Line Focus Solar Stirling Domestic Power Generation

Masters Thesis in Mechanical Engineering

Hamish P. Trolove

April 1994

Department of Mechanical Engineering
University of Canterbury

ACKNOWLEDGEMENTS:

A number of people have helped me to bring this project to completion. I should like to thank my supervisor Dr John Raine, Dr Don Clucas, my Stirling Engine advisor, Neville Foot for his great work with the heat pipes, and for his support after the accident. I should also like to thank Professor Arthur Williamson, Ron Tinker, and Eric Cox for their advice and ideas, Otto Bolt, and Ken Brown who built a lot of the apparatus I made use of, and the technicians in electrical engineering who advised on things electrical, and loaned me some of their equipment. A very special thanks also to Don Clegg from Chemical Engineering whose speed and efficiency after the accident was much appreciated.

TABLE OF CONTENTS

ABSTRACT:

This thesis has found that to generate electricity for a domestic supply, the use of a two stage line focus concentrator coupled to a Stirling engine by way of a heat pipe is very inefficient, and the end result (useful power) could be better achieved by a line focus system with a Rankine cycle heat engine, or by using photovoltaic cells. For larger systems such as that needed to supply a small community, a point focus solar Stirling engine is the most efficient system at this stage, but with the rapid improvements being made in the performance of photovoltaic cells, this may not be the case in the future.

INTRODUCTION

In 1989 research in Stirling cycle machines commenced in the Department of Mechanical Engineering at the University of Canterbury. The initial aim was to design a commercial Stirling engine battery charger for yachts, (Clucas 1993). The reason for the choice of a Stirling engine, was its ability to operate quietly and efficiently on a convenient fuel such as liquified petroleum gas. The project was completed in 1993.

The Stirling engine designed (See Appendix 3) was of a form that had great potential for use in a number of other applications. One of the applications in which Stirling engines have been successfully used, is the conversion of solar thermal energy to electricity. This is normally achieved using a Stirling situated at the focus of a parabolic dish reflector. Systems of this form generate powers within the range 5-25kW.

On farms remote from the electricity grid, the use a solar power generation system capable of meeting the domestic energy demands of a single dwelling, appeared to be a good application for a Stirling engine of the type developed by Clucas (1993). With dish-Stirling systems being suited to higher electricity loads than that needed by a single domestic user, it seemed at the time that this would have been an unnecessarily complex and expensive system.

The alternative was a line focus or trough-Stirling system, whereby the Solar radiation is focused on a tubular, or flat absorber for transport to the Stirling engine heat exchangers. Having a complex shape in only one dimension, the trough reflector system appeared to be cheaper and easier to produce than the more complex parabolic dish. The trough reflector system, had the attraction of originality as very little research had been done into the use of line focus solar Stirling power generation systems. Thus the system investigated in this thesis is a line focus solar Stirling co-generation system. The configuration of the optics and how they are related to the Stirling engine is discussed in detail in Chapter 5.

Concept design, and testing of the concept became the focus of the research. The design had to be cheap, simple to produce, and require a minimal amount of maintenance. Being for a rural situation, the area of the reflector system was not of prime importance. Concept design for each of the components comprising the system had to be investigated. These were:

- The optics system (Chapter 5)
- The heat transfer system (Chapter 7)
- The heat exchanger system on the Stirling engine. (Chapter 7)

As the Stirling engine had already been designed, no redesigning other than the heater heads would be done. To control the system, a microcomputer and servos for tracking would also be required, but these were not to be considered in any detail, as this would be beyond the scope of this thesis. Research into the energy demands of an average household determined the size of the system. This is covered in chapter 4.

To optimise the concept design, a computer model had to be devised. The details of this are outlined in chapter 6. To allow for easy operation, and an easy output of data, the model was run through a spreadsheet package. The output from the model was the optimised temperature for the solar concentrator absorber. This determined the performance of the system, and the nature of the working fluids to be used in the heat exchangers.

For this application it was necessary that the heat exchangers for transporting heat from the solar concentrator to the Stirling engine, be capable of passing a large heat flux through a small cross-sectional area It also needed to have a minimal temperature drop between the heat input at the concentrator focus, and the heat output at the Stirling engine. Heat pipes fulfilled these requirements.

A heat pipe is a two phase heat transfer device. It operates through the evaporation of a working fluid at the point of heat application, and the condensation of the vapour at the point of heat rejection. The heat is therefore transferred through the latent heat of vapourisation of the working fluid.

It became evident from the computer model that the temperature at the absorber was within a range for which there are very few suitable heat pipe working fluids. A larger portion of the project was concerned with the evaluation of a few potential working fluids. They were:

- Sulphur/iodine
- The organic fluids diisodecyl phthalate, Benzyl Benzoate, and Dowtherm A. The suitability of these was indicated by the testing of Dioctyl Phthalate.
- Mercury
- Potassium

First the candidate fluids were found through literature searches, and the application of a "Merit Number" that could compare the working fluids properties (Chapter 8). Calculation of the operating limits for the working fluid's determined the form of the heat pipes, and gave a size for the pipe.

Evaluation of the working fluids was achieved through the construction of model heat pipes based on the system to be used as the absorber for the solar arrays, and the subsequent testing of these using electrical heating. The heat flow, and temperature profiles over a time indicated the performance of the heat pipes, from which suitability could be deduced. Chapters 9-12 give the results and conclusions drawn for each of the working fluids tested.

Drawing on the information gained from the heat pipe tests, and the performance prediction model, an estimate of the system's viability was made. This conclusion is presented in Chapter 13.

1. THE STIRLING ENGINE

1.1 Introduction

As will become evident from reading Chapters 1 and 2 of this thesis, the Stirling engine is a device well suited to a large number of applications and has a lot of very desirable performance and environmental qualities. Working on the idea of a domestic power supply for dwellings away from the national electricity grid, and a desire for a clean source of electrical energy and hot water, a Solar heated Stirling engine generator set was looked at for this project. The design was to be based around the 200W Stirling Battery Charger system designed by D.M.Clucas for his Doctorate Thesis (Clucas, 1993) within the Department of Mechanical Engineering at the University of Canterbury.

1.2 Stirling Engine History

During the early part of the nineteenth century the predominant industrial prime mover was the reciprocating steam engine. Manufacturing techniques of the time were not of a very high precision nor very reliable. These, when applied to the production of steam engines, meant that there was a considerable danger of the boilers exploding (Goetz 1990). This prompted a minister of the Church of Scotland, Robert Stirling (1790 - June 6th 1878), to invent a reliable, and safe engine based on the expansion and contraction of a contained mass of air within a cylinder, heated by an heat source external to the cylinder. He was granted a patent for the new machine in 1816. This new machine was the Stirling cycle engine otherwise known as the Hot-air engine.

His design included a regenerator which is a short term heat storage component that greatly increased the efficiency of the engine.

Through till the early 1900s the Stirling engine enjoyed some attention, though the materials available greatly hampered its continued development. An example of the state-of-the-art Stirling engine available in 1885 was a German 1.5kW unit weighing 4100kg and having a volume of 21m^3. It is therefore with little surprise

that the internal combustion engine and electric motors that were starting to be used by the turn of the century quickly superseded the cumbersome stirling engine.

The next major step in the history of the stirling engine occurred in 1938 and was due to the efforts of N.V.Philips Gloeilampenfabrieken in the Netherlands who began a Stirling Research Program (Meijer 1988). During World War II, the Philips company concentrated on theoretical research so as not to draw the attention of the occupying forces as they would have done had they started producing new machines. With the finish of the war Philips found a market niche for the Stirling engine as a small electrical generator for powering radios and communication equipment in the field where large batteries would be awkward or simply not available. The Stirling engine's ability to operate on most fuels made it ideally suited to this application.

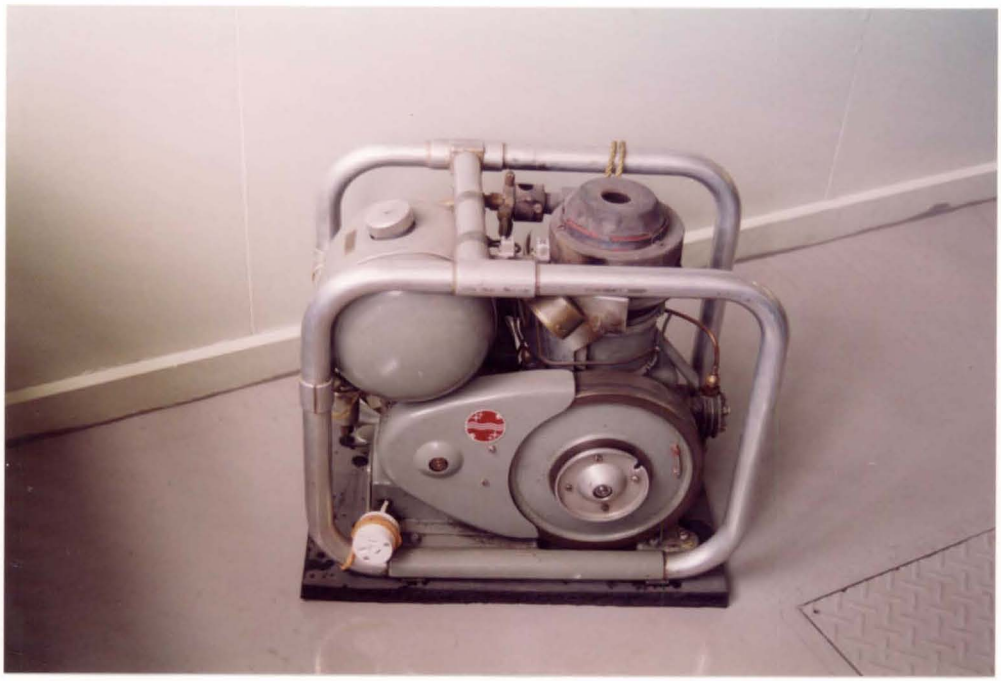

Figure 1.1 Philips 200W Bungalow Set

Philips became the principle researchers and developers of Stirling technology, and designed a large number of machines with a wide range of powers for various applications. From this research, a few new mechanisms and configurations were devised. Of particular significance is the rhombic drive and the Rinia or Siemens

configuration.

A small 200W generator known as the "Bungalow Set" (See Figure 1.1) was designed and a pre-production batch of about 150 built in 1948 - at about the time transistors were invented. New radios based on the transistor technology no longer needed large power supplies and so the "Bungalow Set" became obsolete. The 150 generators produced in the pre-production run were eventually donated to various universities all over the world - the University of Canterbury being one of these.

With the loss of the field generator market, Philips turned its attention to automotive applications for the Stirling engine, eventually producing and successfully demonstrating two Stirling powered Ford Torinos in 1976 - just in time to have Ford terminate its exclusive Stirling engine license because of difficulties in the automobile industry and the need to concentrate on short term problems. At this point Philips also gave up. The work done by Philips was picked up by one of their licensee companies called Stirling Thermal Motors Inc (STM).

Despite the lack of success in the pursuit of the Stirling engine as a marketable power source, Philips had, in 1945, invested in research involving the Stirling cycle as a refrigeration plant. Under the guidance of Dr. J.W.L. Köhler, the Cryogenerator Division of Philips become a world leader in its field, with a large range of commercial cryocoolers.

The oil crisis of the 1970's helped the Stirling engine become the focus of a renewed interest, because of its potential high efficiency. However this interest failed to grow due to the return to plentiful oil supplies and the pressure from internal combustion engine producers. With the growing environmental awareness of the general population through the 80's and early 90's, the Stirling engine has slowly been gaining familiarity and renewed interest. In the United States, Solar power generation plants based around the Stirling engine coupled to a point focus parabolic dish concentrator have been successfully used.

The Mechanical Engineering Department of the University of Canterbury in New

Zealand, in 1989 initiated a research project for the development of a commercial Stirling Battery Charger for use on board yachts. Normally battery charging is done by running the main diesel engine for long periods of time, which, being at low load, is wasteful, while also being noisy (Clucas 1992).

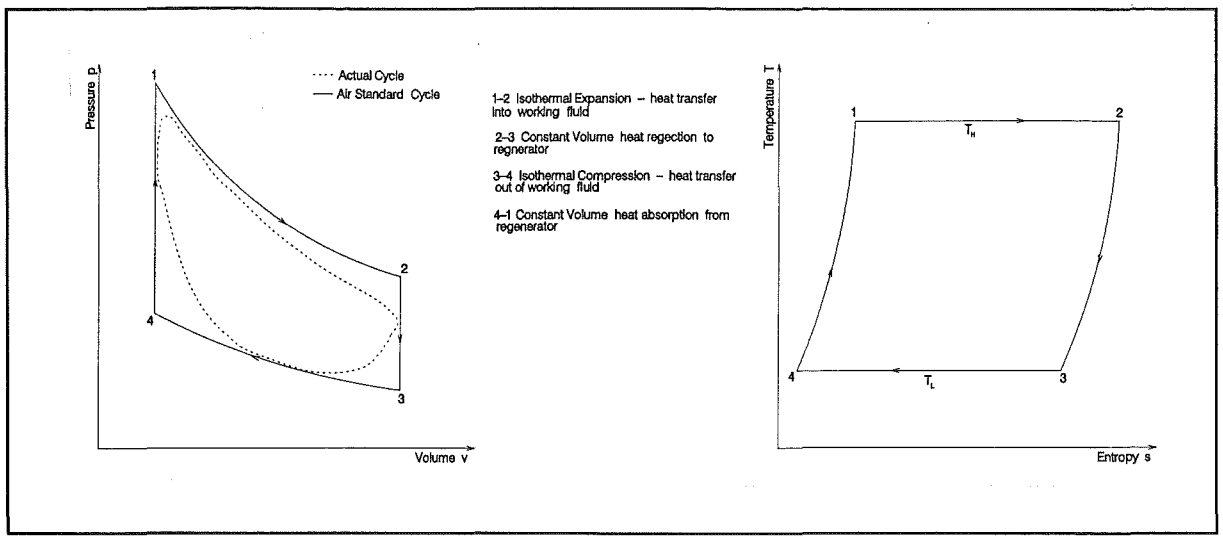

Figure 1.2 Air standard Stirling cycle represented on a) Pressure-Volume diagram and b) a Temperature-Entropy diagram for the working fluid. The PV cycle followed by an actual Stirling engine has been represented by a dotted line.

1.3 Stirling Cycle

The ideal Stirling cycle is comprised of four separate processes (Karlekar 1983) which can be seen in Figure 1.2. The first is an isothermal (constant temperature) expansion with heat transfer into the working fluid from outside the cylinder, and is represented on the diagram by curves 1-2. 2-3 is an isochoric process (constant volume) where the working fluid is moved from the hot expansion space to the cold compression space usually being passed through a regenerator into which heat is rejected. Process 3-4 sees the working fluid being cooled and the subsequent isothermal compression that occurs as heat is dumped out of the cycle. The cycle is completed by the isochoric process, 4-1, when the cold working fluid is moved from the compression space to the expansion space, again passing through the regenerator, picking up the stored thermal energy as it goes.

A more practical representation of the cycle has been given in Figure 1.3 which

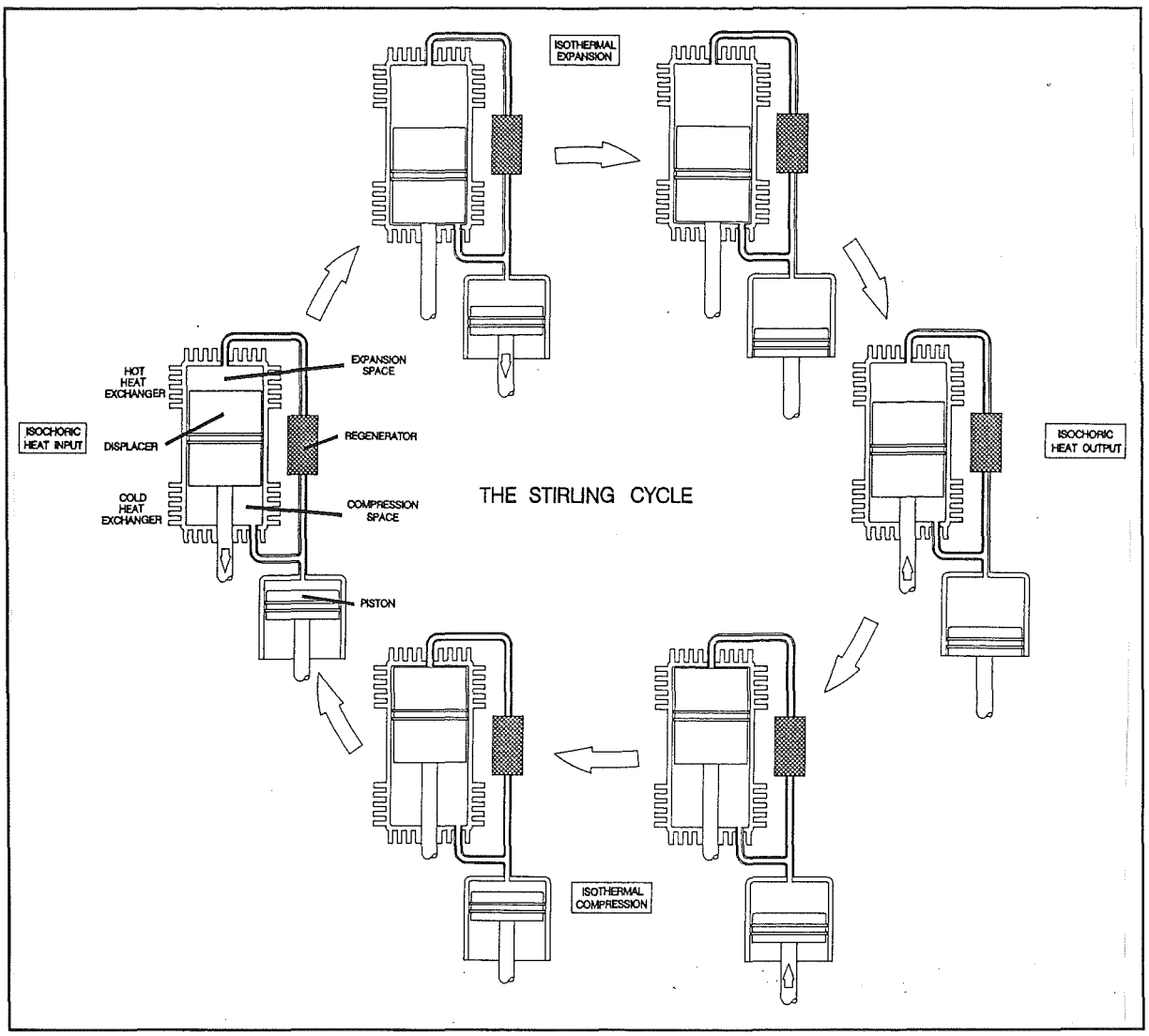

Figure 1.3 Representation of a practical Stirling cycle as executed by a gamma configuration engine

shows a representation of one of the many Stirling engine configurations[1]. For ease of visualisation, two extra diagrams have been included in the representation shown by Figure 1.3.

Starting at the top of the diagram, the engine is engaged in the isothermal expansion phase. As can be seen, almost all of the working fluid in the cylinder is above the displacer and therefore in the hot space. The gas heats up from heat transfer through the cylinder walls, and expands, thereby increasing its pressure and forcing the piston down, until it reaches the bottom of its stroke. At this

[1] The configurations will be looked at in more detail in Section 1.5.

point, the displacer begins moving up, displacing the working fluid from the hot space, through the tube, and regenerator, into the cold space. The diagram in the lower right of Figure 1.3 shows the displacer at the top of its stroke. Almost all the working fluid is now below the displacer, inside the compression or cold space. Heat is rejected to the walls of the cylinder where it is dumped to the atmosphere or to an alternative cooling system. With the cooling of the working fluid, the pressure in the cylinder drops below the ambient pressure or the pressure in the crank-case which produces an upward force on the piston. The piston rises, and continues to compress the working fluid until it reaches the top of its stroke, whereupon the displacer begins to move back down the cylinder, causing the working fluid to be displaced back to the hot expansion space after passing through the regenerator and picking up any thermal energy stored there.

Because of the continuous motion produced by the mechanisms needed for practical systems, the Air Standard Stirling cycle cannot be achieved and the processes involved are less distinct as can be seen in Figure 1.2a.

1.4 Operational features of the Stirling Engine

Most of the desirable properties of the Stirling engine are due to the combustion or source of heat being external to the cylinder. These are;

- Possibility of running the Stirling cycle engine on any heat source, i.e. Natural Gas, Coal, Biomass, Geothermal, Solar energies (Kolin 1991).
- Reduced need for maintenance, particularly of the seals within the cylinder. The reason for this is that there are no combustion products within the cylinder to cause degradation of the surfaces and components.
- Quiet operation. With no periodic explosions occurring, the noise from a Stirling cycle engine is very low, most being due to the combustors (if a combustion heat source is used.), and the drive linkages.
- Complete combustion of fuels (if used) due to the continuous nature of the combustion, and the abundance of oxygen.
- Having the same unit of gas trapped in the cylinder without being passed out each cycle means that the engine can be charged with exotic gases which have good thermal and transport properties e.g. Helium, and Hydrogen.

There are draw-backs with external combustion, the major one being the problem of getting the heat into the cylinder efficiently. The design of the heat exchangers in Stirling cycle engines is very critical and there has been a large amount of research done to address this problem. As with most design problems, there are trade-offs needed, and in this case there are three main ones; pressure drop through the heat exchangers, good heat transfer coefficient, and keeping the gas volume down. Unfortunately, these requirements all conflict with each other, leading to an interesting design optimisation problem.

Also due to the external combustion is the fact that the hot end heat exchangers are generally made of materials which have a considerable mass, and so it takes time for the engine to heat up and cool down. This means that the Stirling cycle engines will not respond very quickly to changes in the heat input, which means that power control has to be achieved by some other means, which are generally very complex and therefore expensive.

With the heat input being continuous at a high temperature, there are considerable problems associated with the materials for the hot end heat exchanger. This was one of the main problems behind its loss of ground to the internal combustion engine where the temperatures are high but only for a very short time. It has only been with the advent of new high strength, high temperature alloys that the temperatures in the cylinder have been able to reach a sufficiently high temperature for the Stirling engine to once again be viable.

Another reason for the downfall of the Stirling cycle engine was the low specific power output when compared to the internal combustion engine. If we look at the West equation 1.1 (West 1986). We can see that the mean cycle pressure p_{mean}, has a large effect on the power output of a Stirling cycle machine of a given size. By increasing the mean pressure, the power per unit weight power output can be improved. With the new alloys, the mean pressure could be increased, with as much as 20MPa being used in some machines. At these pressures, the power per unit weight is in excess of that found in an internal combustion engine.

$$P = W_n p_{mean} f V_o \frac{T_H - T_C}{T_H + T_C} \qquad \text{(1.1) West equation}$$

P = Power output from cycle (W)
W_n = West Number - a factor usually between 0.25 and 0.35 and is chosen by the designer and shows how confident they are of their design's ability to approach the theoretical Carnot efficiency.
p_{mean} = Mean cycle pressure. (Pa)
f = Frequency of cycle (Hz)
V_o = Volume variation in the cycle (m^3) which depends on the configuration of the engine: Alpha engines use $V_o = 1.414 V_s$, while Beta and Gamma engines use $V_o = V_s$. (Refer to section 1.5)
V_s = Swept volume of expansion piston (m^3).
T_H = Hot end temperature (K).
T_C = Cold end temperature (K).

Associated with the high internal pressure, there is a need for special care in the design of the seals and lubrication of the engine, for otherwise the high pressure gas charge will be lost with consequent loss of power and performance. Lubrication is a problem in Stirling engines because of the need to avoid hydrocarbon lubricants which could burn, or thermally decompose to produce contaminants in the engine working fluid which would foul the regenerator and heat exchangers or cause the engine to wear out prematurely.

The theoretical efficiency of a Stirling cycle engine is the same as the Carnot efficiency which is the theoretical maximum for a heat engine. Real Stirling cycle engines fall short of attaining the theoretical efficiency, but they may approach it more closely than most other engines of similar size and power outputs. Within reasonable limits, the thermal efficiency of a real Stirling cycle engine is almost independent of the engine speed. This is very useful for applications with changing loads. Similarly, torque varies little with changing engine speed.

1.5 Stirling Cycle Engine Configurations

The configuration of Stirling engines is based upon the arrangements of the cylinder(s), not upon the overall form due to the vast number of mechanisms that

have been designed to produce the appropriate motions. Typical types (West 1986) are shown in Figure 1.4. These illustrations are very general, and do not take into account the many other variations of the same types, such as radial forms, or "V" cylinder arrangements, and any number of others. There also exists the rotary engine which is based on the Wankel engine (Walker 1973).

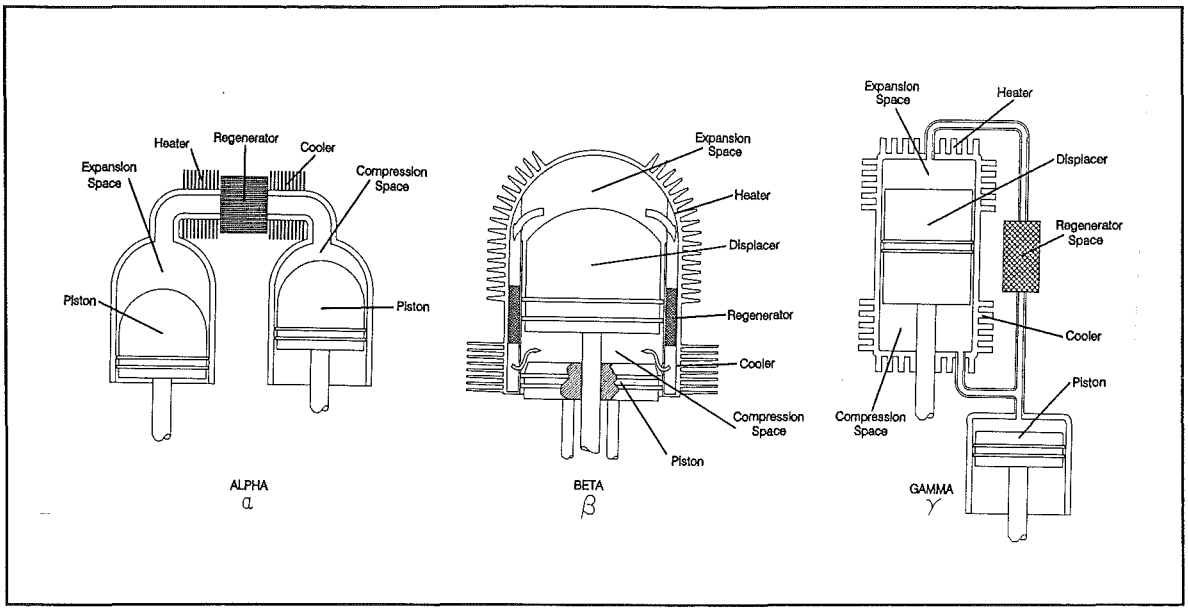

Figure 1.4 Typical single acting engine configurations.

1.5.1 Alpha Configuration

This is a typical single acting two piston engine. In this arrangement, there is no displacer, as the two pistons are phased such that they shuttle the gas between their two cylinders through the regenerator, and heat exchangers. They have several main subgroups within them. Shown in Figure 1.4 is the parallel cylinder arrangement, there is also the V-cylinder, opposed piston, and the rotary cylinder (see Walker 1973 for representations of these systems). The mechanisms for alpha engines can be relatively simple such as a pair of slider crank mechanisms, or something more complex like the Ross linkage (West 1986).

1.5.2 Beta Configuration

The Beta configuration machine makes very efficient use of cylinder space and size, being a single acting single cylinder piston-displacer engine. There are very

few variations of this type. One variation is as shown in Figure 1.4, while another has the regenerator mounted on the displacer itself so that the gas flow is then through the displacer into the compression or expansion spaces. The Beta configuration Stirling cycle engines are generally as shown in the diagram which requires a seal to be built into the piston. To get around this problem, another arrangement exists where the displacer rod is passed out through the top of the cylinder. Beta engines usually have very complex mechanisms to achieve the appropriate motion, the most notable being the rhombic drive. Free piston Stirling cycle engines are also of this type. These are engines where there are no kinematic mechanisms, and all the phasing between the piston and displacer is achieved by gas springs and fluid dynamics.

1.5.3 Gamma Configuration

The possible arrangements and mechanisms available for this type of configuration are very wide. The basic requirement for a Gamma engine is that it has a piston, a displacer, two cylinders and be single acting.

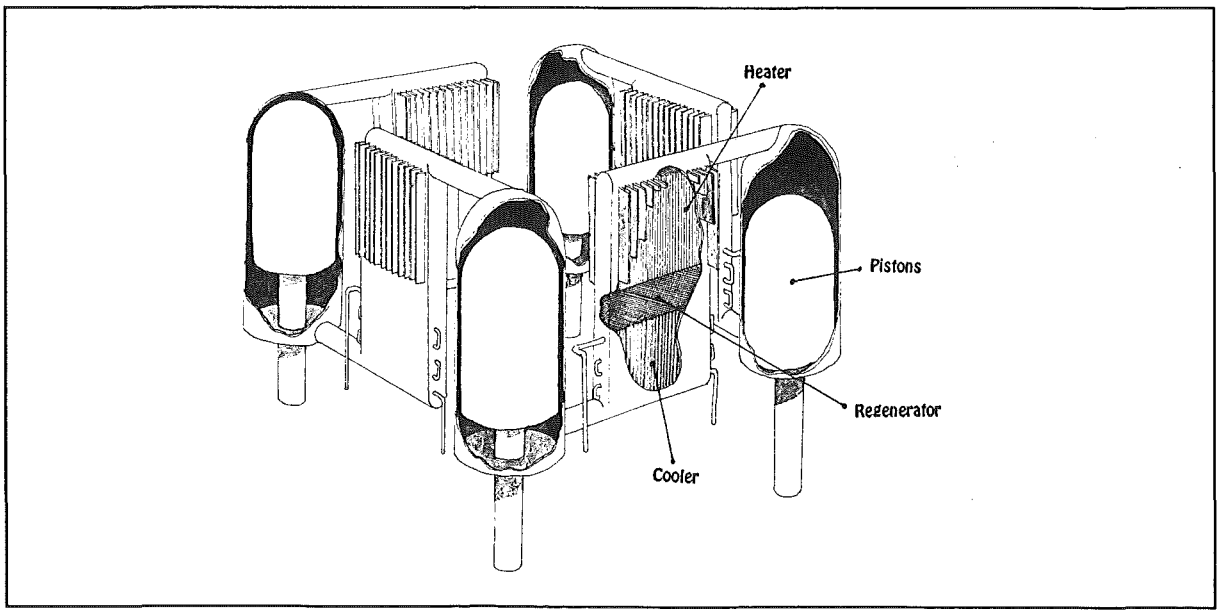

Figure 1.5 Double acting Siemens configuration Stirling engine.

1.5.4 Double Acting Siemens Configuration

This is most similar to the alpha configuration engine except that each cycle is between the space over one piston, and the space under the piston in the adjacent

cylinder, as in Figure 1.5. The normal number of cylinders is four with each of the cycles being phased 90° apart. Both in-line and square arrangements exist with various mechanisms to produce the correct motion being employed for each type. The usual is the swash plate drive. For the engine developed by Clucas (1993), the Siemens configuration was used, with a new mechanism called the "wobble yoke".

2. STIRLING ENGINE APPLICATIONS

2.1 Introduction

As was shown in the preceding chapter, the Stirling cycle engine has a number of qualities which make it suitable for a very wide range of applications. The key attributes that are responsible for this are its multi-fuel capability, and the fact that it has very good part load performance.

2.2 Remote Power Generator Sets

This is the application which best suits the Stirling engine, particularly in locations where there is difficulty in obtaining petrol for an internal combustion engine. In this case, the ability to run on low grade fuel (biomass or coal) is of high importance (West 1986). There is a commercially available Stirling engine developed by Sunpower, designed to burn rice husks, wood chips, and straw with a third world market being targeted. This engine can be used to drive water pumps, mills, or generator sets (Lockwood 1984, Gaegauf 1993). In developed countries, the Stirling engine when used as a power generator would supply electricity to yachts (Clucas 1993), and holiday homes, with the advantage being that the Stirling engine is much quieter and less invasive than its equivalent internal combustion counterpart.

Another factor that makes Stirling engines useful for remote power generation, is its reliability. They can operate for a long time without maintenance, supplying power to navigational aids in lighthouses, communications equipment, and meteorological stations.

In this application, the need to have a high specific power output is reduced, with the need for engine speed regulation being of only moderate importance. This means that the Stirling engine can compete on an equal footing with the internal combustion engine. The size of motor desired generally falls within the range 200-500W with the largest size being about 5kW.

2.3 Space Power

As an extension of the remote power generation application, the Stirling engine is well suited to space power due to its ability to run on any source of heat, and its reliability. When the Stirling engine is being used in space power applications it is generally a Free-Piston Stirling engine, where the piston and displacer motions are controlled by gas springs and pneumatic forces caused by the varying pressure in the working gas, instead of heavy and less reliable kinematic linkages. Because of the lack of shafts and need for any external drives, the free piston Stirling engine can be totally sealed, which makes it unaffected by the outside environment.

The heat sources available in space for the operation of the Stirling engine are;

- Solar Thermal Energy
- Radioisotope decay
- Anaerobic Chemical reactions
- Thermal Storage Device

2.4 Solar Powered Stirling Engines

Considerable research has been carried out in the field of solar Stirling power generation with a number of commercial systems available. The power range of the generators used is generally 5kW to 25kW and are usually part of a solar power station. Fitted into the focus of a parabolic dish reflector, the efficiencies of the Dish-Stirling systems (around 30%) (Ross 1992, Erbeznik 1992, Bean 1992) are comparable to those of the best photoelectric cell[1] currently available. However, photoelectric cells are getting better and cheaper all the time. This will be expanded on in later chapters.

Because of the nature of the incoming energy, the Solar Stirling application tends to have a much higher overall efficiency compared to its combustion heated counterpart operating with the same temperature differential, as the parasitic losses due to heat being lost up chimneys and through the combustion chamber walls are not present here. In most currently available systems the configuration used is a single cylinder beta arrangement, which allows for a fairly even heat flux

---

[1] point contact crystalline silicon cell 25% conversion efficiency and gallium aluminium arsenide, gallium arsenide, and silicone stack junction cells having a theoretical efficiency of 40% (San Martin 1992).

into the cylinder head. However with the more recent models, and multi-cylinder engines like the DMC5 (Clucas 1993) developed in the Department of Mechanical Engineering at the University of Canterbury, a heat pipe absorber system has to be used to avoid hot spots.

For lower temperature operations, a parabolic trough can be used, which has cheaper but larger concentrator arrays. Unfortunately with this system, the efficiency is very poor - being only about 3% total energy conversion to electricity (Refer to Chapter 6).

Like all other Solar Thermal systems the Solar Stirling system suffers from the problem of night-time when the system cools off and does not produce any power. This inconvenience means that the system has to be restarted every morning which may take a considerable amount of time due to the system's thermal mass.

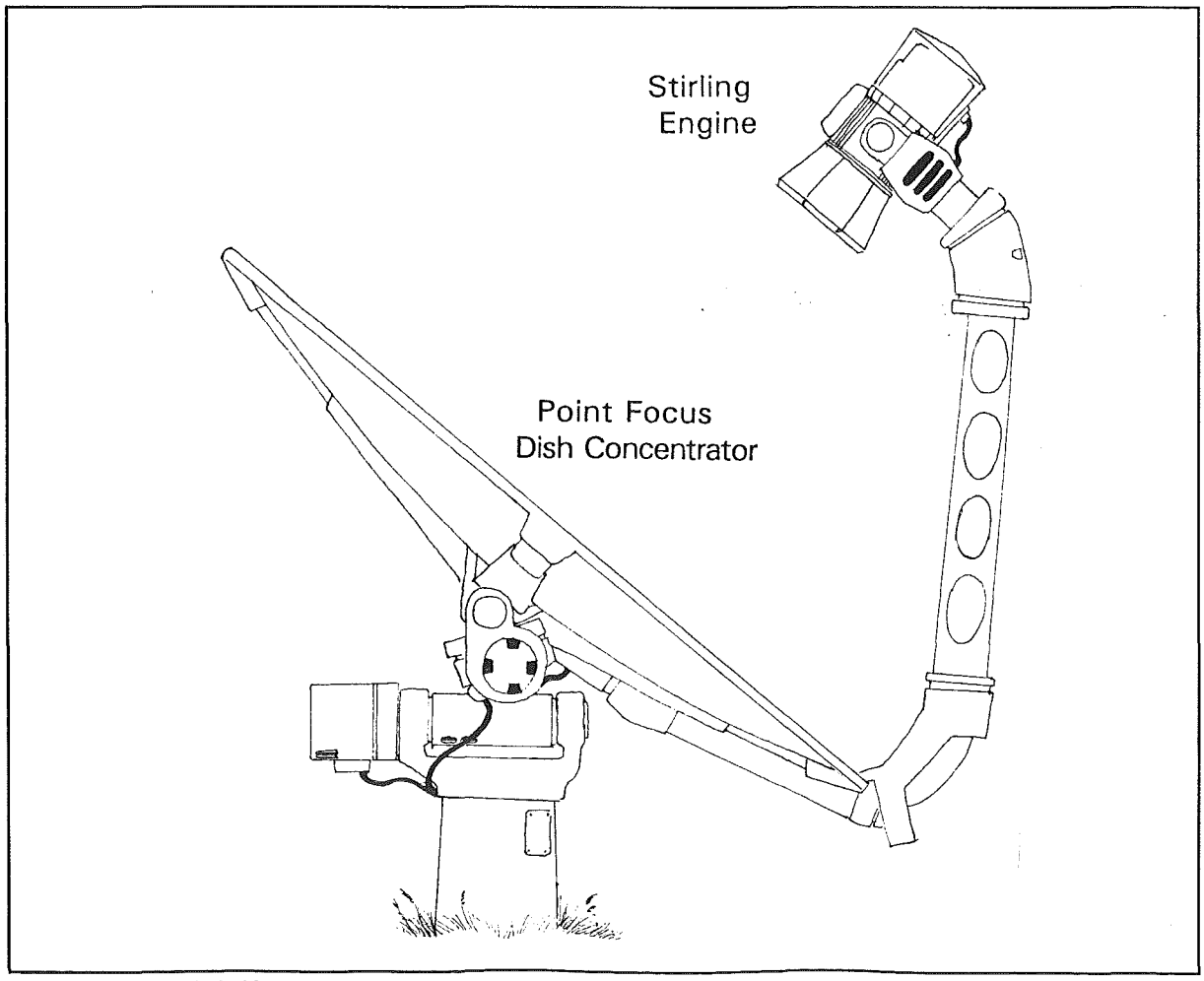

Figure 2.1 Dish/Stirling power generator

The lower insolation during the first and last couple of hours of daylight are also a problem because the temperatures achieved will not be high enough to drive the system. To get around this problem energy storage of some kind would be needed, be it a thermal or chemical battery. The possibility exists that the energy could be stored as potential energy in a hydrolake, or in unburnt fuel, if a national electricity grid was nearby. This would depend on the power authorities allowing the domestic solar power system owners to feed the power generated during the day into the grid, and reclaim it at night.

2.5 Co-Generation

Co-generation refers to the design of a system to cater for several energy demands at the same time, the typical example being the need for electricity, hot

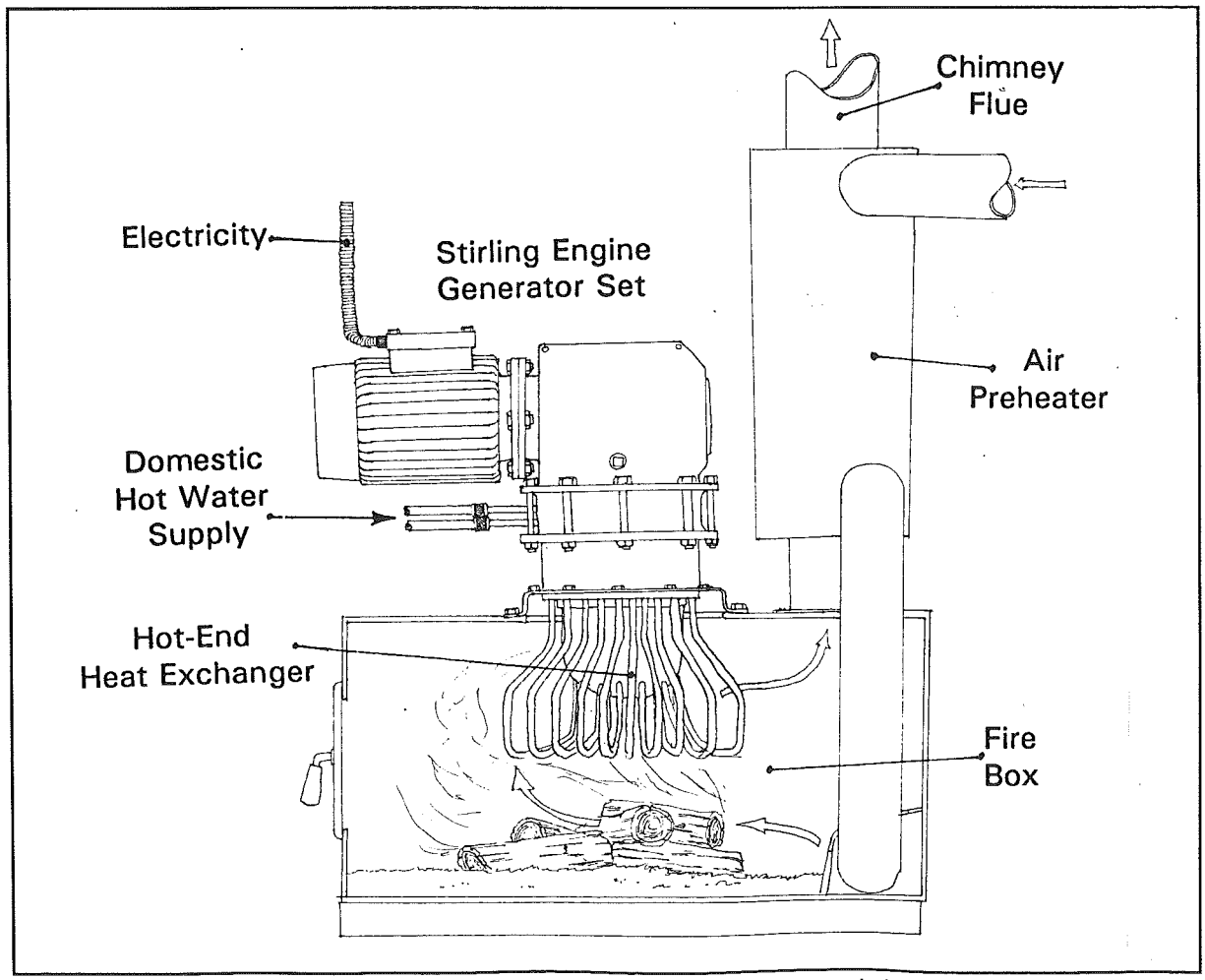

Figure 2.2 Wood burner fitted with a Stirling engine supplying electricity and hot water in a domestic situation.

water, and heating. Some projects exist in this field based around a Stirling engine supplying domestic power and hot water demands. The typical system for this would consist of a power management device, 1.5kW Stirling engine, combustor, battery storage, and hot water storage/circulation system. The water from the cooling of the Stirling engine would be at a suitably high temperature and of sufficient quantity and cleanliness for all domestic needs, while the battery storage combined with the electricity generated would supply all electricity demands, and be able to meet the peak loads that would occur.

In an application such as this, the source of heat will usually be a domestic gas, or oil furnace, depending on the local supplies and laws governing heating systems. Wood burners are another possible source of heat while coal burners would be very

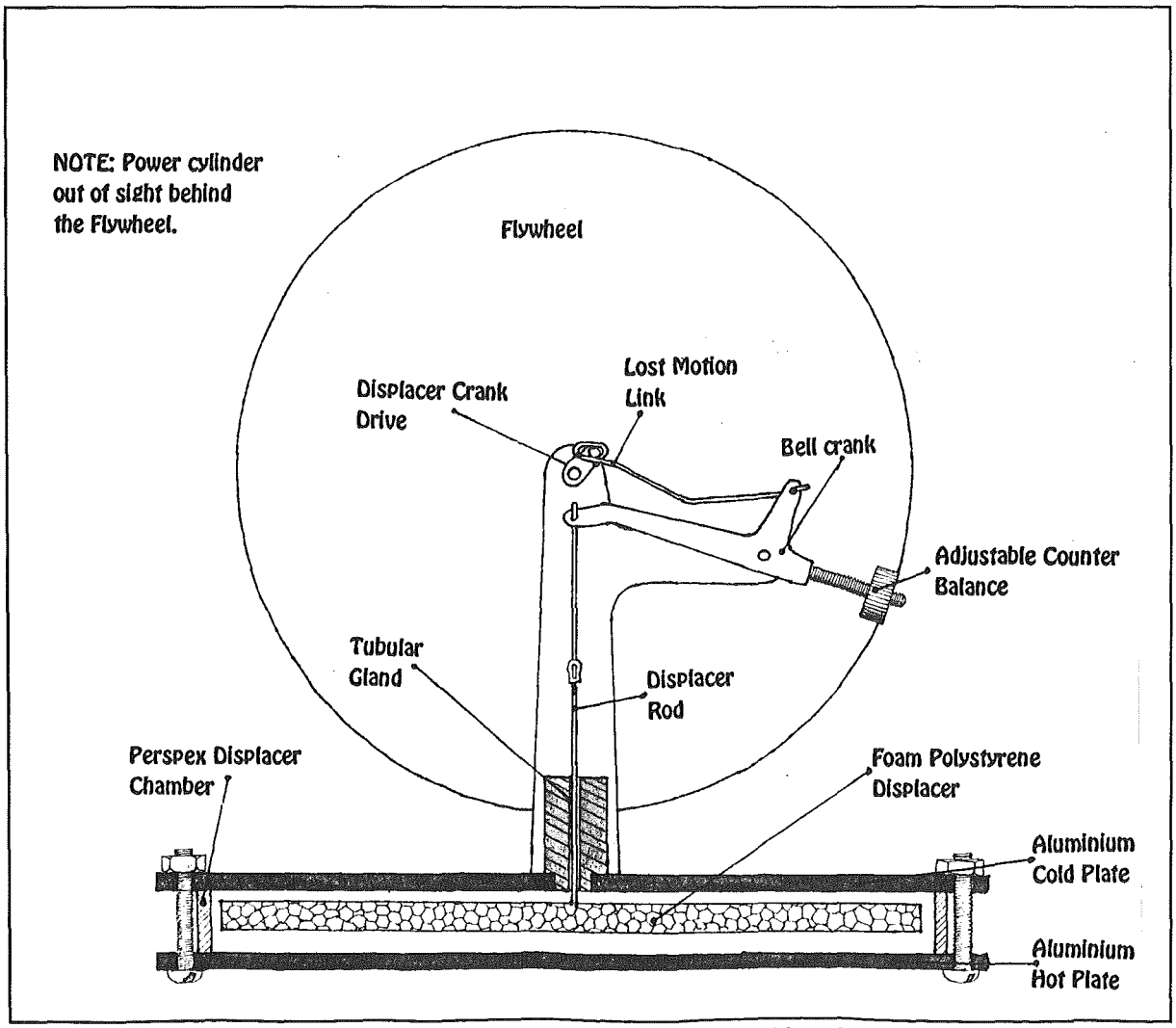

Figure 2.3 A low temperature model Stirling engine. (Senft 1991)

good but suffer from being a non-renewable resource as well as dirty. A final possibility exists in the use of solar energy to heat the engine. Space heating could be achieved through circulation of the hot water produced.

On a larger scale, small power stations running on biogas could supply the electricity and hot water for a number of houses.

The qualities making the Stirling engine a viable option here is that it has a reasonable efficiency at the temperatures experienced, while the reliability is the chief factor. Being stationary, the weight and specific power are not critical. Powers below 10MW (Walker 1986) give the Stirling engine a cost advantage over the Rankine cycle co-generation units because to achieve a good efficiency at the lower powers, the turbines would have to be replaced by the less reliable, reciprocating steam engine. In this case, a condensing cycle would have to be used, making for large and expensive heat exchangers.

2.6 Model Stirling Engines

Stirling engines are a great attraction to model engineering enthusiasts because of their ability to run on any source of heat, the fact that they generally have more complex and interesting drive linkages than their internal combustion counterparts, while not requiring any extreme precision to build (Walker 1986, Lista 1991, Fox 1991). The power range for these engines is within the range from less than 1W up to 40W from cylinders of about 6 - 30cm^3. A competition held each year for model engineers always has a number of Stirling engines of ingenious design, both pressurised and unpressurised (Fox 1993). The drive systems employed by the builders are as many and varied as are the designs for full scale devices, with a few more besides. Figure 2.3 illustrates a small model Stirling engine capable of running from the temperature differential between the ambient air and the temperature of a person's hand.

It is through laboratory models, and hobbyist models that the general public come into contact with the Stirling engine. To cater for this market, there are a number of companies world wide who produce the engines (Lista 1991, Fox 1991) covering a range of power outputs, fuel types, configurations, and costs.

2.7 Underwater Power Systems

Silence of operation, and the ability to work on stored thermal energy (usually molten salt), reaction heat, or radioisotope heat are the prime characteristics of the Stirling engine that make it so well suited to this application (Walker 1986). When used with fuels such as diesel and methanol, the combustion is carried out in pure oxygen at high pressure (to match the ambient pressure at the maximum depth so as to allow for disposal of the exhaust if the "exhaust trail" produced by this is tolerable). Some of the heated exhaust gas is recirculated in order to keep the flame temperature within reasonable limits as with pure oxygen, temperatures of 4000°C are possible (Nilsson 1988, West 1986). Much research has gone into using the Stirling engine in underwater applications, particularly for the powering of submersibles.

2.8 Marine Engines

With an abundance of water present around boats, the problem of where and how to dump the waste heat is solved (Walker 1986). The engine size of most significance for Stirling engines is about 10kW to act as an auxiliary propulsion and power plant for yachts, and luxury craft, where their silent operation would be appreciated.

Larger engines up to 600kW have been developed for coastal vessels such as tugs, and commercial fishing vessels. These are usually diesel burning, but coal is also a possibility. Engine sizes in excess of this are unlikely to be developed due to the extreme cost to produce a new working engine, while the less efficient and noisy diesel engine can easily satisfy the small demand for engines of this size.

General Motors, at one time, developed a 600kW unit for the propulsion of a coastal vessel requiring good manœuverability. To achieve this, the designers came up with a cunning method of changing the phase angle 'α' between the pistons and displacers, thus allowing power control, and also a method for reversing.

2.9 Automotive Engines and Heavy Vehicle Power

Stirling engines are least suited to this task and cannot compete at the present

$$P = W_n p_{mean} f V_o \frac{T_H - T_C}{T_H + T_C} \qquad \text{(1.1) West Equation}$$

time against internal combustion engines due to their cost, lower specific power, lack of support from the larger companies, and very importantly, the difficulty involved with power control. In addition to this, the Stirling engine, when used in this application, requires a substantially larger radiator than its Otto cycle counterpart. Compared with the internal combustion engine, more of the heat rejected from the system has to pass into the cooling water, as the gas charge cannot be expelled with each cycle. The Stirling engine is better at constant speed applications where its thermal mass will not cause problems. However, used as the primary powerplant in an automobile where the engine directly drives the wheels, the power requirement is constantly changing. A number of systems have been devised to try to overcome this problem. If we refer back to the West equation (1.1) from Chapter 1, it can be seen that by varying the mean pressure p_{mean} of the cycle, the power can be changed. This is one method that has been used. To do this means that a compressor capable of supplying a very high pressure[2] needs to be present in the car, or alternatively a large and heavy cylinder of compressed gas. This also means that the working fluid would have to be air for safety and cost reasons, which falls short of the extremely high performance that can be achieved with helium and hydrogen. Another method of power control works on the variation of the swept volume V_o. The mechanisms to achieve this are complex, but respond quickly. In addition to the stroke variation, some device for varying the fuel rate must be included so as to protect the engine from overheating when operating at part loads. A large proportion of the Stirling engine powered vehicles that have been produced use the double acting Siemens configuration. This lends itself very well to volume control as the arrangement is analogous to the power control used in hydrostatic drives using swash plate pumps.

---

[2] To have a high specific power equivalent to that of an internal combustion engine the mean cycle pressure has to be of the order of 10 MPa.

To get over this problem there is an alternative where the Stirling engine is run at a more constant rate, together with another system better suited to quick variations in power output. There are two main possibilities for this: Electric Hybrid vehicles, or Stirling engines coupled to hydrostatic drives.

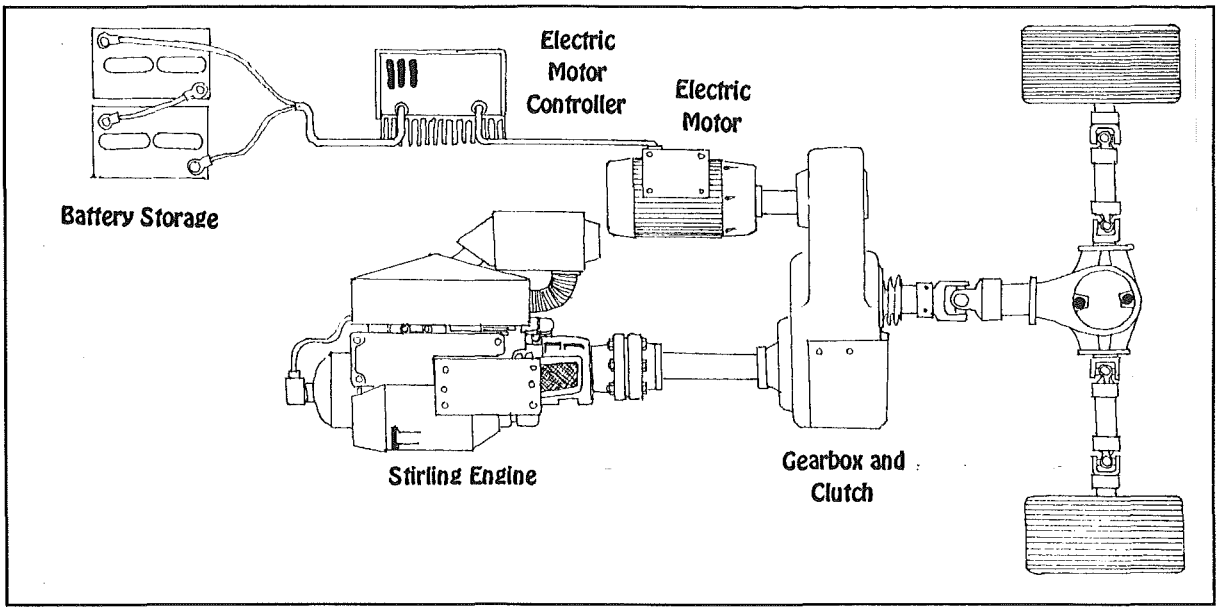

Figure 2.4 Parallel Hybrid Electric Vehicle Schematic

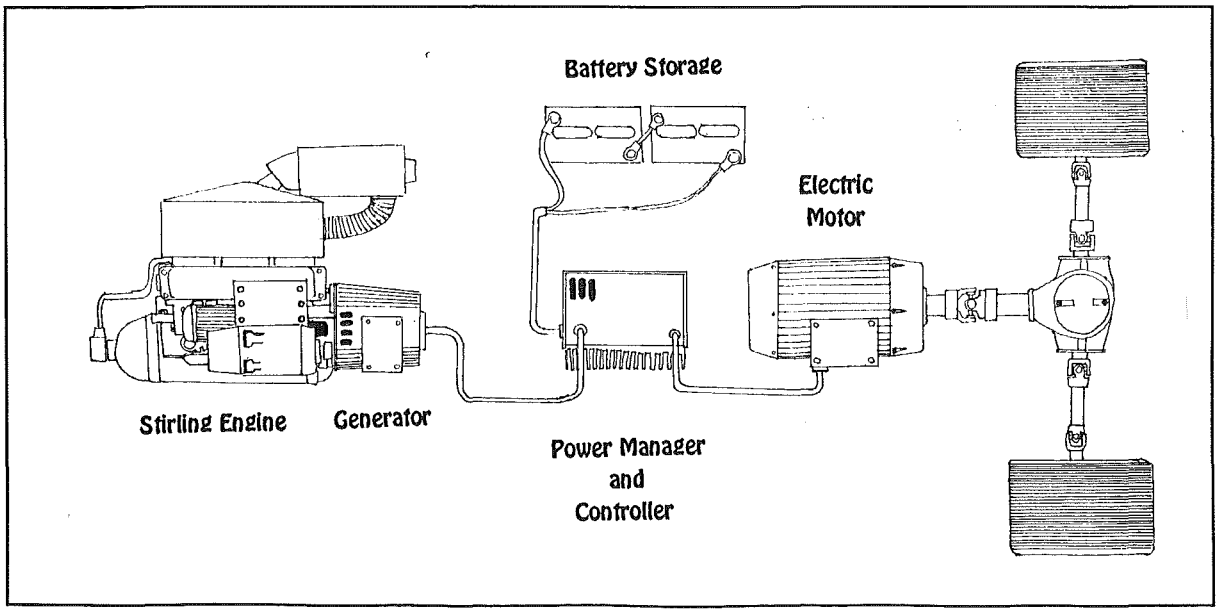

Figure 2.5 Series Hybrid Vehicle Schematic

Within Hybrid electric vehicles there is a choice: Parallel, or Series systems. A parallel system (See Figure 2.4) is arranged such that the heat engine (Stirling or Internal Combustion), drives - through a gearbox - the drive wheels. Peak power

can be added by electric motors which are also driving onto the wheels through the same gear box. This system is better suited to internal combustion engine hybrids because a certain degree of power control is still needed. Of the two systems this is the more efficient.

The Series arrangement (Figure 2.5) has the heat engine operating at a constant speed and power, (the engine can be optimised for this condition), which is driving an alternator. Power from the alternator is used to drive the electric motors, or stored in batteries for such time when the power demand exceeds the heat engine output, and so draws on the stored energy. This arrangement is well suited to the Stirling engine although not as efficient as the parallel system. Both systems can operate on battery power alone should there be a need for emissionless running.

Comparison of the two electric hybrid vehicle configurations:

Parallel

- Neither motor has to take full load so both the heat engine and the electric motor can be smaller.
- The losses incurred by the energy conversions ie mechanical to electric (to chemical) are reduced.
- The heat engine is not isolated from the load and so can be disturbed from its optimal operating point.
- The transmission system is larger and more complex without much freedom in placement of the components.
- More efficient system due to the reduced number of energy conversions.

Series

- Allows for easy conversion of existing electric vehicles.
- Because the link between the driving wheel and the heat engine is through a power cable with a motor controller in between, the heat engine cannot be disturbed from its operation.
- With its more modular nature, the Series engine can be worked on easily.
- Rotational Inertia is less than with a Parallel hybrid vehicle because of the lack of gearbox and if there is an electric motor for each drive wheel, the differential may be left out.
- The efficiency is lower due to the mechanical to electrical energy conversion.

This means that the heat engine has to be larger to account for this.

- The electric motor(s) must be able to handle the full load, and so need to be larger than for the equivalent parallel configuration.

The other type of hybrid system uses hydrostatic drives with Stirling engines. This system does not have any long term storage capacity as do the electric hybrids, and so the engine would have to be bigger to be able to drive the hydrostatic pump with enough power to take up the peak loads. Some companies have experimented using heat engines (internal combustion engines) in parallel with an electric motor system, connected in series with a hydrostatic variable speed drive (Billingham 1979, Preston 1984)

The hydrostatic drive option is best suited to heavy mobile machinery such as tracked vehicles, and locomotives, taking the place of the diesel engines. A large number of conceptual studies have gone into the running of locomotives (Jingwei 1984, Walker 1982) on coal in a fluidised bed combustor from which heat is

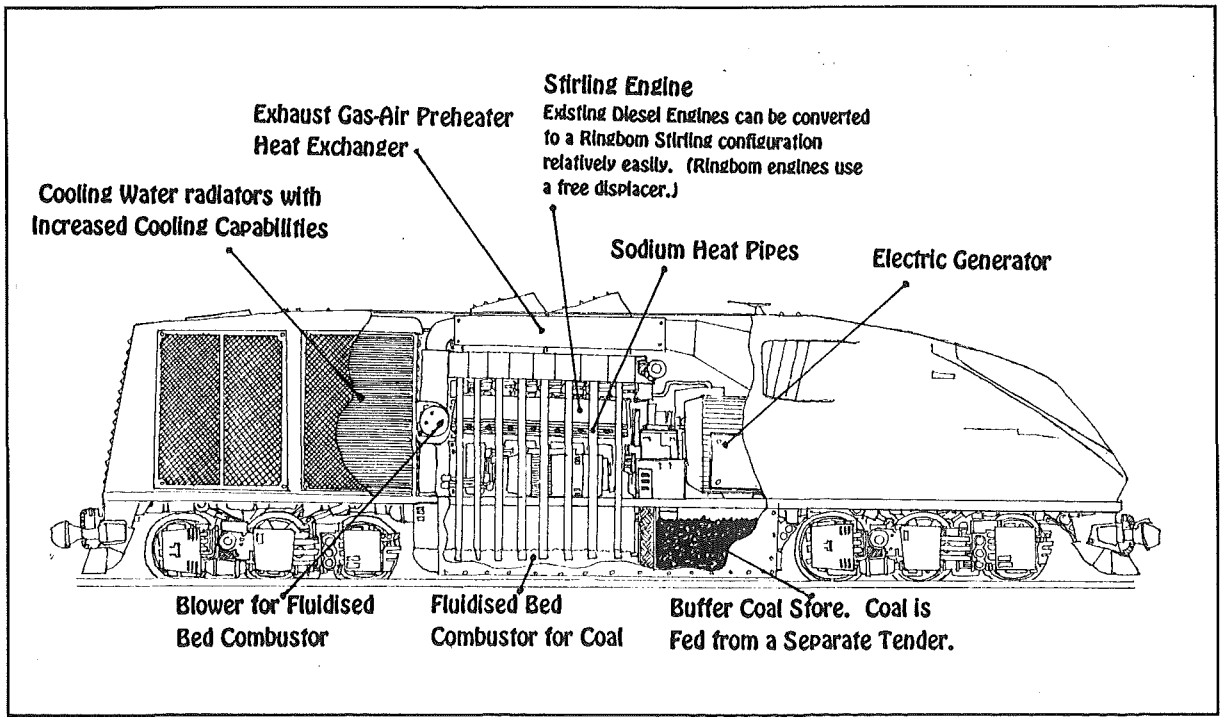

Figure 2.6 Stirling\Electric Hybrid locomotive burning coal in a fluidised bed combustor.

transported to large Stirling engines through heat pipes. In these cases, the Stirling engines drive an electric generator, and electric motor set, as in the series hybrid system, without the battery storage, and exactly the same as the existing Diesel-electric locomotives.

2.10 Cryogenic Cooling Engines

Nearly all Stirling cycle machines in production at present are for the cryogenics industry. The range of types here is as wide and varied as for the Stirling engine systems. Philips, the principle producers of Stirling cryocoolers, manufacture units with cooling abilities of fractions of a watt up to several kilowatts. The smaller sized coolers find considerable use in infrared night vision and missile guidance systems due to their small size, efficiency, being lightweight, and being cheaper than the other alternatives. The larger sizes are used in the production of large quantities of liquified gases. By the use of double expansion, these machines can achieve temperatures as low as 20K. Future developments with superconductors promise an even greater use of Stirling cycle machines. As yet, little has been done with the machines for the more moderate temperatures (100K and above). A rough test carried out in the 1950's found that the coefficient of performance of a Stirling cycle machine was less than the equivalent vapour compression cycle machine (Walker 1973) for temperatures greater than 230K. However the Stirling Cycle Machine used in the test had not been

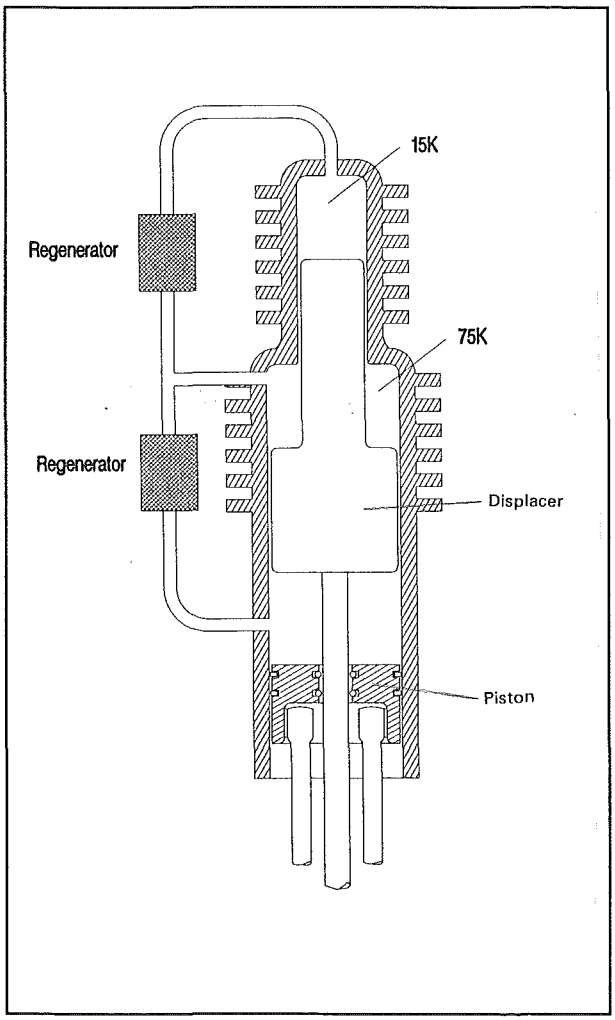

Figure 2.7 Multistage Stirling Cycle Cryocooler.

optimised for either performance or design.

An interesting extension to this application is the use of a Stirling engine to drive a Stirling cycle refrigeration machine (Walker 1986) and is known as the Duplex Stirling machine. The use envisaged is to liquify natural gas from wells which are remote from the pipelines. Some of the waste gas would be burnt to drive a Stirling engine which would be directly coupled to the Stirling cycle cooler.

2.11 Heat Pumping

There are two possibilities for the use of Stirling engines in this application;

1. A gas fired Stirling engine is used to drive a reversed Rankine cycle machine.

or 2. An electric motor is used to drive a reversed cycle Stirling engine thereby making it act as a refrigeration machine.

For efficiency of gas usage, the former is the better system because the waste heat from the Stirling engine can be added to the heating provided by the heat pump. The Stirling cycle machine acting as the heat pump itself has the advantage over the Rankine cycle machine in that its performance is less dependent on the temperature difference between the heat source and heat rejection (West 1986). This allows more heat to be extracted from the air than would be possible with the Rankine cycle machine.

2.12 Artificial Hearts

In the search for a total heart replacement, the Stirling engine is one of the few contenders that has managed to satisfy most of the requirements for an artificial heart system. The Stirling engine would provide power to a blood pump, its heat source either being a thermal storage device, or an alpha particle emitting radioisotope source (Alpha particles because they require less shielding than Beta or Gamma rays.) The Stirling engine's quality of being reliable and silent running are big bonuses in this application. In the early 1970's an experiment was carried out with the implanting of a radioisotope-fuelled Stirling powered artificial heart in a calf (Walker 1986).

3. STIRLING CYCLE ENGINES ON RENEWABLE RESOURCES

3.1 Introduction

This Chapter will take a deeper look at the use of renewable energy resources to drive Stirling engines that are in a stationary power generation application. The two resources that will be concentrated on are:

- Biomass
- Solar Heat

There are others which are of high interest, and are used, but to cover all of the possibilities would be outside of the scope of this thesis. However a brief mention will be made of some of the others available.

3.2 The Sun

Located at an average distance of 149 598 000km it is the nearest star to Earth. A yellow dwarf star with a diameter of 1 392 000km and a mass of 1.99×10^{30}kg, it is wholly unremarkable, and quite safe to live next door to for the next 6×10^{9} years, which is considerably longer than humans will be in existence. It is classified as a star of spectral class G2 and can be found in the middle of the main sequence of the Hertzsprung-Russel diagram Figure 3.1, a diagram used to group stars into types and their expected histories and futures.

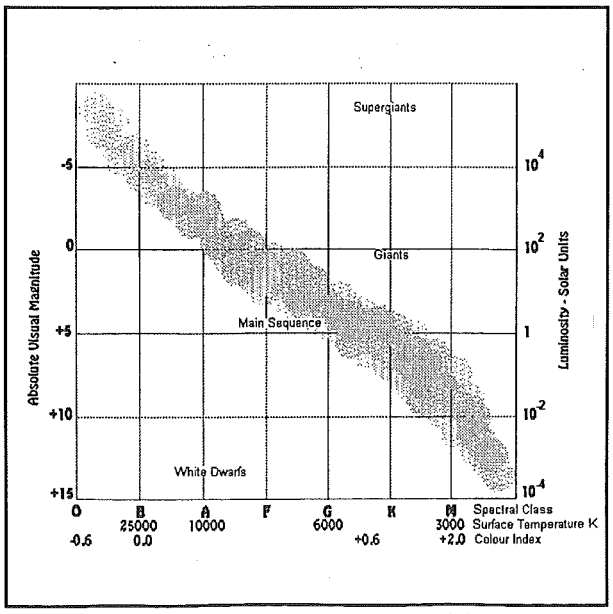

Figure 3.1 Hertzsprung-Russel Diagram

In the sun's core the pressures are so high (4.1×10^{16} Pa), that fusion reactions can occur between hydrogen atoms to form Helium. This reaction sees the conversion of mass into

energy[1] at a rate of 3.85×10^{26}W which corresponds to a mass of 4.7×10^{9} kg of matter every second, and produces temperatures near 14000000K within the core. The gamma radiation from this reaction begins to travel to the surface, intercepting atoms, being absorbed, and emitted many times. Finally after several hundred thousand years the much degraded energy reaches the sun's surface in the form of lower energy radiation such as infrared, and visible light. The energy flux passing through the sun's photosphere ("surface") is about 8kW/cm^2 where the temperature is about 5800K. Most of the energy disappears off out into deep space, but a tiny fraction of it, only 1 part in 2 200 000 000, reaches earth. Of this tiny amount, less than 75% of it gets to the planet's surface, through the atmosphere, without being reradiated back into space. Of the energy that reaches the Earth's surface, most is absorbed by the sea, where upon it causes evaporation and eventually rain. Temperature differences caused by the absorption of the sun's radiation in different regions of the land and sea, produce convection currents in the atmosphere. However neither of these renewable energy sources are much good for Stirling engines because they involve no temperature changes. Some of the Sun's energy, is absorbed by plant life. The plants store the energy within chemical bonds, and this energy can be released by burning (Biomass), or decomposition within the body of a living creature. Animal life when it processes any food, never extracts one hundred percent of the energy available within it, and so the waste from the animals is also very high in energy content. If a device is built to encourage anaerobic decay of the animal waste, a useful gas is given off, namely methane (Biogas).

The sunlight falling on the oceans causes layers of different temperatures to occur, because of the lack of vertical mixing that occurs within the ocean. Therefore a heat engine could be run between the different temperature layers.

A very insignificant proportion of the sunlight produced by the sun may fall into the concentrating collector array of a solar thermal power generation device. The radiation flux becomes concentrated and is able to create very high temperatures allowing the use of Stirling engines with very high efficiencies to generate power.

---

[1] Initially the energy is released as Gamma radiation and neutrinos.

Ultimately, all renewable energy resources are the direct or indirect conversion of the sun's radiation. Sunlight itself is, strictly, a non-renewable resource; however we are in no immediate danger of running out of it, nor can we control the sun to conserve its remaining fuel, so we may as well use it.

3.3 Solar Thermal Power

Solar Thermal Power generation involves the conversion of incoming solar radiation into heat which is then used by a heat engine to drive an electrical generator, and so photovoltaic cells do not fall within this category.

Outside of the Earth's atmosphere, the radiation flux is $1370 \pm 6 W/m^2$ with a variation of $\pm 3.4\%$ due to the elliptic nature of the Earth's orbit.[2] Of this, 8% is Ultraviolet radiation while 47% is in the visible light wavelength band, and the remaining 45% is Infrared (San Martin 1992). At the Earth's surface the flux incident on a horizontal surface varies with a peak at approximately $1 kW/m^2$ at midday with no cloud cover or atmospheric hazing. Over the course of a day, the amount of solar energy incident on the horizontal plane at sea level, will range up to $7 kWh/m^2$. At higher latitudes, the flux is less because of the much lower elevation of the sun position.

There are a number of other heat engines competing against the Stirling engine in this application. They are the Rankine cycle engines and the Brayton cycle engines (Gas Turbine). The different types are suited to different operating temperatures. Historically Rankine cycle engines have been used where heat sources at a lower temperature have been available. Using a lower temperature heat source they do not need very high sunlight concentrations, and it is possible to not use any concentration at all (M. Amor 1991). High concentrations are needed for the Stirling engine based generators, while very high temperatures and therefore concentrations are needed by the Brayton cycle engines. The temperature of the waste heat from the Brayton cycle engines makes them ideally suited to run in combination with a Rankine cycle engine to give a power generation system of very high efficiency. However this system is not suited to

---

[2] This figure is known as the Solar Constant.

supplying the needs of just one house, because of its high cost, high maintenance, and difficulty in controlling it. Therefore it will only be commercial sized solar thermal power stations that will have systems of this type.

For the isolated farm or village that only requires a few kilowatt-hours of electrical energy each day, a more realistic alternative exists in the Stirling engine based systems.

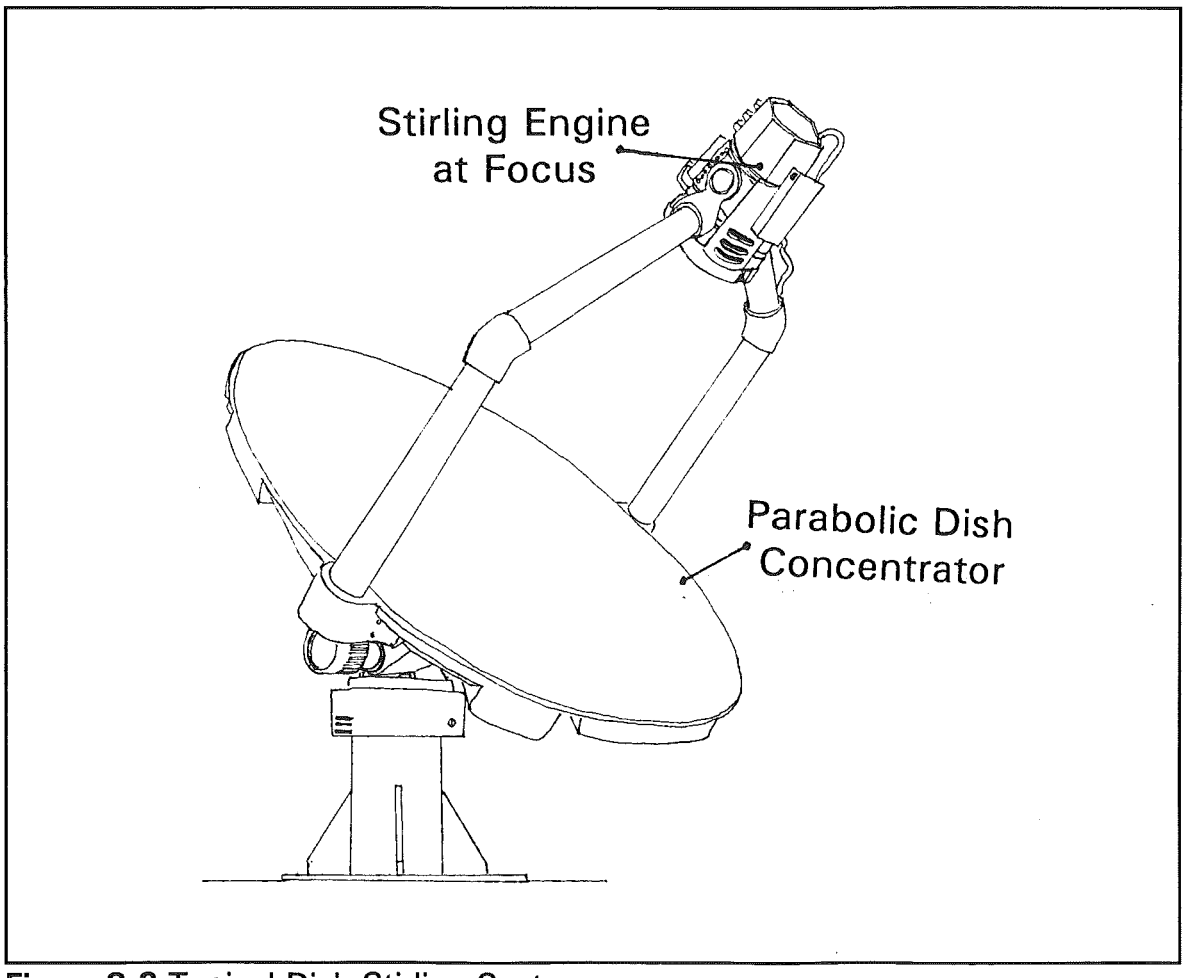

Figure 3.2 Typical Dish Stirling System

Two possibilities exist for the concentration of the solar radiation for the Stirling engine; Parabolic dish collectors (point focus), or parabolic trough collectors (line focus), refer to Figures 3.2 and 3.3. Most research into the field of solar Stirling power generation has been concerned with the use of point focus collectors with the Stirling engine situated at the focus. The reason for this is that the high

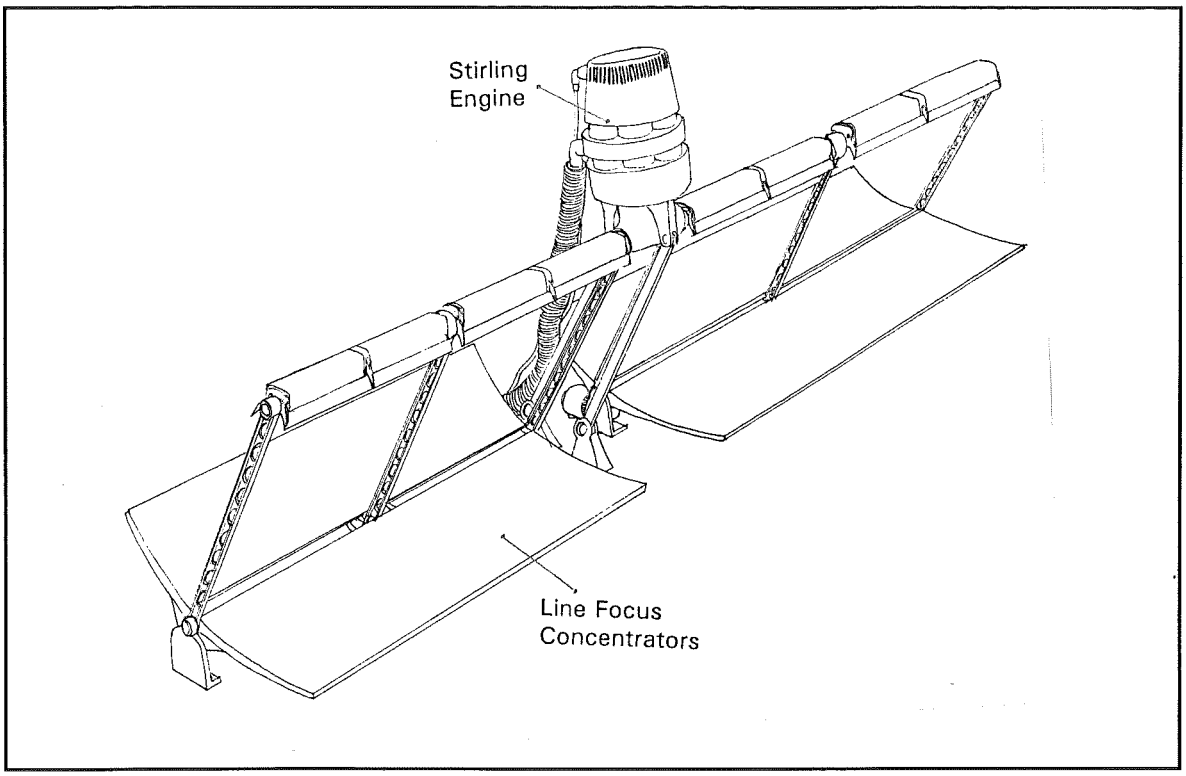

Figure 3.3 Line Focus Collector with Stirling Engine

temperatures achieved at the focus of the parabolic dish allow the Stirling engine to operate with a very high conversion efficiency which would not be achievable with the Rankine cycle or the Brayton\Rankine cycle combination outlined earlier on this small scale. A large number of solar dish/Stirling systems have been successfully run at sites all over the world, with very promising results, achieving mean daily efficiencies as high as 25%, and peak efficiencies exceeding 30% (Schiel 1993).

The methods for getting the heat into the working fluid are many and ingenious. Direct heating of the engine heater heads or heat exchange tubes is one of the methods regularly used on single cylinder engines. One particular arrangement had a quartz glass cylinder top so that the focal beam from the concentrator could get into the cylinder and heat a number of mesh layers within the cylinder (Isshiki *et al* 1989). The machine produced had the mesh layers built into the displacer, resulting in a lighter and simpler heat exchanger system, and claimed to have a lower dead volume than other methods. The collector system for this project was also quite ingenious in that instead of the engine being mounted out at the focus of the parabolic dish, it was mounted down behind the surface of the dish. To

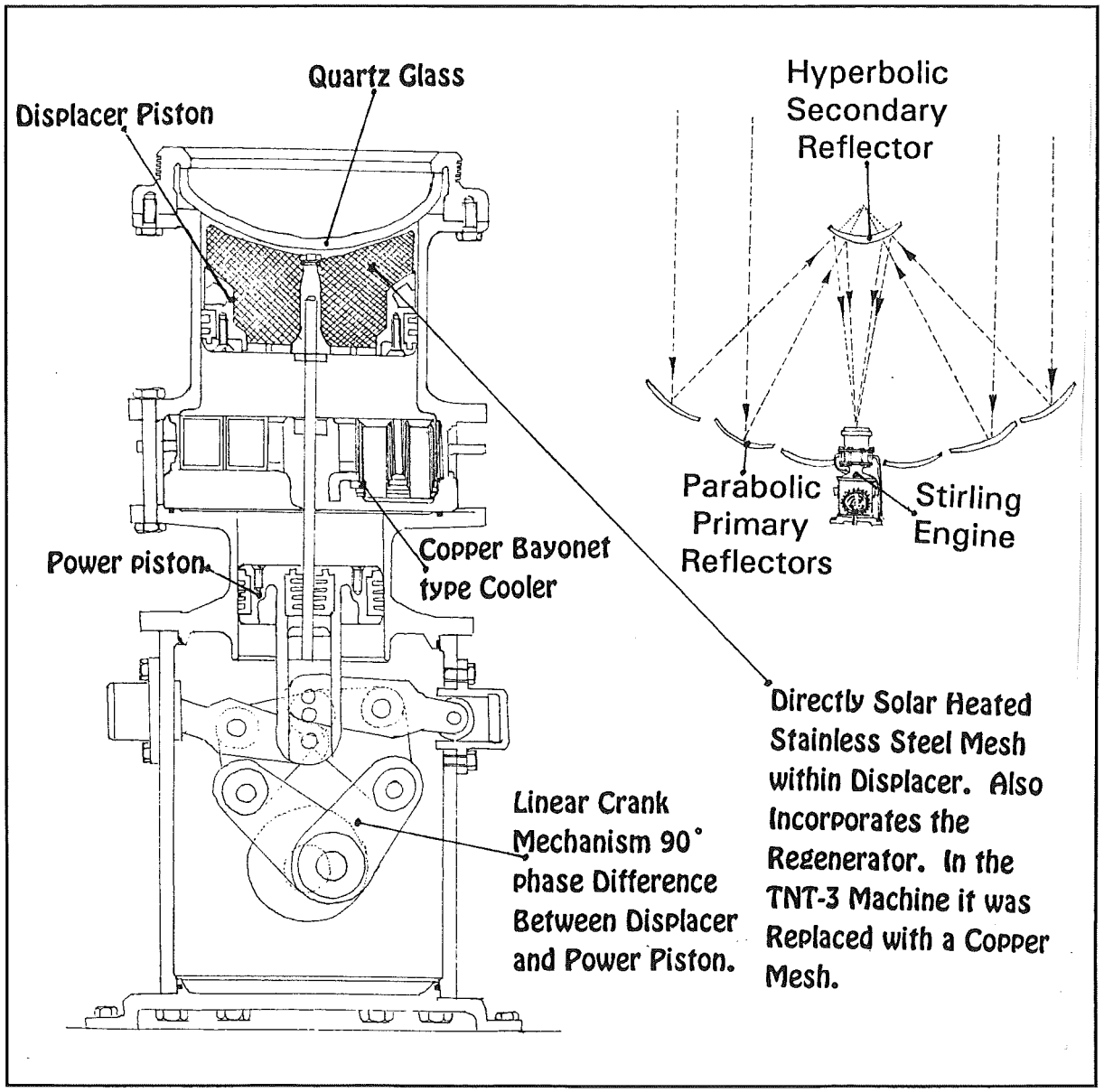

Figure 3.4 The TNT-1 solar Stirling engine (Isshiki *et al* 1989, Shishido *et al* 1993). Shown is the collector arrangement and a sketch of the internally heated Stirling engine.

reflect the radiation to the engine, a secondary reflector was placed at the parabolic dish focus. Shifting the Stirling engine from the parabolic dish focus made the system less prone to wind damage, and gave less rotational inertia for the servos to work against (Shishido 1993).

Other methods include the use of cavities into which the beam is passed. The inner walls of the cavity are lined with the heater tubes of the engine. This allows most configurations of engine to be run. There are however problems with the use

of direct solar heating of the heat exchangers, one of these is the occurrence of hot spots, which if too severe will cause the quick demise of the system. Allowing for hot-spots also means that if the hot spot is at the maximum permissable temperature, then the rest of the heater will be at a lower temperature and therefore the system will not be running at the high efficiency and power that it could run at if the entire heat exchanger were operating at the maximum temperature.

To get over this problem, indirect heating can be used. In this, a heat pipe is used (Figure 3.5). A heat pipe is a two phase heat transfer system where an evacuated space has a quantity of a fluid in it[3]. The fluid boils and the vapour travels to the cooler regions in the space, which are usually the heater tubes of the

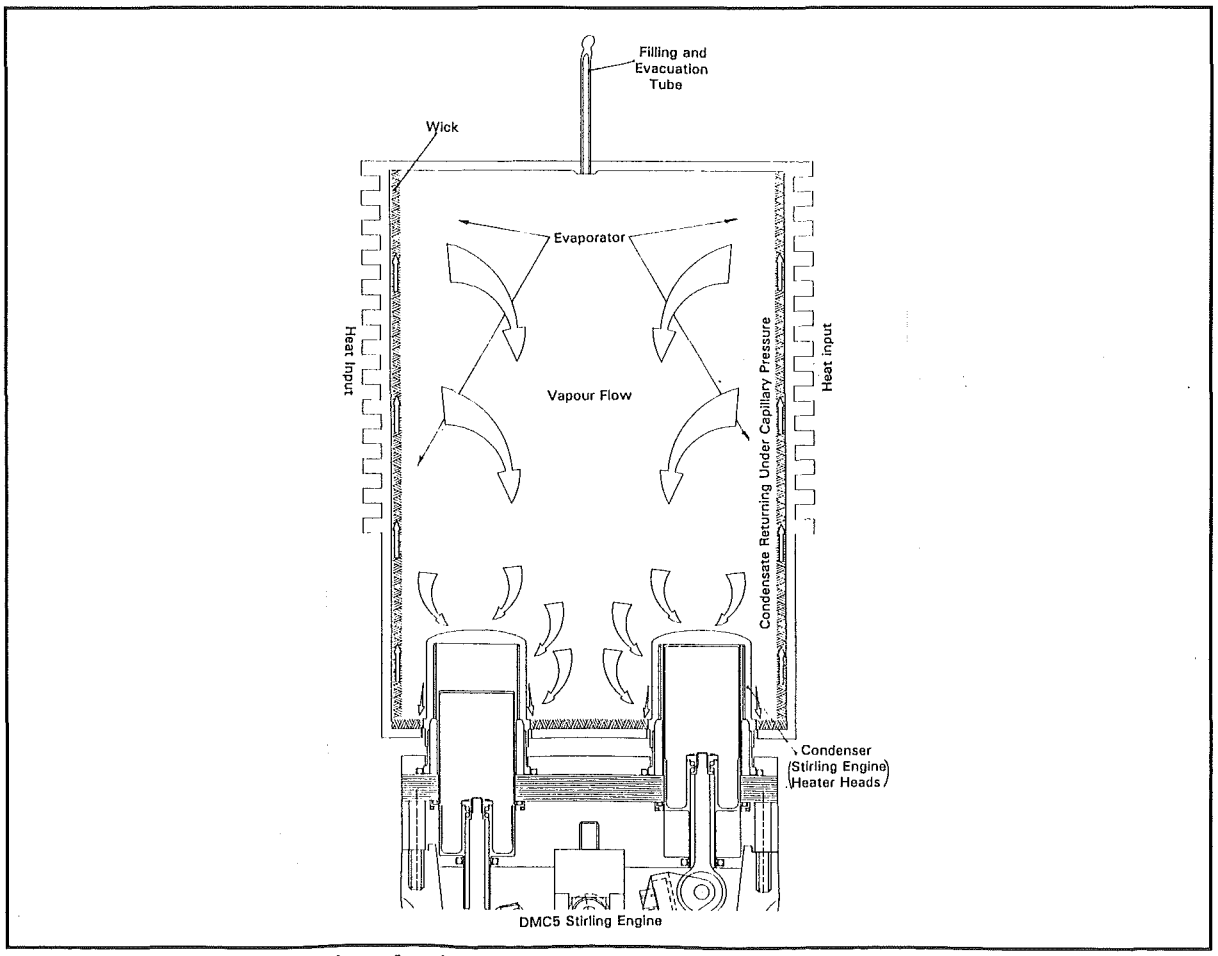

Figure 3.5 A Schematic of a heat pipe attached to a Stirling Engine.

[3] The working fluid normally used for this application is Sodium, or occasionally the NaK Eutectic heat transfer alloy.

Stirling engine, where it condenses giving up its considerable latent heat to the cooler heater tubes, or wall as the case may be. The liquid then travels back to the evaporator, through capillary action within a wick, or simply by the action of gravity. The features of a heat pipe that make them so useful are; that the heat transfer is nearly isothermal, they have an extremely high heat conductivity, they are lightweight, and can act as thermal transformers[4]. It is the quality of being almost isothermal that makes them so good for eliminating hot spots. Should a hot spot occur on the Stirling engine heater tubes, then no condensation will occur there, and so the spot will be allowed to cool to whatever the rest of the heat exchanger is. If a hot spot should appear in the evaporator section where the focus of the collector is, then preferential evaporation will take place at that point drawing away the extra heat, and transferring it to all the cooler parts of the pipe.

It is heat pipes that make line focus concentrators a possibility with the Stirling engine. The important feature here is the ability to transform the low heat flux along the focus, to the high heat flux at the heat exchanger of the Stirling engine. The alternative to this is the circulation of a single phase fluid which is run through a heat exchanger on the Stirling engine. This is similar to the system used by Rankine cycle solar power systems except that the fluid in that case is normally used to produce steam. The advantage in the use of the cylindrical concentrators is that they are cheaper to produce, and the control system is simpler as only one axis need be tracked. Because of the high temperatures needed for the Stirling engine to make it viable against the Rankine cycle engines, it is necessary to use high solar concentrations with the parabolic trough collectors which means that tracking does need to occur with a system that will adjust every two or three minutes to the new sun position. To achieve the high concentrations which are approaching the practical maximum possible with line focus concentrators, it is necessary to employ a relatively new type of reflector called the non-imaging reflector (These will be looked at in more depth in Chapter 5).

---

[4] A thermal transformer means that it can take a low heat flux input over a large area, and transfer the heat to a small region and a high heat flux, and visa versa.

3.4 Ocean Thermal Energy Conversion (OTEC)

First suggested in 1881 by A.d'Arsonval, this scheme uses the difference in temperature between the heated upper layers of the ocean and the colder deeper layers. It relies on a heat engine operating between the temperature difference, with water being pumped up from depths of around 1500m. However the temperature difference being operated on is very small and so is not very suitable for the operation of Stirling engines. The OTEC's that have been built so far have produced up to 1000kW (San Martin 1992) using ammonia in a closed Rankine cycle machine.

3.5 Biomass

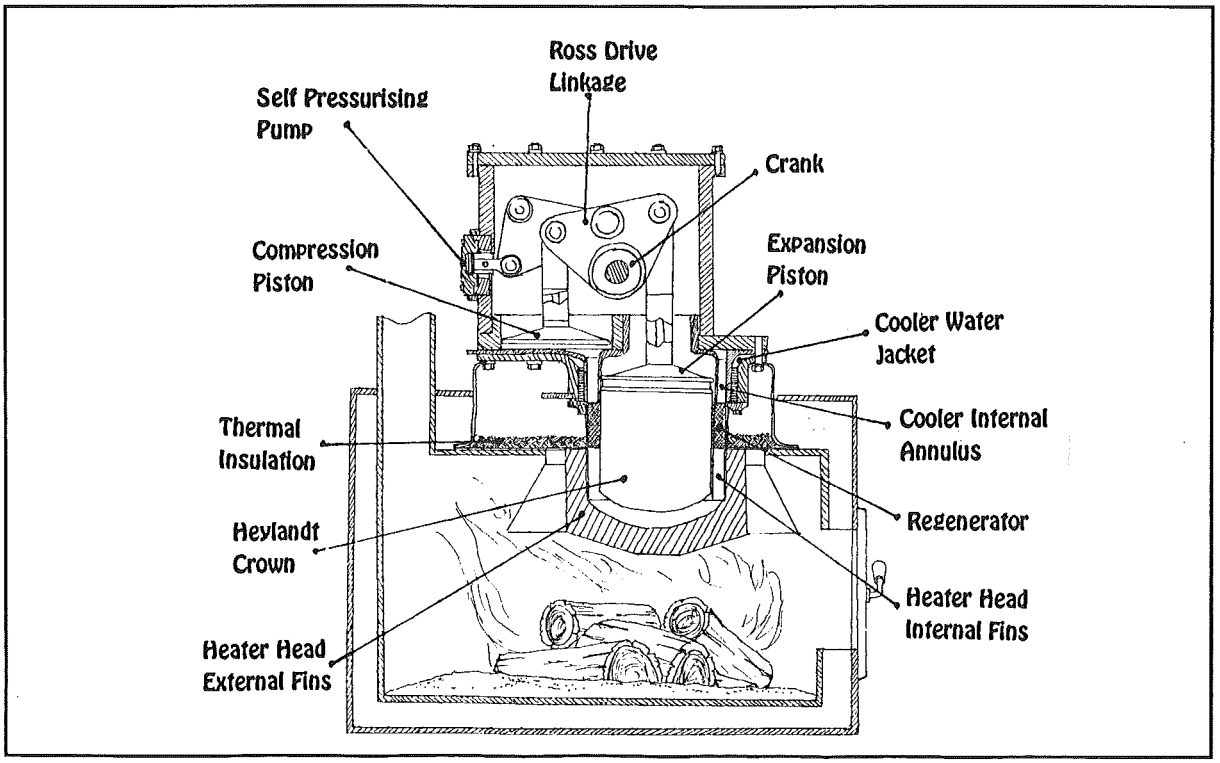

Figure 3.6 3kW Wood-Fired Air-Charged Ross-Stirling Engine (Atkins *et al* 1990)

Biomass covers the range of energy sources where solar energy has been stored within biological systems, be it plant matter or animal waste. Recovery of the energy can be achieved in various forms; Direct burning, gasification, or digestion. The production of biogas is through the digestion of biomass (normally waste) and will be covered briefly in section 3.6.

The gasification of biomass is about 80% efficient and involves the introduction

of air to the biomass to produce a nitrogen rich low calorific value gas as well as heat from the reactions of oxygen with the biomass. This low calorific value gas is what is burned for the production of useful power. Other methods of gasification of biomass use pure oxygen to react with the biomass to give off synthesis gas which is a mixture of carbon monoxide and hydrogen. Methanol can also be produced from various of the gasification methods.

The form of most interest is the direct combustion of biomass, especially in the form of wood logs, wood chips, waste paper briquettes, and waste from grain production. A number of Stirling engine based systems have been built and tested to use biomass for the production of power. They range from the humble rice husk burners (Lockwood 1984) in third world countries to small electric power generators attached to a domestic wood burner (Atkins 1990).

In the domestic situation the quietness, low maintenance, relative cheapness, and the fact that the heat rejected by the heat engine may be put into the domestic hot water supply, makes the Stirling engine the ideal choice. The amount of heat rejected is quite large in normal use, and will be more than enough to meet the hot water demands of an average family[5] (Refer to Chapters 4 and 5). It will be seen that an average house will need a 1.5kW$_e$ engine to supply their electricity demand, if there is battery storage used to cater for peak loads, and a power management system in place, providing the heat rejected from the stirling engine goes into the hot water system. The 3kW unit proposed by Atkins will be large enough to supply even the peak loads and would not need any electricity storage ability, but this means that the engine will not be operating at its peak performance for most of the time and will require a very large burner running at full power.

Wood has a much lower heating value than fossil fuels, being only about 20MJ/kg when dry (less when wet) compared with 48MJ/kg for petroleum, and 31MJ/kg for coal (San Martin 1992). This means that the temperatures available within a biomass combustor are generally lower than those for a fossil fuel burner.

---

[5] This 1.5kW value is the average power consumption of an average New Zealand family and so does not take into account the peak loads. The figure is for power use without an energy management system or the use of high efficiency components such as heat pumps and fluorescent lights. It does however ignore the load due to water heating, as this would be adequately serviced by the engine cooling, and also some of the space heating load as the log burner will be able to cater for most of this.

Great care must be taken in the design of the combustor and Stirling engine heater so as to minimise the losses up the flue and to keep the temperature drop between the combustion gases and the Stirling engine working fluid to a minimum.

Air preheating is desirable in trying to design an efficient small scale co-generation unit such as the one about to be described. This would reduce the flue losses considerably as well as aid combustion. One danger of extracting heat from the flue gases is the problem of taking too much heat out. Dropping the temperature below 150°C will allow some of the gaseous combustion products to condense within the flue. These products are chemicals such as water, and creosote which will deposit themselves on the flue wall and cause corrosion.

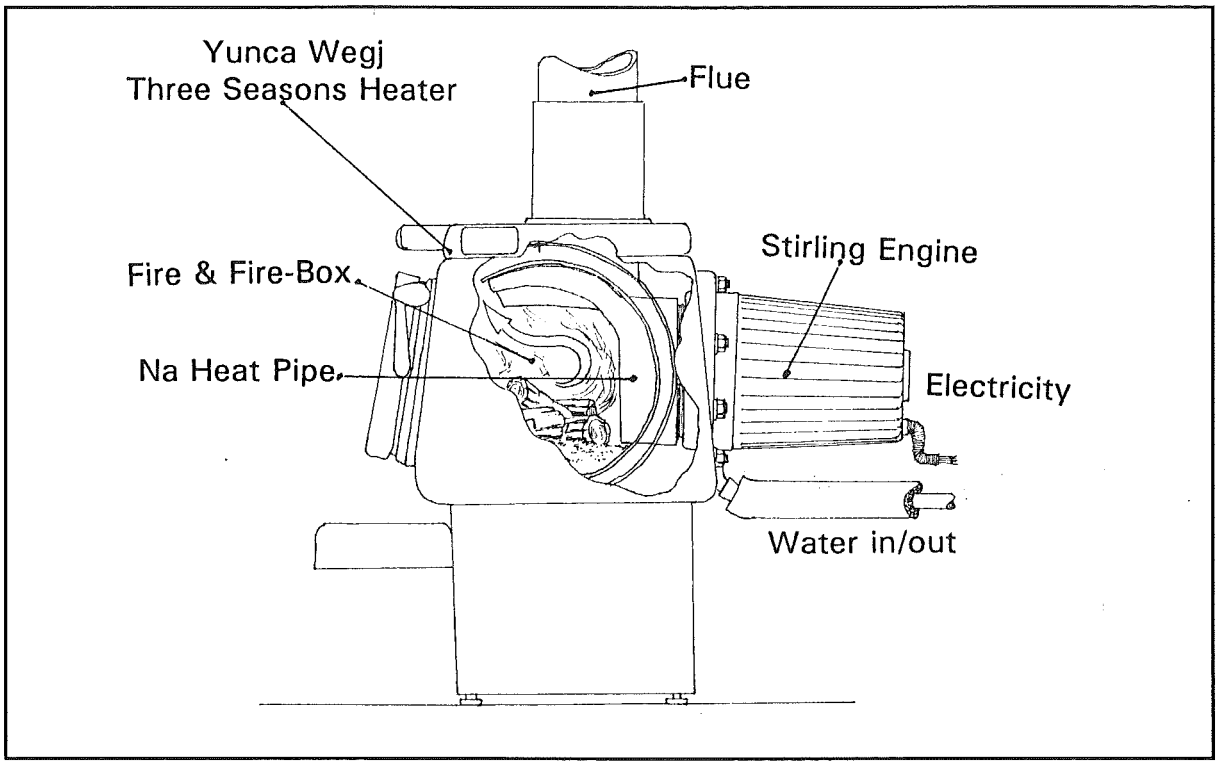

Figure 3.7 An impression of the Co-generation unit based on the scaled up DMC5 Stirling engine, fixed onto a commercial wood burner.

A proposal to produce a co-generation unit based around a commercial log burner and a scaled up DMC5 Stirling engine (Clucas 1993), was investigated in the course of this thesis (Figure 3.7). It was to use battery storage to allow for a slower burning of the fire and make for a more compact unit that could be more easily incorporated into a house. With approximately half the electricity load of a house due to water heating, the total power needing to be generated as electricity

would be greatly reduced by using the Stirling engine cold end heat exchanger as a water heater. Because of the lack of combustion in the engine, the water would remain clean despite multiple passes through the heat exchanger in the course of a day. Using batteries does however cause the problem of reducing the overall efficiency due to the charge-discharge efficiency being about 60%. As indicated in section 2.5, by designing for an average power, and having battery storage, the engine designed will be much smaller as it does not need to meet the peak demands. The batteries were decided to be deep cycle lead-acid batteries because they have a very good charge capacity and, though slow to charge, have a very good current output thereby being able to easily meet the peak power demands expected. For a domestic supply with an average demand of 6.4kWh/day, it would be necessary to have an engine with a power output of 1.5kW_e .

From the manufacturer's data available, commercial log burners can produce heat outputs up to 20kW with an efficiency 60-75%. For normal operation, a wood burner produces out about 7kW. This means that about 4kW of heat are being lost up the flue. It is possible to recover this energy by passing the flue gases over a heat exchanger to transfer the heat to a Stirling engine; however, the problems associated with the dew point become significant while the heat transfer is less efficient due to the lower temperatures. Better performance can be obtained by inserting the Stirling engine heat exchangers into the fire box itself, and gaining good heat transfer from the direct impinging of flames on its surface. Greater efficiency can be achieved by passing the flue gases through a heat exchanger with the heat being used to preheat the incoming air. This second arrangement has the disadvantage of needing to custom modify the burner to take the engine. This second arrangement was the one decided on for the brief investigation carried out in the course of this thesis.

Using simple component efficiencies, the requirements from the engine and heater can be determined.

The average New Zealand household uses 7570kWh annually (Wright 1986). Of this approximately 4000kWh/yr goes into water heating. Electricity savings of about 1250kWh/yr can be achieved through the use of solid fuel burners for space

heating. This then leaves an electrical load of about 2320kWh/yr to be supplied by the co-generation plant, as the domestic water heating can be met by the Stirling engine heat rejection. If this figure is averaged over an entire year, the generation that must be achieved each day is about 6.4kWh. It is reasonable to assume that the owners of the cogeneration system would be able to run the burner for about six hours every day without it interfering with their normal activities.

Electrical load seen at battery terminals	6kWh/day
Load seen at alternator terminals if charge/discharge efficiency is taken to be 60%	10kWh/day
If 6hrs of generation occurs each day then the average load seen at the alternator terminals is	1.67kW ≃ 1.5kW
With a typical alternator efficiency of 60%[6] the mechanical power of the Stirling engine must be	2.5kW

The typical temperature to be found in a wood burner is about 600°C to about 1000°C. Given that the burner will be burning quite hot, with preheated air, the Stirling engine heater head temperature will be taken as 750°C. Domestic hot water supplies are recommended to be no more than 55°C, and so the assumption will be made that the gas temperature in the compression space of the Stirling engine will be about 60°C. With these values, an estimate of the Stirling engine efficiency can be made using a Carnot efficiency with a scaling factor (3.1).

$$\eta_{stirling} = 0.4 \times \left(1 - \frac{T_C}{T_H}\right) \qquad (3.1)$$

Where $\eta_{Stirling}$ is the thermal efficiency
T_H is the peak temperature in the hot space (1023K)
T_C is the temperature in the cold space (333K)

The 0.4 factor allows the ideal stirling efficiency expression to approximate that expected in a real Stirling engine.

Substituting these values into the expression yields a conversion efficiency 0.2. Thus 20% of the heat entering the heater head is converted to mechanical energy.

---

[6] This value is conservative, and alternators of this size with efficiencies greater than 80% are available.

The remainder is rejected into the domestic hot water system and lost through radiation from the engine block. If the mechanical power produced is 2.5kW, then the heat input to the Stirling engine is 12.5kW and must come from the log burner. Catalogues claim that a normal log burner will produce about 14kW at full power, which means that to run this system quite a large burner would be needed so as not to reduce the life of the firebox by long term operation at its maximum condition. Of the 12.5kW entering the Stirling engine, approximately 10kW would be rejected into the domestic hot water supply. If the system is generating for 6hrs every day, this is 60kWh of hot water where the average house only requires 11kWh/day. It is conceivable that further power savings can be achieved by using the hot water as space heating, and by using the hot water tap to fill jugs, and pots when boiling water is needed.

The critical part of this system would be the hot end heat exchanger. It would have to be designed very carefully to ensure that most of the heat produced in the firebox could be captured by the engine, and also that the burner would still supply some space heating. Therefore the placement and shape of the heat exchanger would be of the utmost importance.

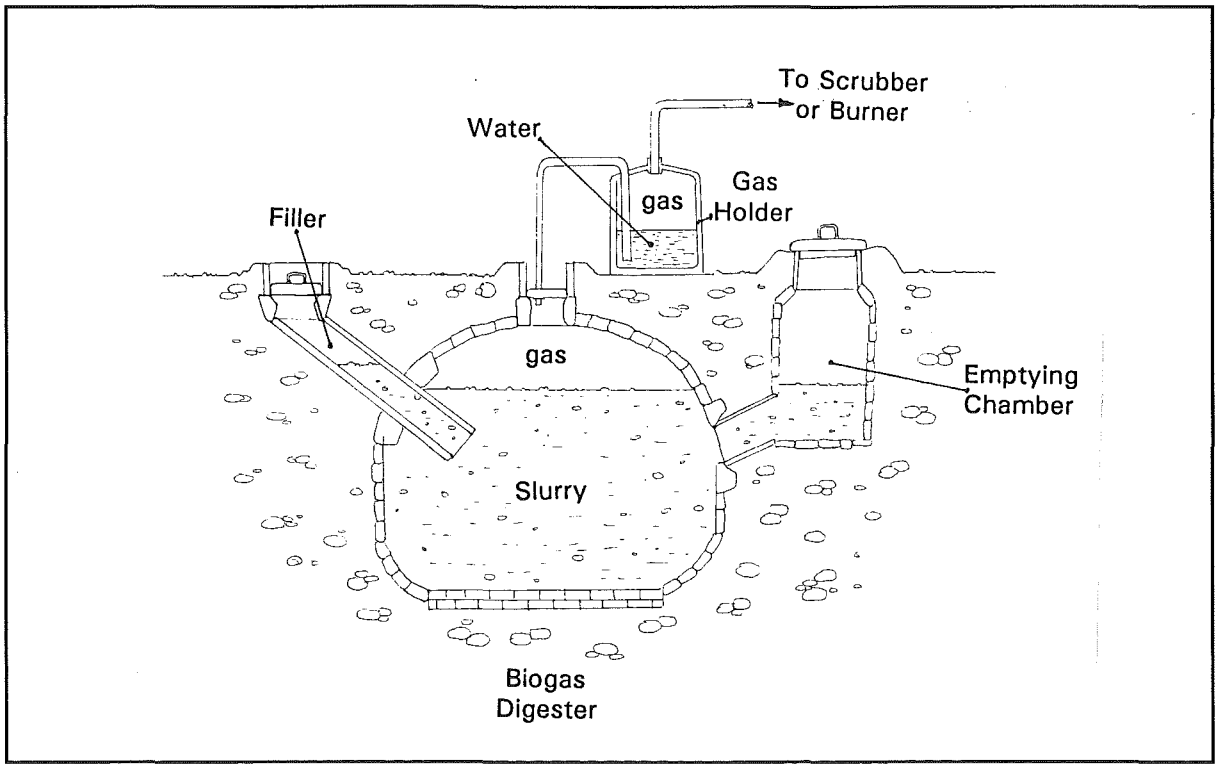

Figure 3.8 Rural biogas digester

3.6 Biogas

There are very large possibilities for this source of renewable energy, in that the scale and use of the units is very wide. Vehicles running on biogas have been around for some time now. These use the internal combustion engine and require scrubbed[7] biogas. The advantage of the Stirling engine operating on biogas is that it does not need the gas to be cleaned or processed in any way before it is used. The best use of the biogas Stirling system is in cogeneration systems for farms, and the small power stations working on the gas produced by municipal waste ie. sewerage, and dump sites. The chief competition here comes from the gas turbine and steam turbine generation systems.

The key component in this system is the digester (Figure 3.8) within which the waste (biomass waste such as dung, food scraps, reject fruit etc.) is broken down anaerobically by bacteria to produce a mixture of carbon dioxide and 50-70% methane. A large number of these already exist in China and India providing methane for lighting, cooking, water heating, and running engines. Generally the scale of these is large, catering for a small community rather than individual households (Perlack 1990). With a number of these digesters in existence already it would be relatively easy to introduce Stirling technology to these countries.

3.7 Geothermal Power

This is not really a renewable energy source, but then neither is the sun. When the earth was formed from the disc of dust and gas surrounding the sun, it was very hot and molten. Over many millions of years, it cooled down and formed a crust, upon which life was able to establish itself. The earth is still cooling and still has a molten interior only a few tens of kilometres below the surface (35-40km under the surface of the land masses, 60-70km thick under mountains, and only 6km thick under the oceans (Currie 1989)). In places the crust has been broken and cracked, allowing the molten rock (magma) to come close to the surface or to burst out onto the surface. Water reaching the magma is heated and when it gets to the surface will form hot pools, geysers, and steam vents. It is these that can

---

[7] Scrubbing is the process where CO_2 is removed from the biogas so that the remainder is predominantly methane.

realistically be used to generate useful energy, as the reliability, and safety in trying to harness a volcano's energy directly are questionable. New Zealand utilises its geothermal energy for electricity production with a steam turbine power station. It is possible to run a Stirling engine on geothermal energy but the temperatures involved are generally low, and so best suited to the steam turbines.

4. DOMESTIC POWER CONSUMPTION

4.1 Introduction

In this chapter we will briefly investigate the power consumption in an average New Zealand household. Special attention will go to the miscellaneous demands, that will make up most of the electrical load that the Stirling engine will experience.

New Zealanders are by no means energy efficient, and tend to waste a large amount by leaving lights on, heating larger areas than are needed, driving a car instead of using public transport or cycling. They therefore follow trends in the rest of the western world. The values presented here will be a low estimate for the developed countries because of New Zealand's mild climate.

4.2 Average Annual Values

The energy consumption for the country as a whole in 1984-1985 was 32.4PJ (Wright 1986), a figure which includes the power used in the commercial sector. In 1985 there were 1 188 700 domestic consumers of which 1 099 800 were households that were occupied for most of the year.

In 1985, the average domestic user in New Zealand used 7570kWh for the year, where the average domestic user was a household of 3 people. Water heating by electricity along accounts for a huge 4003kWh/yr. With such a large proportion of electricity going into the production of hot water, there are good reasons for trying to reduce this value by the use of better insulation of the hot water cylinders, use of a heat-pump, solar panels, a wet-back for a fire, or a hot water heater that heats the water only when it is required. With the Stirling engine based systems, heat rejected from the cycle can be dumped into a domestic water supply without fouling it with oil or combustion products. As will be seen in Chapter 6, the thermal efficiency of the Stirling Engine involved in this project is not very high, due to the low hot-end temperature. This means that for a given amount of mechanical work out, a much larger proportion of the heat entering the cycle must be dumped as a low-grade heat into a reservoir, in this case the

domestic hot water supply. The energy dumped in this case is of the order of 60kWh/day when the average house hold requires only 11kWh/day. This opens the possibilities of further electricity savings in that the extra heat would have to be disposed of in some way. Therefore it is conceivable to use the hot water supply for space heating, and to save electricity by filling hot water jugs and pots directly from the hot tap.

Annual total domestic electricity usage for a single household	7570kWh
Annual hot water heating electricity usage	4003kWh
Annual miscellaneous electricity demand is therefore	3567kWh

The figure for the miscellaneous electricity usage does not include savings achieved by the use of the hot water for space heating, as this option may not be followed by the user, and they may still use electric heaters despite the extra space heating provided by the hot water system.

It is interesting to note the reduction in energy usage over time. In 1980 electricity usage was about 30.44kWh/day (Peet 1982). With the increased occurrence of high efficiency appliances such as microwaves, and a higher rate of unemployment meaning less people with high power consuming devices such as power tools and dish washers, the power consumption steadily declined (Possibly people are tougher now than they used to be). The figure in 1985 was:

$$\frac{7570 kWh/yr}{365 days/yr} = 20.7 kWh/day$$

a saving of almost a third. Because of their availability, it is the 1986 figures which have been used. The power demand will have dropped a little more because of some of the recent hydro-lake water shortages enforcing power conservation, and the increased push by some of the electricity companies for greater use of hot water cylinder insulation, and more efficient lighting. As has been suggested already, with a power management system the power demand could be further reduced.

4.3 Component Breakdown of Power Demand

The following section will look at the components involved in a household and the amount of energy they use. The figures will not add up to the average figure above because not all houses have all of the components mentioned here. Data was for the year 1985 and was found in Wright (1986). Identifying the appliances and their component of the total power usage will help high-light potential areas for energy savings.

4.3.1 Appliance Frequency

Not all of the appliances will be found in every house, and so a probability of finding them in a given house has been presented here (Table 4.1), with the probability expressed as a percentage of households.

Table 4.1 Appliance Frequency

Refrigerator	98%	Electric Frying Pan	75%
Freezer (separate)	73%	Toaster	90%
Clothes-dryer	50%	Electric Kettle	92%
Dishwasher	15%	Iron	100%
Colour Television	85%	Vacuum Cleaner	100%
Washing Machine	96%	Lighting	100%

4.3.2 Appliances and Their Power Usage

The figures below are directly from Wright 1986 and are annual values.

WATER HEATING

If all water heating is achieved by electricity alone, then the annual power consumption is 4003kWh per household. In the South Island, if a wet back is installed on the solid fuel burner, then the electricity consumed is only 2950kWh per year per household.

ELECTRIC COOKING

This covers only the household ovens and stoves, and does not include appliances such as toasters, waffle makers, etc.

A typical oven is rated at 3.5kW while each cook-top element has a mean value of 1.2kW. In general 2 elements are running at any given time. The elements of an oven are controlled by a thermostat, and so are not on all the time that an oven is running. Therefore a fraction of in-use time that this maximum power is drawn can be defined. In the case of the oven it is 0.25 and for the cook-top it is 0.5

Microwaves are an efficient way to cook, without as much waste heat as a conventional oven. Microwaves are generally 1.3kW and draw this power for 0.5 of the time that they are operating. For electric frying pans, the power is generally 1.2kW and the fraction of in-use time that they pull the full power is also 0.5.

The power consumption due to cooking is summarised below in Table 4.2.

Table 4.2 Electric Cooking Annual Power Consumption

Cooking Facility	Mean use Time minutes/week	Estimated Energy Consumption kWh/year
Oven	230	174
Elements	296	308
Total for Range		482 kWh/year
Microwave	15	9
Electric Frying Pan	34	18

OTHER KITCHEN APPLIANCES

The figures (Table 4.3) here include the fraction of in-use time at full power and has been called the rating factor.

Table 4.3 Other Kitchen Appliances Annual Power Consumption

Appliance	Mean use Time (minutes/week)	Typical Power (W)	Rating Factor	Calc. Energy Consumption (kWh/yr)
Electric Kettle	80	1500	1.0	104
Toaster	36	900	1.0	28
Crockpot	15	150	0.25	0.5

FOOD STORAGE

There are various combinations of refrigerators and freezers available on the market and so variation exists in the power consumption of a household where food storage is concerned. The following values are annual power consumption figures.

Refrigerator only	340 kWh/yr
Refrigerator/Freezer units	615 kWh/yr
Separate Freezer	470 kWh/yr

LIGHTING

Incandescent lights are very inefficient (10%) and fluorescent lighting could be substituted to save a large amount of electricity, but in 1985 only 5% of residences had fluorescent lighting, a figure which will not be much different now due to the high initial cost of the fluorescent bulbs.

The values here are again given as an overall annual power consumption value.

Kitchen Lighting	275 kWh/yr
Living Space Lighting	240 kWh/yr
Remaining Household Lights	185 kWh/yr
Total Lighting	700 kWh/yr

MISCELLANEOUS APPLIANCES

The figures given here are estimates of the total power consumption for one year.

Dishwasher	500 kWh/yr - 1 cycle per day
Washing Machine	55 kWh/yr - 5 cycles per week with 0.2 kWh/cycle
Clothes Dryer	605 kWh/yr - 4 kWh/cycle
Colour Television	240 kWh/yr - 5hrs a day
Video Recorder	22 kWh/yr - 2hrs per day at 30W
Iron	50 kWh/yr - (obviously not a student flat!)
Vacuum Cleaner	60 kWh/yr
Misc.	40 kWh/yr

SPACE HEATING

This is another major user of electricity, and is very dependent on the climate, and the preferences of the household. The value is also influenced by the use of solid fuels.

On electricity alone it may be up to 3740kWh/yr in Christchurch (for people liking a very warm dwelling), and 1190 kWh/yr in Auckland. With the use of solid fuels the electricity consumption reduces to about 2490kWh/yr for the people living in Christchurch, and only 790 kWh/yr for Auckland.

4.4 A More Efficient Home

There are many ways in which New Zealand households can be made more energy efficient. New homes now have good insulation in the walls which creates considerable savings with regard to space heating, but a number of other points can be targeted. For electric water heating, a large amount of energy is lost through the cylinder walls and the pipes; this could be reduced with insulation, thereby saving up to 13% of the energy input to the cylinder. Good maintenance of the hot water system fittings will also make for significant savings. For instance, a dripping tap can cause up to 1.5kWh/day loss of energy. Employing a heat pump to heat the water is another way of improving the energy efficiency of the hot water system as the energy saved may be as much as 1990 kWh/yr. However, as the system in this project is going to be generating up to 6 times the amount of hot water needed, the problems of conserving the heat in the hot water system are of little importance, and it would be beneficial to encourage the heat to leave the system so that the engine will operate with a reasonable efficiency, and not over-heat.

Lighting is another suitable target for considerable power savings because of the extremely poor efficiency of the incandescent light bulb. For example a 25W fluorescent bulb or tube will replace a 100W incandescent bulb. Therefore if all of the incandescent bulbs in a residence were to be replaced by fluorescent lights, the 700kWh/yr quoted in 4.3.2 would be reduced to a mere 175kWh/yr.

Cooking is another large user of electricity, and can be made more efficient by the increased use of microwave ovens. It the microwave were to totally replace the conventional oven[1] the total consumption would be only 361kW/yr as opposed to the 600kWh/yr if only a range were used. Generally the use of a microwave oven saves the household about 187kWh/yr in electricity.

Changes in the habits of people to save more electricity such as turning off

---

[1] For most consumers this is not an attractive option. An alternative is to down size the conventional oven, as a smaller volume is more efficient, as well as being quicker to heat up.

lights, and having showers instead of baths, are much harder to implement, but the possibility exists.

5. SOLAR-STIRLING CONFIGURATION

5.1 Introduction

In this chapter, the concept design of the solar-Stirling system for this thesis will be discussed. The niche being targeted with this project was the supply of electricity to remote farms. This meant that the area that the device covered would not be so restricted, and the technology had to be simple and reliable.

The question of the type of heat engine to use for this project was decided from the outset as being a Stirling engine, simply for the fact that this was the field that the author wanted to work in. However with the configuration chosen, the use of a Rankine cycle machine could have worked equally well, possibly better.

5.2 Point or Line Focus

The first step in the concept design was the determination of the overall form of the system. There were two options: the dish or point-focus collector, and the trough or line-focus collector.

A considerable amount of research and development has already gone into the Dish-Stirling systems with a number of successful plants operating around the world. The power output from these devices is typically in the range 5-25kW. Because of the high temperatures attained by the point focus concentrators the system efficiency is very high (About 30% thermal input to electrical output (Schiel 1993)). However, as discussed in the previous chapter, the power needed from the project in this system is only 3567kWh/yr which is roughly 1.4kW$_e$ if generating occurs for about 7hrs per day (Based on data from Western 1990 and Ross 1992). Point focus dish concentrators are quite expensive to produce because of the complex shape and the accuracy to which the optical components must be built. In addition to this, sophisticated tracking devices must also be provided to allow the high sunlight concentration possible to be attained. Therefore a point focus system to provide only 1.4kW$_e$ would be prohibitively expensive. An estimate of some of the specifications of a Dish Stirling system to fulfil the demands placed on it by an isolated farm, are listed below in Table 5.1.

TABLE 5.1
Dish-Stirling Basic Specifications

Electrical Power output from batteries	1.4 kW_e
Overall System efficiency (Including batteries)	10%
Solar to Electrical efficiency (No Storage)	17%
Concentration ratio	2412
Rim Angle	30°
Acceptance Half Angle (related to the Sun Half Angle)[1]	1°
Absorber Temperature (Insolation 600W/m²)	1583 K
Collector Diameter	5.5 m

The concentration used in the above example is far below the maximum attainable (x45000), but the use of the 1° acceptance half angle allows the system to continue working well even if there is some atmospheric diffusion occurring.

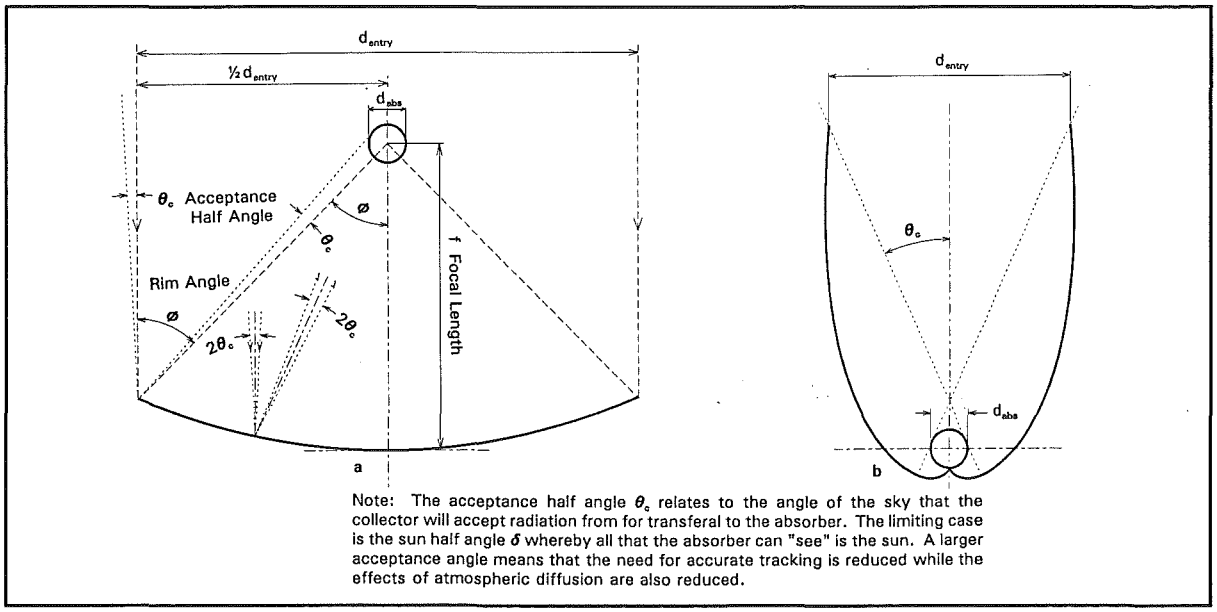

Note: The acceptance half angle θ_c relates to the angle of the sky that the collector will accept radiation from for transferal to the absorber. The limiting case is the sun half angle δ whereby all that the absorber can "see" is the sun. A larger acceptance angle means that the need for accurate tracking is reduced while the effects of atmospheric diffusion are also reduced.

Figure 5.1 Nomenclature used in solar concentrator equations (both dish and trough). (a) is the simple parabolic concentrator (SPC), and (b) the compound parabolic concentrator (CPC).

A considerable advantage of the point focus collectors is that because they can focus the solar insolation onto a smaller area due to their very high concentration ratios, the losses due to reradiation, and conduction-convection to the surroundings

[1] The sun half angle is half the angle of view that the sun covers. The sun ordinarily covers 0.54° of the sky, thus a sun half angle $\delta = 0.27°$. By using a larger angle (acceptance half angle) in the calculations, the maximum concentration possible is lowered, but the effects of atmospheric hazing, diffusion of the sunlight, and tracking errors, are reduced.

are reduced, thereby increasing the overall efficiency.

Line focus concentrators are also produced commercially and used in large solar power stations, and domestic solar water heating, but these are generally either low concentration, or fitted to steam turbine boilers. Because of the lower temperatures involved, the materials involved in the manufacture of the line-focus systems are cheaper and the processes used are cheaper due to the complex shape only being in one direction. Within the line focus type of concentrators, there are two distinct families: Imaging, and non-imaging. The definition of an imaging concentrator is one that will produce an image at its focus of the light sources situated at a large distance from it. Simple parabolic dishes, simple parabolic troughs, and lens based concentrators (albeit a little distorted in the case of the line focus systems) are capable of this. However the need to form an image limits the size of the area that an imaging concentrator can concentrate the light down to. In the case of solar power, the sun's half angle is the limiting factor due to the laws of thermodynamics (as explained in Section 5.2.1).

To avoid the limit imposed by forming an image at the focus, another type of reflectors known as non-imaging concentrators, may be used. These can achieve the theoretical maximum concentration, and are discussed in further detail in section 5.2.2.

5.2.1 Theoretical Limit for Solar Concentration

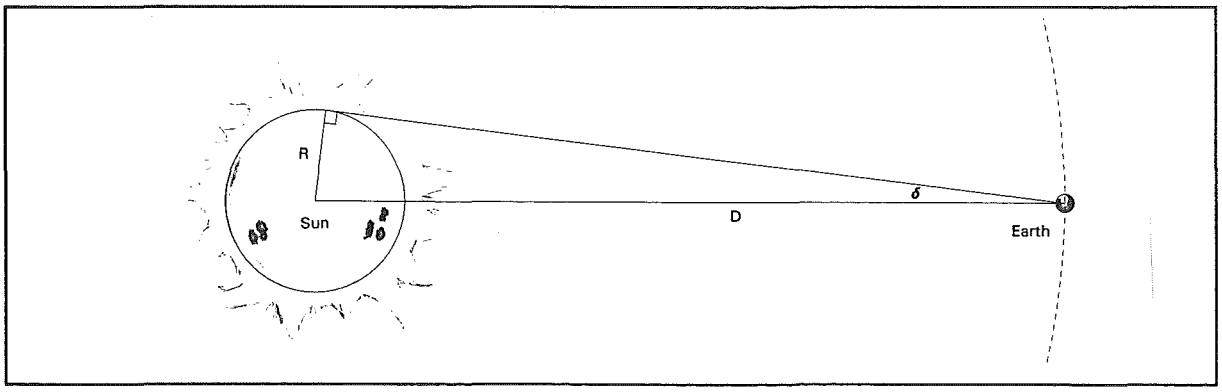

Figure 5.2 Thermodynamic limit diagram and Nomenclature to be used.

As was mentioned, it is the laws of thermodynamics that govern the highest

solar concentration. If a solar concentrator could produce a sunlight intensity corresponding to a temperature greater than the temperature at the sun's surface, then a heat engine could operate successfully between the concentrator's focus and the surface of the sun and extract energy at no cost, which is therefore a perpetual motion machine (Winston 1991). Figure 5.2 shows diagrammatically the mathematics behind the theoretical maximum as applied to point focus systems. The total solar energy leaving the sun is calculated through the intensity I_{sun} at the sun's surface multiplied by the sun's surface area $4\pi R^2$.

$$E_{solar}=I_{sun}\times 4\pi R^2$$

This energy must all pass through the sphere[2] containing the Earth's orbit, which means that the intensity I_{earth} of the light going through the sphere is the total solar energy E_{solar} divided by the surface area of the sphere $4\pi D^2$. Thus

$$I_{earth}=\frac{E_{solar}}{4\pi D^2}=\frac{I_{sun}4\pi R^2}{4\pi D^2}=\frac{I_{sun}R^2}{D^2}$$

The laws of thermodynamics state then that the intensity of the light on the earth cannot exceed the intensity on the sun, therefore:

$$I_{sun}=\frac{D^2}{R^2}I_{earth}$$

If the sun half angle = δ, then from trigonometry, the maximum concentration ratio given by D^2/R^2 is:

$$\frac{D^2}{R^2}=\frac{1}{\sin^2\delta}=45031$$

once the value of $\delta=0.27°$ is substituted into the equation. The calculation of the theoretical limit for the line focus systems is analogous to that above except that the spheres are replaced by circles and their perimeters, to give a maximum of:

$$C_{max\ 2D}=\frac{D}{R}=\frac{1}{\sin\delta}=212$$

---

[2] For the purposes of simplicity we shall assume that the Earth's orbit is circular.

Concentrations higher than these have been achieved by the use of refractive materials in the concentrators to cause the light to be refracted to an even smaller point. This technique has produced concentrations of sun light as high as 84000 giving an intensity at the focus 15% higher than that found at the surface of the sun (Winston 1991).

Image forming concentrators fall short of the theoretical maximum by a significant amount. In the case of the parabolic dish this factor is about ¼. For the line focus case, the limit for the parabolic trough is ½ of the theoretical maximum. Figure 5.3 shows the nomenclature to be used in the following derivation for the line focus case. The derivation for the parabolic dish is analogous. An assumption will be made that the trough of length L will not have any end effects, and that the target at the focus will not shade the reflector surface.

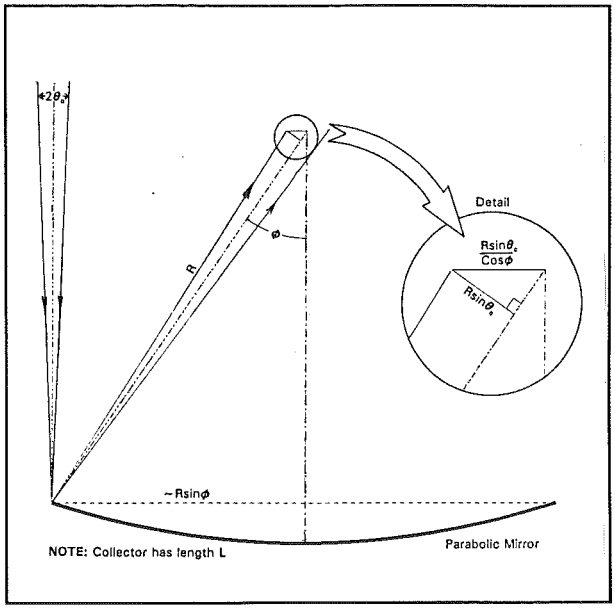

Figure 5.3 Parabolic trough collector with Nomenclature for the derivation of the theoretical maximum concentration ratio.

$$A_{reflector}=2RL\sin\phi$$

$$A_{absorber}=2RL\frac{\sin\theta_c}{\cos\phi}$$

The above expressions were derived through simple trigonometric relationships, where ϕ is the rim angle, and θ_c is the acceptance half angle. (Concentration is a maximum when the acceptance half angle θ_c equals the sun half angle δ. See Figure 5.1). These then may be used to determine the theoretical concentration ratio $C_{parabolic\ trough}$ that the line focus parabolic trough is capable of. The concentration ratio is calculated as the ratio of the frontal area of the reflector, to the absorber area.

$$C_{parabolic\ trough}=\frac{A_{reflector}}{A_{absorber}}=\frac{2RL\sin\phi\cos\phi}{2RL\sin\theta_c}=\frac{\sin\phi\cos\phi}{\sin\theta_c}=(\frac{1}{2})\frac{\sin2\phi}{\sin\theta_c}$$

Therefore when ϕ is 45° the concentration ratio is ½ of the theoretical maximum concentration ratio for line focus systems if θ_c is allowed to equal δ.

$$C_{max}=(\frac{1}{2})\frac{1}{\sin\delta}$$

5.2.2 Non-Imaging Solar Concentrators

By using non-imaging optics, the theoretical maximum concentration ratio can be achieved. Non-imaging concentrators act as a funnel for light; all light that falls into its entrance is reflected to the exit aperture or absorber as the case may be. Figure 5.4 shows the simplest compound parabolic concentrator (CPC), similar to the type of non-imaging concentrator that we are concerned with in this project. The generation of this particular CPC profile is achieved by the construction of two parabolic arcs with their axes parallel to the lines diagonally joining the two apertures, but passing through the opposite edge of the exit aperture.

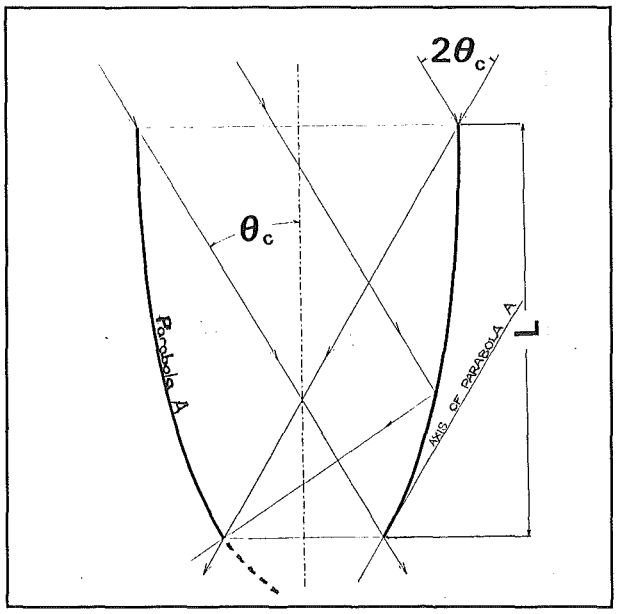

Figure 5.4 Compound parabolic concentrator with an exit aperture where a flat absorber could be mounted.

Increasingly, the CPC collectors are finding use in applications such as domestic solar water heaters, due to their high efficiency, and good concentration ratios. In the case of the basic CPC as shown here in Figure 5.4. The concentration for a line focus system is:

$$C_{CPC\ line\ focus}=\frac{1}{\sin\theta_c}$$

where θ_c is the acceptance half angle of the collector. If the acceptance half angle

were to be set to be equal to the sun half angle, then the theoretical maximum concentration ratio would be achieved. However most CPC's in use have acceptance angles of about 15-30° giving concentrations of 4-2 times. With the larger acceptance angles, the need to track the sun is eliminated, or reduced to a seasonal adjustment. For the higher concentrations, the acceptance half angle is reduced. This however means that the collectors become very deep, and therefore more expensive to produce due to the increased amount of material, while also being more prone to wind damage. For this reason it is the simple parabolic collectors that have the advantage over the CPC's when concentration ratios over 10 are required (Grimmer 1979). For this concentration, both types would require diurnal tracking, but the CPC would have an acceptance half angle of 6° or less, making for an exceptionally deep collector which would cost about 4.4 times that for the equivalent simple parabolic collector.

To get the best of both worlds, it is possible to use both a simple parabolic collector and a compound parabolic collector in the one system. In this case the simple parabolic collector reflects into a compound parabolic collector which further concentrates the light onto the absorber. This system has the high concentration ability of the CPC without the problem of the CPC being very deep. This therefore was the system chosen for this project. Secondary reflectors have been proposed for point focus systems, either on a large scale in combination with a heliostat field or to reflect sunlight back down onto a heat engine mounted level with the main array (Isshiki *et al* 1989, see Figure 3.4)

With a system such as this, the acceptance half angle of the CPC is governed by the rim angle and the acceptance half angle of the simple parabolic collector.

5.3 The Absorber Shape and Insulation

The system for transporting the heat from the solar collectors to the Stirling engine was decided to be through a heat pipe (see chapter 7). The easiest shape for fabrication of the heat pipes was tubular which meant that the design of the collector profiles could go ahead. This also gave the advantage in being able to set up a system where the absorber supports, and CPC system, could rotate around the absorber without the profile needing to be changed. This would be necessary

because of the tracking method that was to be used (see section 5.7). The working fluid for the heat pipes was never resolved and so the actual final diameter of the pipes was never finally resolved as this would depend on the heat pipe performance and its ability to transfer the required heat through as small a diameter as possible. However this would not change the profile of the collectors, just the scale. Thus, knowing the shape of the absorber was all that was needed to continue with the collector design. From preliminary calculations it appeared that for a sensibly sized system, the width of the simple parabolic troughs should be approximately 1m, This meant that the absorber if tubular would be of a very small diameter, which would then cause problems in not allowing the desired heat transfer to the Stirling engine. To alleviate this problem, the absorber was set such that only a portion of its surface would be heated, thereby allowing the absorber to be able to reach the required temperature, and keeping the simple parabolic trough about 1m across, while also allowing a sufficiently large vapour space in the heat pipe for good heat transfer.

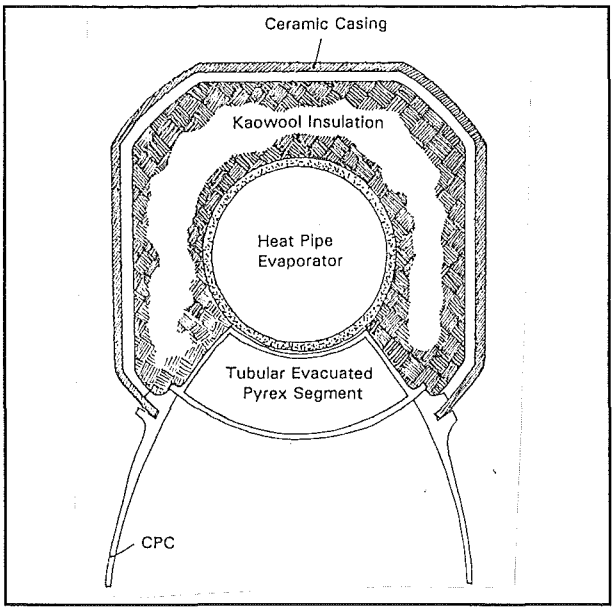

Figure 5.5 Insulation around the heat pipe absorber.

Now that there was a large amount of unheated absorber which would be hot, insulation was needed around the pipe. In most other systems existing, the heat transfer into the working fluid (normally single phase heat transfer fluid) occurs around the entire surface of the absorber, and an evacuated gas container surrounds the absorber to provide insulation from convective and conductive losses. For this project, the use of evacuated glass tubes surrounding the entire absorber was ruled out by a number of factors;

- The use of a secondary reflector would interfere with the glass cover.
- The evacuated glass tube would not prevent increased radiative losses from the unheated portion of the absorber.

- With the need to rotate the collectors relative to the absorber for the purposes of tracking, the glass case would be subject to damage as well as being a complex shape with a number of glass to metal seals.

Solid insulation around the unheated portion of the absorber was the best option, while the strip receiving the radiation would be insulated by an evacuated glass (pyrex) segment. The insulation was to be a rock wool in a "rack" which would allow the absorber to move relative to it, and at the same time, hold the secondary reflectors in place. This would all be covered by a thin weather shield of ceramic. See Figure 5.5.

5.4 Collector Orientation

There are two choices for the orientation of the collectors;

- East-West orientation where the troughs run in the east-west direction and the sun travels in a plane which is also in the same direction. Figure 5.6a.
- North-South orientation where the sun travels across the collectors. Figure 5.6b.

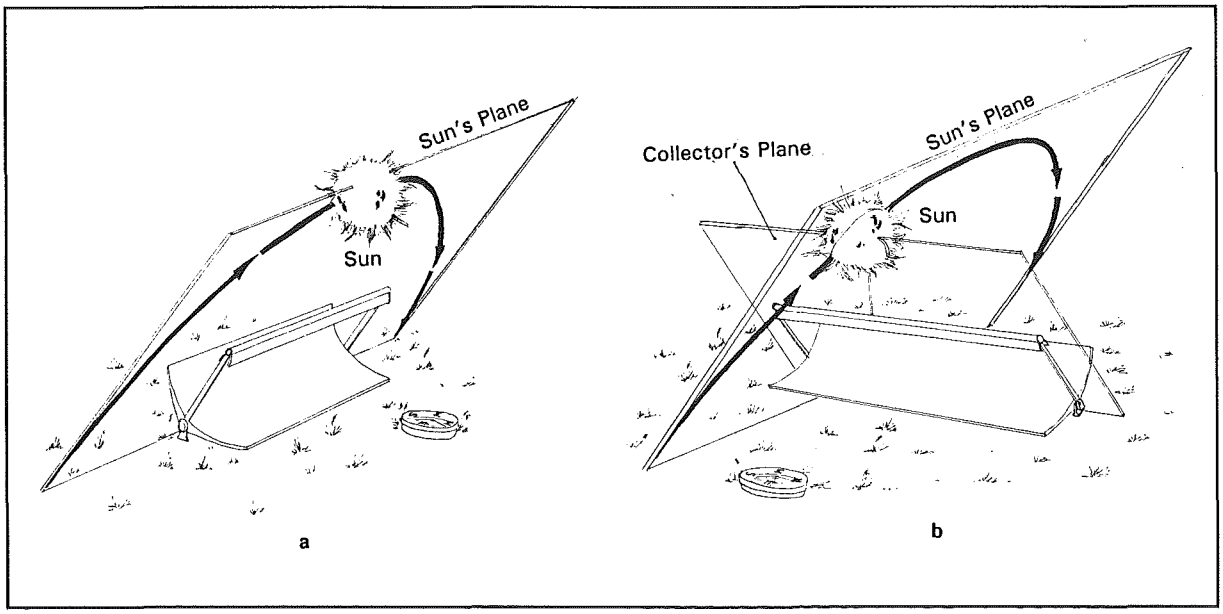

Figure 5.6 Orientations of the collector arrays. (a) East-West, (b) North South.

During the course of a day, the sun follows a path that deviates from a plane by only 6°. This means that if an acceptance half angle θ_c of 3° were used, then no tracking device would be needed other than a manual change to account for

seasonal variation. However this would not allow a high enough concentration to be achieved for our purposes. With the North-South orientation, tracking has to be used otherwise even with a large acceptance angle, operation will only occur for a short time each day. As the seasons change, the plane of the sun's path changes, the change becoming more pronounced the further from the equator one goes, and so to account for this the North-South oriented systems must have one end of the collector array's height adjust to present the maximum possible face area to the sun especially during winter. If this was not done, then a large amount of energy would be missed. Because of the length and size of the full scale system ($81 m^2$), this would be a very large, ungainly, difficult to handle, and extremely ugly system while being liable to be damaged by the wind. Although the sun's elevation is quite low in the mornings and evenings, these times are not prime generating times. The East-West system with a small tracking device to cater for the 6° deviation in the sun's path is the better system. This would also eliminate the need for seasonal manual adjustment. Power wastage during the night as the tracking device returns the array to a suitable position to pick up the morning sun would be minimal. Using the tracking device also allows a very small acceptance half angle to be used, so that a higher concentration and system efficiency may be achieved. An added bonus for the East-West oriented system is that should there be a failure of the engine, or simply too high an insolation, then with a small expenditure of power, the arrays could be tracked away from the sun and left off line.

5.5 Generating the Collector Profile

Generating the profile for the primary concentrator was a matter of choosing a basic size for the primary aperture which could be scaled as needed, deciding on an appropriate acceptance half angle, and then choosing a suitable rim angle which would then determine the focal length.

The acceptance half angle was chosen to be 1°. The reason for this extremely small acceptance angle when compared to most trough systems, is that this would allow the absorber temperature to be higher while also restricting the amount of exposed absorber thereby increasing the system efficiency. The orientation of the

collectors, and the use of diurnal tracking, made this both possible and desirable for good all-day performance.

Rim angles play a significant part in the concentration ratio and so it is important to choose one that will increase the efficiency of the system. Other factors are also present when using a two stage system and affect the choice of size for the rim angle. If the rim angle is large, then the primary concentration will be large, but the contribution from the secondary will be small as its acceptance half angle is approximately equal to the rim angle of the primary. If on the other hand the rim angle is small, then the secondary becomes dominant, but this means then that the secondary becomes large and its shadowing effect on the primary will become quite significant, while also making the system tall and prone to greater wind effects.

Calculations and preliminary designs (Appendix 10) showed that the best theoretical performance would be obtained through the use of a 20° rim angle, giving an absorber temperature 4°C higher than a 30° rim angle unit. The gain in efficiency was of the order of 0.02%. Rim angles below 20° were unsuitable due to the size of the secondary. The model used to compare systems was concerned entirely with the generation of electricity and the associated power flows and did not take into account the shape of the unit. A rim angle of 30° was eventually chosen because the performance it gave was not significantly below that of the 20° rim angle unit, and it balanced a reasonable small secondary with a suitably sized primary.

The rim angle directly affects the secondary reflector's acceptance half angle. The exit aperture of the secondary CPC should be able to see no more or less than the full face of the primary, and given that the secondary reflector's entry aperture is situated at the focus of the primary, its acceptance half angle must equal the rim angle of the primary less the acceptance half angle of the primary, as shown in Figure 5.7. Therefore the CPC had an acceptance half angle of 29°.

The size of the primary entry aperture was set at 1m for convenience and was to be scaled as appropriate once the final size of the absorber was known.

5.5.1 Primary Reflector Focal Length

With the dimensions needed to calculate the focal length of the primary present, an iterative expression was set up for this purpose. The expression for a parabola is given below:

$$y=\frac{x^2}{4f}$$

where **y** is the vertical axis, **x** is the horizontal axis, and **f** is the focal length. Figure 5.8 shows the nomenclature and sizes used in the derivation of the iterative expression for finding the focal length.

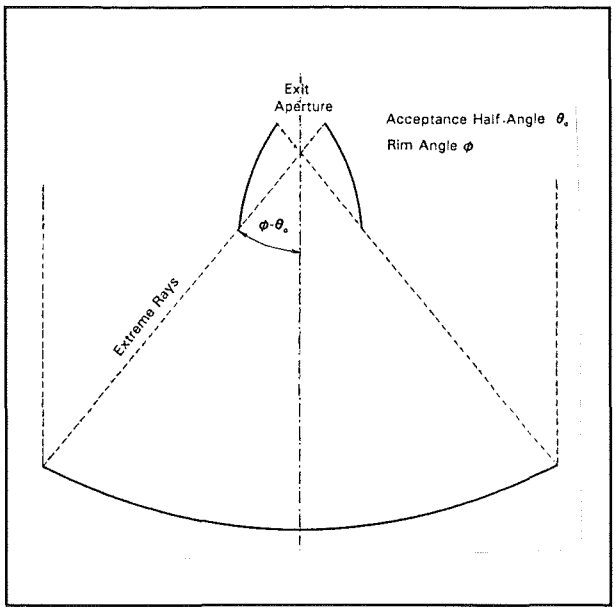

Figure 5.7 Relationship between the acceptance half angle of the CPC and the rim angle of the SPC.

Knowing the size of the primary aperture **2a** and the rim angle ϕ, similar triangles can be used to find the iterative expression for **f**. In the small triangle shown in the detail in Figure 5.8, the base length **b** is found through simple trigonometry:

$$\tan\phi=\frac{b}{a^2/4f}$$
$$\therefore b=\frac{a^2\tan\phi}{4f}$$

This then means that the width of the base of the large triangle has been found.

$$\frac{f}{a+b}=\frac{a^2/4f}{b}$$
$$\text{where}\quad a+b=a+\frac{a^2\tan\phi}{4f}$$
$$\therefore f=\frac{a^2/4f}{a^2\tan\phi/4f}\left(a+\frac{a^2\tan\phi}{4f}\right)$$
$$\text{so}\quad f=\frac{a}{\tan\phi}\left(1+\frac{a\tan\phi}{4f}\right)$$

The values to be substituted in are: ϕ = 30° therefore $\tan\phi = 1/\sqrt{3}$
a = 500

Thus the expression for this rim angle and basic size is:

$$f=500\sqrt{3}\left(1+\frac{500}{4\sqrt{3}f}\right)$$
$$=500\sqrt{3}+\frac{500^2}{4f}$$
$$=866.025+\frac{62500}{f}$$

From a starting point at 900mm, three iterations were needed before the focal length settled on 933mm.

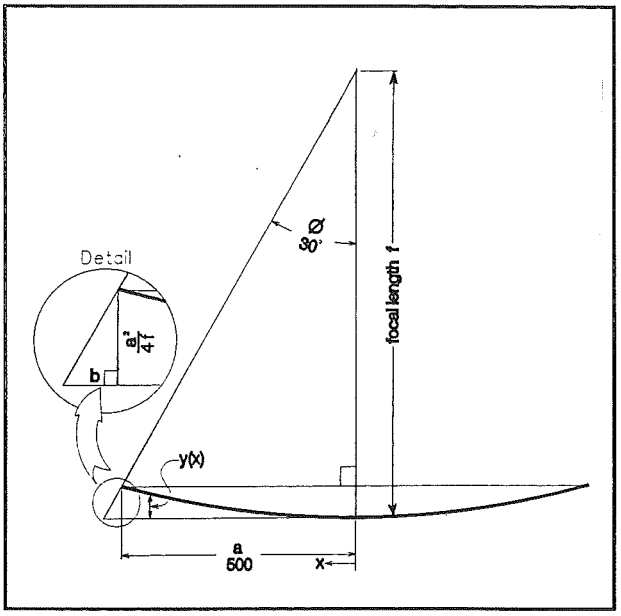

Figure 5.8 Focal length of the primary reflector, and construction lines used in the derivation of the iterative expression.

5.5.2 Size of the CPC Exit Aperture

This is determined again through the geometry and the edge-ray principle (Welford 1978), which states that all extreme rays entering the concentrator at the acceptance angle, must emerge from the rim of the exit aperture. Therefore, as long as a ray is within the acceptance angle, it will fall into the exit aperture.

In the case of the secondary reflector, the extreme rays come from the rim of the primary reflector at an angle differing from the rim angle by the primary concentrator's acceptance half angle which in the case of this project is 1°. Therefore the acceptance angle of the CPC secondary must be 29°. A relationship between the distances between the apertures of the primary and secondary have been shown to be:

$$AP'-AP=Q'Q$$ refer to Figure 5.9

The height of the CPC entry aperture above the rim of the SPC primary reflector is given by the focal length minus the depth of the SPC.

$$SPC\ depth=\frac{500^2}{4\times933}=67mm$$

$$\therefore CPC\ Entry\ Aperture\ Height=focal\ length-SPC\ depth=933mm-67mm=866mm$$

$$So\ \ AP'=\frac{866}{\cos31°}=1010.3mm\quad and\ AP=\frac{866}{\cos29°}=990.1mm$$

$$\therefore Q'Q=1010.3-990.1=20.2mm$$

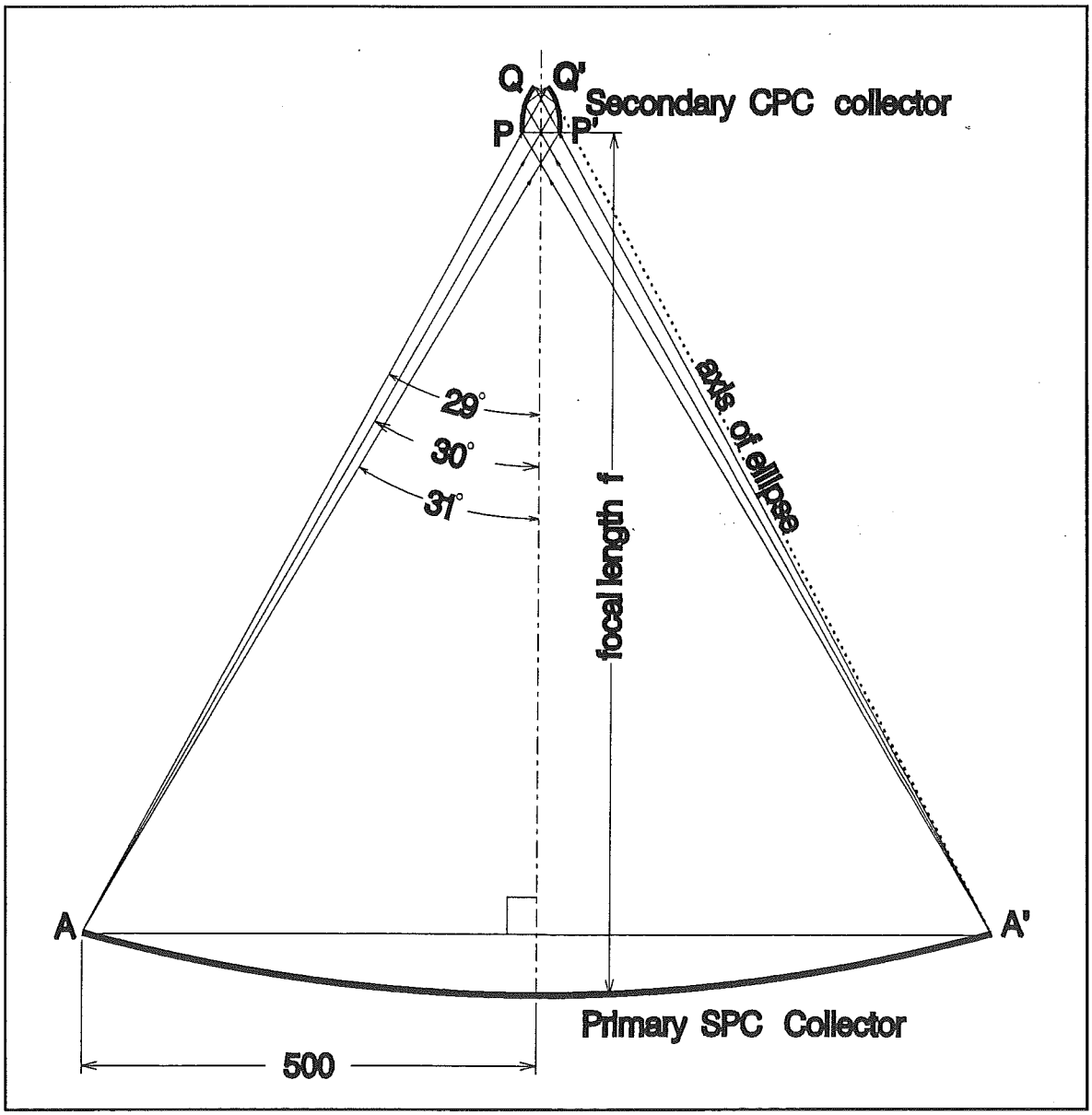

Figure 5.9 Two stage SPC-CPC combination showing the relationship between the entry and exit apertures.

The CPC exit aperture size is constant for this arrangement with a 1m primary entry aperture, a 30° rim angle, 1° acceptance angle, and a secondary CPC, no matter the shape of the absorber. With different absorber shapes, it is the profile of the CPC that changes.

5.5.3 Size of the CPC Entry Aperture

The entry aperture of the CPC (represented by **PP'** in Figure 5.9) can be determined through trigonometry.

$$CPC\ entry\ aperture = 866 \times (\tan 31° - \tan 29°) = 40.3mm$$

5.5.4 Concentration Ratios of the Reflectors

Just through the consideration of the aperture sizes, the concentrations of the two reflectors can be determined. The concentration ratio is the ratio of the area of the entry aperture to the exit aperture. Therefore for the primary simple parabolic concentrator:

$$C_{SPC} = \frac{d_{entry}}{d_{exit}} = \frac{1000}{40.3} = 24.8\times$$

To account for the shading caused by the secondary, approximately one exit aperture width will be shaded so the concentration ratio is in fact $C_{SPC} = 23.8x$. For the CPC, the concentration ratio is calculated in the same way, providing a concentration ratio $C_{CPC} = 2x$. Concentration ratios for two stage reflector systems are the product of the two component concentration ratios, therefore:

$$C_{\text{Two Stage Concentrator}} = 47.6x$$

5.5.5 CPC Profile Generation

At this point it becomes very important to have determined the size of the absorber, because this will significantly change the profile shape. Preliminary estimates put the absorber diameter at about 25.4mm if mercury was to be used. Of this, only a portion would be heated, this portion being an arc with a length of

20.2mm as calculated for the CPC exit aperture size.

There are a number of methods for generating the profiles of CPCs that have non planar absorbers and light sources at a finite distance, all of which are based around the edge ray principle. The simplest is the use of a piece of string to simulate a light ray, and its reflection from the concentrator's surface onto the absorber. In some cases this is the only way to generate the profiles, but with simple absorber shapes it is possible to set up equations to describe the rays, and their reflection. This method was the one used here. The following is an adaptation of the method presented by Welford (1978).

Welford proves the theory in his book "The Optics of Nonimaging Concentrators-Light and Solar Energy" and so a rigorous proof will not be presented here. He showed that a differential equation could be set up, which upon solving would yield an ideal profile for the line focus CPC's. The equation was for a CPC with a light source at an infinite distance, and with any non-planar absorber shape. Figure 5.10 shows the nomenclature used by Welford. Because of the condition that light is coming from a source an infinite distance away, all the light rays approach the concentrator at the acceptance half angle, as these are the ones that are of concern.

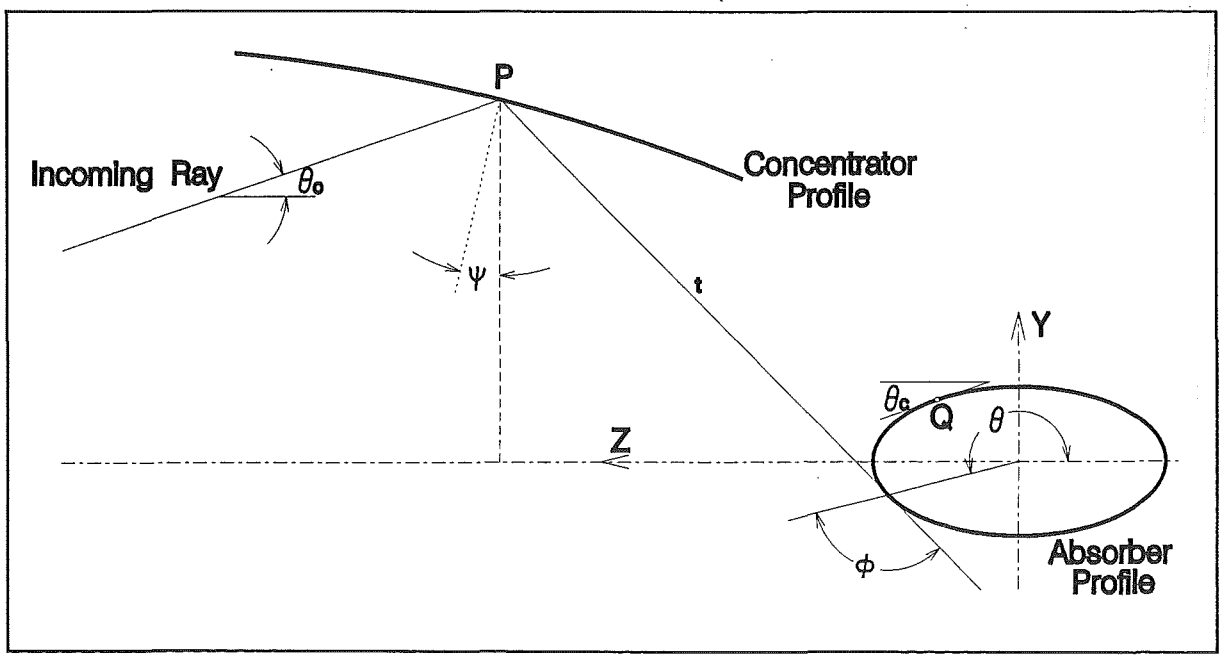

Figure 5.10 ray trace of a 2D concentrator with a non-planar absorber.

The coordinates of point P on the CPC profile are given by:

$$y = r\sin\theta - t\sin(\theta+\phi)$$
$$z = -r\cos\theta + t\cos(\theta+\phi)$$

In the general case this produces a first order differential equation as shown below in (5.1):

$$\frac{\frac{dr}{d\theta}\sin\theta + r\cos\theta - \frac{dt}{d\theta}\sin(\theta+\phi) - t\cos(\theta+\phi)(1+\frac{d\phi}{d\theta})}{-\frac{dr}{d\theta}\cos\theta + r\sin\theta + \frac{dt}{d\theta}\cos(\theta+\phi) - t\sin(\theta+\phi)(1+\frac{d\phi}{d\theta})} + \tan\frac{1}{2}(\theta_c+\theta+\phi) = 0 \qquad (5.1)$$

In a normal CPC profile with a tubular absorber, there is an involute portion for reflecting light onto the back side of the absorber. The differential equation for this is:

$$\frac{dt}{d\theta} = \sqrt{r^2 + \left(\frac{dr}{d\theta}\right)^2} \qquad (5.2)$$

A closed form solution can be achieved for (5.1) by the use of a "string method" where s is the perimeter of the absorber, θ_o is the polar angle to point Q where the shadowed portion of the absorber begins. For $\theta > \theta_o$:

$$t = \frac{[s + s(\theta_o)] - r\cos(\theta-\theta_o) + r(\theta_o)\cos(\theta_o-\theta_o)}{[1-\cos(\theta+\phi-\theta_o)]} \qquad (5.3)$$

The involute portion where $\theta < \theta_o$ is defined by:

$$t = s \qquad (5.4)$$

For the special case where the absorber is circular in cross section, then $dr/d\theta = 0$, $\phi = \pi/2$ reducing (5.1) to:

$$\frac{dt}{d\theta} - t\tan[\theta - \frac{1}{2}(\theta_c+\theta+\frac{\pi}{2})] - r = 0 \qquad (5.5)$$

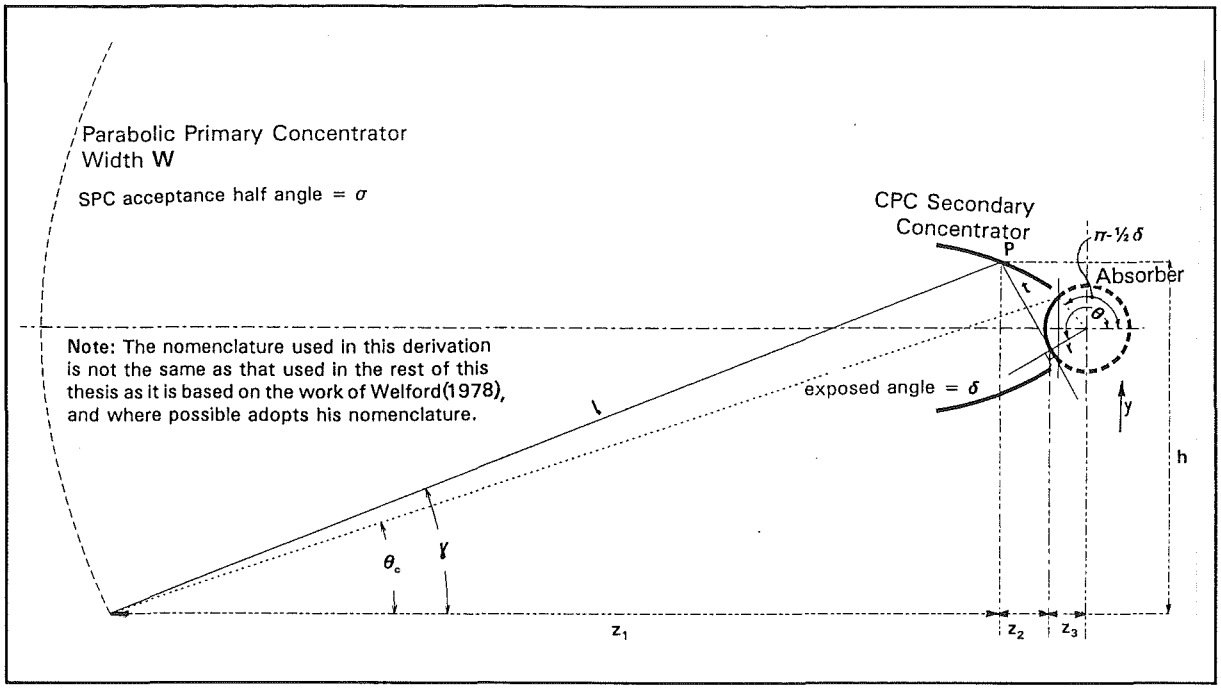

Figure 5.11 Ray trace for a 2D CPC which is a secondary reflector in an optical system.

It is from this expression that the expression for the secondary CPC of the solar concentrator is derived. As there is no shaded region on the absorber for the system described within this thesis, there is no involute region, and so the only expression needing to be solved is that above in (5.5). However before solving could be started it needed to be adapted to be able to describe the profile that would be suitable for a light source at a finite distance, ie. from a primary reflector. In this case the incoming light is no longer at a constant angle θ_c, instead entering the CPC at an angle of γ (refer to Figure 5.11). With these conditions then, the expression 5.5 becomes:

$$\frac{dt}{d\theta} - t\tan\left[\frac{1}{2}\left(\theta - \gamma - \frac{\pi}{2}\right)\right] - r = 0 \qquad (5.6)$$

where γ is a function of t and θ and can be found through the geometry of the system. So equating the distances along the z-axis:

$$z_1+z_2+z_3=CPC\ depth+focal\ length-SPC\ rim\ height+zdist\ CPC\ exit\ to\ abs\ centre$$

$$where \quad CPC\ depth=\frac{1}{2\tan\theta_c}(d_{CPC\ entry}+d_{CPC\ exit})$$

$$d_{CPC\ exit}=2r\sin\left(\frac{\delta}{2}\right)$$

$$d_{CPC\ entry}=\left(f-\frac{w^2}{16f}\right)(\tan(\phi+\sigma)-\tan(\phi-\sigma))$$

$$focal\ length-Rim\ height=f-\frac{w^2}{16f}$$

$$zdistance\ CPC\ exit\ to\ absorber\ centre=r\cos\left(\frac{\delta}{2}\right)$$

(5.7)

The nomenclature is shown in Figure 5.11.

The constant length $z_1+z_2+z_3$ must be the same as that obtained by the ray trace, therefore:

$$\begin{aligned} z_1&=l\cos\gamma \\ z_2&=-t\sin\theta \\ z_3&=-r\cos\theta \\ \therefore\quad z_1+z_2+z_3&=l\cos\gamma-t\sin\theta-r\cos\theta \end{aligned} \tag{5.8}$$

If $z_1+z_2+z_3$ is constant, then the expression after combining (5.7) and (5.8) is then;

$$\begin{aligned} l\cos\gamma-t\sin\theta-r\cos\theta&=constant \\ \therefore\quad l&=\frac{const+t\sin\theta+r\cos\theta}{\cos\gamma} \end{aligned} \tag{5.9}$$

Then if the **y** direction is considered, an expression is also produced:

$$\begin{aligned} h&=\frac{w}{2}-r\sin(\theta-\pi)+t\cos(\theta-\pi) \\ &=\frac{w}{2}+r\sin\theta-t\cos\theta \end{aligned} \tag{5.10}$$

Using simple trigonometric relationships, an expression for γ can be obtained from (5.9) and (5.10).

$$
\begin{aligned}
& l \sin\gamma = h \\
& \frac{const + t\sin\theta + r\cos\theta}{\cos\gamma}\sin\gamma = \frac{w}{2} + r\sin\theta - t\cos\theta \\
& \therefore \quad \tan\gamma = \frac{\frac{w}{2} + r\sin\theta - t\cos\theta}{const + t\sin\theta + r\cos\theta}
\end{aligned}
\qquad (5.11)
$$

This is all that is needed to generate the profile; however to solve this would be awkward and time consuming, so the solution was attained using a numerical mathematics computer package. The package was MATLAB and the numerical solution function was ODE23 for solving ordinary differential equations, where the ordinary differential equation that was to be solved was (5.6).

5.5.6 MATLAB Program Listings

The program was written to be relatively general, and could be quickly changed if the sizes of some of the components were changed, although some settings would need to be calculated out manually and re-entered, ie integration limits etc. The first listing here is called **PROFILE.M** and ran the ordinary differential equation solver, changed the output to cartesian coordinates, and plotted them. Note the variable change used - t is the θ value, and y is the t value.

```
% A program to operate the CPC profile generating differential
% equation
r=12.7;
[t,y]=ode23('cpc',2.346246113,4.206243497,0,1.e-4);
a=sqrt(r.^2+y.^2);
psi=t-pi/2-atan(y./r);
x=a.*cos(psi)
z=a.*sin(psi)
plot(z,x)
grid
```

The ODE23 operation calls on the function contained within the file **CPC.M**, below, which contains the differential equation to be solved, and the expressions involved in finding the value of the constant in the $\tan\gamma$ expression. Again the same variables as above have been used.

```
function cpc=profile(t,y);
% t is the theta value, y is the t value.
r=12.7;
% r is the absorber radius
s=20.2;
% s is the aperture size of the CPC exit
delta=s/r;
w=1000;
f=933;
% w is the entry aperture width SPC, f is the SPC focal length
acc=0.506145483;
phi=pi/6;
% Phi is the rim angle of the SPC; acc is the CPC acceptance angle
sigma=pi/180;
centry=(f-w.^2/(16.*f)).*(tan(phi+sigma)-tan(phi-sigma));
cexit=2.*r.*sin(delta./2);
% sigma is the SPC acceptance angle, Centry & exit are the CPC aptures
zk=r.*cos(delta/2)+f-w.^2./(16.*f)+1./(2.*tan(acc)).*(centry+cexit);
% t is the theta value, y is the t value.
num=w./2+r.*sin(t)-y(1).*cos(t);
den=zk+y(1).*sin(t)+r.*cos(t);
tang=num./den;
cpc=[y(1).*tan(0.5.*(t-atan(tang)-pi/2))+r];
```

The output from the package is in the form of a plot, and the display of the z and x coordinates of the profile, where the z coordinate is the distance in the vertical axis taken from the absorber centre, and the x axis is the horizontal axis with its origin also at the absorber centre. The data points can then be entered into a CAD package and joined by a curved line string to form the accurate curve for production and checking. To check the curves, the use of a CAD package makes it possible by simulating the light rays entering the CPC at different angles in the same way as the string-ray tracing technique.

5.6 Solar Concentrator Materials

The choice of materials for the reflectors is governed by a number of factors;

- Cost
- Ability to form the material accurately into the desired curves and then hold that shape.
- Reflectivity
- Resistance to weathering
- Heat resistance - particularly important for the CPC.

For the simple parabolic reflector, the temperatures are low, and the shape simple, therefore the chief factors here are the formability, reflectivity, and weather resistance. A suitable system for producing parabolic troughs of accurate shape, and using cheap, simple techniques, was outlined by Heiti and Thodos (1983).

In their technique a master mould was first produced out of wood using metal templates accurately shaped to fit the parabolic expression: $y = x^2/4f$

The surface was finished with a filling compound. From this mould, accurate fibreglass shapes could be pulled. Over the fibreglass, a layer of aluminised acrylic film laminate was applied to provide the reflective surface. Surface protection was provided by a glass cover plate that lay across the SPC entry aperture. The reflectivity of this material was of the order of 0.86.

For the system described in this thesis, the same technique would be used to create the base shape using fibreglass, but the reflective surface would be a front surface[3] aluminised mylar which has a reflectivity of 0.88 (Kreider 1981). Better reflectivity could be obtained by using silvered plastics instead, but this leads to greater costs in the system. On the whole, metallised plastics have a very good surface quality, but have less abrasion resistance than glass, while also suffering from UV embrittlement if UV stabilizers are not added. If the surface is carefully kept clean, the loss of reflectivity after two years amounts to only a few percent.

At the secondary reflector, the requirements are much more stringent, requiring a good temperature resistance, very good reflectivity, and a good formability. As the size of the secondary reflector is not very big, the material costs will not be high. The ideal material for this part is a polished aluminium. This has the advantage of being able to withstand the high temperature that will occur with the high solar fluxes present. The wear resistance of aluminium is very good, and it has a high reflectivity typically in the range 0.85 to 0.87. Aluminium reflectors are known to have good resistance to UV radiation and will not lose their reflectivity

---

[3] Front Surface refers to the reflective layer being applied to a substrate, and then an overcoat of a protective material added. This does however mean it is more prone to damage from scratching, and other weathering effects.

even after an extended time of outdoor exposure.

5.7 Solar Tracking System

Because of the orientation of the reflectors, it will be necessary to have a solar tracking device that can follow the sun actively and be capable of responding to a control system that will direct it away the sun should a failure occur, or the insolation be too high. Therefore the solar tracking device will be a very integral part of the operation of the whole system as it will be connected into the temperature monitoring circuits as well.

The system envisaged is comprised of;

- a servo motor, and worm drive to the concentrators
- a pair of optical sensors,
- a comparator for the optical sensor outputs,
- a controller receiving data from the engine, the batteries, the heat exchangers, and the comparator.

The optical sensors will be fixed into a holder such that if they are not pointing directly at the sun, then they will be shaded, or partially shaded. The signals will vary depending on the degree of shading, and so by using the comparator, it will determine whether the servo will have to be activated to bring the concentrator back into line, and also which way it should run to achieve this.

A worm drive attached to the servo motor was decided on because it cannot be back driven, which means that the motor will not need to work constantly against gravity, or wind loadings. Only moving 6° in a day, the servo will not need to operate frequently, for any length of time which means that the tracking system will not be a significant drain on the energy generated by the system.

5.8 Thermal Storage Batteries

Thermal storage of the solar energy has been proposed on a number of occasions with other systems, and in the concept design of this one. Thermal storage is a very efficient method of storing energy for a moderately long time, because of the lack of energy changes that occur.

Thermal energy storage comes in two types, latent heat, and sensible heat. In latent heat or phase transition thermal storage, the energy is stored in a material

that changes phase. This is a very efficient form of storage with a high energy density being possible. Sensible heat is storage of energy in the specific heat capacity of the material. A common example of this is the use of bricks, and sand to store heat.

Both latent and sensible heat storage are excellent for solar thermal systems where a high heat output is not needed. Unfortunately with the system proposed here, the Stirling Engine would be supplying all loads, including the peak load which would mean that an engine capable of producing up to $5kW_e$ would be needed, and at 10% heat to electrical energy conversion, the thermal storage system must be capable of supplying 50kW of heat to the engine. To do this, the storage must have a very complex and expensive heat exchange system, as well as a system for clearing the solid away from the heat exchange surfaces when it forms in the latent heat storage system.

The need to be able to cater for the peak electricity demands with the Stirling engine also makes this system quite big, and uses an unnecessarily large and expensive engine.

In the practical system, the thermal storage would need to be mounted very close to the collector system so that heat transport to the thermal storage unit is efficient with minimal loses, which is a problem in that the heat losses from the system will be wasted in heating the outside air. In addition to this, the system for connecting the collector heat exchangers to the thermal storage would have to be flexible to allow for the movement of the collectors as they track the sun.

5.9 Finalised System Concept

The finalised concept design used electric battery storage. Although not as efficient as a thermal battery, the electric batteries have the advantage of being able to meet very high peak currents. As the Stirling engine is only meeting the mean power demand, the size of the engine is reduced, and its operation can be optimised to meet that demand.

In the final concept design, heat pipes were to be used to transport the heat from the two stage line focus (SPC-CPC) solar concentrators to the Stirling engine heater heads (Chapter 7). An East-West orientation would be used for the arrays.

6. SYSTEM PERFORMANCE PREDICTION MODEL

6.1 Introduction

For the purpose of sizing the components, and predicting the overall system performance under various conditions, an iterative computer spreadsheet model was produced. This allowed the array size to be predicted, and a suitable temperature at the absorber to be found which would optimise the system performance. The spreadsheet model was based on component efficiencies, and heat losses to the surroundings.

The computer spreadsheet package used was VP Planner, a program similar in operation to Lotus 123 and most other spreadsheets.

6.2 Collector Optical Efficiency

The optical efficiency η_o refers to the proportion of the incoming radiation $IA_{SPCentry}$ that reaches the absorber surface $\dot{Q}_{abs\text{-}Surf}$.

$$\eta_o = \frac{\dot{Q}_{abs\text{-}Surf}}{IA_{SPCentry}} \qquad (6.1)$$

In the two stage concentrating reflector for this project, the optical efficiency is the product of the reflectivities of each of the reflector surfaces. Had the CPC been truncated, then the optical efficiency would be lower due to the loss of some of the radiation back out into the environment. The reflectivity of the aluminised mylar surface of the primary is $\rho_{SPC} = 0.86$, and the reflectivity of the aluminium CPC is $\rho_{CPC} = 0.87$. Therefore the collector optical efficiency is:

$$\eta_o = \rho_{SPC} \times \rho_{CPC} = 0.86 \times 0.87 = 0.75 \qquad (6.2)$$

6.3 Total Power Transmitted to the Absorber

All materials have some degree of reflectivity even when treated with a black coating. This means some of the radiation reaching the absorber surface will be

reflected. The measure of the fraction of energy being absorbed into the absorber is called the absorptance α. If a black sulphide or one of the black oxides is plated onto a steel absorber, then the solar radiation absorptance is about 0.95. Thus the heat entering the absorber is:

$$\dot{Q}_{abs}=\alpha \dot{Q}_{abs-Surf} \tag{6.3}$$

6.4 Heat Transfer to Heat Engine

Knowing the diameter of the absorber, its material, and estimating its length, the efficiency of the heat transfer from the collectors to the heat engine can be predicted. The calculations here make the assumption that all the heat, once in the working fluid of the pipe, will be transferred to the heat engine except for that lost by re-radiation and convection to the surroundings.

$$\dot{Q}_{in}=\dot{Q}_{abs}-\dot{Q}_{Rerad}-\dot{Q}_{Cond} \tag{6.4}$$

6.4.1 Re-radiative losses

Radiative losses occur at all points of the absorber, but it is insignificant where insulation is present, so the assumption that negligible radiative losses occur in these places has been applied. Therefore the only radiative losses from the system come from those parts that are exposed to the incoming radiation or are uncovered.

Energy losses due to radiation are calculated using the Stefan-Boltzman law:

$$\dot{Q}_{re\ rad}=\epsilon A_{abs}\sigma(T_a^4-T_{amb}^4) \tag{6.5}$$

Where σ = Stefan-Boltzman constant = 5.67×10^{-8} W/m².K⁴
ϵ = the emissivity of the material ≈ 0.15 for a steel absorber at high temperatures.
T_a is the absorber temperature
T_{amb} is the ambient temperature
A_{abs} is the exposed absorber area which can be calculated from the CPC exit aperture and the lengths of the collector arrays.

6.4.2 Conductive-Convective Losses

The losses due to convection and conduction can account for a very significant energy loss if care is not taken with the method of insulation.

In chapter 5.3, the choice of insulation material was a rock wool ideally with a ceramic weather guard around it to keep it dry and free of dirt build up and also provide an air gap for added insulation. There are a large number of different types of rock wool insulation available on the market, with varying thermal properties. The thermal conductivities of these fall in the range of 0.15 W/mK down to 0.1W/mK. It will be taken that the insulation material used here has a thermal conductivity of 0.12 W/mK.

A simplification of the shape of the insulating shell will be made by approximating it with a uniform cylinder. By doing this, the uncovered portion of the absorber will also contribute to the convective loss where the thermal resistance will come from the zone of heated air held under the secondary reflector. The expression then becomes:

$$\dot{Q}_{conv} = -\frac{2\pi L f_c (T_{amb} - T_a)}{\frac{1}{r_o h_1} + \frac{1}{k_{ins}} \ln\left(\frac{r_{ins\text{-}air}}{r_{ins}}\right) + \frac{1}{r_{ins\text{-}air} h_2} + \frac{1}{k_{cer}} \ln\left(\frac{r_o}{r_{air\text{-}cer}}\right)} \qquad (6.6)$$

Where
k_{ins} = thermal conductivity of insulation material = 0.12 W/mK
k_{air} = Air thermal conductivity = 0.04 W/mK
k_{cer} = the thermal conductivity of the ceramic casing = 0.5 W/mK
L = the length of the absorber.
h_1 is the heat transfer coefficient for the air on the outer surface of the ceramic casing = 15 W/m²K.
h_2 is the heat transfer coefficient for the air between the insulation and the outer casing = 7 W/m²K.
f_c = proportion of absorber covered by insulation.
r_{ins} = internal radius of the insulation.
$r_{ins\text{-}air}$ = the radius for the insulation to airgap interface.
$r_{air\text{-}cer}$ = the radius for the air gap to ceramic cover interface.
r_o = the outer casing radius.
T_{amb} = the ambient air temperature.

The model does not take into account the losses to be found around the engine heater head, but as there is sufficient room for a large amount of insulation, the heat losses will be relatively insignificant.

6.5 Engine Conversion Efficiency

This factor has been based on the theoretical Stirling engine efficiency with a factor of 0.4 included to more accurately approximate the real system efficiency.

$$\eta_{Stirling}=0.4\times\left(1-\frac{T_c}{T_a}\right) \tag{6.7}$$

T_c is the temperature in the Stirling engine compression space.

When this efficiency is applied to the heat that reaches the heater heads, the result is the mechanical work output from the system.

6.6 Electricity Generation and Storage

To model the mechanical to electrical energy conversion through the alternator, a constant efficiency of 60% has been taken. This is reasonable for a standard vehicle alternator. It should be noted that there is available, a generator developed by British Gas that has a conversion efficiency of approximately 90% (Starr 1994). This generator is a suitable size for use in future Stirling engine research within the Department of Mechanical Engineering at the University of Canterbury.

Similarly, the Charge/Discharge efficiency of the lead acid batteries, has been taken as 60% which again is average for lead acid batteries.

6.7 Solar Concentration Ratio

As an expression, the concentration ratio for the two stage array is given by:

$$C_{two\ stage}=\left(\frac{\sin\phi\cos(\phi+\theta_c)}{\sin\theta_c}-1\right)\frac{1}{\sin(\phi-\theta_c)} \tag{6.8}$$

where ϕ is the rim angle = 30°

θ_c is the primary concentrator's acceptance half angle = 1°

Expression 6.8 is comprised of the product of the two separate concentration ratios for each stage. The expression (6.9) for the concentration ratio of the primary SPC (simple parabolic concentrator) has been adjusted to account for the effects of shading by the absorber. The expression given below (A.Rabl 1976) has been derived for the case of an SPC with a flat plate absorber.

$$C_{SPC}=\frac{\sin\phi\cos(\phi+\theta_c)}{\sin\theta_c}-1 \qquad (6.9)$$

The secondary concentrator has its concentration ratio given by:

$$C_{CPC}=\frac{1}{\sin(\phi-\theta_c)} \qquad (6.10)$$

6.8 Operation and Construction of the Spreadsheet

The spread sheet has been constructed to iterate when the **F9** key is pressed. A change to the constants is made and the sheet is iterated until no further values change. This is valuable for finding the optimum temperature for the absorber, and therefore allows the selection of an appropriate working fluid to be carried out. By referring to Figure 6.1, the information transfer between the cells can be seen.

To start the spreadsheet, a value must be put in place of one of the formula cells involved in the iterative process, for example an initial value for the absorber exposed area. Once this value is in, the cell can be changed back to its formula, and the iterative system will be able to continue, as it will have values to work on.

To find the optimum temperature at the absorber for a given concentrator geometry, a value is entered into the absorber temperature cell. This will influence the efficiency of the Stirling engine, the reradiative, conductive, and convective losses. This will change the system efficiency. As the power from the Stirling engine is set, the spread sheet will change the array size to match the incoming radiation to the required heat for the engine, and to counter the heat losses. The model is iterated, until the calculated values stabilise. The system efficiency can then be recorded. By varying the absorber temperature over a range, and observing the system efficiency that is calculated after the model has been iterated, an absorber temperature may be found that maximises the system efficiency for a given concentrator area.

With minor changes, the spreadsheet can be used to compare dish collectors, and different heat engines to the Trough-Stirling system. With the design presented here, the initial optimum temperature was 420°C at the absorber which

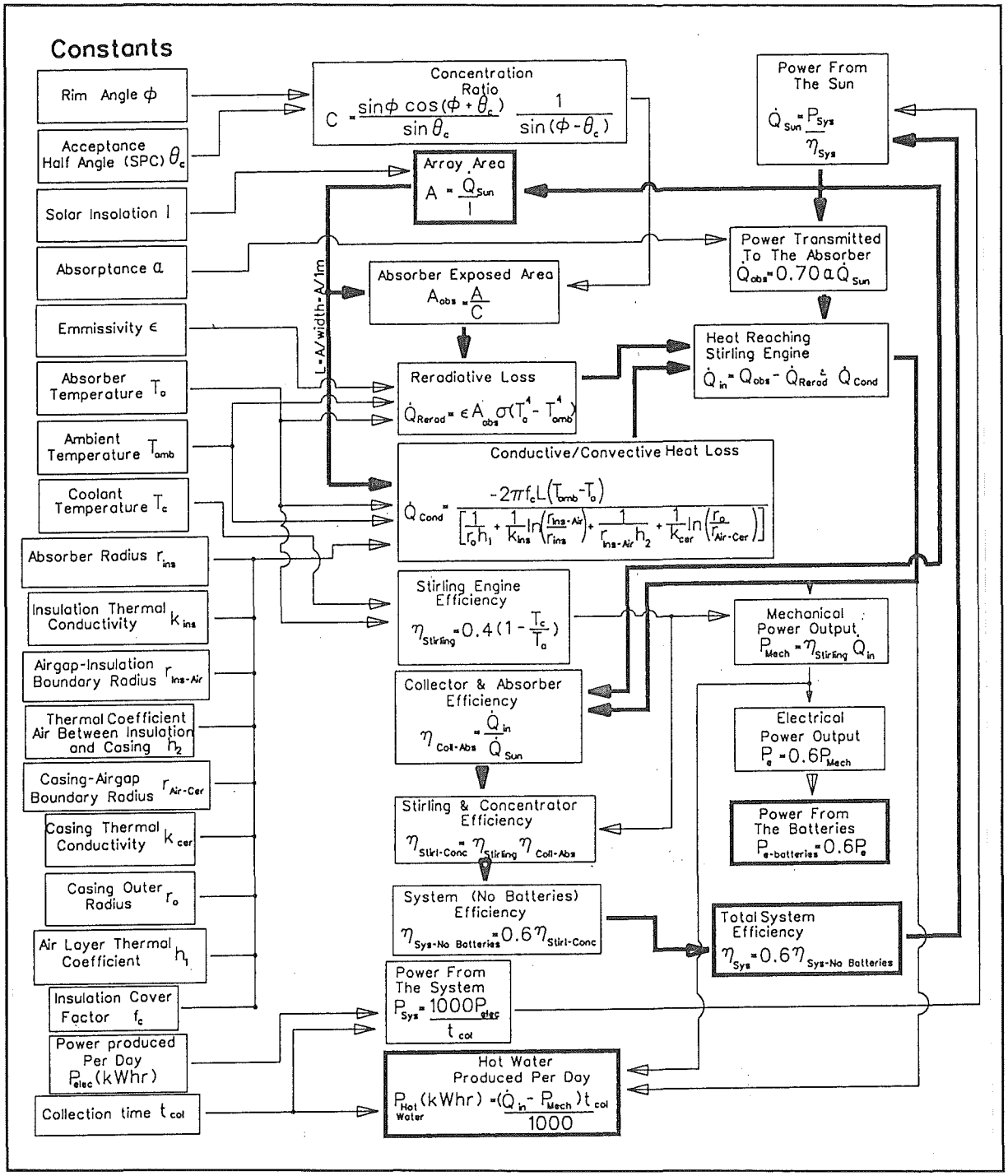

Figure 6.1 Diagram of the flow of information in the Spreadsheet. The Dark arrows indicate the iterative pathway, and the dark boxes are the most valuable outputs.

was a tubular design with its entire surface being the CPC exit aperture, and being surrounded in an evacuated glass tube. However with the tests on the working fluids, the tube size needed for such a system was too small to allow adequate heat transfer, and so partial surface exposure of the absorber had to be used. This

ruled out the use of the evacuated tube insulation system because of the high reradiative losses that would occur. This meant that the conductive convective losses would be higher, thus the new optimum occurred in the region 330-350°C.

6.9 Worked Example for the 200W$_e$ System

The following is the manually worked values from the spreadsheet. The basic values can be found in Appendix 1. Values used are:

SPC rim angle ϕ = 30°
SPC acceptance half angle θ_c = 1°
SPC entry aperture width w = 1m
Absorber exposed length L = 7m
Solar radiation flux density I = 600W/m²
Collector optical efficiency η_o = 0.75 (expression 6.2)
Absorptance α = 0.95
Absorber temperature T_a = 617K
Absorber emissivity ϵ = 0.15
Stefan-Boltzman constant σ = 5.67x10^{-8} W/m²K⁴
Ambient air temperature T_{amb} = 288K
Thermal conductivity of insulation material k_{ins} = 0.12 W/mK
Thermal conductivity of ceramic casing k_{cer} = 0.5 W/mK
Air heat transfer coefficient on outer surface of ceramic casing h_1 = 15W/m²K
Air heat transfer cefficient for air gap between insulation and ceramic casing h_2 = 7W/m²K
Internal radius of the insulation r_{ins} = 12.7mm
Radius for the insulation to airgap interface $r_{ins\text{-}air}$ = 30mm
Radius for the air gap to ceramic cover interface $r_{air\text{-}cer}$ = 35mm
Outer casing radius r_o = 40mm
Temperature of the water cooling system T_c = 333K
Alternator efficiency η_{alt} = 60%
Battery charge\discharge efficiency η_{bat} = 60%

The concentration ratio for the solar concentrators is calculated through the use of equation 6.8.

$$C_{two\ stage}=\left(\frac{\sin 30^\circ \cos(30^\circ+1^\circ)}{\sin 1^\circ}-1\right)\frac{1}{\sin(30^\circ-1^\circ)}=48.6\times \qquad (6.11)$$

This value is higher than that calculated in section 5.5.4, this is because of the different techniques used. In the method above the rounding errors have been minimised as the two parts for the calculation are not separated out. It is also worked from the basic rim angle, and acceptance half angle so that the aperture

widths do not need to be calculated, thus reducing the source of cumulative errors.

The heat from the sun is calculated from the heat flux, and the entry aperture area of the concentrator array (6.12).

$$\dot{Q}_{sun}=LwI=7\times1\times600=4200W \tag{6.12}$$

Not all of the radiation entering the SPC entry aperture, reaches the absorber, because the reflective surfaces will not be perfect. The optical efficiency accounts for this. Therefore the energy reaching the absorber surface is:

$$\dot{Q}_{abs\text{-}Surf}=\eta_o\dot{Q}_{sun}=0.70\times4200=2940W \tag{6.13}$$

Of this energy, a portion is reflected back out of the concentrator, by the absorber surface.

$$\dot{Q}_{abs}=\alpha\dot{Q}_{abs_{Surf}}=0.95\times2940=2793W \tag{6.14}$$

The area of the absorber exposed to the incoming radiation is found through the entry aperture, and the concentration ratio such that:

$$A_{abs}=\frac{Lw}{C_{two\ stage}}=\frac{7\times1}{48.6}=0.144m^2 \tag{6.15}$$

The absorber surface is at 610K. This means that there will be some re-radiation occurring from the exposed part of the absorber. Referring to equation 6.5, and taking the value of the exposed absorber area from 6.15, the re-radiative loss is:

$$\dot{Q}_{rerad}=\epsilon A_{abs}\sigma(T_a^4-T_{amb}^4)=0.15\times0.144\times5.67\times10^{-8}\times(617^4-288^4)=169W \tag{6.16}$$

Through the insulation surrounding the absorber there is a considerable heat loss. Before this can be calculated the proportion of the absorber covered by the insulation must be calculated.

$$f_c=1-\frac{w}{C_{two\text{-}stage}2\pi r_{ins}}=1-\frac{1}{48.6\times2\pi\times0.0127}\approx0.75 \tag{6.17}$$

Returning to the heat loss through the insulation and referring to equation 6.6, and applying the values given at the start of this section, the loss is:

$$\dot{Q}_{conv}=\frac{-2\pi L f_c(T_{amb}-T_a)}{\frac{1}{r_o h_1}+\frac{1}{k_{ins}}\ln\left(\frac{r_{ins-air}}{r_{ins}}\right)+\frac{1}{r_{ins-air}h_2}+\frac{l}{k_{cer}}\ln\left(\frac{r_o}{r_{air-cer}}\right)}$$

$$=\frac{-2\pi\times7\times0.75\times(288-617)}{\frac{1}{0.04\times15}+\frac{1}{0.12}\ln\left(\frac{0.03}{0.0127}\right)+\frac{1}{0.03\times7}+\frac{1}{0.5}\ln\left(\frac{0.04}{0.035}\right)} \qquad (6.18)$$

$$=783W$$

The total heat transferred to the engine is the heat that enters the absorber less the losses due to reradiation and convection-conduction losses. This is expressed in equation 6.4.

$$\dot{Q}_{\epsilon}=\dot{Q}_{abs}-\dot{Q}_{rerad}-\dot{Q}_{cond}=2793W-169W-783W=1841W \qquad (6.19)$$

Of this heat, a fraction is used by the Stirling engine for the production of mechanical power. The remaining energy is dumped into the water cooling system which in this case is also the domestic hot water supply. The energy conversion efficiency of the Stirling engine is given below and in equation 6.7.

$$\eta_{Stirling}=0.4\times\left(1-\frac{T_c}{T_a}\right)=0.4\times\left(1-\frac{333}{617}\right)=0.184 \qquad (6.20)$$

From 6.20, the mechanical power can be calculated.

$$P_{mech}=\eta_{Stirling}\dot{Q}_{\epsilon}=0.184\times1841=339W \qquad (6.21)$$

This means that 1570W of heat is going into the domestic hot water supply.

The electrical power out at the terminals of the batteries is found through the efficiencies of the alternator, and the batteries.

$$P_{e-batteries}=\eta_{alt}\eta_{bat}P_{mech}=0.6\times0.6\times339=122W \qquad (6.22)$$

Therefore the overall conversion efficiency of the system is:

$$\eta_{sys}=\frac{P_{e\text{-}batteries}}{\dot{Q}_{sun}}=\frac{122}{4200}=0.029 \qquad (6.23)$$

At 3% efficiency, the system conversion of solar energy to electricity is very poor. It does, however, provide large amounts of hot water.

In the course of a day the system described in Appendix 1 will produce 0.84kWhrs of electricity.

7. COLLECTOR TO STIRLING ENGINE HEAT TRANSPORT

7.1 Introduction

With the configuration determined, the choice of heat transport systems could be investigated. There were two options, that would be suitable for the line focus collectors and Stirling engine;

- The use of a pumped single phase working fluid heat transfer system operating in a circuit.
- Heat pipe heat exchangers running along the focus of the troughs.

Presented in this chapter is the comparison between the two systems.

7.2 Heat Pipes

A heat pipe is a very efficient technique for the transfer of heat with a minimal temperature gradient between its heat input and heat output points, while also being very compact for the amount of heat that they can transport.

7.2.1 The Typical Heat Pipe

Heat pipes consist of an evaporator, condenser, a vapour space, and a wick or similar arrangement for returning condensate to the evaporator. (Figure 7.1) All heat pipes have a working fluid within them, which is in equilibrium with an atmosphere normally[1] composed entirely of its own vapour at the vapour pressure corresponding to the temperature of the condenser and evaporator. The working fluids are chosen for their good thermal conductivity, high latent heats, good transport properties, and over the desired temperature ranges, they must not break down thermally, or have too high a vapour pressure. There are many other requirements that are more specific to the particular design of the heat pipe, and the application to which it will be applied.

---

[1] In some heat pipes, inert gases such as helium are added to give some control over the heat pipe's performance, and conductivity.

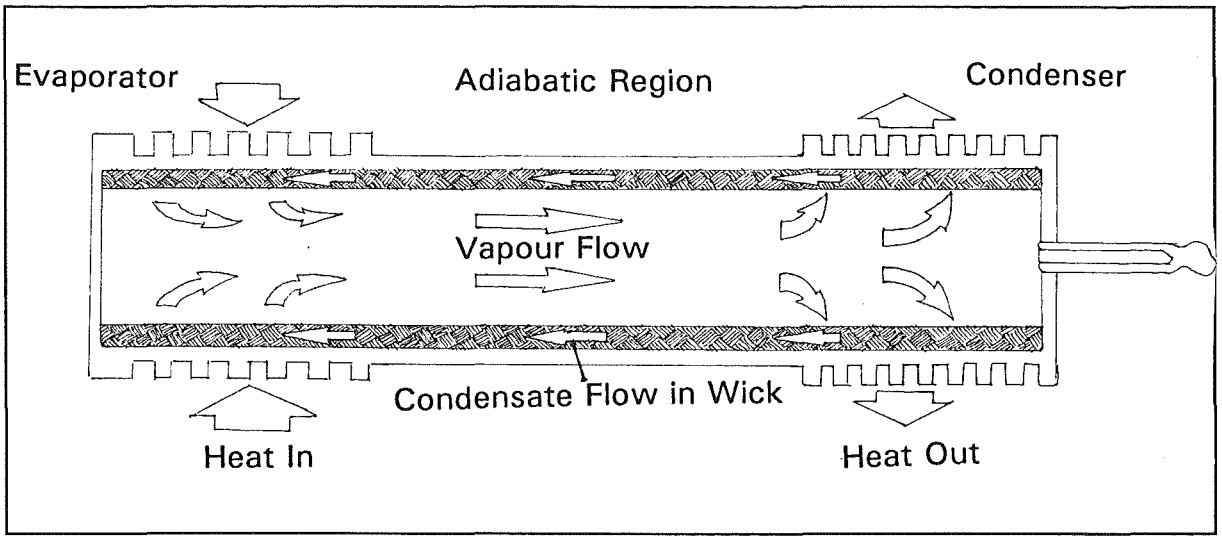

Figure 7.1 A typical Heat pipe.

7.2.2 How the Heat Pipe Works

A heat flux is applied to the evaporator of the heat pipe and boils the working fluid there, which picks up latent heat. Refer to Figure 7.1. The vapour leaves the wick, and joins the vapour flow towards the condenser, which occurs because of the lower pressure present there caused by the vapour in the condenser condensing. Having reached the condenser, the vapour loses its latent heat to the walls of the heat pipe or to whatever cooler surface is present, and enters the wick. Under the action of gravity, or capillary action, the liquid runs back towards the evaporator, to start the cycle again.

Because the heat is transported as latent heat, the temperatures occurring along the heat pipe are very nearly isothermal, while a large amount of heat can be transported by very little fluid. It is this isothermal property that makes the heat pipe very attractive for use with Stirling engines. A major problem with heat exchanger design in Stirling engines is the occurrence of hot spots which can profoundly shorten the life of a heat exchanger. By using a heat pipe, the problem of hot spots can be eliminated because the vapour will not condense on a surface which is hotter than those around it. It is this reason also that has seen so many heat pipes used in the point focus dish-Stirling solar power systems. In the system being designed here, another property of the heat pipe is also being utilised, and that is the ability to act as a thermal transformer, taking a low flux over a large area and transferring it to a high flux over a small area as is found around the

Stirling engine heater heads.

7.2.3 Limits of Heat Pipes

The maximum heat flux that a heat pipe can pass is governed by a number of factors and limits which are dependent on the properties of the working fluid, and therefore the temperature of the pipe (see Figure 7.2). If the temperature is low compared to the normal operating temperature of a heat pipe charged with a particular heat transfer fluid, then the *Sonic Limit* is the major limiting factor. At the low temperatures, the vapour is of a very low density and so, to carry a given amount of heat, the vapour needs to travel faster than it would at a higher temperature when the vapour density would be higher. If the heat flux is too high, the vapour will reach sonic velocities and this will limit the heat flux. Upon start up of a heat pipe, large axial temperature gradients can occur due to this, however as the evaporator temperature increases, so the vapour density increases, and the sonic limit also will increase until another limit becomes the dominant factor.

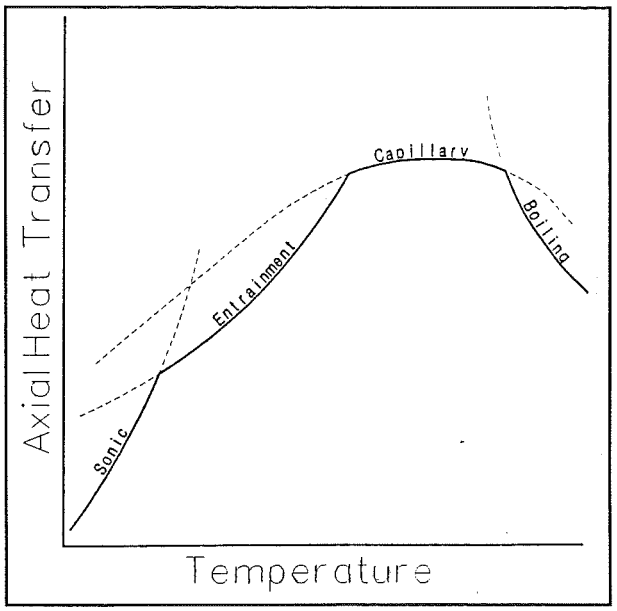

Figure 7.2 Heat transport limitations in heat pipes.

The following are two expressions for the sonic limit of a heat pipe:

$$\dot{Q}_{sonic}=0.474A_{vap}\lambda\sqrt{\rho_v P_v} \qquad (7.1)$$

(P.D.Dunn 1982) and alternatively

$$\dot{Q}_{sonic}=\frac{a\lambda\rho_v}{\sqrt{2(1+\gamma)}}A_{vap} \qquad (7.2)$$

(G.Rice 1984) where *a* is the speed of sound in the vapour and is given by:

$$a=\sqrt{\gamma RT_v} \tag{7.3}$$

Here A_{vap} = cross-sectional area of the vapour space (m^2)
λ = latent heat of vaporisation
ρ_v = the vapour density
P_v = the vapour pressure
γ = the vapour specific heat ratio which has the value 1.67, 1.4, and 1.33 for monoatomic, diatomic, and polyatomic vapours respectively.
T_v is the vapour temperature which under steady operating conditions, is close to the temperature of the evaporator wall
R is the gas constant of the working fluid which can be found by dividing the universal gas constant R_o = 8.314 J/K mol by the working fluid's molecular mass.

As the vapour density increases, the problem of sonic velocities occurring reduces, but if the vapour flow velocity is high enough, it can pick up liquid from the wick and blow it back to the condenser, interrupting the return flow of condensate, and allowing the evaporator to dry out. This is the *entrainment limit*. This is influenced by the type of wick used. A wick consisting of axial grooves is very prone to this problem, whereas a fine wrapped screen wick is not. The expression for the maximum rate at which heat can be transferred when the entrainment limit is dominant, is:

$$\dot{Q}_{ent}=A_{vap}\lambda\sqrt{\frac{\sigma\rho_v}{2r_{hs}}} \tag{7.4}$$

(S.W.Chi 1976) σ = the surface tension of the liquid.
r_{hs} = the wick surface pore hydraulic radius.

Eventually the vapour density is sufficiently high that it can travel relatively slowly to transfer the same amount of heat. However the limiting factor in this case is the ability of the wick to return the liquid to the evaporator fast enough, and is known as the *wicking limit*, or the *capillary limit*. This depends on the nature of the wick, the slope of the heat pipe, and the properties of the fluid which will influence its capillary pumping capabilities, and flow characteristics. The expression presented here is a simplistic method, and it is recommended that

S.W.Chi 1976 is a good reference for more general expressions.

$$\dot{Q}_{wick}=\frac{A_{wick}K\lambda\rho_l}{L_{eff}\mu_l}\left(\frac{2\sigma}{r_{hs}}-\rho_l gL\right) \tag{7.5}$$

(G.Rice 1984) where:

A_w is the cross-sectional area of the wick.
ρ_l the liquid density.
μ_l the liquid viscosity.
g is the acceleration due to gravity.
L is the total heat pipe length, and is given by: $L=L_{evap}+L_{adiabatic}+L_{cond}$
L_{eff} is the effective heat pipe length, given by: $L_{eff}=\frac{1}{2}L_{evap}+L_{adiabatic}+\frac{1}{2}L_{cond}$
L_{evap} is the length of the evaporator region.
$L_{adiabatic}$ is the length of the adiabatic region.
L_{cond} is the length of the condenser region.

The factor K is the permeability of the wick in the direction of the liquid flow, and is given by:

$$K=\frac{d_w^2\varepsilon^3}{122(1-\varepsilon)^2} \tag{7.6}$$

d_w is the diameter of the screen wire, and ε is the porosity of the wick. For a wrapped screen wick:

$$\varepsilon=1-\frac{\pi N d_w}{4} \tag{7.7}$$

and N is the number of apertures per unit length of the mesh screen.

Eventually the boiling in the evaporator becomes sufficiently vigorous for the vapour forming to hold the flow of liquid away from the evaporator wall, and so the wall temperature begins to rise much higher than the vapour temperature. This is the *boiling limit*. The expression for simple prediction of the boiling limit is given by S.W.Chi 1976:

$$\dot{Q}_{boil}=\frac{2\pi L_{evap}k_{eff}T_v}{\lambda\rho_v \ln\left(\frac{r_i}{r_v}\right)}\left(\frac{2\sigma}{r_n}-P_c\right) \tag{7.8}$$

P_c is the capillary pumping pressure which may be approximated by:

$$P_c=2\sigma/r_{hs}.$$

r_i = the internal radius of the pipe.
r_v = the vapour core radius.
r_n = the nucleation radius of the vapour bubbles. This has been found experimentally to be between 2.5×10^{-8} and 2.5×10^{-7}m for a very clean heat pipe, however for a conservative estimate the value is recommended to be within the range 2.5×10^{-5} and 2.5×10^{-7}m (S.W.Chi 1976).
k_{eff} is the effective thermal conductivity of the liquid saturated wick, and is approximated by the following expression:

$$k_{eff} = \frac{k_l[(k_l+k_w)-(1-\epsilon)(k_l-k_w)]}{[(k_l+k_w)+(1-\epsilon)(k_l-k_w)]} \qquad (7.9)$$

where k_l is the liquid thermal conductivity.
k_w is the wick material thermal conductivity (Wrapped wire screen wick).
ϵ is the volume fraction of liquid which is the ratio of the liquid volume, to the total volume of the saturated wick.

Not all of the limits described will be relevant to an individual heat pipe because of the nature of the design, the wick used, or the working fluid properties. In the case of a mercury heat pipe, the capillary limit would be very significant if the pipe were horizontal or working against gravity, because the contact angle of mercury would not allow the liquid to wet the wick. However if it is operated as a gravity assisted heat pipe, the wicking limit would no longer be a problem. Still with the example of mercury, it is prone to the boiling limit when operating at high temperatures because of its inability to wet the heated surface allowing a vapour film to form very easily between the liquid and the wall.

7.2.4 Form of the Heat Pipe

The use of the two stage line-focus solar concentrator means that the heat pipe evaporator will have to be long and circular in cross-section because of the tracking requirements. The condenser around the Stirling engine can be a number of different forms, preferably of such a design to allow the condensation to occur directly on the hot end heat exchangers. Further form design depends on the working fluid. As the heat pipe is to be quite long (3.5m out each side of the unit for the 200W test rig), capillary action would not be strong enough for returning the condensate to the evaporator, and so gravity return or mechanically pumped

return were the only options. Since gravity is free, reliable, and simple to use, this was the option chosen. To this end, the Stirling engine was designed to be held upside down with the condenser space collecting the condensate and returning it via a down tube to the evaporator. (Figure 7.3)

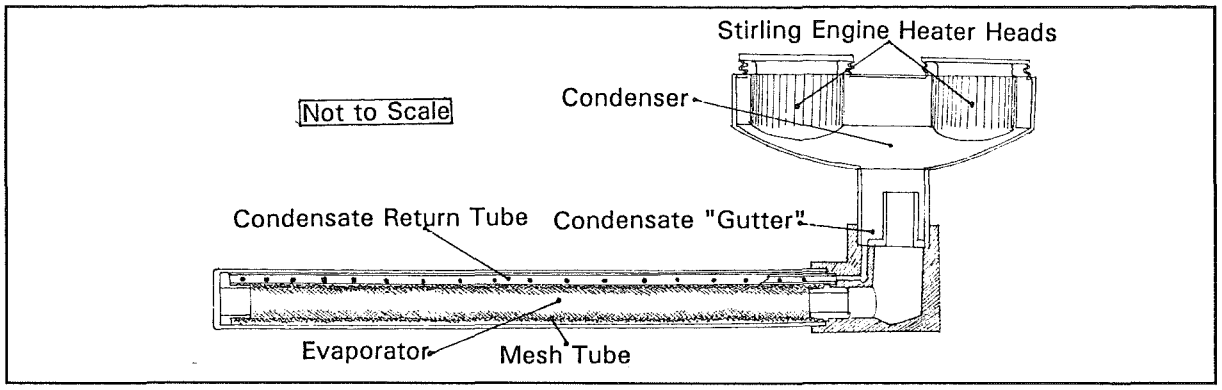

Figure 7.3 Heat pipe arrangement for the Solar-Stirling power system based on a two stage concentrator, and a DMC5 Stirling engine.

One of the main disadvantages of the heat pipe in this particular application is its vulnerability to leaks. If a leak should occur in a heat pipe system, the pressure inside the pipe will become atmospheric which, depending on the working fluid could either shut the device down or cause it to fail catastrophically should some reaction with air take place. The other main difficulty exists in trying to find a suitable working fluid. In the range 200°C to 500°C there are very few suitable working fluids.

For control of the heat pipe in emergencies such as the need to shut it down fast, and dump some of the heat if it is a particularly hot day, the possibility of adding a small water pipe around the heat pipe exists. This would be empty most of the time, but should the system controller need to suddenly cool the system it would turn the collectors away from the sun, and run water from the domestic hot water supply into the cooling tube.

7.3 Single Phase Circuits

Here the working fluid is pumped around a circuit picking up heat from the concentrators with a corresponding rise in temperature as it passes through the absorber, and then losing the heat to the Stirling engine working fluid. Figure 7.4 shows an impression of a pumped single phase heat transfer circuit.

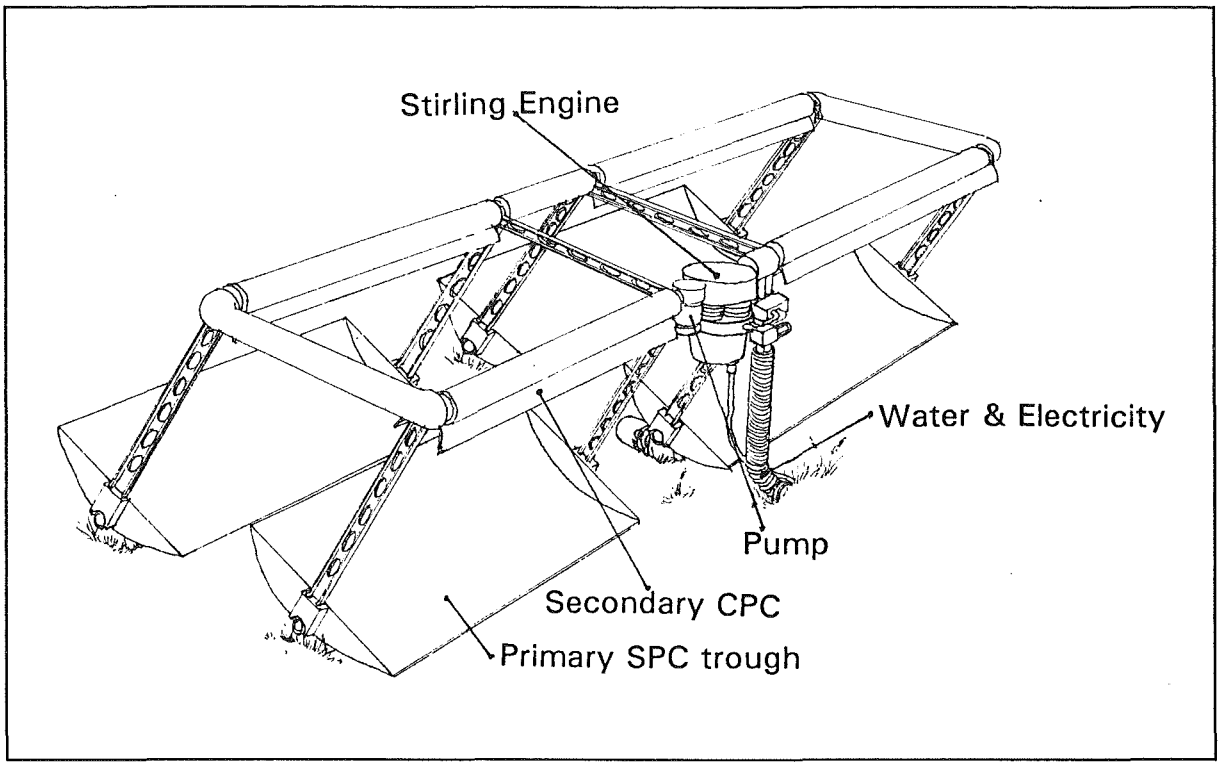

Figure 7.4 A solar-Stirling system based on a circulating single phase working fluid.

The requirements for the working fluid in this system are a lot less demanding than for a heat pipe, and there are a number of commercial fluids that would be suitable. The main draw-backs are:

- that the mass flow rate has to be quite high relative to the heat pipe to transport the same amount of heat, and so a pump must be used. This is an added load for the Stirling engine and therefore makes the system even less efficient.
- although the heat exchanger design at the absorber is very straight forward (being just a tube, due to the lower heat flux.), the Stirling engine heater must be designed very carefully to avoid any large temperature drops occurring between the circuit working fluid and the Stirling cycle working fluid, and also to avoid large pressure drops that would cause the pump to have to work harder to overcome the resistance.
- compared to a heat pipe, the amount of working fluid in the system is much larger and this has the disadvantage of having a larger thermal mass. With a system that is heated up in the morning and cools off over night, this would be quite undesirable because of the waste of useful generating time, as the fluid

temperature heats up or cools off through the temperature ranges that the Stirling engine cannot operate at.

With the single phase system, the problems of sealing are not as critical as that for the heat pipe, especially if the working fluid is chosen such that its vapour pressure is below atmospheric at the operating temperature. Should the need arise to suddenly cool the system, a similar system as for the heat pipe could be used, or a valve could be used to run some of the fluid into a radiator, or to a water heater.

7.3.1 Stirling Engine Heater Head Configurations

A number of different configurations of heat exchanger were considered. However a major restriction was the fact that the DMC5 Stirling engine already existed, and so the size and shape of the heat exchangers would have to fit this. Two main types existed, these were, the external heat transfer fluid flow path type, and the use of an "internal radiator" which would be included within the Stirling engine gas flow paths. These are shown in Figure 7.5.

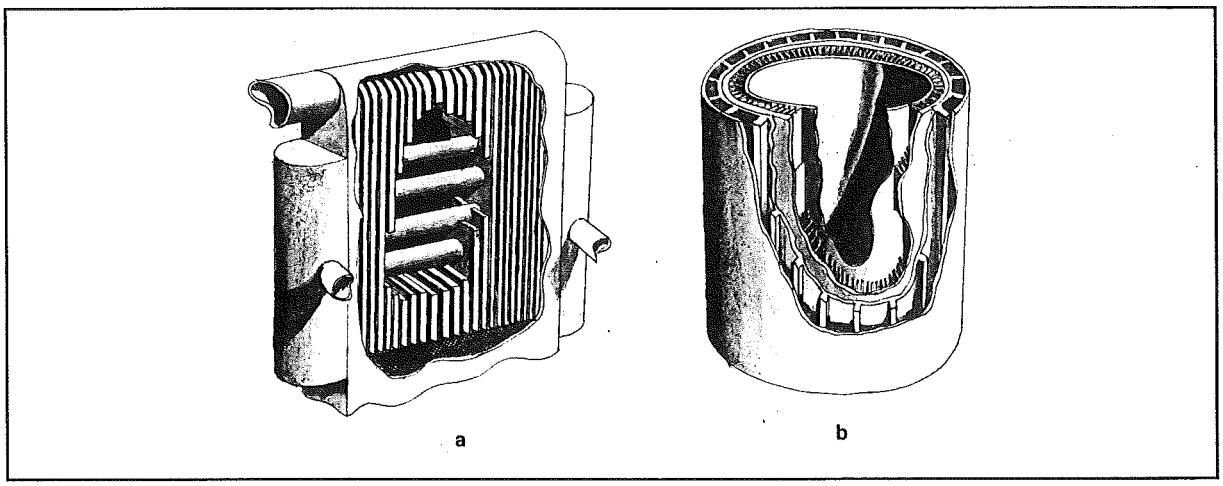

Figure 7.5 Different forms of Stirling engine heat exchanger. **(a)** "Internal Radiator" heat exchanger, **(b)** Heat transfer fluid flow paths outside the cylinder.

The two systems when compared had very little difference between them with regard to performance, but the system using the external heat transfer paths, though having a slightly poorer heat transfer coefficient, is closer to the existing Stirling engine design, and so was the chosen form. The calculations used to determine the temperature drops were based on steady flow conditions, and so not

of any high accuracy, but were sufficient for obtaining approximate figures. The calculations were based around the heat flow into one cylinder. The working fluid that was used for the calculations was Marlotherm S, a mixture of isomeric dibenzyl toluenes.

With the rough estimate system used, the heat transfer from the heat transfer fluid to the Stirling engine cylinder wall produced a temperature drop in the region of 20°C to 30°C (Appendix 11).

A program was written to start evaluating the temperature drop between the heat transfer fluid, and the Stirling engine working fluid, to a greater accuracy, but was never completed because of the return to looking at the heat pipe systems.

7.4 Conclusion

With its greater heat transfer capability, lower thermal mass, isothermal properties, and with gravity condensate return, the heat pipe system was the final system chosen. This made for a system that could be manufactured relatively easily, would start quickly, and would work efficiently. However the working fluid was still unknown.

8. HEAT PIPE WORKING FLUIDS

8.1 Introduction

In the temperature range 300°C to 550°C there are very few suitable working fluids for heat pipes available. This chapter will look at what properties make a good working fluid, and the subsequent selection of candidate working fluids for the Solar-Stirling power system.

8.2 Properties of Heat Pipe Working Fluids

Listed below are the qualities that a working fluid must have to be used in a standard heat pipe. However not all of these qualities need to be met in the case of heat pipes with gravity condensate returns or pumped condensate returns.

- High latent heat of vaporisation. This is very important because it is this that determines the amount of heat that a given mass of fluid can transport,and therefore the velocity that the vapour must flow at.
- High thermal conductivity. This helps the heat transfer between the pipe wall, the wick, and the fluid. At lower temperatures, the only working fluids are organic compounds and water, neither having very good thermal conductivities.
- High surface tension. For ordinary heat pipes, this is particularly important, because it limits the length of the heat pipe, and the amount of rise it can work against, as capillary pressure is dependent on the surface tension. In the case of thermosyphons, it is important in that it affects the entrainment limit (Section 7.2.3), because it is the surface tension that keeps the liquid from being blown out of the wick.
- Good wetting behaviour. Of very high importance within ordinary heat pipes because of the use of capillary action to return the condensate, but also important within the thermosyphons in that it will affect the boiling behaviour of the fluid. With a non-wetting fluid, the formation of vapour will allow the liquid to break contact with the heat pipe wall and therefore reduce the heat transfer. This is a serious problem for mercury.
- A low viscosity in both the vapour and liquid phases. This allows the condensate to return easily and quickly and the pressure losses in the vapour flow to be minimal.
- Vapour pressure must not be too high or too low over the desired operating temperature range. If it is too high, material problems may occur in trying to hold the high pressure, as well as there being the danger of an explosion should the pipe fail. If the vapour pressure is

low, it will cause problems with the sonic limit because the vapour, being of a very low density, would have to travel at high velocities to transfer the desired amount of heat.

- Compatibility between the fluid and the wick, and wall materials. One of the major causes of heat pipe failure, is the gradual erosion or weakening of the heat pipe wall or wick material by reaction with the working fluid. The heat pipe can fail by the build up of reaction products in the evaporator, or by the loss of pressure.
- The freezing point must be compatible with the desired operating temperature as it affects the time taken for a heat pipe to start up. It is conceivable that a heat pipe with a frozen working fluid could boil off the working fluid in the evaporator successfully, only to have it freeze at the condenser, and not return at all, thereby quickly causing the evaporator to dry out.
- High liquid density. This means that the liquid flows in the wick will be slow, and so the pressure losses will be less.

8.3 Comparing Working Fluids

For the purposes of finding a suitable working fluid for a given application at a certain temperature, a "Merit Number" (Dunn & Reay 1982) can be used. This is a grouping of property values in such a way that the higher the merit number the better suited the candidate fluid is for the proposed application. For ordinary heat pipes it is given by Dunn & Reay as;

$$M=\frac{\rho_l \sigma \lambda}{\mu_l} \qquad (8.1)$$

where M is the merit number, ρ_l = liquid density, σ is the surface tension, λ = the latent heat of vaporisation, and μ_l is the viscosity of the liquid. Using this expression produces a graph like Figure 8.1 when several working fluids are plotted against temperature. Units of the Merit number M are, kW/m², a flux measure.

However for the system devised here, the ideal properties of the working fluid are a little different with different priorities. Working with a gravity return and no porous wicks, the wetting behaviour of the fluid is less critical (This was not accounted for in 8.1 anyway), and the surface tension was not so critical for the same reasons. As with the above expression a high liquid density and heat of vaporisation were of importance as well as a high liquid thermal conductivity k_l because of the need to keep all temperature drops to a minimum. Keeping the liquid viscosity low and the vapour pressure P_v low were also of high importance,

though the vapour pressure should be kept within reasonable limits so as not to cause the sonic limit to become a problem. To allow the heat transfer system to be able to respond quickly to changing heat inputs, a low liquid specific heat capacity c_p was of importance. This yielded a pair of new merit numbers (8.2). The units of $Merit_1$ are m^2/s^2K, and $Merit_2$ is a dimensionless group.

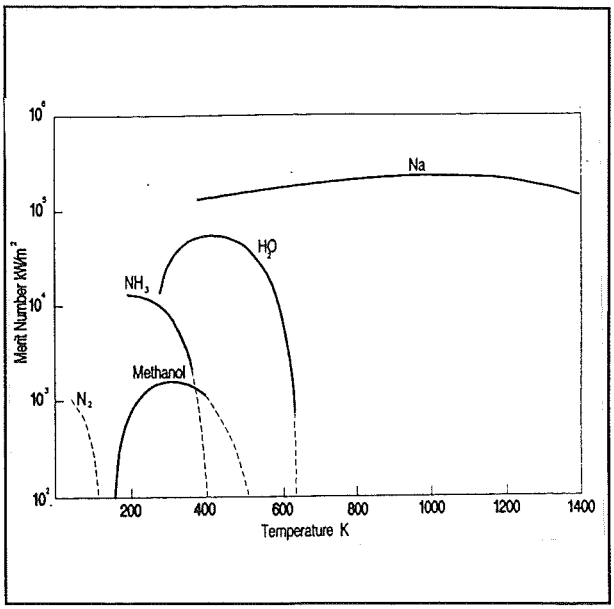

Figure 8.1 Merit Number of Selected Working Fluids (Dunn & Reay 1982)

$$Merit_1 = \frac{\rho_l \lambda k_l}{P_v \mu_l} \qquad (8.2)$$

$$Merit_2 = \frac{\rho_l \lambda k_l}{P_v \mu_l c_p}$$

It was these two merit numbers that were used to determine the candidate fluids for this project. The merit numbers were calculated using candidate fluid's property values at the predicted system operating temperature

8.4 Selection of the Candidate Fluids

Finding tables of thermal properties and transport properties of a large number of chemicals is a problem, and so any search for a good working fluid will be limited by the information available. However a search through chemical data books produced a list of possible working fluids, through consideration of the melting points and boiling points. Having narrowed the field somewhat, the merit numbers were used to select out a number of chemicals that showed suitable characteristics for use in a gravity assisted heat pipe. The following table is for the working fluids at 330°C.

TABLE 8.1 Merit Numbers for Candidate Materials at 330°C

Properties Working Fluid	Liquid Density kg/m³	Vapour Pressure Pa	Latent Heat Vaporisation J/kg	Liquid Therm. Cond W/mK	Liquid Viscosity Pa.s	Liquid Specific Heat Capacity J/kgK	merit1 m^2/s^2K	merit2
Potassium	765.8	84.78138	2188093	41.5904	0.0002178	768.8893	3.774E+12	4909000000
Mercury	12832.78	58513.05	296722.6	11.9438	0.0009028	135.3152	860933507	6362430.14
Benzyl Benzoate	811.062	107966	274947	0.08711	0.000107	2245.4	1681513.13	748.870194
1-Nonyl Naphthalene	707.8233	46001	245202	0.07668	0.0002109	2723.8	1371788.36	503.630356
Linoleic Acid	660.6771	51069.95	263731.8	0.085186	0.0002313	2924.585	1256547.51	429.649851
Dihexyl Adipate	644.7184	62593.02	218927	0.05707	0.0001285	2614.655	1001493.72	383.030923
Dibenzyl Ether	773.3661	236105	248577	0.076166	0.0001	2488.651	620157.553	249.194264
Diisodecyl Phthalate	763.3877	4654.74	199641	0.055872	0.003	2565.199	609778.953	237.712143
1-Decylnaphthalene	703.878	35038.32	242668.6	0.07594	0.0006606	2729.081	560402.062	205.344606
Tridecyl Benzene	610.4744	75117	228378	0.064482	0.0002884	3004.649	414979.583	138.112499
Dodecyl Benzene	624.3343	100058.8	230897	0.06459	0.000251	2984.499	370741.974	124.222516
Tetraethylene Pentamine	735.6824	85440	401692	0.09435	0.0008928	3343.74	365519.063	109.314439
Dodecyl Thiol	590.6232	281601.6	223111.7	0.06882	0.0001558	2928.302	206702.126	70.587708
Oleic Acid	668.6725	44047.66	267935.5	0.03	0.0004012	4552.036	304145.371	66.8152384
1,1-Diphenyl Ethane	728.1318	280887	248098	0.082	0.0011893	2531	44342.8963	17.5199116
Sulphur	1684.106	12526	297405	0.17056	0.6078579	1068.413	11219.6783	10.5012559
Dibutyl Phthalate	731.7439	75592.29	231759.8	0.09126	0.0160927	2411.353	12722.465	5.27606908
Dioctyl Phthalate	740.2474	24822.15	206769	0.09186	0.1039442	2611.489	5449.40521	2.08670425

As can be seen from the data in table 8.1, the best working fluid according to the merit numbers is potassium; however at this low temperature, the vapour density is too low, and the sonic limit is extremely restrictive. However, in the initial calculations for the system, the working temperature was calculated to be 420°C which meant that potassium was even more favourable, and the sonic limit less of a problem. In the table above, the second best material was mercury, which has poor wetting characteristics, but was still suitable, although its toxicity is a problem. Should a mercury heat pipe operating at 330°C fail, it will have a pressure below atmospheric inside it, and so it would shut down, and would not send jets of vaporous mercury into the atmosphere. Benzyl Benzoate, an organic compound used for flavouring chewing gum, a perfume solvent, fixative, and insect repellent, is suited to working as a heat pipe working fluid, despite its poor thermal conductivity. A problem was foreseen in that it has an autoignition temperature at 753K, but testing under heat pipe conditions was needed to confirm it. Near the bottom of the list is sulphur. The merit number here is for pure sulphur and its unusual viscosity behaviour makes it unsuitable if used on its own. A common classroom experiment in high school is to add iodine to sulphur which keeps its viscosity low as it heats up (Further explanations can be found in Chapter 9). And so at higher temperatures, with iodine present, sulphur becomes a reasonable heat pipe candidate material. At the higher temperatures calculated in the initial test,

Diisodecyl phthalate turned out to be a very suitable candidate material, but it had a problem with the operating temperature being very close to the autoignition temperature.

8.5 Selected Program of Testing

Because of its non-toxicity and its recommendation in various texts (Dunn & Reay 1982, D.L.Timrot *et al* 1981) it was decided that a sulphur-iodine heat pipe should be tested first as a proof of concept. This would be followed by the testing of a Dioctyl phthalate heat pipe. The use of Dioctyl phthalate (DOP) over Diisodecyl phthalate (DIDP) was to assess whether the working fluid would break down at the elevated temperatures, and because the DOP was easier to obtain, while also having a similar autoignition temperature, and molecular structure. The tests from this would give an indication of the feasibility of using Benzyl Benzoate. Tests on mercury would follow if the organic DOP failed. Potassium was not considered until very late in the project because of the problem with the sonic limit.

9. THE SULPHUR HEAT PIPE

9.1 Introduction

Over the 300°C to 600°C temperature range, there are very few working fluids available that will be able to last for long periods of time, and have a good heat transfer coefficient. Most of the organic fluids break down rapidly at these elevated temperatures, forming lighter fractions which separate out and cause large axial temperature gradients. This would also mean that the heat pipe would have to be recharged at regular intervals, a process that could generate considerable amounts of toxic chemical waste. Boiling limitations are also a problem at these temperatures, with the organic fluids boiling so rapidly, that they begin to form a layer of vapour adjacent to the wall which effectively insulates the liquid, and leads to large temperature drops between the evaporator surface and condenser. Liquid metals on the other hand are generally unsuitable because their vapour pressure is too low, and so sonic velocities can occur within the pipe. A sulphur-iodine heat pipe was therefore constructed to test its suitability for use in a Solar-Stirling application.

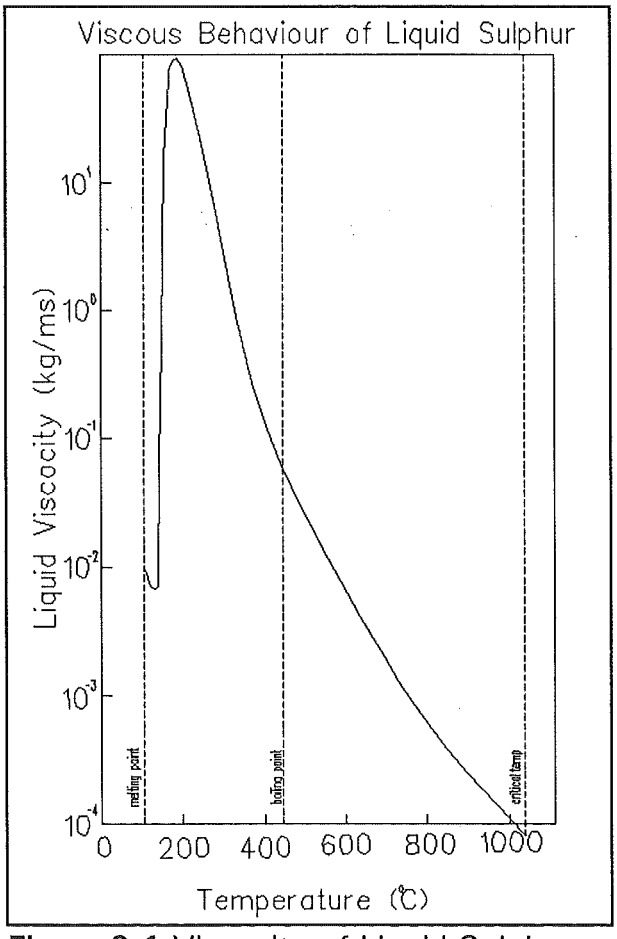

Figure 9.1 Viscosity of Liquid Sulphur

9.2 Sulphur as a Heat Pipe Working Fluid

Timrot *et al* (1981) and Polasek (1976) proposed sulphur as a possible working fluid for the 300°C-600°C temperature range. Use of Chrome-Aluminium alloys were also proposed to overcome the problem of Sulphur

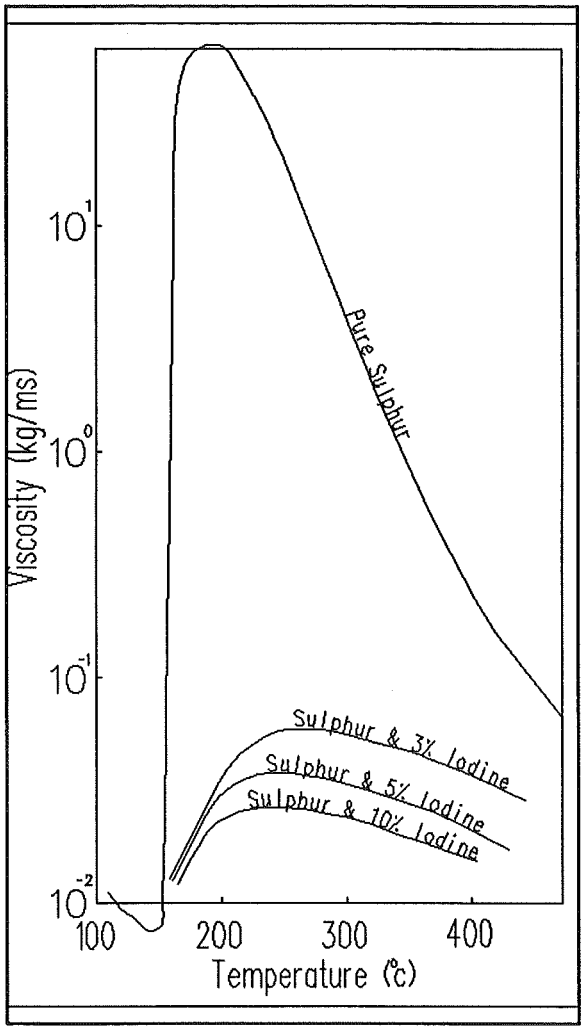

Figure 9.2 Viscosity of Sulphur-Iodine mixture with Temperature.

forming a low melting point Eutectic with Nickeliferous steels. The advantage of sulphur was its non toxicity, cheapness, and the fact that being a pure element, it would not thermally decompose or otherwise break down. The major disadvantage of Sulphur is a feature of its physical behaviour. Sulphur melts from its yellow crystalline S_8 rings at 115°C and becomes a fluid with a very low viscosity, also comprised of S_8 rings. As the fluid is heated further, from 160°C to 190°C the viscosity rises very rapidly (See Figure 9.1). Thereafter, further increases in the temperature cause the viscosity to gradually decrease until it returns to the original level at about 330°C. The reason for this abnormal behaviour is due to the S_8 rings breaking and linking together to form long chains which tangle and cause the sharp increase in the viscosity. The chains break down after 190°C into S_4, and S_3.

During start up on days of low insolation, this would be a very serious problem because of the lack of liquid return that would occur, leading to a burn out condition within the evaporator. The addition of iodine causes the chains that form to be terminated by the iodine atoms, thereby keeping them short, and so the viscosity is kept low. The addition of 6% Iodine to a charge can reduce the viscosity from about 27 kg/ms to 0.07 kg/ms at 250°C. Using different proportions of Iodine changes the degree to which the viscosity is modified(See Figure 9.2).

9.3 The Test Heat Pipe

9.3.1 Construction

The sulphur heat pipe (Figure 9.3) built was a simple wickless heat pipe made from hydraulic steel tube with an internal diameter of 20mm. End caps were welded on along with the filler tube which was a length of 6mm OD seamless hydraulic tube. Into the pipe was put 2.25g of Iodine, and 45g of Sulphur, making a mixture of 5%Iodine by weight. The pipe was temporarily sealed and heated to just above the melting point of the sulphur to allow the iodine to mix into the sulphur and reduce the amount lost to sublimation during filling. Having let the

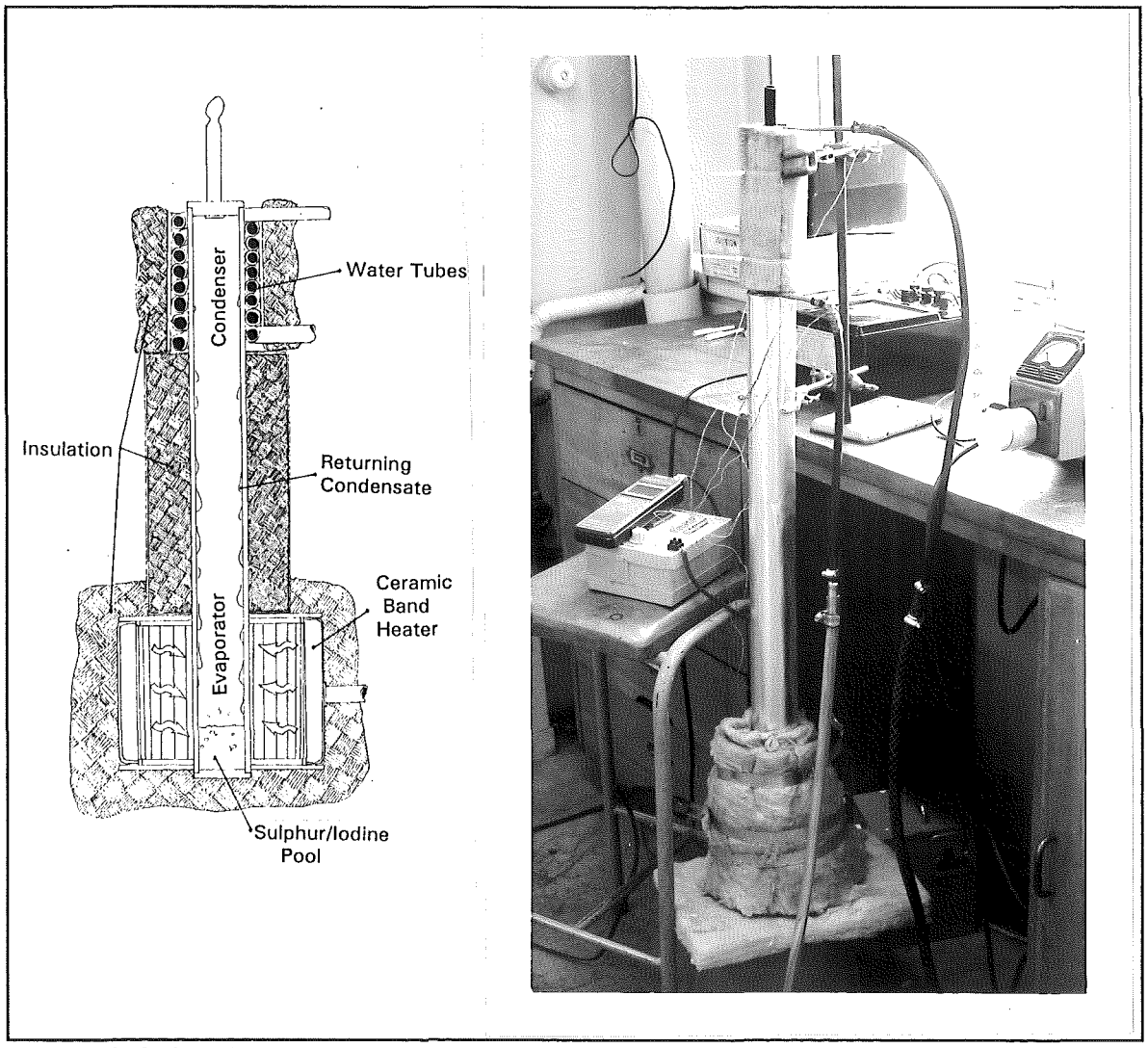

Figure 9.3 Sulphur heat pipe and photograph of the sulphur heat pipe rig.

mixture freeze again, the heat pipe was transferred to an evacuation line, evacuated, and its filler tube pinched off. An initial test showed that a heat front did progress up the pipe but stopped advancing a considerable distance from the top, indicating the presence of non-condensing gases. The pipe was allowed to cool to ambient temperature and opened up. During the reevacuation, gas was drawn off some of it being identified as H_2S. Another test had the heat pipe heating to its very end, so rig insulation and instrumentation could proceed. A ceramic-insulated band heater with a variac provided the heat source for the test rig, relying on radiant heat transfer. A wrapped water tube around the condenser with thermocouples on the inlet and outlet provided the calorimetry. After the attachment of a number of thermocouples, the entire pipe was insulated.

9.3.2 Experiments and Results

The first test with a 700W heat input showed that nothing happened until the evaporator surface reached 180°C, then a very steep thermal gradient began moving up the pipe towards the condenser, isothermalising at 350°C when the heating source was turned off. The isothermal region is represented by an almost flat plane in the temperature/time/distance graph as seen in Figure 9.4.

The total amount of heat transfer through the heat pipe was 390W, as determined by the calorimetry. The remaining 310W were lost through the heater surround, and insulation.

As can be seen from the xyz-plot the heat pipe (Figure 9.4) did not isothermalise very well, having a considerable temperature drop along its length of 150K. A very steep thermal gradient existed between the last thermocouple in the adiabatic region, and the condenser thermocouple. Also noticeable is the local peak temperature that occurred at about the same time as the heat front reached the condenser which coincides with a localised temperature peak at the condenser as well. This phenomenon can be easily seen in all subsequent test runs.

In operation, the sound produced by the heat pipe was a very harsh and crisp "pinging" as would be expected with a good vacuum and with a low viscosity fluid.

The second experiment was a repeat of the first to check whether the peak

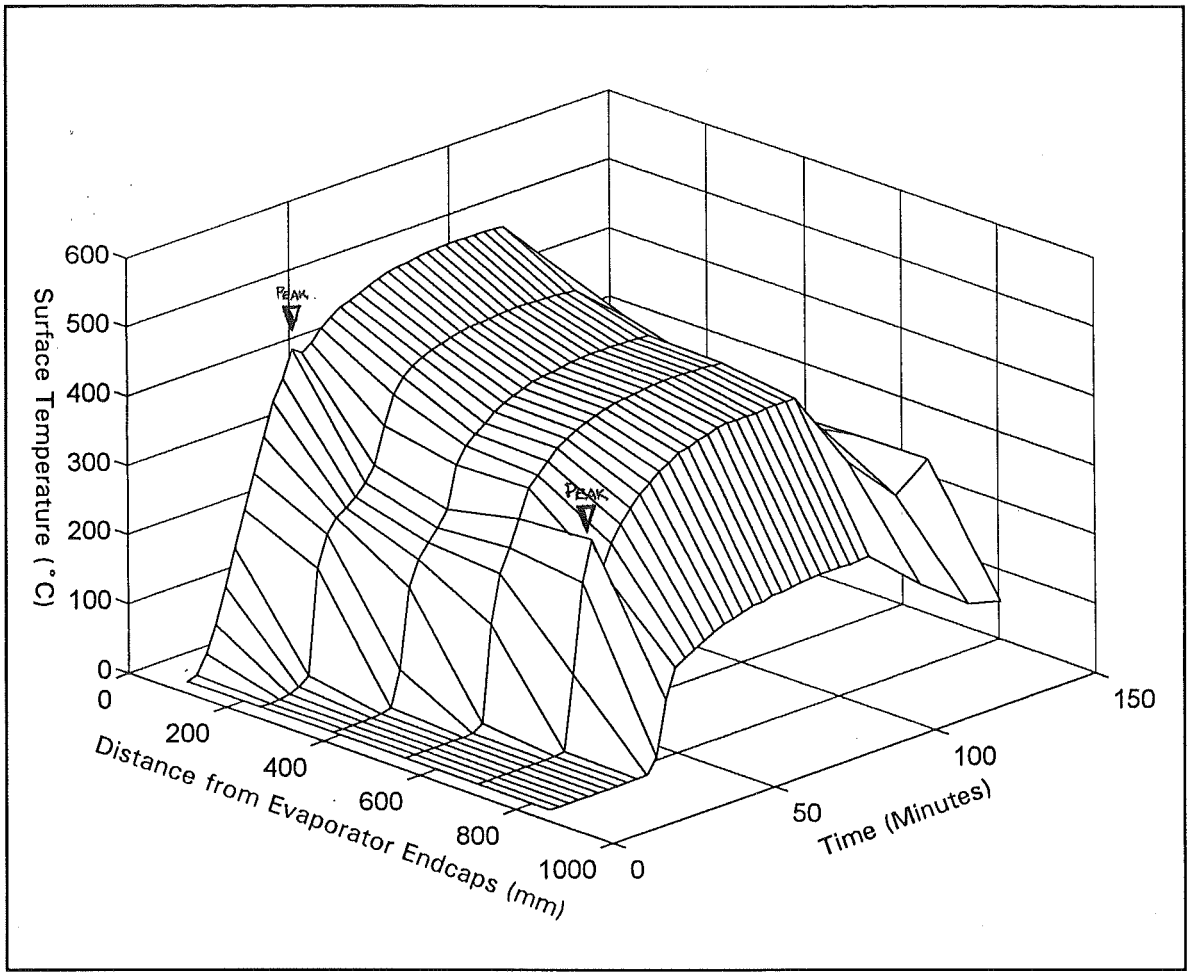

Figure 9.4 Sulphur heat pipe performance at 390W transferred, and water cooling.

observed in the first test run was a repeatable phenomenon, and to observe any degradation of the performance with time. (Figure 9.5) Again, 390W of heat was transported through the heat pipe. This time the maximum temperature was lower, the axial temperature drop slightly larger, and the local peak even more pronounced, indicating that some degradation of the working fluid had taken place. As sulphur cannot thermally decompose as organic working fluids do, it had to be reacting with chemicals on or in the heat pipe walls, to form noncondensing gases, or losing the iodine from solution.

Again, careful note was taken of the sound of the heat pipe. It started a crisp "popping" at 120°C which continued until the evaporator reached 250°C whereupon the sound became dulled. This would mainly indicate the steady increase in

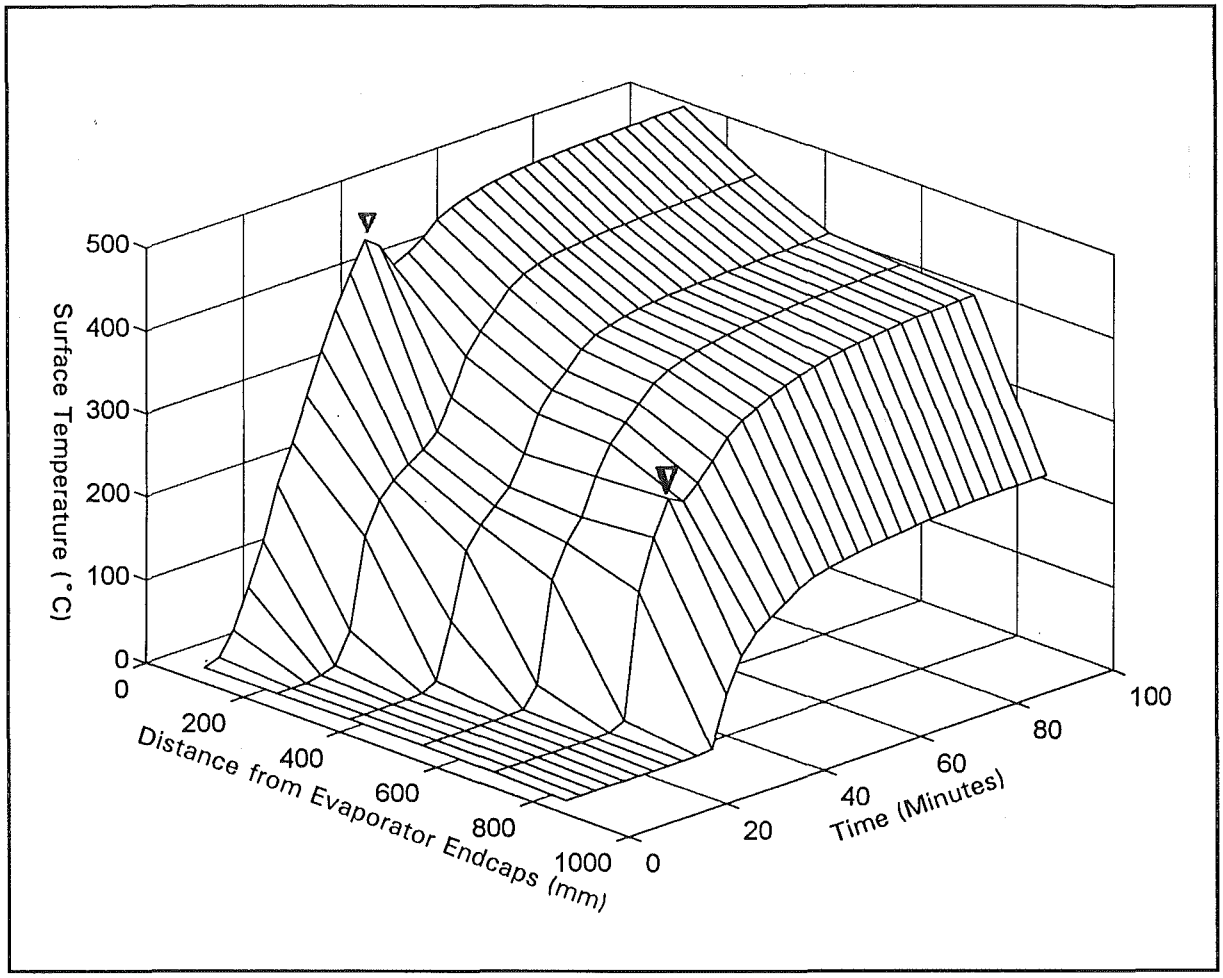

Figure 9.5 Sulphur heat pipe transporting 390W. Repeatability test for the first experiment.

vapour over the boiling pool which would serve to dampen the sound.

With the third experiment shown in Figure 9.6, the heat pipe was run with 500W heat input. The calorimetry showed that 280W of heat was passing through the heat pipe when its temperature had stabilised after a hour of operation. The temperature peak experienced in this run was much more pronounced than the previous two tests, and the axial temperature gradient was again 150K of having a very clear boiling sound, the heat pipe has a muffled sound for the duration of the test. The lower heat flux causing the liquid to boil less vigorously, and the possibility of non-condensing gases increasing would help explain this.

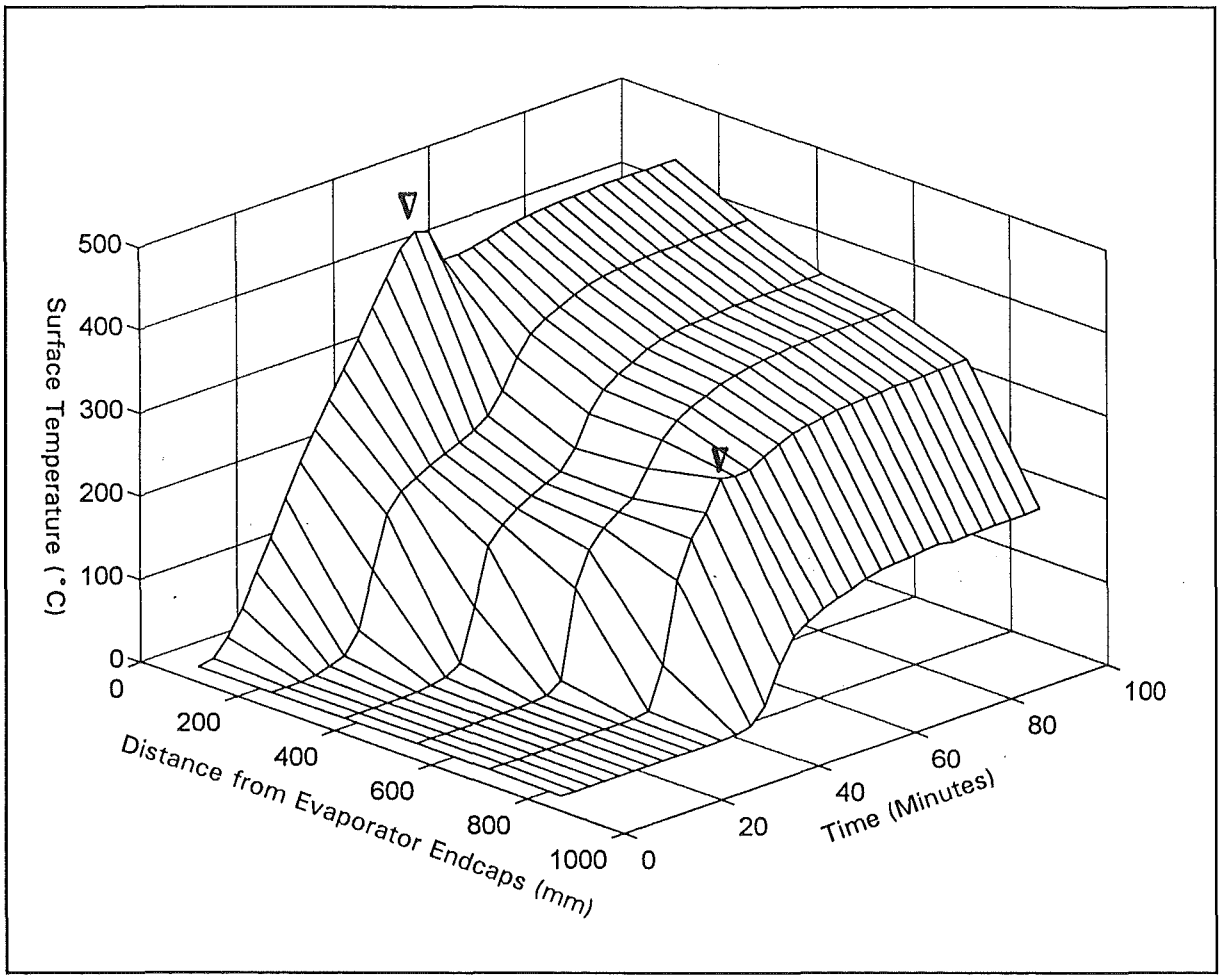

Figure 9.6 Sulphur heat pipe with 280W being transported, and water cooling applied to the condenser.

Figure 9.7 shows the temperature\time\distance plot for the heat pipe operating with only natural air convection cooling and with a 700W electrical input to the heater. The heat pipe was heated at 700W, and then held for a short time at 300W before turning the heater off. The highest temperature was maintained with the electrical input to the heater being 300W. The drop in temperature evident after the maximum temperature was reached was from monitoring and recording the temperatures after the heater had been turned off.

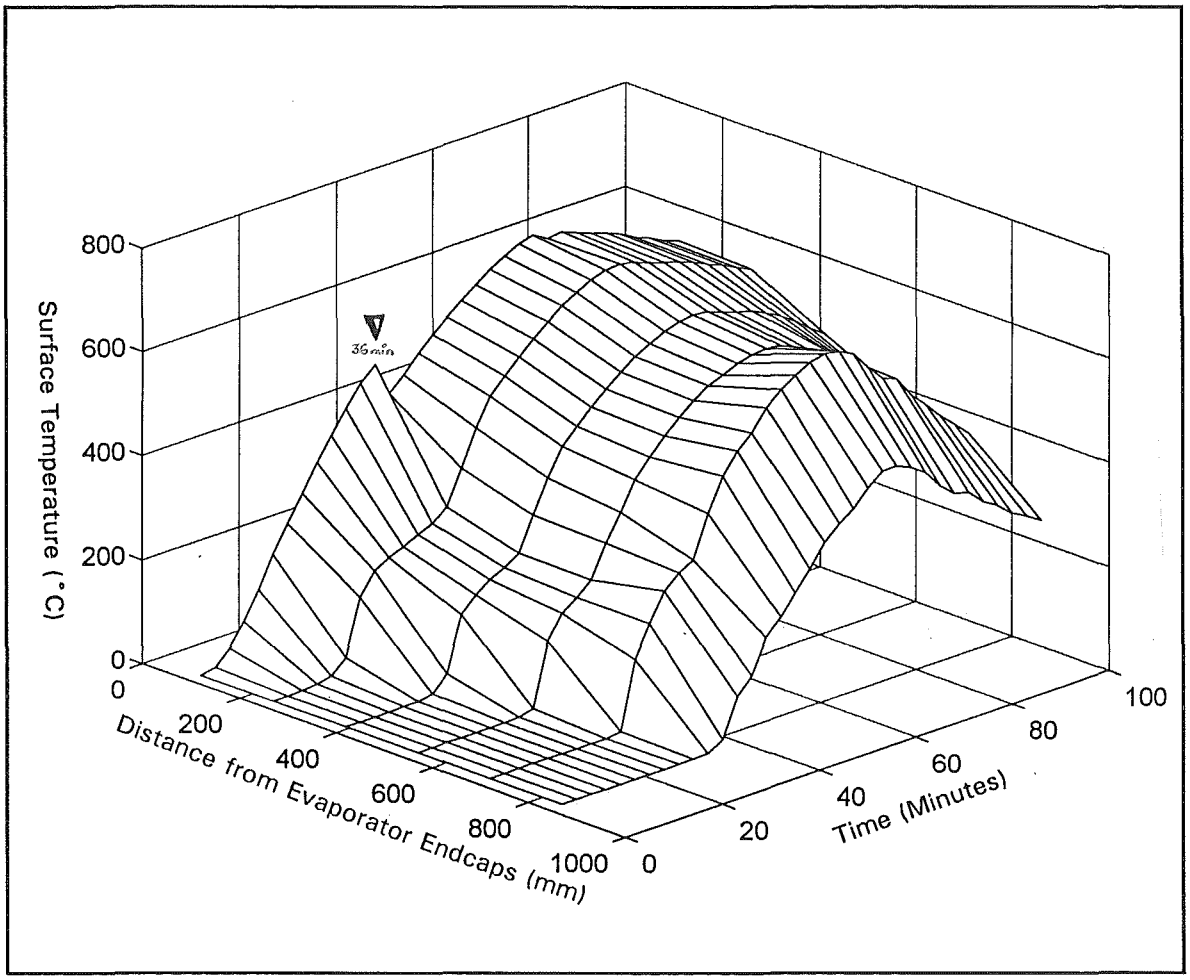

Figure 9.7 700W heat input to the sulphur heat pipe run without the water calorimeter.

The local evaporator temperature peak occuring at about 36 minutes, is very pronounced in this experiment, and still coincides with a local peak occurring close to the condenser. Also evident is the temperature gradient that exists between the two thermocouples closest to the condenser. Without the water cooling to cause a depression of the temperature, it is fair to say that a considerable length of the

pipe is rendered ineffectual by the presence of non-condensing gases. The axial temperature gradient was less for this case at only 30K between the evaporator, and the last thermocouple in the adiabatic region, with an 80K temperature drop between the evaporator, and the lowest temperature measured (disregarding the last thermocouple because of the suspected non-condensing gas effect).

Because of the high heat flux and high expected temperatures, a close record of the sounds produced was kept. The heat pipe started with some very loud "pops" and "pings" at 140°C, these were quite audible up to two metres away. Over the temperature range 200°C to 500°C the sound was a very rapid and faint bubbling. Coinciding with the sharp peak (501°C), the sound changed with the sudden drop in temperature from the quiet rapid boil to a very loud "pop" settling to a loud "chugging" suggesting slug boiling or large vapour bubbles. From the 494°C, to which the evaporator temperature had dropped, and the 550°C maximum temperature, the thick slug boiling became replaced by a rapid light boiling as of a low viscosity fluid. As the temperature increased, the sounds became first very fast high frequency bubbling, and then faded away all together - a possible evaporator boil-dry condition having been reached.

The final of the heat pipe experiments was with a lower heat input (to reduce the chances of a boil-dry condition occurring.), with the pipe operating at a near horizontal angle, and having natural air convection cooling. Its temperature/time/distance graph is show in Figure 9.8.

Although this has a local temperature ridge, it did not have the peak that the previous tests had. The axial temperature drop in this case was very large being a maximum of around 200°C. From the sounds of the heat pipe, it boiled very lightly as would be expected with the lower heat flux, but then went quiet for a period. The explanation for this would be that the evaporator boiled dry for a period because of the slow fluid return rate (The pipe was on a small angle otherwise there would have been no fluid return at all.)

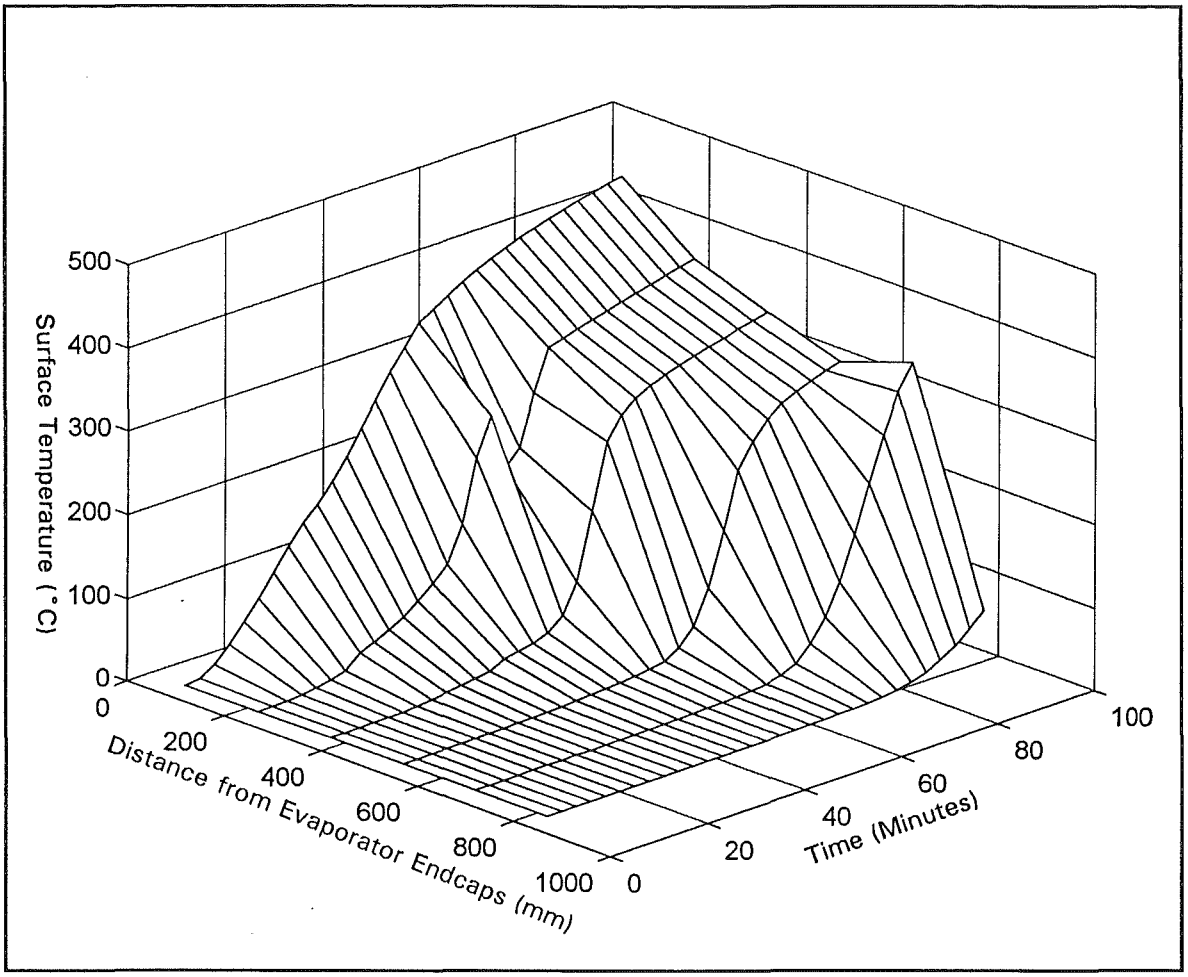

Figure 9.8 300W into the heater with the heat pipe operating in a near horizontal position.

One final experiment was carried out using an empty pipe with water cooling, in the vertical position, and 500W electrical input to the heater, for the purposes of comparing the temperature profiles of a control with the profiles of the heat pipe. The result of this test run is shown in Figure 9.9. As can be seen, the profile is completely different, and no heat reached the calorimeter in the period of the experiment.

9.3.3 Assessment of Sulphur as a Heat Pipe Working Fluid

Although sulphur can be used for a heat pipe working fluid in the range 300°C to 600°C, it has severe drawbacks which make it unsuitable for the solar-Stirling system.

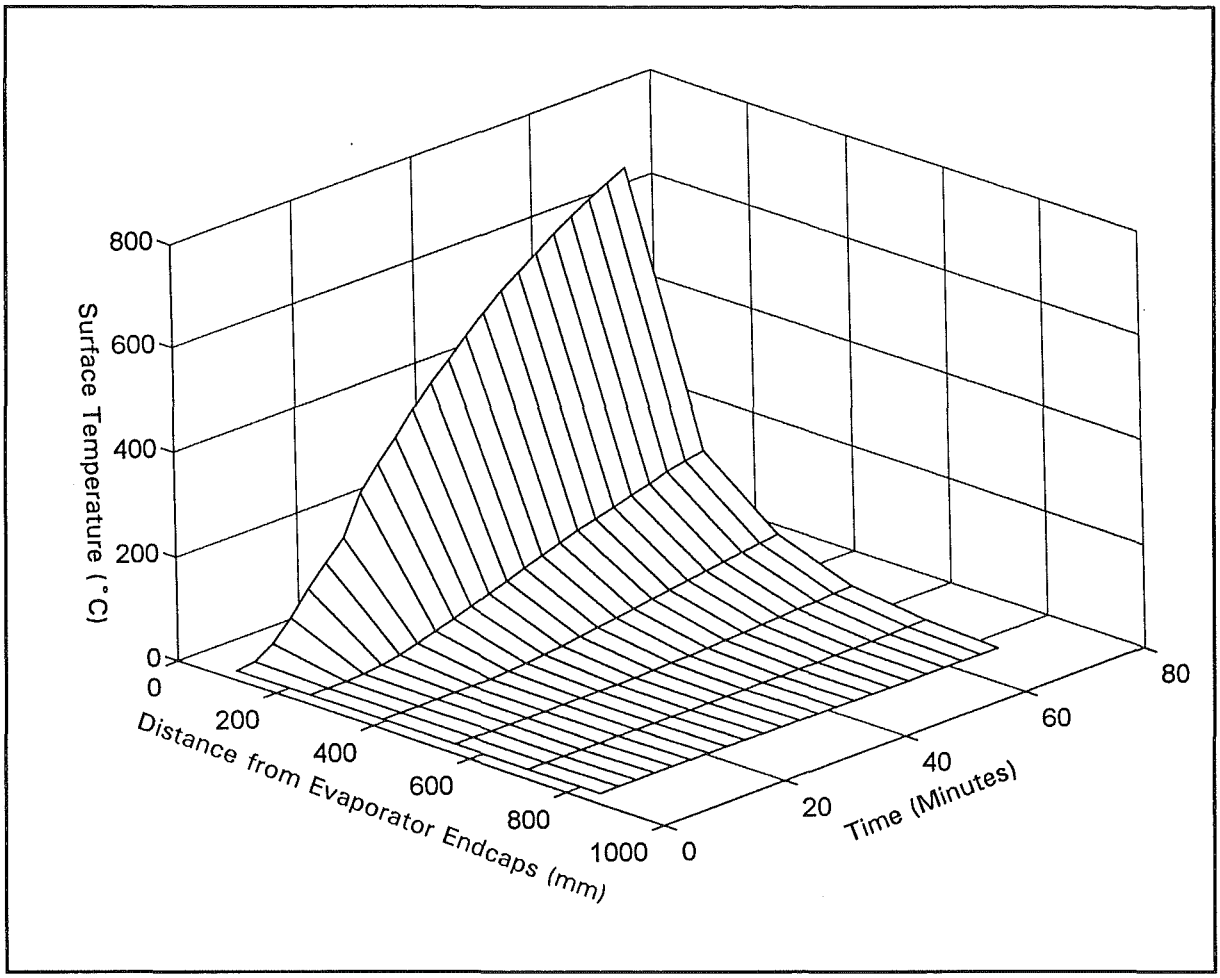

Figure 9.9 Control Experiment with an empty pipe with water cooling, and 500w input going into the heater.

For the solar-Stirling system, it is important that the heat transfer system be able to operate over a reasonable temperature range (200°C to 450°C). Sulphur and Iodine could provide such a working fluid except that as is suggested by the drop off in temperature in the condenser region, there is a build up of non-condensing gases in the condenser as time goes by. This is suspected to be iodine which, when the liquid sulphur Iodine mixture boils, is released as a gas after separating from the sulphur chains. The vapour flow carries this gas to the evaporator. The sulphur then condenses and runs down the wall leaving the iodine in the condenser. Without the iodine, the returning sulphur would become very viscous depending on the temperature of the fluid and walls. In support of this theory, it was found that when the heat pipe was cut open, that around the condenser region, a large amount of iodine was present, while the remainder of the pipe had

very little.

Because of the high melting point of the sulphur, there was a possibility of sonic velocities occurring within the vapour space which would limit the operation of the heat pipe and cause large temperature drops to become evident between the evaporator and condenser. To check this, the limit expressions given by S.W.Chi (1976) for heat pipes, were used. Because the heat pipe does not have a wick the capillary limit was not relevant, and the boiling limit would only be a problem with higher temperatures and a larger heat flux. The two remaining limits that were of concern were the Sonic limit, and the Entrainment limit. The expressions for these are given below in equations 9.1 and 9.2 respectively. Upon calculating the values for the limits using the heat pipe vapour diameter (20mm) and pure sulphur properties over a range of temperatures, the curves in Figure 9.10 were found. These indicated that the sonic limit was far above the heat transfer rates being experimented with. However, the theoretical entrainment limit was lower than amount of heat actually transferred. As will be discussed later, fluid was returning to the evaporator, and so the entrainment theory was not applicable here either. Thus any temperature drops along the pipe were due to non-condensing gases, and effects linked to the high viscosity of the returning fluid (until the temperature was sufficiently high to keep it at a low viscosity.)

$$\dot{Q}_{sonic}=A_{vap}\rho_v\lambda\left[\frac{\gamma RT_v}{2(\gamma+1)}\right]^{\frac{1}{2}} \qquad \textbf{(9.1)}\ \text{Sonic Limit}$$

$$\dot{Q}_{ent}=A_{vap}\lambda\left(\frac{\sigma\rho_v}{2r_{hs}}\right)^{\frac{1}{2}} \qquad \textbf{(9.2)}\ \text{Entrainment Limit}$$

where $\dot{Q}_{sonic}$ = Heat transfer W
A_{vap} = Cross-sectional area of vapour space ($3.14 \times 10^{-4} m^2$)
λ = Latent heat of evaporation J/kg
ρ_v = vapour density kg/m^3
σ = surface tension N/m
r_{hs} = hydraulic radius of pipe (taken as 7.5mm to account for surface roughness.)
R = Gas constant for sulphur (259J/kgK)
γ = Specific Heat ratio for Sulphur (1.6)
T_v = Stagnation temperature of vapour K

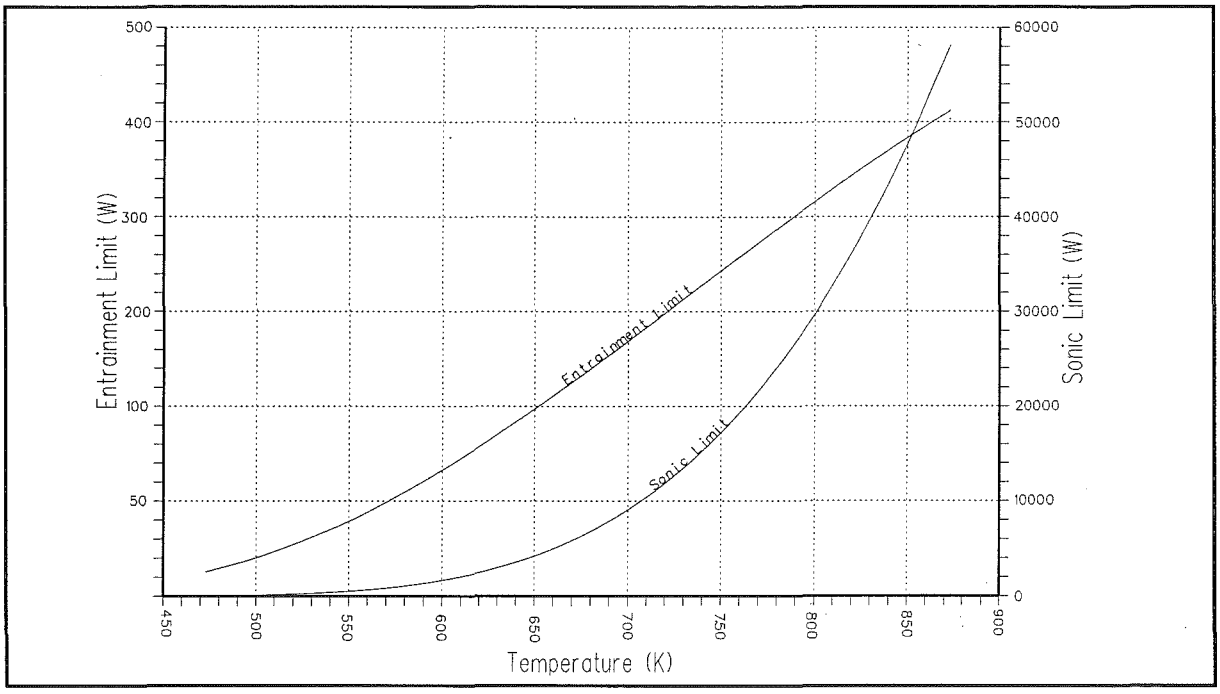

Figure 9.10 Sonic and Entrainment Limits predicted for the sulphur heat pipe.

The evidence for the return of the fluid is found through the consideration of the temperature peaks occurring in each run. The explanation for this would be that the liquid pool boils, and the vapour transports itself to the closest lower temperature region whereupon it condenses. If the wall temperature is very low, the condensing sulphur will become very viscous or solidify, therefore meaning that there will be no condensate return, or at least very little. More vapour will condense, thereby raising the temperature of the wall and the condensed fluid or solid. Without the cooling provided by the returning condensate, the evaporator becomes very hot, and the vapour leaving it is very hot too. Eventually the condensing vapour is at a high enough temperature to cause the fluid to lose

enough viscosity that it will begin moving, and therefore run back into the evaporator. When this occur, the evaporator cools quickly, producing the very sharp temperature drop seen in all of the performance plots. Each time the heat pipe was run, the peak was more significant, indicating that the iodine was slowly differentiating out and becoming resident in the condenser.

From the performance plots it can be seen that there was a smaller peak occurring at the entrance to the condenser (or at least the portion not covered by the non-condensing gases) corresponding to the temperature peak occurring in the evaporator. A possible explanation for this is that the heat front, by the time it arrived at the condenser, is made of very hot vapour produced by the almost dry evaporator. Not having any condensed sulphur already present to absorb some of the heat, most of the heat is transferred directly to the wall, whereas further down, the condensate requires heat to melt or become less viscous, and so acts as an insulator for the wall.

9.4 CONCLUSIONS

For the application, sulphur as a heat pipe working fluid is unsuitable for a number of reasons:-

- It has a large temperature drop occurring along the length of the heat pipe due to the presence of Iodine as a non-condensing gas, and the liquid solidifying and acting as an insulator in the early stages of operation.
- The iodine separates out thereby allowing the condensing fluid to become very viscous. The viscous behaviour of sulphur could cause the evaporator to boil dry, a condition that will result in a high axial temperature drop.
- Because of the unusual viscous behaviour and the occurrence of solid sulphur, the start up time for the heat pipe is very long, making it difficult or impossible to start on a cold day, because of the slow working fluid return rate.

In other applications with a steady heat input at a temperature over 500°C and

with a tolerance for an axial temperature drop of a considerable amount, a pure sulphur heat pipe could prove to be a cheap, non-toxic, and useful device. However the use of Iodine is not recommended because of its eventual separation from the sulphur and ultimate failure to fulfil its function, and disadvantage caused by it being present as a non-condensing gas. For the temperatures above 500°C the liquid metals have the advantage over sulphur as they have higher heat conductivities, low liquid viscosities, and all round better behaviour with much lower axial temperature gradients (of the order of 15K per metre). However they are in general harder to handle because of their reactivity, or else extremely toxic in the case of mercury.

10. ORGANIC HEAT PIPE WORKING FLUIDS

10.1 Introduction

There are many organic working fluids used in heat exchange systems, some of which are suitable for use in heat pipes. Generally, the organic fluids are restricted to lower temperature applications from -80°C up to 200°C. There are a few that can operate up to 400°C such as Thermex, and Dowtherm A, but these working fluids break down rapidly around this temperature, and so the heat pipe would fail after a short period, and have to be recharged. From the search outlined in chapter 8, several candidate working fluids appeared to be suitable for the originally planned 400°C, but they had to be checked for chemical stability at these high temperatures. The candidates were then benzyl benzoate ($C_{14}H_{12}O_2$), and diisodecyl phthalate ($C_{28}H_{46}O_4$).

10.2 Testing Diisodecyl Phthalate and Benzyl Benzoate

Both benzyl benzoate, and diisodecyl phthalate (DIDP), are based around benzene rings, as in Figure 10.1, and are readily available in the plastics industry as plasticizers. The main doubt in their ability to operate as a heat pipe working fluid is the size of the molecules, especially in the case of DIDP, but also the presence of oxygen within the structure. Being within an evacuated system it was suspected that the autoignition temperature might correspond to a thermal break down of the working fluids into lighter fractions, but this also was unknown, and so a simple heat pipe was rigged up with a representative working fluid. The working fluid used was DOP or dioctyl phthalate ($C_{24}H_{38}O_4$), a simpler relative of DIDP which, though not a good working fluid, would indicate the suitability of DIDP and Benzyl benzoate as candidate working fluids provided it did not thermally breakdown at the high temperatures. Its structure is shown in Figure 10.1.

10.2.1 Experimental Method

The heat pipe case was a 400mm wickless steel tube, with a filler tube. It was first filled with a small measure of DOP (17mL), and then attached to the evacuation rig. A combination of shaking and heating was used to release the

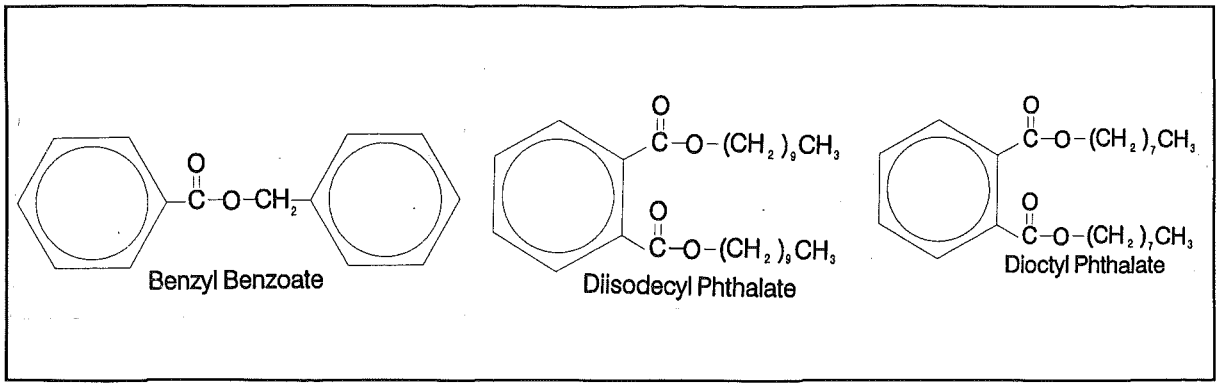

Figure 10.1 The chemical structures of Benzyl Benzoate, Diisodecyl Phthalate, and Dioctyl Phthalate.

entrapped gas from within the liquid. This was continued until the jump in pressure observed when the heat was applied and the heat pipe shaken, was negligible. At this point the filler pipe was pinched off and welded to make a good seal.

A water calorimeter was added to the end, and a ceramic-insulated band heater placed around its base. Insulation was placed around the adiabatic region as for the sulphur heat pipe test rig.

Data was gathered from several thermocouples along the tube's length, and the temperature of the water inlet and outlet was also taken. To start the pipe, it was first run at 700W electrical input to the heater, and then cut back to 570W to keep a stable 420°C until a total operating time of 4 hours had elapsed.

After the prolonged operation, the pipe would be opened up, and the contents checked for thermal decomposition, as evidenced by changes in colour or smell.

10.2.2 Results

The results of the test are presented here on a Temperature\time\distance xyz-graph in Figure 10.2.

The largest highest heat transfer rate passing through the heat pipe was 260W which was at 70 minutes, almost at the maximum temperature reached, which was during the 700W of electrical input to the heater. During the stable temperature period of operation, the heat transfer rate was about 180W.

The DOP followed heat pipe start-up trends for the first ½hr, but then as the

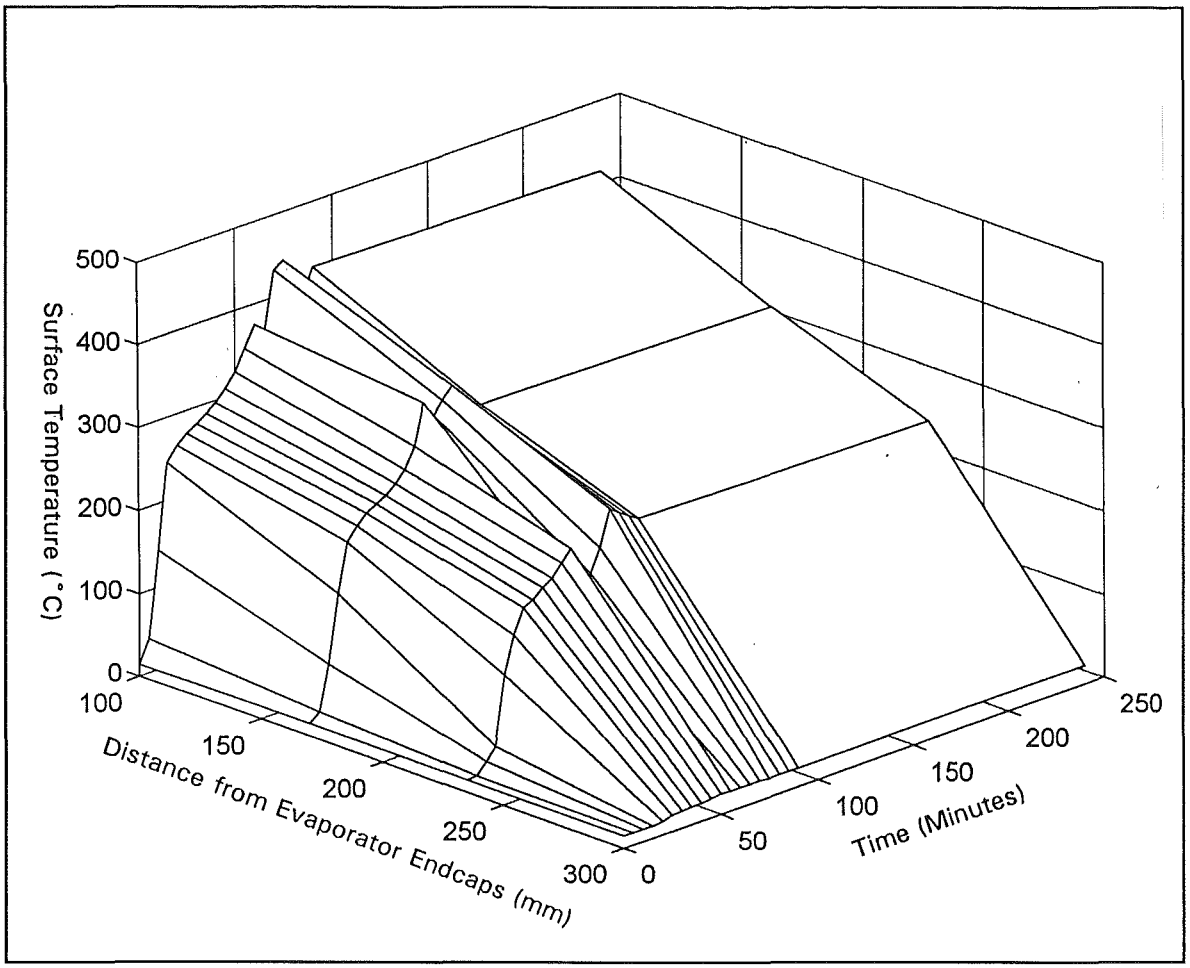

Figure 10.2 Temperature\Time\Thermocouple Location graph of the experiment with Dioctyl Phthalate as a heat pipe working fluid, operating with 570W electrical input to the heater to maintain a steady temperature for several hours.

time increased, and the temperature as well, the temperatures became unstable, and the thermal gradient along the pipe increased.

Upon opening the pipe once it had cooled down to ambient temperature, a high pressure jet of vile smelling yellow vapour was released. Had there been no decomposition, the pipe contents should have been under a vacuum, with a clear light oily liquid with almost no smell. More liquid was poured out, and this was a yellow-brown, smelly, liquid with a very low viscosity.

10.2.3 Conclusions Drawn

The Dioctyl phthalate broke down under the high temperatures to a number of lighter fraction chemicals, and so failed as a heat pipe working fluid. This indicated

that diisodecyl phthalate would be unsuitable. Using the same reasoning, it is reasonable to assume that the Benzyl Benzoate would also exhibit the same thermal breakdown, but probably at a slower rate, due to the smaller size of the molecule, and the higher autoignition temperature.

10.3 Dowtherm A

Dowtherm A is a commercially produced heat transfer fluid comprised of a Eutectic mixture of diphenyl/diphenyl ether which has been used successfully in heat pipes before. It has a structure as shown below in Figure 10.3.

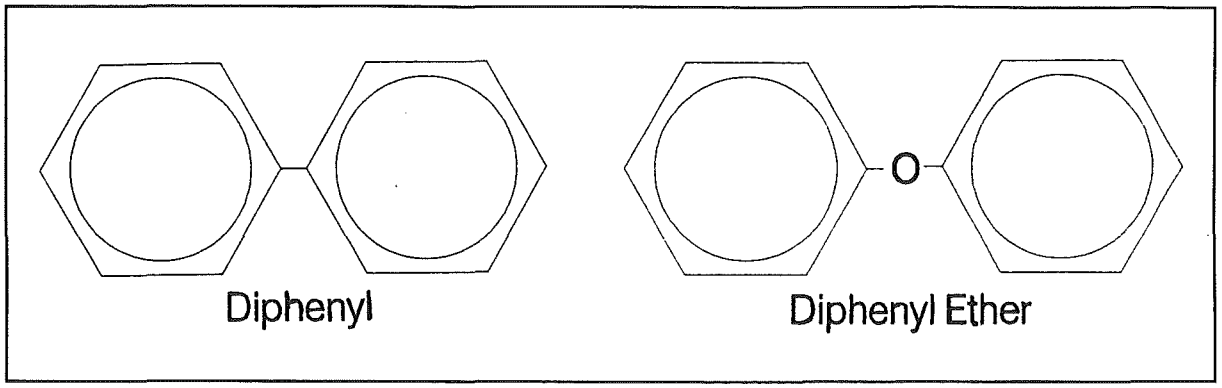

Figure 10.3 Molecules of diphenyl, and diphenyl ether used in Dowtherm A heat transfer fluid.

This working fluid was not tested in the end because its boiling limit with a reasonable sized heat pipe was too low being only 36W at 400°C for a 4m pipe. It also had a vapour pressure of 10.9bar at 400°C which could be a problem to try and contain at the elevated temperatures.

11. THE MERCURY HEAT PIPE

11.1 Introduction

Liquid metals have great advantages for use as the working fluids in heat pipes in that they have high latent heats of vaporisation, and very high thermal conductivities; however they are either highly reactive as in the case of the alkali metals, or very toxic, as in the case of mercury, and the other heavy metals. Generally the liquid metals are used where the temperatures are above 600°C because their vapour pressures are too low, and the sonic velocities limit the heat transfer possible with a reasonable sized tube. However mercury is one working fluid that will operate at the more moderate temperatures between 250°C and 500°C.

11.2 Characteristics of Mercury

Mercury is one of only two elements that are liquid at room temperatures and pressures[1], the other being bromine. It is a very unreactive metal but will form amalgams (alloys) with a number of other metals, such as copper, and aluminium, and does not react with water or decompose acids. It is also extremely rare, comprising 8×10^{-6}% of the earths crust by mass, making it even rarer than platinum and gold, but the high concentrations of its deposits make it cheap and readily obtainable.

One of the main disadvantages of mercury as a heat pipe working fluid is its very poor wetting characteristics. It is a well known and easily observable fact, that the meniscus of mercury concave downwards which is the opposite to water, this means that instead of capillary action drawing mercury up a thin tube, it will in fact depress the mercury level; this is known as *capillary depression*, and is illustrated in Figure 11.1.

---

[1] By observing trends in the periodic table, it has been shown that the radioactive element francium would probably be a liquid at 23°C (For an element to be listed as a liquid it must be liquid at 25°C). However being an alkali metal it is predicted to be very reactive, as well as its most stable isotope having a half life of only 21 minutes, getting enough francium together to measure the melting point without it immediately vaporizing because of the heat of reaction, would be a task in futility. (Chang 1984)

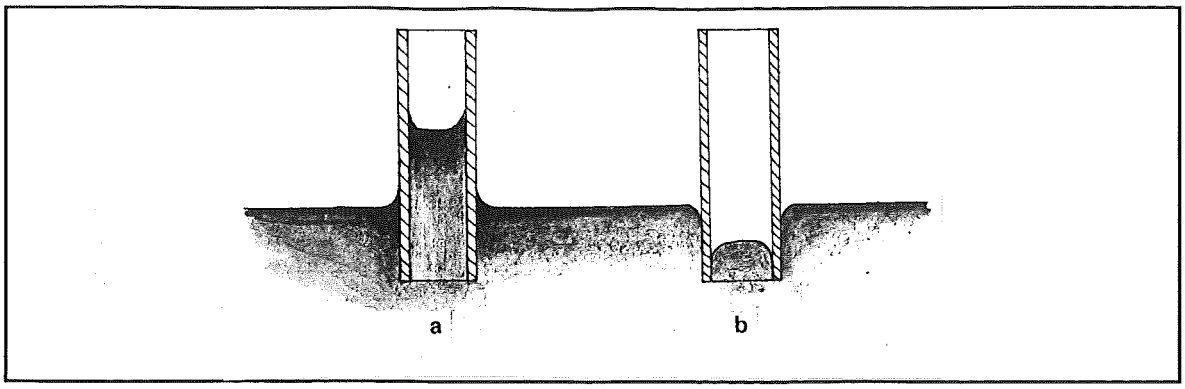

Figure 11.1 Capillary action on **(a)** a wetting fluid ie. water, and **(b)** a non-wetting fluid ie mercury.

A very real concern for using mercury in a system such as the one outlined in this thesis, is that if they are to be produced commercially, then it will be impossible for all of the mercury heat pipes produced never to break. Because of the high temperatures, when a mercury heat pipe of this type breaks it will spill large quantities of vaporous mercury into the environment.

Mercury as a liquid is relatively harmless if not handled for any prolonged period, as it can be absorbed through the skin. It is also possible to drink a small amount of the liquid metal without suffering any ill effects. It is the compounds of mercury, and the vaporous mercury that pose the danger. Inorganic compounds of mercury vary in toxicity depending on their solubility. Mercurous chloride (Hg_2Cl_2) which is insoluble is not regarded as very toxic, and has been used as a purgative. Mercuric salts (Hg^{2+}) on the other hand are more soluble and, considered toxic. Of all the mercury compounds the most toxic are the dimethylmercury, $(CH_3)_2Hg$ and, the methylmercury ion $(CH_3Hg)^+$ which can pass through the membranes separating the bloodstream from the brain. The effects of mercury poisoning are; liver and kidney damage, brain damage, erethism (uncontrolled spasms and emotional disturbances). Vapour inhalation causes irritation and damage to the lungs. (Chang 1984)

Mercury freezes at -38.9°C, and boils under atmospheric pressure at 357°C. This means that it will take a very hard winter to cause problems with the system freezing up, and under the operating conditions calculated (330°C-350°C see chapter 6), the mercury, should it escape from the heat pipe, would be just about to boil.

11.3 A Solution to the Wetting Problem

The poor wetting ability of mercury is a concern because it means that a regular wrapped wire screen wick cannot be used to distribute the liquid around the evaporator, because the mercury will not enter it, and thus will be kept from contact with the heat pipe wall. A simple solution to this would be to use pool boiling instead, which means have a pool of mercury in the tube with no wick. This has a problem in that the absorber would have to be exactly level, otherwise the mercury will all run to one end, and the absorber would over-heat in part, and burn out. It was observed that a wire mesh when pushed into the surface of a mercury pool would displace the pool around the mesh while also allowing a free surface from which evaporation could take place. It was this phenomena that was used in the design of the mercury heat pipe used in the tests.

11.3.1 Wire Mesh Pressure Testing Apparatus and Method

To check the hypothesis and concept design of using a wire mesh to hold back a quantity of mercury, and a pressure, a small rig was built to take a number of different types of mesh and measure the pressure head that they could withstand. It consisted of a glass "T" section with a plunger in one end, and a holder for the wire mesh on the other. This is illustrated in Figure 11.2. The holder was fitted with a pair of rubber rings that would seal the mesh edges which would have been disturbed by cutting and would otherwise give false readings by leaking first.

The plunger pushed on a volume of mercury between it and the mesh. The mercury would rise up the vertical tube, and thereby increase the pressure at the mesh. When the first drops of mercury began to pass through the bottom of the mesh, the distance from the bottom of the mercury pool (this was where the leakage occurred, and where the pressure was highest) to the top of the mercury meniscus was measured.

11.3.2 Wire Mesh Pressure Testing Results

Table 11.1 contains the results from the test rig with several mesh sizes. The mesh numbers refer to the number of apertures per inch, and the diameter of the wire used in millimetres.

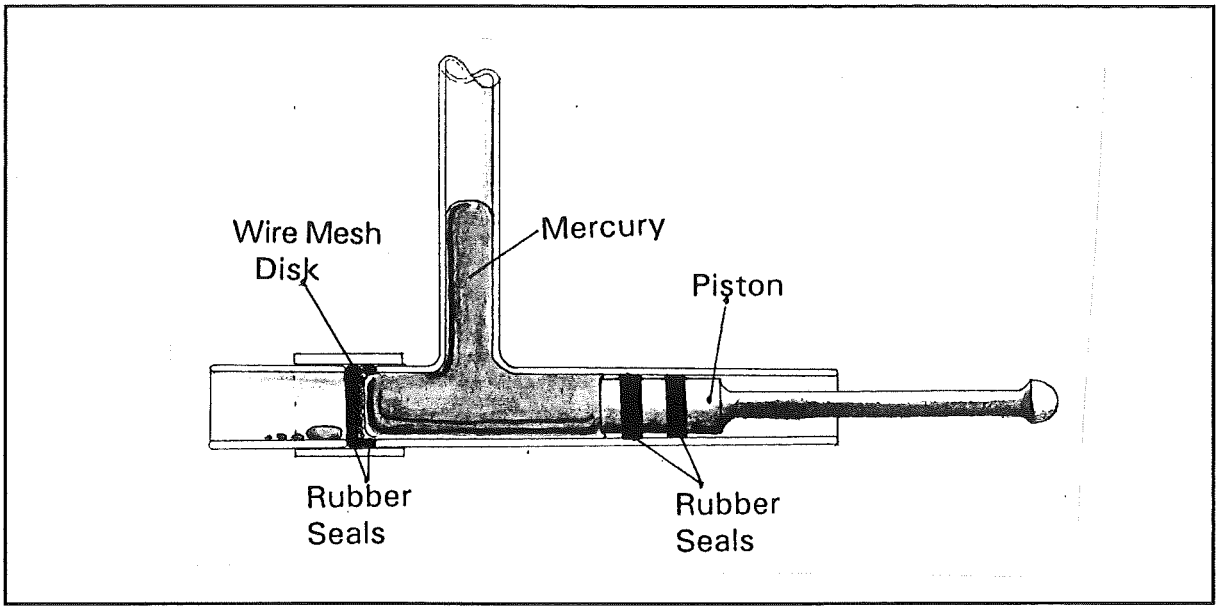

Figure 11.2 Wire mesh-mercury pressure testing apparatus.

A general feature observable from the table is that some of the tests had a reasonable variation in the pressure that the mesh was able to hold back. With the first set of tests, a lubricant had to be applied to the piston to allow it to slide smoothly otherwise pressure shocks would spoil the results. Some of this lubricant, was able to reach the wire mesh, and caused the mercury to flow through the mesh more easily and thereby reduce the static head. The mechanism that caused this is unknown. After several tests, the lubricant had been pushed out, and the static head improved. In the later tests, a problem did occur with the first of the 200 mesh tests, in that the piston ring seals had gaps large enough that they would leak before the mesh did. This was remedied with new seals.

It is expected that the behaviour of the mercury at the higher temperatures will not be much different than that at the atmospheric conditions because the surface tension does not change much with temperature, but the density of the liquid mercury reduces a little, so the pressure that the mesh can hold may be slightly increased.

The graph of the results, Figure 11.3, shows that the relationship between the static pressure differential and the mesh size is nearly linear. It was decided then that a reasonable mesh size would be a 150 mesh which would be capable of holding a head of about 80mmHg, enough to cater for errors in the levelness of the

heat pipe absorber, and to allow a sufficient head to drive the condensate return tube lines.

TABLE 11.1 Results of Wire Mesh - Mercury Pressure Tests

Mesh	Test No.	Lower Datum (mm)	Upper Level Reached (mm)	Differential (mm)	Pressure Differential (Pa)
20x.42	1	47	60	13	1728
	2	48	61	13	1728
	3	48.5	62	13.5	1794
	4	47.5	61	13.5	1794
	5	48	62.5	14.5	1927
	6	47.5	61.5	14	1860
40x0.42	1	46.5	70	23.5	3123
	2	47	71	24	3189
	3	46	70	24	3189
	4	46	70	24	3189
60x0.14	1	54	85	31	4119
	2	53.5	84	30.5	4053
	3	53.5	85	31.5	4186
	4	53.5	85	31.5	4186
80x0.14	1	51	108	57	7575
	2	52	109.5	57.5	7641
	3	52	109	57	7575
100x0.1	1	56	122	66	8770
	2	53	117	64	8505
	3	54	118.5	64.5	8571
200x0.1	1	51	151	100	13289
	2	51	169	118	15681
	3	52	163	111	14750
	4	52	162.5	110.5	14684

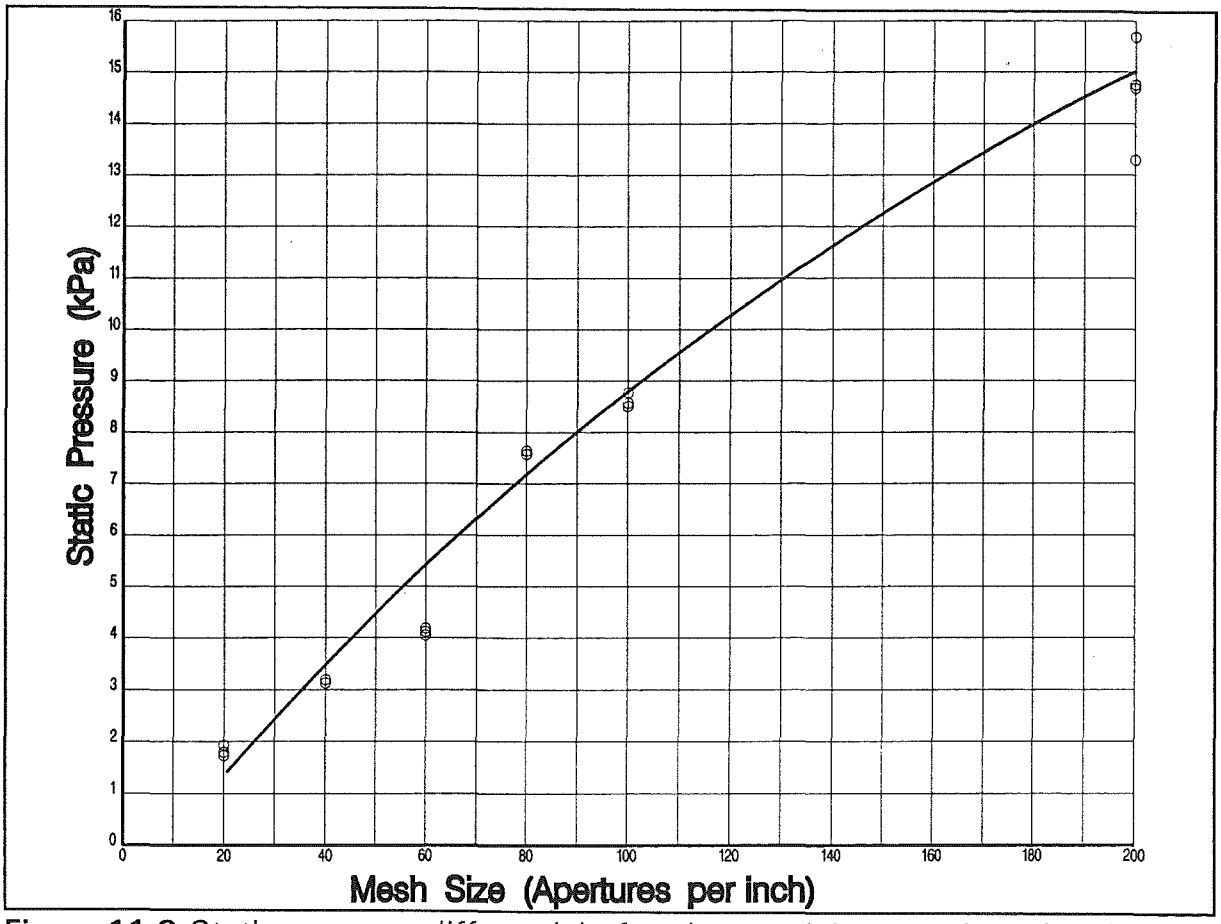

Figure 11.3 Static pressure differential of various stainless steel meshes holding back mercury.

11.3.3 Conclusions Drawn from Test

The experiment showed that the concept would work, and that a 150 mesh would be quite adequate for the heat pipes to be used in the full sized solar thermal power system, as well as the small test heat pipe. To apply this to the heat pipes, a mesh tube would be employed inside the heat pipe to hold a layer of mercury against the evaporator wall, thereby ensuring a good contact between the working fluid and the heated surface, allowing a good heat transfer to occur. This is illustrated in Figure 11.4. Using a technique like this uses the poor wetting to advantage. Poor wetting is desirable for condensation heat exchange, as it encourages dropwise condensation, a much more effective and efficient form of heat transfer, which normally requires expensive and not overly effective chemical treatments to achieve when using other heat transfer media, such as water.

11.4 Heat Pipe Concept Design

Having shown that the use of a wire mesh screen to hold mercury against the tube wall would be successful, the design of the heat pipe could proceed. Mercury with its high liquid density and low viscosity was ideally suited to a simple gravity return for the condensate. Therefore, all that was needed was to raise the condenser section relative to the evaporator. The problem then was how to transfer the liquid mercury from the condenser back to the outside of the mesh tube. The solution was to use an external liquid return pipe (later to be internalised) running from the condenser (The condenser was angled to encourage pooling), back into the evaporator directly into the space between the heat pipe wall and the mesh tube. In the process of designing for this, the need to transfer liquid forming

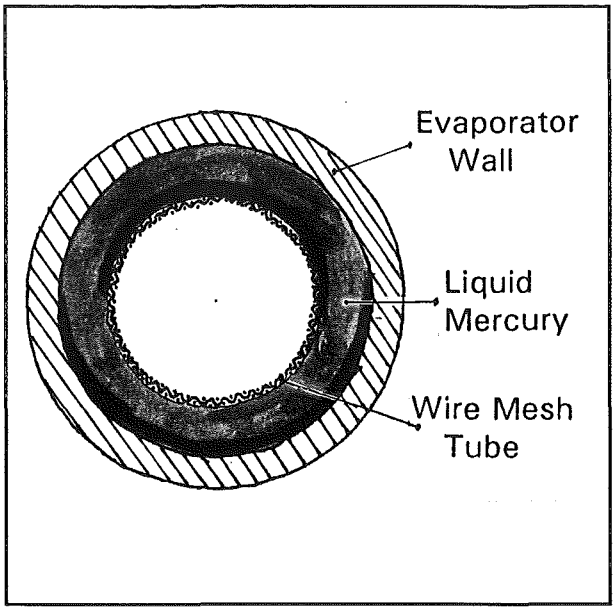

Figure 11.4 The mesh tube inside the heat pipe holding mercury against the pipe wall.

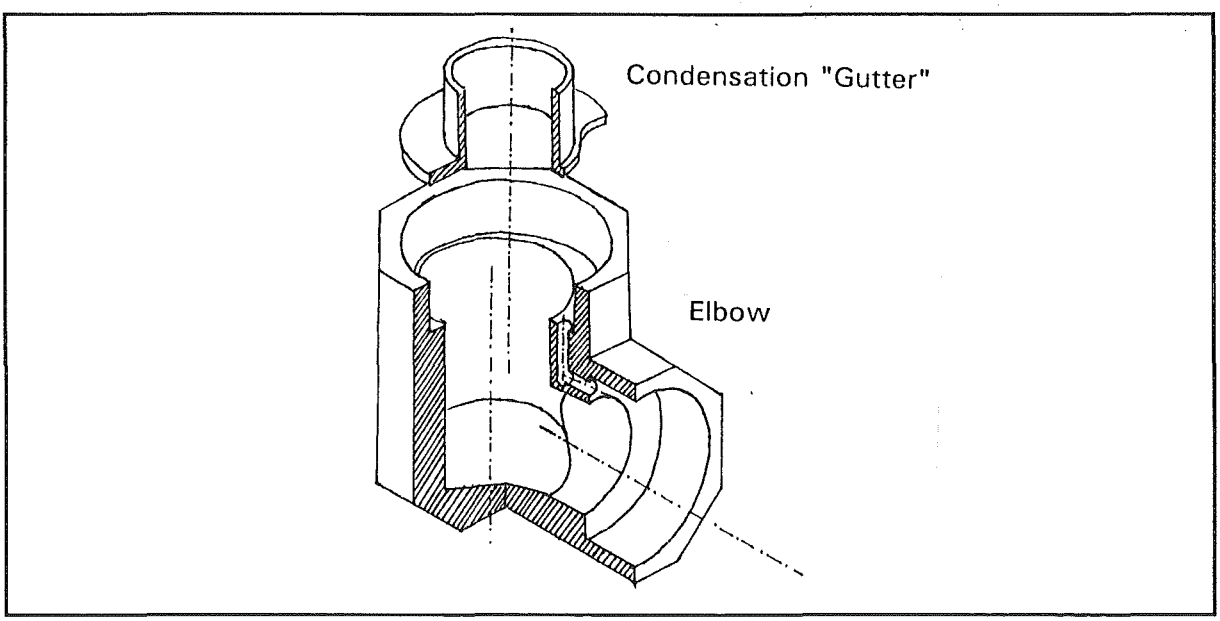

Figure 11.5 isometric cutaway view of the elbow, and "gutter" for returning condensate from the evaporator region to the liquid region between the heat pipe wall and the mesh tube, also used for locating the mesh tube.

outside of the condenser region back to the space between the evaporator wall and the wire mesh tube became apparent. To partially alleviate the problem, a system to capture, and guide the condensing liquid back into the liquid region, was devised. However it is impossible to solve this problem completely, but axial heat flow within the heat pipe walls would help reduce it by re-evaporating the liquid when it runs into the hotter regions. What was produced was an elbow bend, with a "gutter" for catching the condensate running down the walls of the adiabatic section. Three small holes allowed the condensate to return to the region between the heat pipe wall and the mesh tube. (Figure 11.5). The complete cut away heat pipe circuit is shown in Figure 11.6. As can be seen the mesh tube was fitted to a pair of ends, one of which rested inside the heat pipe, and the other was firmly pressed into the elbow section by means of a specially made tool. The seam of the mesh tube was lapped, and spot welded together with a very low powered spot welder so as not to cause holes to be burnt into the mesh. To stop the mesh tube being crushed by the mercury, a series of thin steel rings were mounted inside the tube to add strength, while another ring was mounted externally to the mesh tube.

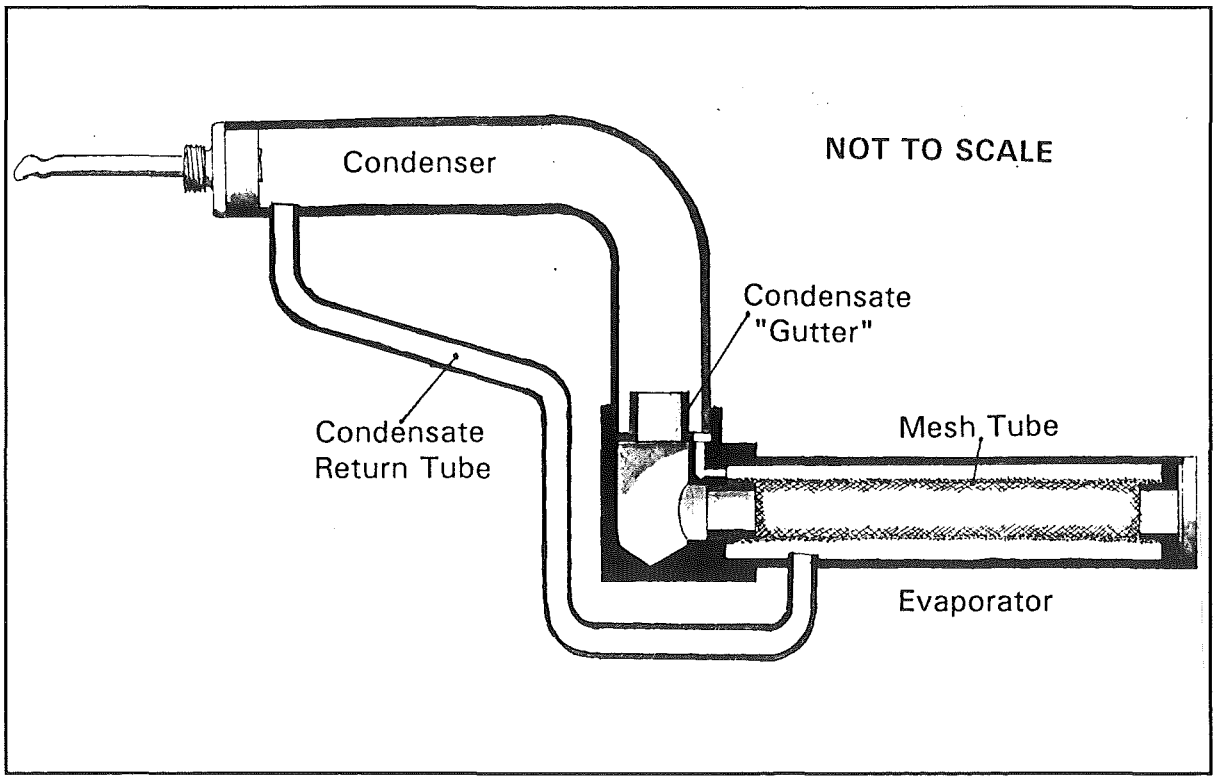

Figure 11.6 The complete circuit for the flow of vapour and return of condensate.

The external ring had channels cut into its edge to allow a free flow of liquid to occur.

11.5 Mercury Heat Pipe Calorimetry

It was desired to have a more controllable calorimetry than that used for the previous heat pipe experiments, particularly with mercury's very good condensation heat transfer characteristics. This would mean that if the heat transfer to the calorimeter working fluid was too good, then the heat pipe would remain at a low temperature and not be able to be assessed at the desired operating temperature. Therefore it was decided to use air flowing through a heat exchanger for the calorimetry, and using a variable speed fan to alter the air speed, and consequently the heat transfer of the calorimeter. To measure the heat transported, thermocouples on the inlet and outlet of the calorimeter were to be used. The air flow would have to be measured, and kept at as low a rate as possible.

To help reduce the flow-rate, the heat exchanger was designed to pass air past the condenser three times, thereby maximising the temperature rise in the air, increasing the pressure drop through the heat exchanger which in turn would reduce the air speed, and the heat transfer coefficient. Refer to Figure 11.7.

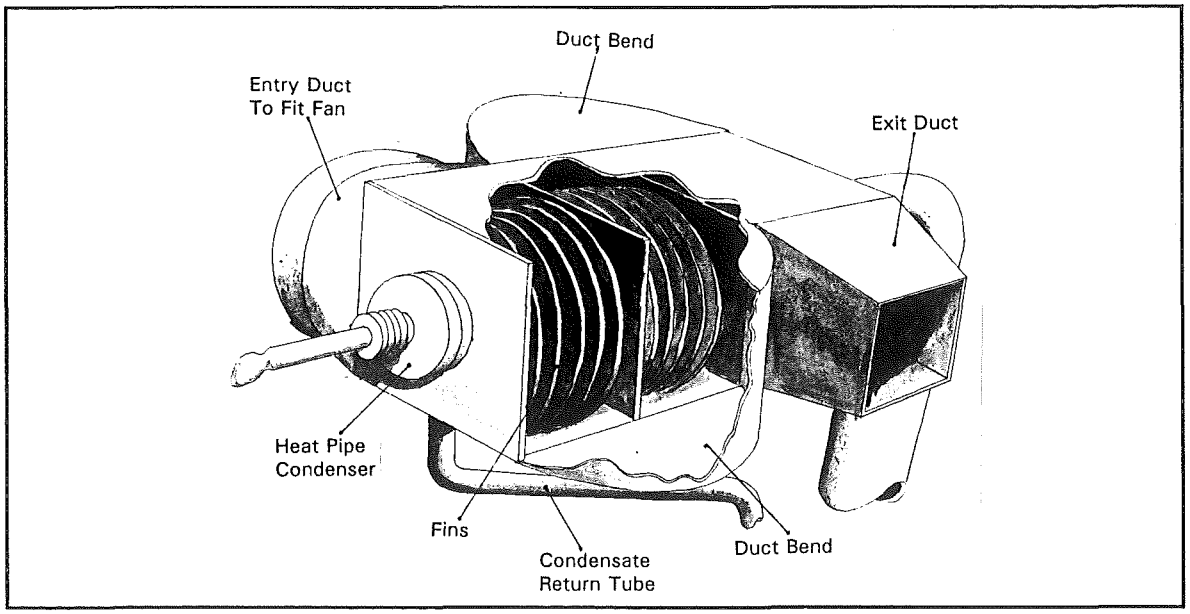

Figure 11.7 Cutaway of Calorimeter around the mercury heat pipe condenser.

11.5.1 Air Flow Metering

Using air in the calorimetry posed the problem that it was much more difficult to meter than water, and a considerable amount of time was spent trying to find a suitable airflow measuring device. Originally this was to be done using an orifice flow meter in the fan intake duct where it would be unaffected by the air temperature changes; however a vane anemometer as shown in Figure 11.8 was available and was supposed to be more accurate for the low air speeds that would

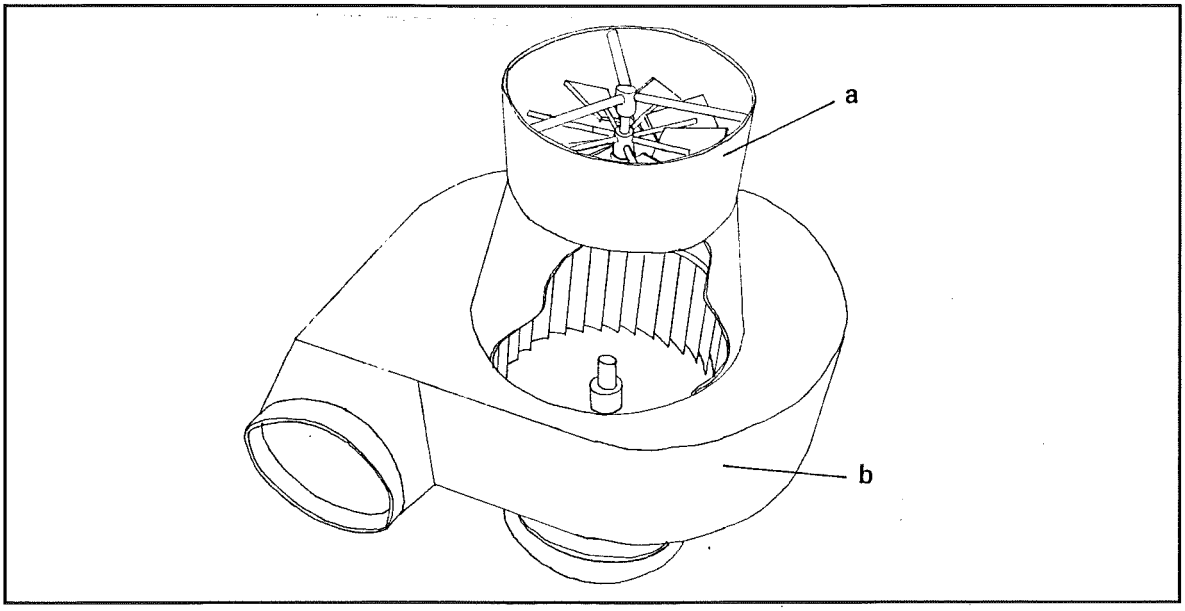

Figure 11.8 Vane anemometer **(a)** fitted into a centrifugal fan **(b)**.

be encountered in the calorimeter. This would have been an ideal solution and given suitably accurate and easy to read measurements, except the meter used was an old damaged one, unusable for its proper function of wind-speed measurement, and as it happened, quite unreliable for the measurements needed in this experiment. Therefore a new air-flow meter had to be devised.

The new meter was based on the Annubars used in air-flow metering for engine performance analysis. It consisted of a tube across the flow with four holes across it facing into the wind direction, another tube behind this had a hole facing the opposite direction. By measuring the pressure difference between the two tubes, an air-speed measurement could be taken.

A floating scale micromanometer was used for reading the pressure differential between the two points. Because of the four holes across the flow, the pressure

Photo A Mercury heat pipe, fan, and air flow meter.

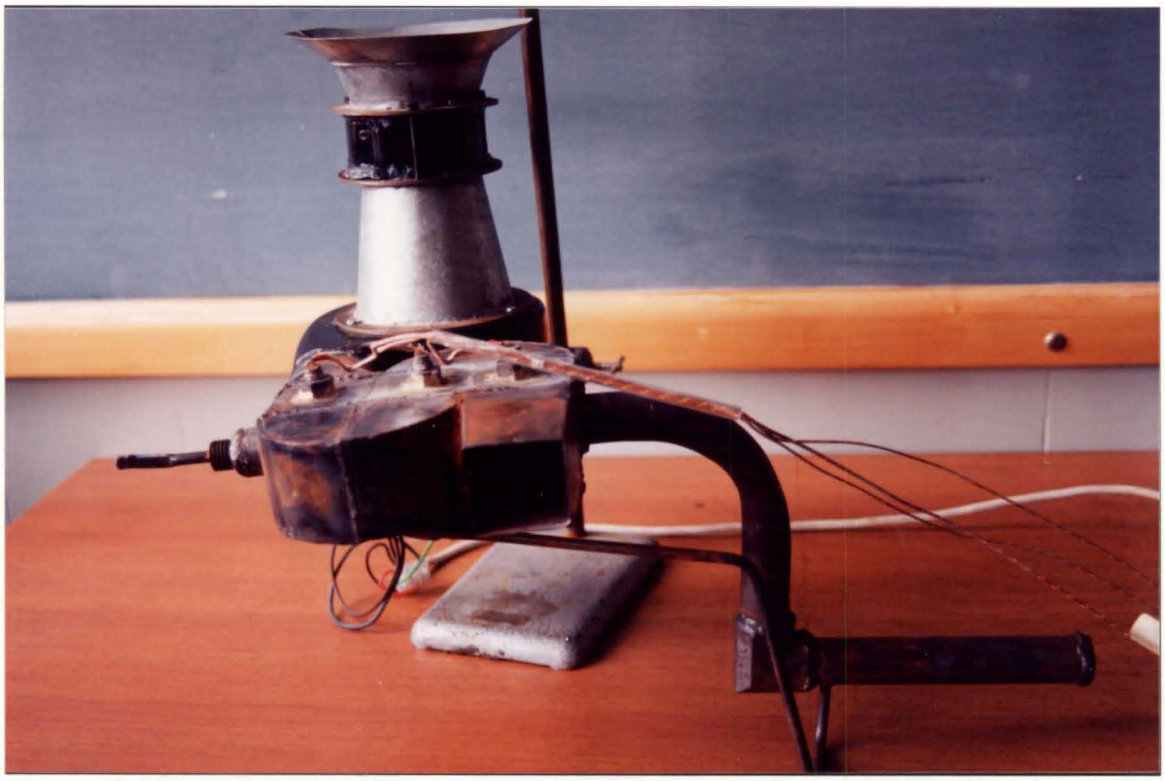

Photo B Mercury heat pipe and air calorimetry equipment.

Photo C The mercury heat pipe and the air calorimeter heat exchanger.

differential relates to the average flow velocity. The Annubar is shown in Figure 11.9.

Due to the ducting being already built up, the size of the Annubar was restricted to being the same as the vane flow meter which meant that it was short and wide. One of the recommendations for a commercial Annubar is to have 6 diameters of straight duct before the Annubar , and then another 4 diameters of straight duct after it. Unfortunately, these conditions were not met, but it was felt that being an averaging flow meter, the errors due to this would be minimal.

The expression derived for the Annubar built for this project is as given below in expression 11.1.

$$v_{air} = \sqrt{\frac{2\rho_{man} g \Delta h R T_{air}}{P_{atmo}}} \qquad (11.1)$$

where v_{air} = the average velocity of the air through the Annubar.
ρ_{man} = the density of the manometer working fluid which in this case is water.
Δh = the head difference read from the manometer.
R = the gas constant for air which is 287 J/kgK.
T_{air} = the air temperature of the air entering the duct.
P_{atmo} = the atmospheric pressure.

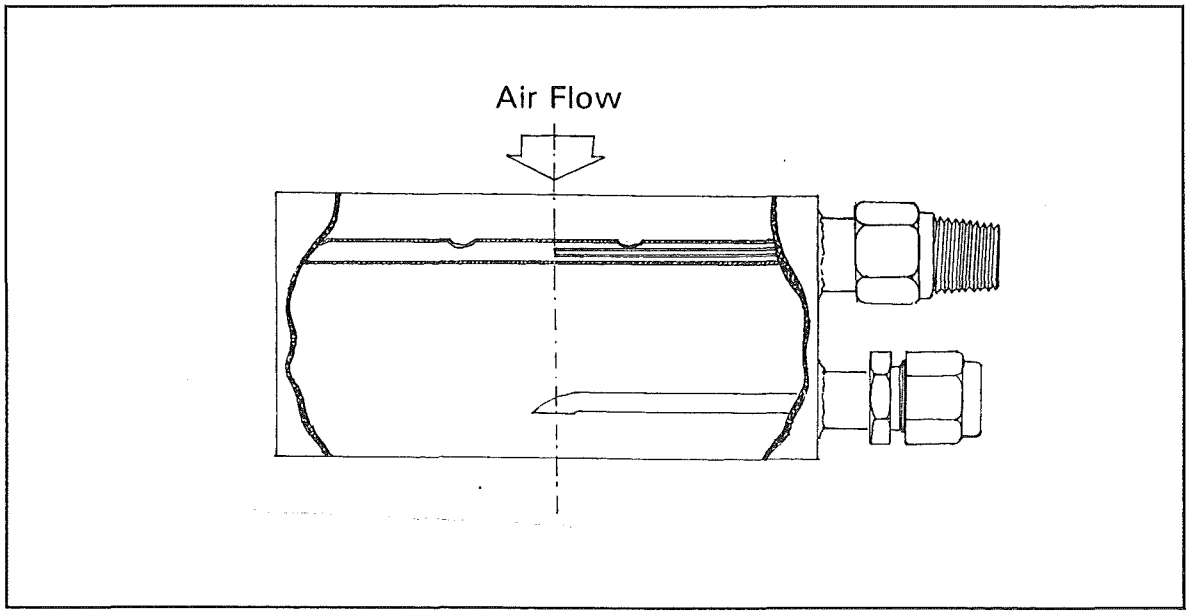

Figure 11.9 Averaging flow meter based on a commercial Annubar.

11.6 Limits of the Mercury Heat Pipe

The mercury heat pipe when operating in the range 330°C-350°C has a high heat flux capacity, but it is necessary to evaluate the limits that are likely to be a problem at this temperature. (Refer to Appendix E for the properties of mercury over a range of temperatures.) As introduced in chapter 7, the relevant limits are;

- The Sonic Limit
- The Entrainment Limit
- The Wicking Limit
- The Boiling Limit

11.6.1 The Sonic Limit

As given in chapter 7 the sonic limit is given by;

$$\dot{Q}_{sonic}=\lambda \rho_v A_{vap}\sqrt{\frac{\gamma R T_v}{2(1+\gamma)}} \qquad (11.2)$$

where λ is the latent heat of vaporisation.
ρ_v is the vapour density.
A_{vap} is the cross sectional area of the vapour space.
γ is the specific heat ratio of the working fluid which in the case of mercury is 1.67.
R is the gas constant for the working fluid which in this case is 41.45 J/kgK,
T_v is the vapour temperature (K).

Therefore at 340°C, and a pipe with an internal diameter of 13mm at its narrowest point, the sonic limit is;

$$\dot{Q}_{sonic}=295\times10^3\times3.0\times\frac{\pi}{4}0.013^2\sqrt{\frac{1.67\times41.45\times613}{2(1+1.67)}}=10500\ W \qquad (11.3)$$

Given that the heat pipes in both the systems will be no more than 4m long a piece, servicing a 1m wide trough with an average collection of 2400W each, the sonic limit will not be a problem.

11.6.2 Entrainment Limit

The unusual arrangement for holding the mercury against the wall of the heat pipe increases the entrainment limit by providing a shield between the vapour and

liquid meaning that the vapour cannot pick up the liquid quite so easily. Had a pool boiling system been used, the entrainment limit would be a much more serious problem. The expression for the entrainment limit as given in chapter 7 is;

$$\dot{Q}_{ent}=A_{vap}\lambda\sqrt{\frac{\sigma\rho_v}{2r_{hs}}} \qquad (11.4)$$

where σ is the liquid surface tension.
r_{hs} is the hydraulic radius of the mesh tube apertures.

r_{hs} is taken to be ¼ of the aperture width of the wire which in the case of a 150 mesh is 0.089mm, so r_{hs} equals 0.0223mm.

$$\dot{Q}_{ent}=\frac{\pi}{4}\times 0.013^2\times 295\times 10^3\sqrt{\frac{0.397\times 3}{2\times 22.3\times 10^{-6}}}=6400\ W \qquad (11.5)$$

11.6.3 Wicking Limit

In a regular heat pipe with a porous wick, the wicking limit is determined by the rate at which the liquid can be returned to the evaporator, and is normally quite low. In the design for the mercury heat pipe to be tested here, the limit is

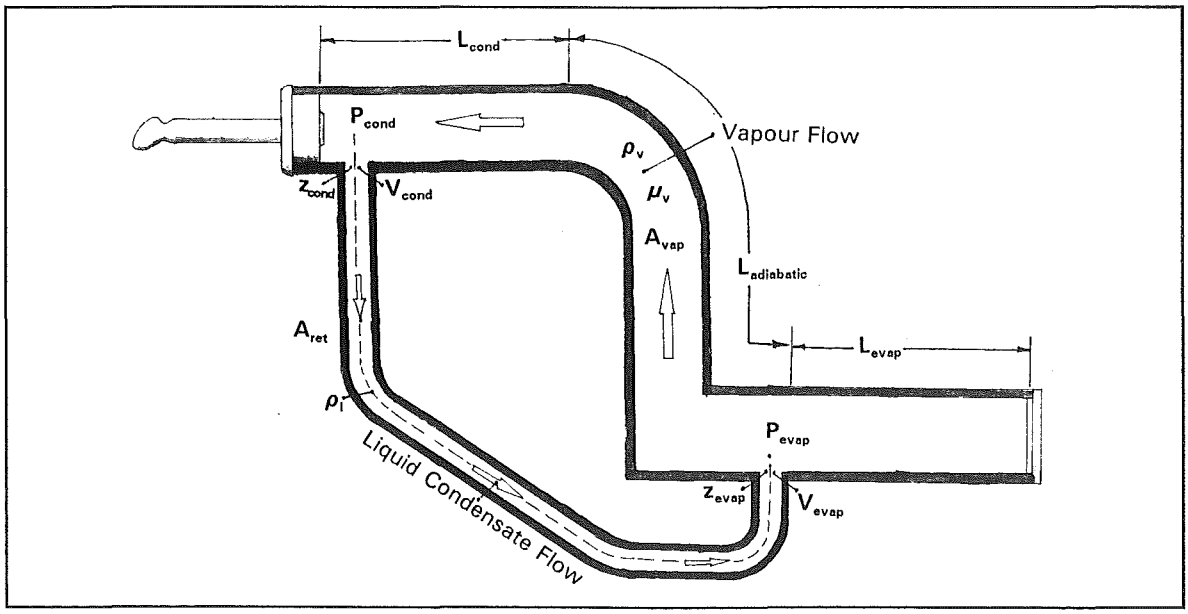

Figure 11.10 Nomenclature used in the limit expression for a heat pipe with a separate condensate return tube.

determined again by the rate at which the liquid can be returned to the evaporator, but in this case the flow is within a tube, with gravity providing the pumping pressure. As the tube is quite large compared with a porous wick capillary path, the amount of flow possible is very high, and consequently, so is the wicking limit. In this case, the use of the wicking limit equation 7.5 is not applicable. A new expression was produced to better approximate the limit to be imposed by the condensate return tube. (Refer to Figure 11.10 for the nomenclature used.)

The first simplification made was that a case of steady state incompressible flow existed in both the vapour space and the return tube. Also it was assumed that the heat pipe was a straight pipe with a diameter equal to the narrowest part of the real heat pipe designed. Bernoulli's equation was applied along a stream line through the condensate return tube, beginning in the condenser where the flow velocity was considered to be zero, and finishing level with the pipe outlet into the evaporator. It was assumed that the flow in the vapour space would be laminar, and that the flow in the condensate return tube would have negligible frictional effects due to the low viscosity of the mercury, and that the return tube would be full at the maximum condition. Bernoulli's equation for a stream line is:

$$P_{evap}+\frac{1}{2}\rho_l V_{evap}^2+\rho g z_{evap}=P_{cond}+\frac{1}{2}\rho_l V_{cond}^2+\rho g z_{cond} \qquad (11.6)$$

Where ρ_l is the liquid density.
V_{evap} is the liquid velocity in the condensate return tube at the evaporator end.
V_{cond} is the liquid velocity at the condenser, and is taken to be zero.
g is the acceleration due to gravity.

The z terms are the vertical heights of the condenser and evaporator relative to a datum which in this case was taken to be the outlet of the condensate return tube.

The pressure differential given by P_{evap}-P_{cond} could be found through the pressure loss due to friction in the vapour space. Given the assumption of a laminar flow present, the Hagen-Poiseuille equation was used. This was combined with the inertial term for pressure (P.D.Dunn 1982), thus:

$$P_{evap}-P_{cond}=\rho_V V_V^2+\frac{8\mu_V \dot{m}}{\rho_V \pi r_V^4}\left[\frac{L_{evap}+L_{cond}}{2}+L_{adiabatic}\right] \qquad (11.7)$$

Where ρ_v is the vapour density.
V_v is the vapour velocity.
$\dot{m}$ is the mass flow rate which is the same around the complete circuit.
μ_v is the vapour viscosity.
r_v is the radius of the vapour space which is taken to be 6.5mm
L_{evap} is the length of the evaporator.
L_{cond} is the length of the condenser.
$L_{adiabatic}$ is the length of the adiabatic region.

Equations 11.6 and 11.7 can be combined. However, to assist in the solution it is worthwhile changing the velocity terms into mass flow rates:

$$V_{evap}=\frac{\dot{m}}{\rho_f A_{ret}} \quad and \quad V_V=\frac{\dot{m}}{\rho_V A_{vap}} \qquad (11.8)$$

A_{ret} is the cross-sectional area of the condensate return tube, and A_{vap} is the cross-sectional area of the vapour space. Substituting 11.8 into 11.6, and 11.7, then combining the two, a quadratic expression in $\dot{m}$ can be obtained.

$$P_{evap}-P_{cond}=\rho_f g(z_{cond}-z_{evap})-\frac{\dot{m}^2}{2\rho_f A_{ret}^2}=\frac{\dot{m}^2}{\rho_V A_{vap}^2}+\frac{8\mu_V \dot{m}}{\rho_V \pi r_V^4}\left[\frac{L_{evap}+L_{cond}}{2}+L_{adiabatic}\right]$$

$$\therefore \dot{m}^2\left(\frac{1}{\rho_V A_{vap}^2}+\frac{1}{2\rho_f A_{ret}^2}\right)+\dot{m}\left(\frac{8\mu_V}{\rho_V \pi r_V^4}\left[\frac{L_{evap}+L_{cond}}{2}+L_{adiabatic}\right]\right)-\rho_f g(z_{cond}-z_{evap})=0$$

(11.9)

The quadratic can be broken down into its roots, and the negative root discarded. The remaining root is the maximum mass flow rate that the tube can carry, and will give the maximum heat flux when put into expression 11.10:

$$\dot{Q}_{wick}=\dot{m}\lambda \qquad (11.10)$$

λ is the latent heat of vaporization of the working fluid.
$\dot{Q}_{wick}$ is the wicking limit maximum heat transfer.

Upon substituting in values for a range of temperatures, the wicking limit was

never the lowest limit, and so was not of concern. For the full size system, at 340°C, the limit was 8600W.

11.6.4 Boiling Limit

The final limit was the boiling limit, the expression for which was given in chapter 7 by expression 7.8, shown here in expression 11.11.

$$\dot{Q}_{boil}=\frac{2\pi L_{evap}k_{eff}T_v}{\lambda\rho_v \ln\left(\frac{r_i}{r_v}\right)}\left(\frac{2\sigma}{r_n}-P_c\right) \qquad (11.11)$$

Where T_v is the vapour temperature.
k_{eff} is the effective thermal conductivity of the saturated wick.
r_i is the internal wall radius of the heat pipe.
r_v is the radius of the vapour space.
r_n is the nucleation radius of the vapour bubbles which for this case is taken to be 2.5×10^{-6}m.
P_c is the capillary pumping pressure and is not relevant here because of the nature of the liquid return, and wick.

To adapt the expression for $\dot{Q}_{boil}$, the boiling limit maximum heat transfer, to the conditions present in the mercury heat pipe described here, the thermal conductivity of the wick was taken as the thermal conductivity of the mercury alone. The reason for doing this is that there is an annular gap filled with mercury instead of a wick. At 340°C, the maximum heat transfer due to the boiling limit, was:

$$\dot{Q}_{boil}=\frac{2\pi 4\times12.06\times613}{295\times10^3\times3.0\times\ln\left(\frac{10}{6.5}\right)}\left(\frac{2\times0.543}{2.5\times10^{-6}}\right)=212\times10^3 W \qquad (11.12)$$

So the boiling limit according to this model was the least of our worries. However, as will become evident from the test heat pipe results, the boiling limit was the most serious problem, because of the poor wetting of the mercury allowing a vapour layer to form adjacent to the heat pipe wall, thereby acting as an insulator. This property of the working fluid is not accounted for within the expression 11.11.

11.6.5 Theoretical Heat Transfer Limits on the Mercury Heat Pipe

According to the theory used in the design and analysis of normal heat pipes, the limit envelope is shown in Figure 11.11. The region is bounded by the sonic limit line, and the entrainment limit line. Due to the nature of the condensate return, the wicking limit does not feature, and the excellent properties of mercury mean that the boiling limit does not feature either; however this fails to take into account the poor wetting of mercury. The size of pipe used in the calculations above is a straight steel hydraulic tube with an internal diameter of 20mm, and a vapour space diameter of 13mm. Its length is 450mm for the test heat pipe, and about 4.5m for one trough of the full size system. The practical heat pipe was much different, having two elbows in it, wider vapour spaces with constrictions down to 13mm diameter, so the theoretical limits predicted can only give an indication of the heat transfer ability, and in general will be conservative due to the narrower vapour space assumed.

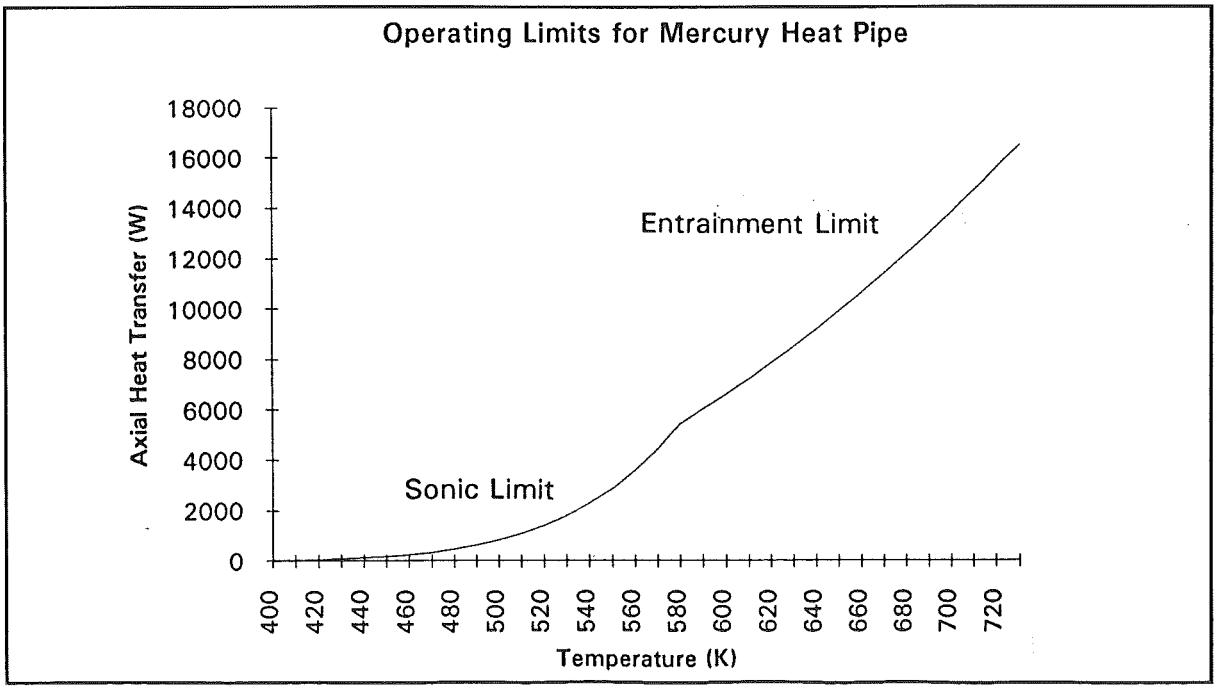

Figure 11.11 Heat transfer limit enveloped for a mercury heat pipe of 4.5m length with a 20mm internal pipe diameter, and a 13mm diameter vapour space.

11.7 Mercury Heat Pipe Experiments

After the fitting of a number of K type thermocouples, the heat pipe was mounted within a thick block of castable ceramic refractory for the purposes of insulation. The thermocouple placements are shown in Figure 11.12, and the number correspond to the numbers used in the 3D results plots. To drive the air calorimeter, a centrifugal fan was mounted in a retort stand, and connected to the calorimeter heat exchanger. This was controlled by means of a variac, and the air speed was measured upstream by a floating scale water micromanometer. Around the evaporator, a ceramic band heater was fitted, and wrapped in kaowool insulation. The electrical power input to the heater was measured by a wattmeter. For safety, the whole unit was placed in a fume cupboard which had been tested to ensure it met the standards required for this type of test - which it barely did.

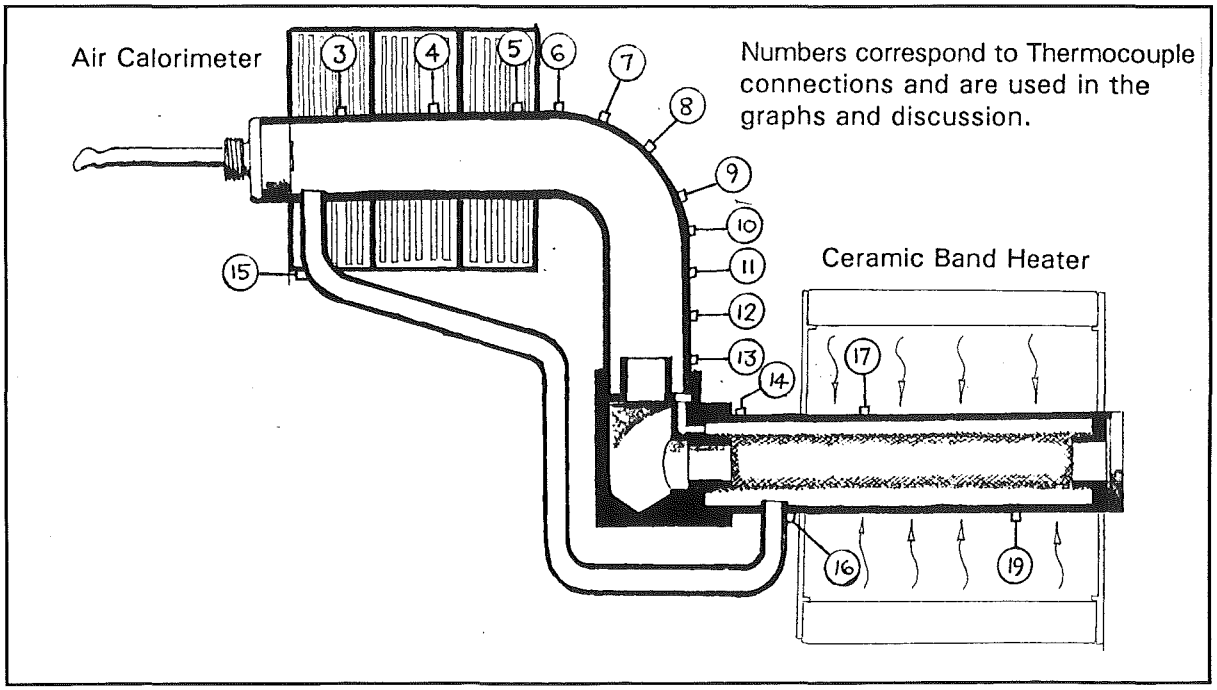

Figure 11.12 Thermocouple placement on the test mercury heat pipe.

The first experiment involved 750W of electrical power to the heater. The heat pipe was allowed to heat up until it reached about 250°C along its length, then the fan was switched on. This is shown in Figure 11.13. Note the sharp drop in the temperature corresponds to the time when the fan was switched on.

The second test had the fan running at all times but at a much slower speed so as to reduce the amount of cooling experienced by the heat pipe, and therefore

allow the heat pipe to operate at a temperature nearer that expected for the solar thermal application. This test was repeated with another thermocouple added to test the validity of the readings coming from the heated surface of the evaporator as it seemed to be giving erroneous readings which were unusually high.

A fourth experiment was run where the heat pipe was operated without any forced air cooling, so the cooling of the condenser came from the slight air movement through the calorimeter, and radiant cooling from the calorimeter. The reason for this test was that the target of 400°C was not being met, because the fan could not run slow enough to allow the heat transfer to the air to be low enough for the heat pipe to be able to reach temperatures much above 350°C.

Some time later it was felt that the reason for the high temperature drops between the evaporator, and the first thermocouple in the adiabatic region was a boiling problem (This will become evident as the results of the experiments are discussed in the following section). To reduce the heat flux, the heater was turned down until it simulated the expected flux from the solar thermal concentrators. To allow the temperature to rise sufficiently high, forced air was not used in the calorimeter.

The final test involved the use of the heat pipe on a small incline, to encourage an uneven distribution of liquid in the evaporator, and so try to ensure that the wall was being wetted, and so whether this could bring down the high temperature differential between the evaporator, and the first thermocouple in the adiabatic region; however with 750W of heat applied, and air cooling, the differential still existed.

11.7.1 Results and Discussion of the Mercury Heat Pipe Tests

Looking at Figure 11.13, there is a significant drop in the last three thermocouples (No.s 3,4, and 5) which are situated in the calorimeter, and touching the heat pipe wall. These thermocouples are subject to forced air cooling, and so will not read the true wall temperature unless the air flow is stopped. In this particular test, the air flow was quite fast, and the cooling was very effective which meant that the heat pipe never reached a temperature much above 260°C. At the other end of the pipe, the thermocouple No 17 on the heated surface of the

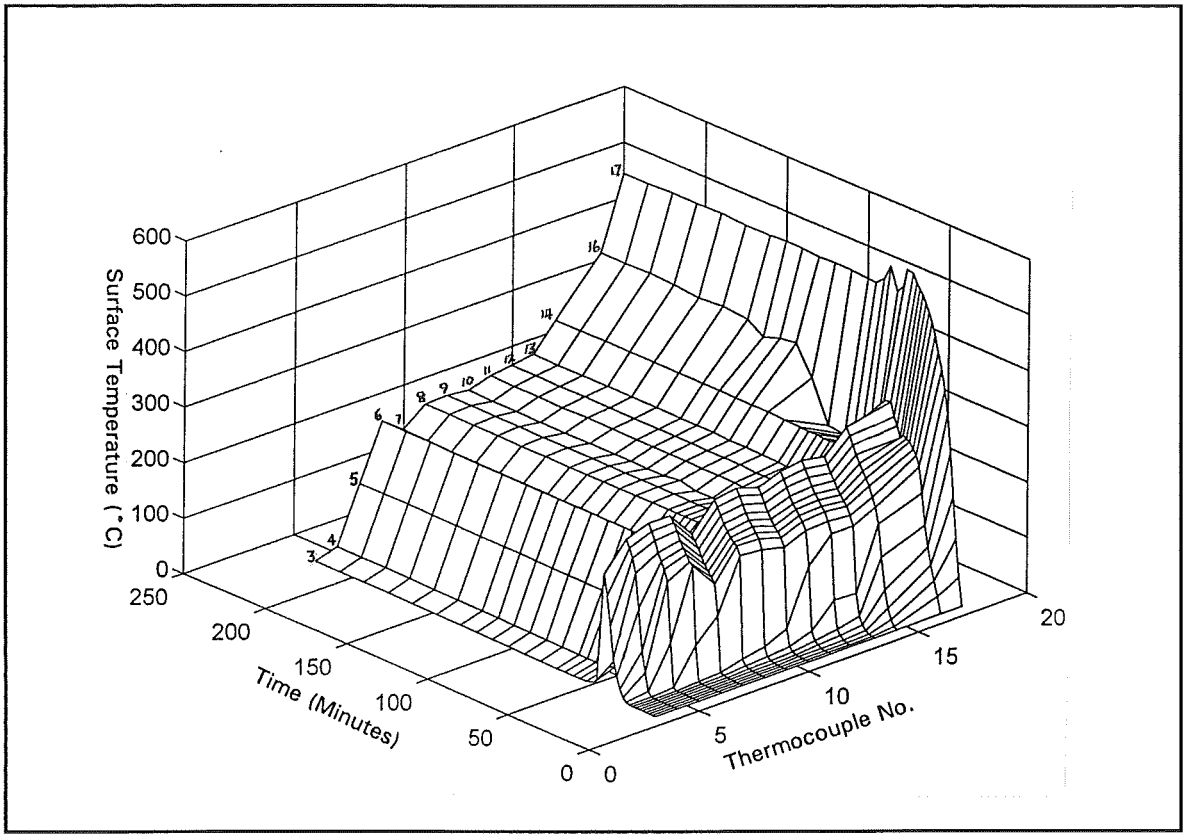

Figure 11.13 The Mercury heat pipe operating with 750W of electrical heating, and forced air cooling.

evaporator, is subject to radiant heating, and so the temperature reading from this is likely to be a little high.

It can be seen that there is a significant ridge along the 32 minute line, the reason for this being that after allowing the heat pipe to heat up, the calorimeter fan was turned on, thereby removing heat and dropping the temperature. The temperature drop is marked, and even, along the whole pipe, demonstrating quite effectively the heat pipe's ability to respond to changes in conditions at the condenser, and isothermalise quickly.

If more detailed attention is paid to the region just prior to and just after the fan was turned on, the thermocouple at the condenser return evaporator end (No. 16) experiences a fall in temperature; this indicates the presence of cooler condensate emerging from the return tube. This effect is quite marked after the fan was turned on because of the condensate receiving additional cooling from the air and the cold condensate return tube, as well as there being a large amount of mercury converging on the condenser instead of heating other parts of the heat pipe. Over

a period of 40 minutes as indicated by the rise in temperature at thermocouple No 16, the condensate return tube heated up, and the operation of the pipe settled down.

At thermocouple No. 7 there is a consistent, temperature drop; this is most likely due to the thermocouple having a bad contact with the heat pipe wall.

It was noted that a large transient heat transfer (607W) occurred immediately after the fan was turned on. During the initial start up when no air cooling was applied, the insulation and heat pipe walls were able to reach quite a high temperature (250°C). When the cooling was applied, the extra heat contained within the walls and insulation was drawn out, giving rise to the large transient heat transfer. Over time, the heat transfer through the pipe settled to a steady state of 410W. The difference between this value and the electrical input to the heater, represents heat that never entered the heat pipe but was instead lost through the insulation surrounding the heater.

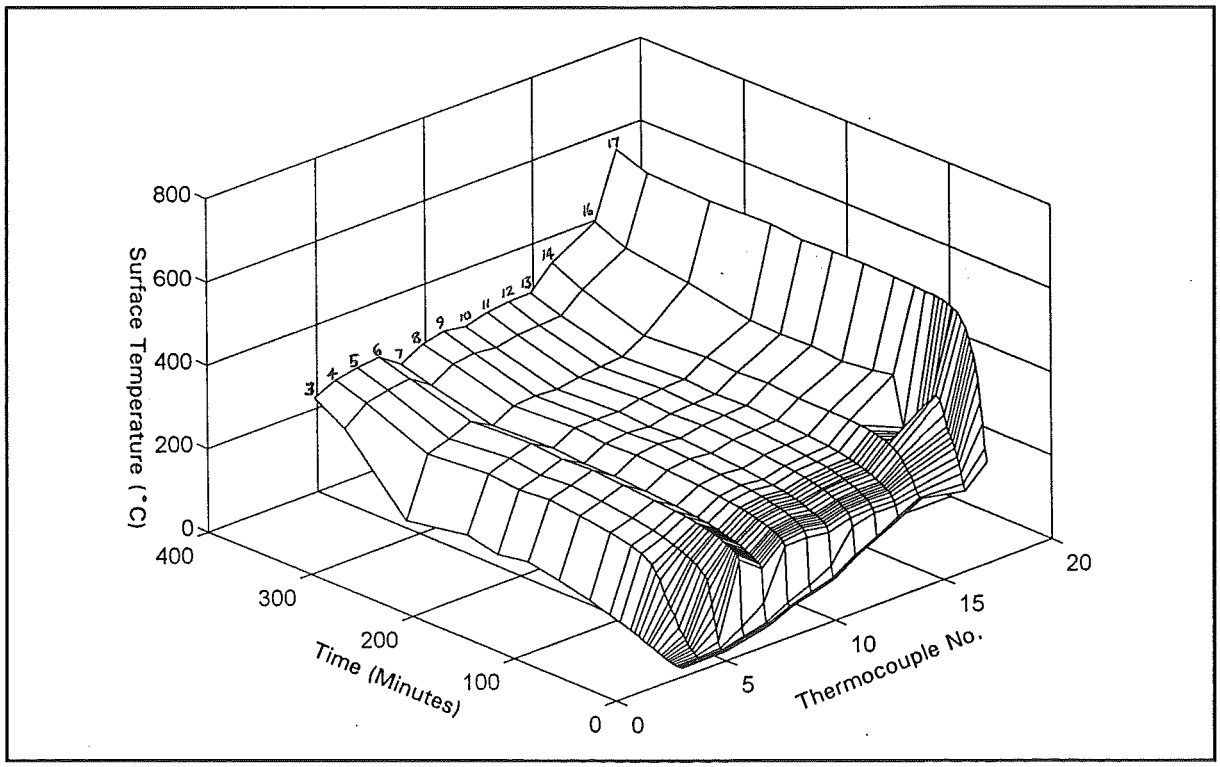

Figure 11.14 Mercury heat pipe operating with 750W electrical input to the heater, and low speed forced air cooling in the calorimeter.

Figure 11.14 shows the experiment where the same amount of heat was applied to the heat pipe, but the calorimeter fan was turned down in an effort to reduce

the cooling effect taking place. The averaging pitot tube flow meter measured a head of 0.11mmH_2O in a duct of 73mm diameter.

The start for this experiment was soon after a short test to determine the accuracy of the wattmeter, which is why the heat pipe does not start from a point of near uniform 20°C along its length. In this experiment, the depression of the temperature at the outlet of the condensate return tube is evident, as it was in the first experiment. Again it coincides with the heat front reaching the condenser region. As with the first experiment, the temperature depression due to this lasts for only a short amount of time because of the heating of the condensate return tube. A large temperature drop still exists between the evaporator heated surface thermocouple No.17 and the thermocouple on the evaporator wall closest to the elbow which would support the idea of additional radiant heating interfering with the measurements, but also supports the idea of a boiling problem. As the thermocouple No.17 was on top of the evaporator surface a third possible explanation was that the mercury level inside the tube was too low, and so heat would have to travel around from the upper surface of the evaporator tube to the mercury pool, through the steel walls, leading to an increased temperature drop.

To deal with the possibility of the mercury level inside the pipe being low enough to allow hot spots to form, another thermocouple (No.19) was fitted to the heated surface of the evaporator, but this time underneath so that the mercury could be guaranteed to be on the other side. The experiment above was repeated with the same electrical input to the heater of 750W, and the same low air speed through the calorimeter (0.11mmH_2O).

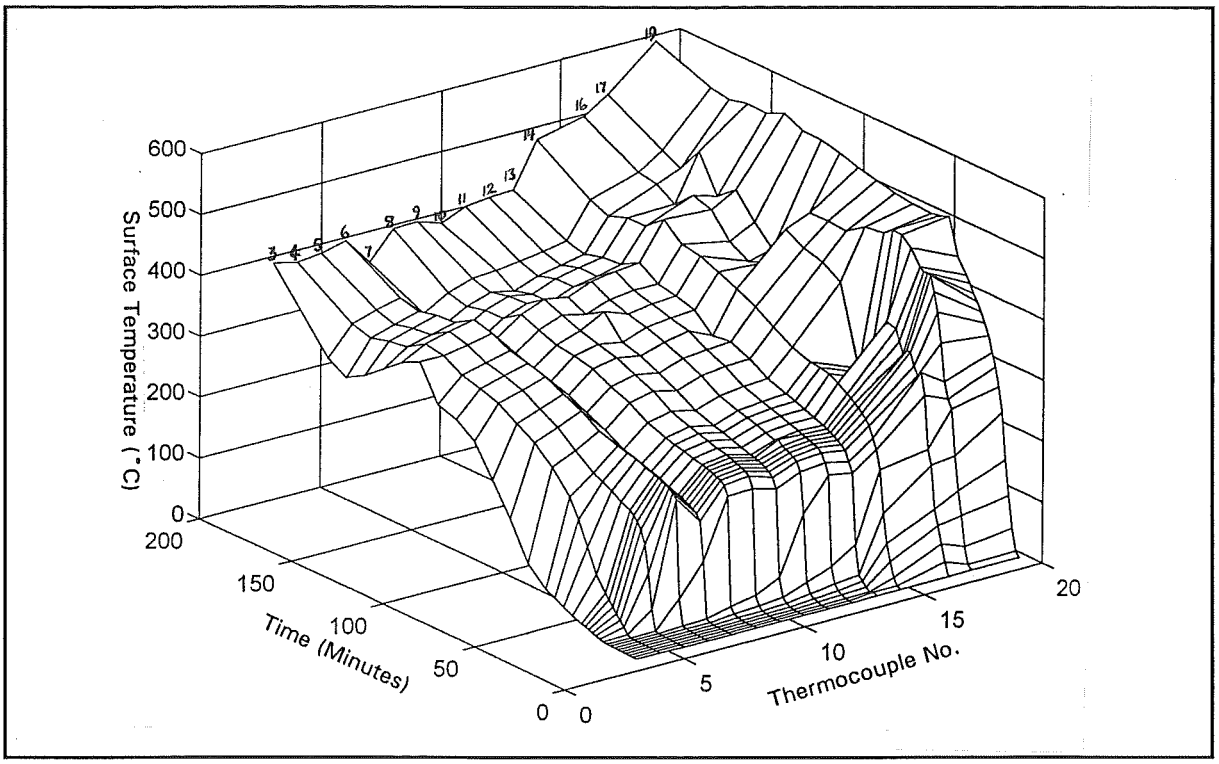

Figure 11.15 Mercury heat pipe operating with a 750W heat input, and a low air speed through the calorimeter. An additional thermocouple has been added to check the validity of the evaporator heated surface thermocouple.

Figure 11.15 shows that the two thermocouples (17 and 19) agreed for most of the time which indicated that the problem was not with the mercury level.

A small rise is evident at about the 120 minute point; this was due to the fan stopping. As with the previous experiments, the depression of the temperature around the condensate return tube outlet occurred at about the time that the heat front reached the condenser.

The next experiment (Figure 11.16) saw the heat pipe operating with 750W of electrical power going into the heater, but the calorimeter fan was not switched on; therefore the only cooling available was natural convective currents around the calorimeter heat exchanger, and radiation through the calorimeter entrance and exit. The heat pipe operated for only an hour, quickly gaining temperature and isothermalising at about 230°C and then continuing to gain heat evenly along its length until it was about 400°C. The temperature drop between the thermocouples on the heated surface of the evaporator (17 and 19) and the

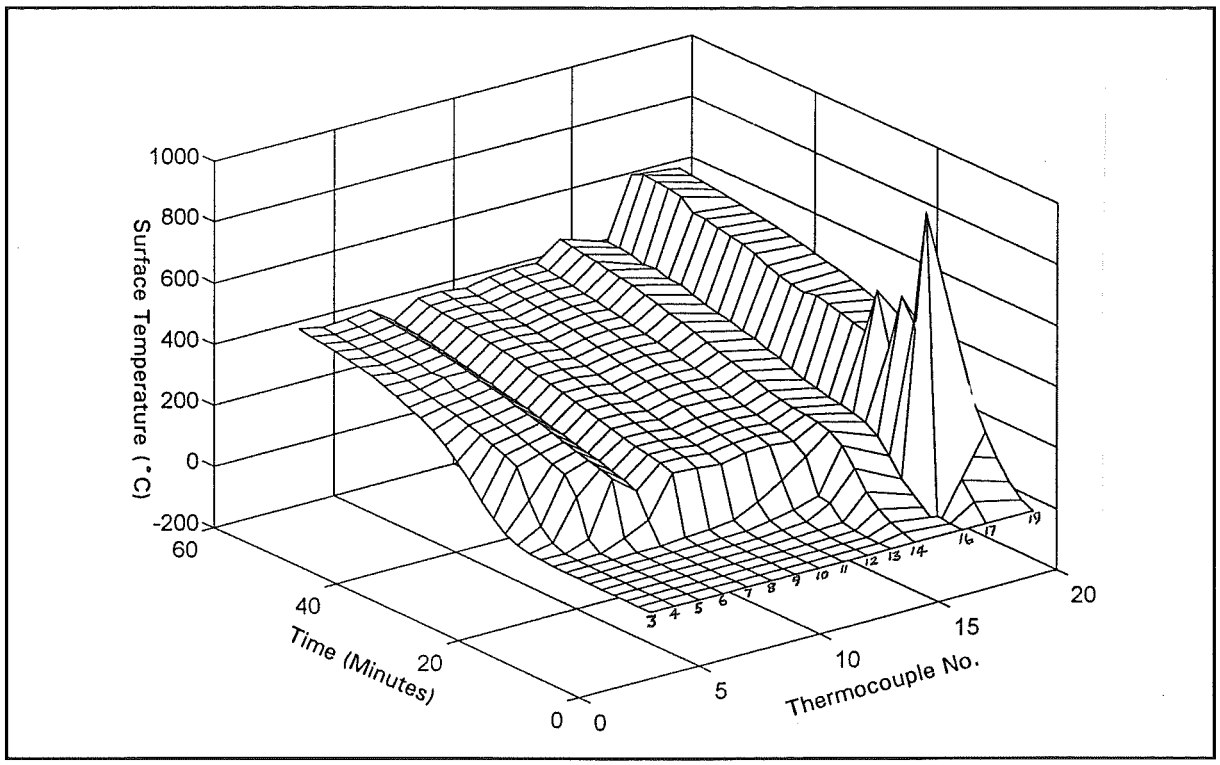

Figure 11.16 Mercury heat pipe with 750W of electrical heat applied, and no cooling applied.

thermocouples along the rest of the pipe remained relatively constant which would seem to indicate that it is a boiling problem that is responsible for it. If it were a result of radiation heating the thermocouple junctions, if they were not in close contact with the heat pipe wall, then the temperature would remain reasonably constant as the temperature of the evaporator would not have a great deal of effect on the outputs from these thermocouples, and so the temperature differential would fall.

The large temperature spikes read from thermocouple 17 were the result of the thermocouple wire insulation being melted away over the previous experiments, and the occasional movement of the heater causing the thermocouple to form a junction against the metal heater endcaps which were uncooled, and so reaching very high temperatures. When the heater was moved to break this contact, the readings immediately agreed with thermocouple 19 on the bottom surface of the heated evaporator.

The fact that the temperatures were constant right to the end of the condenser section indicated that no non-condensible gases had been released in the time that

the heat pipe had been operating. This showed that in production, a good job had been done in degassing, and that there were no reactions taking place to release gases from the pipe walls.

Unlike the previous experiments, the depression of the temperature around the condensate return tube was constant, and only slight. However, after the experiment, when the cooling was applied, very large swings in the temperature of thermocouple No. 16 at the outlet of the condensate return tube indicated large slugs of cooled liquid returning to the evaporator. Therefore during the experiment, only small, quite hot drops of liquid were returning at a slow rate.

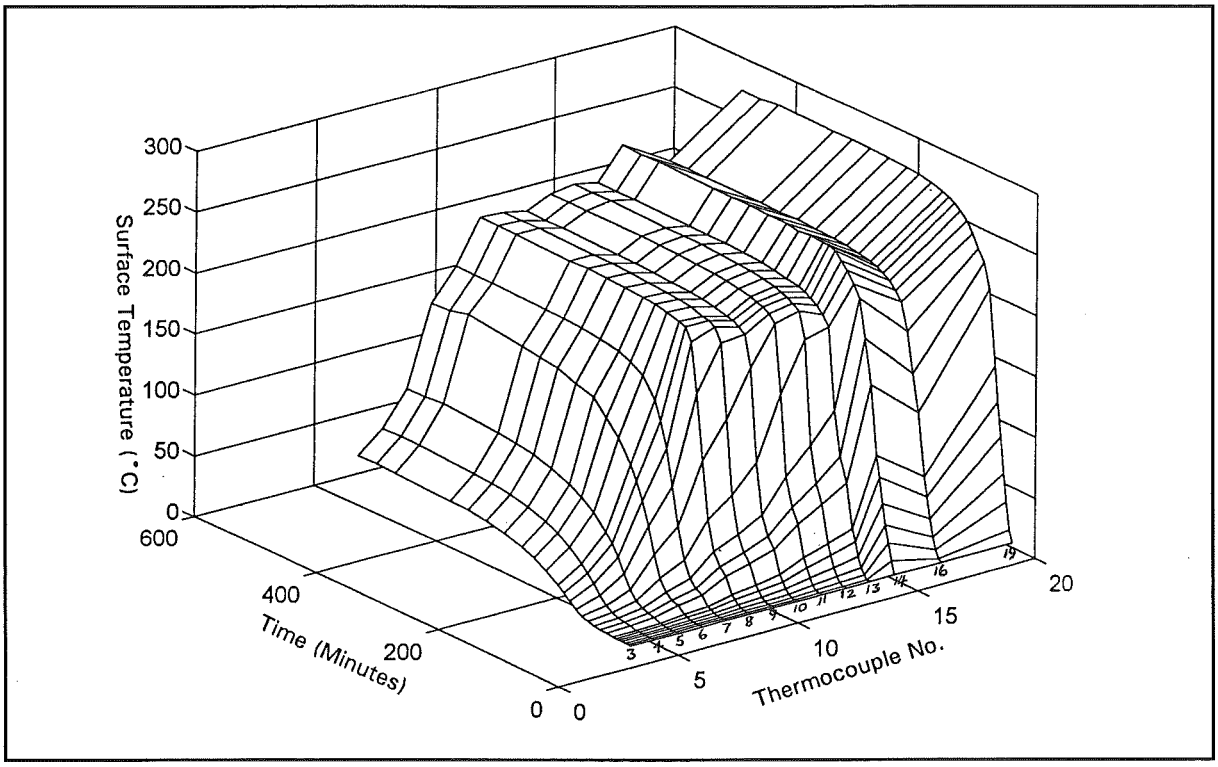

Figure 11.17 Mercury heat pipe operating with 140W heat input, and no cooling applied.

Because of suspicions that the high temperature difference between the evaporator heated surface and the rest of the heat pipe was due to a boiling problem, it was felt that an experiment should be done with a lower heat flux through the evaporator to test whether the temperature difference would be markedly different. It was also decided to simulate the heat flux expected in the solar concentrator system. Thus the electrical input to the heater was set at

140W. The air cooling was left off again to allow the temperature to achieve a reasonably high level. Even without the air cooling, the heat input was not high enough to keep the heat front advancing (see Figure 11.17), and so a large drop off in the temperature existed between thermocouples 3 and 8. It is possible that at this low temperature of only about 180°C along the heat pipe length, there is sufficient non-condensible gas present to shut off the condenser section, and so the heat pipe is operating only between the evaporator, and a point in the top elbow.

The temperature drop experienced between the heated evaporator surface and the rest of the heat pipe was reduced, thereby confirming that the temperature differential was due to a boiling problem. Note that in this experiment only one thermocouple on the heated evaporator surface had been used, because thermocouple No. 17 had become increasingly unreliable, and was giving very erroneous readings ie. 1080°C at one stage.

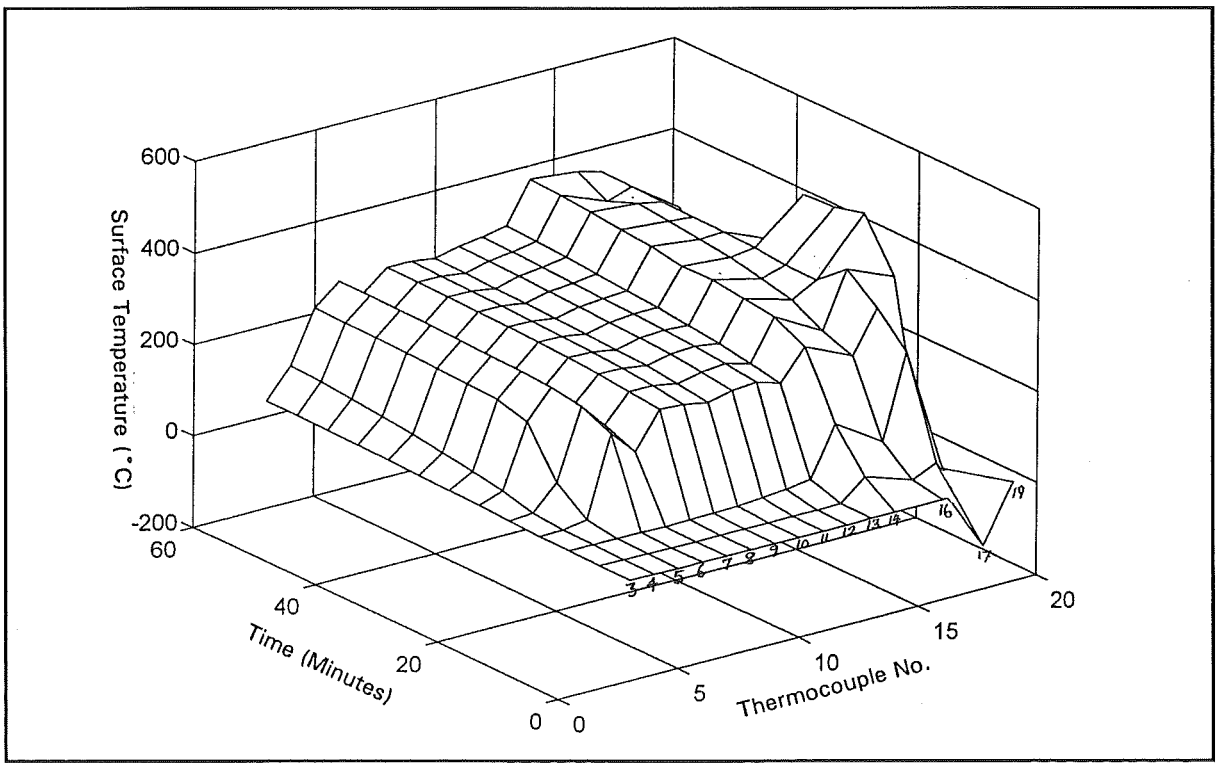

Figure 11.18 Mercury heat pipe with 750W of electrical power into the heater, air cooling, and operated on a slope.

A final experiment was performed with 750W of electricity going into the heater, air cooling applied, and a slope to the heat pipe. The results for this experiment

are presented in Figure 11.18. The temperatures achieved are comparable with those in the third mercury heat pipe experiment, which indicated that the slope was not affecting the performance unduly, while the temperature differential between the heated evaporator surface and the rest of the pipe was lower. This may indicate that sloping the heat pipe achieved a better contact between the mercury and the wall on the underside of the evaporator. Despite the erratic behaviour of the thermocouple 17 due to its loss of insulation, it was possible to get it to settle on a reading a little higher than that on from the thermocouple on the underside of the evaporator. However given that thermocouple No.17 is so unreliable, no conclusion can be drawn about this.

Later the heat pipe was run with a recess in the heater endcap through which a shielded thermocouple probe could be pushed. In this case, the agreement between the shielded thermocouple and the thermocouple No.19 was good.

11.7.2 Assessment of General Behaviour of the Mercury Heat Pipe

The experiments with the mercury heat pipe outlined above tested the concept of the liquid return system, and the use of a mesh tube to retain the mercury within an annular region against the heat pipe wall. The concept appears to work where only a single layer of wire mesh was used. To ensure that no leaks in the mesh cause the system to fail, it is recommended that this system be used but with two or three layers. This will make the production of the mesh tube somewhat easier, as well as improving the entrainment limit.

The variation of the temperatures along the length of the heat pipe outside of the heated region are due to heat flows within the wall material, additional cooling from the calorimeter, and the fact that some of the thermocouple may have pulled away from the heat pipe wall, and so will be reading reduced temperatures. The temperature along the unheated length is quite uniform and, taking into consideration, the effects mentioned above, probably no more than 5K variation exists. The ideal condensation properties of mercury make it very good for a system like the one proposed for the heat transfer into the head of a Stirling engine. All other thermodynamic properties make it very well suited to the

proposed application as well.

Despite the very good heat transport properties of mercury, there is a serious problem that occurs within the evaporator. This is the problem of the high temperature gradient between the heat pipe wall, and the vapour space. It is proposed that this is due to the poor wetting ability of mercury. Non-wetting fluids experience repulsive forces between the liquid and the solid walls, which causes the fluid to curve away from the surface (Dunn & Reay 1982). The angle made between the wall, (see Figure 11.19) and the liquid where it contacts the wall is known as the contact angle, and in the case of non-wetting fluids is greater than 90°. For this reason, the mercury will break contact with the wall given the chance. When the liquid boils or vaporises, the liquid pulls away from the wall, and so a vaporous annulus forms which acts as an insulating layer (see Figure 11.20). It is this insulation that causes the high temperature gradients.

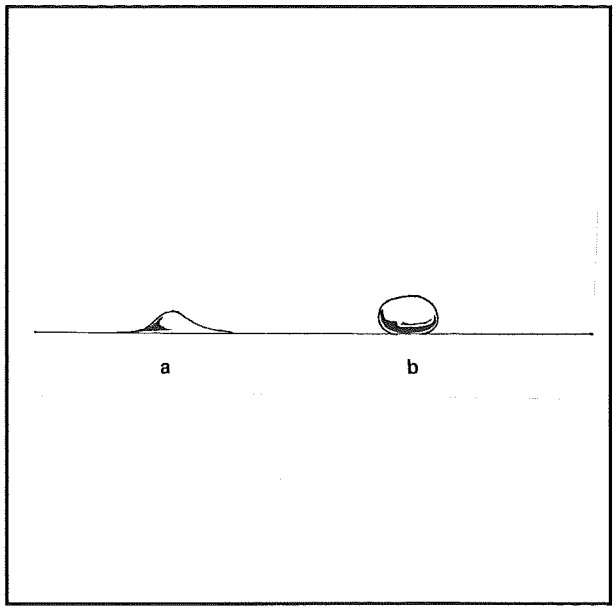

Figure 11.19 Wetting and non wetting fluids. **(a)** wetting **(b)** non-wetting.

A couple of methods of combatting this problem do exist, one would need careful testing as it is completely hypothetical at this stage, the other has been done previously (Deverall 1969). The latter is the suggestion to use an additive to the mercury that will cause it to wet better. It has been found that additions of small proportions of Titanium $4x10^{-3}$% by weight, and magnesium $8x10^{-3}$% by

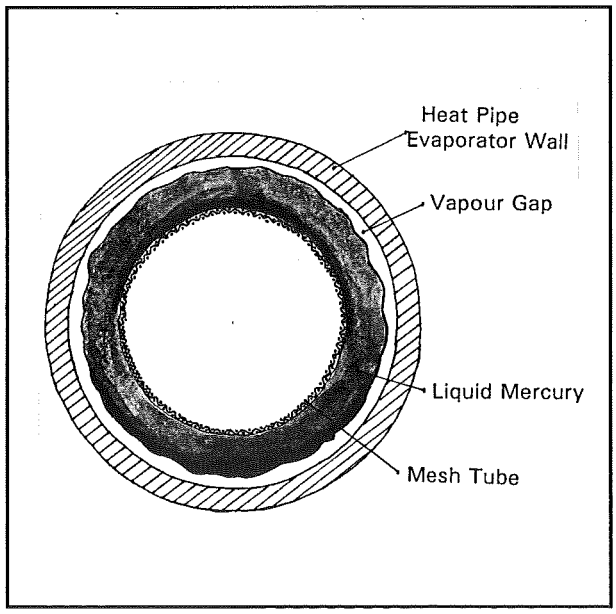

Figure 11.20 Proposed failure of the heat pipe evaporator because of the formation of a vapour annulus.

weight, improve the wetting characteristics of mercury. The magnesium acts as a cleaner for the wick by removing oxygen, while the titanium inhibits corrosion. This allows a clean surface to exist which will allow the mercury to more effectively wet. In the experiment described by Deverall, the heat fluxes attained in a 12 inch long ¾inch OD stainless steel tube with a 100 mesh wire wick were as high as 1030W. Unfortunately the design used would be unsuitable for the solar concentrator system because the capillary liquid return system would not be fast enough for the very long solar heated heat pipes. A combination with a return tube using a wire mesh wick to distribute the liquid once back in the evaporator, with the magnesium and titanium additions, could conceivably work.

The second suggestion makes use of mercury's ability to amalgamate with various metals (Williamson, 1993). A layer of aluminium would be deposited within the evaporator, and the mercury would form an amalgam with a high melting point. because of the presence of mercury within the heat pipe wall, it will wet the inside surface of the evaporator while also retaining its ability to not wet the wire mesh tube, and still have a good dropwise condensation.

Unfortunately, it is the extreme toxicity that makes this working fluid unsuitable for commercial production of a domestic solar power system using mercury heat pipes, as there is nothing that can be done to reduce its toxicity. It is an impossibility for every mercury heat pipe produced never to leak or burst.

The experiments could have been improved by the use of cartridge heaters in close contact with the pipe instead of the ceramic band heater which was separated from the heat pipe surface by quite a distance, and had to rely on radiant heating of the heat pipe which would have interfered a little with the true thermocouple readings for those that were on the evaporator outer surface. The use of a different form of calorimetry would have been easier and more effective too. The type that would be better suited is the water cooled gas-gap calorimeter like the one used by Deverall. This has the ability to have the heat transfer coefficient of the gas gap varied by changing the gas, while the metering of a water stream is easier and more accurate than trying to meter airflow ie. a measuring cylinder and stopwatch will do just as well.

11.8 Conclusion

Because of its extreme toxicity, mercury is unsuitable for a commercial domestic heat pipe. With its poor wetting leading to a large temperature drop appearing between the evaporator heated surface, and the thermocouple points further down the heat pipe, further experimentation was discontinued, with the possibility of continuing it using various techniques to improve the heat pipe wall to liquid contact. The heat pipe outside of the evaporator worked very well, with a good heat transfer ability, and showed a good ability to respond rapidly to changing conditions at the condenser. The design using a mesh tube to trap liquid mercury against the wall, and let vapour through into the vapour space also appeared to work, though it is recommended that the mesh tube be made of several layers of mesh.

In hindsight, there are a few changes to the experiment that could be done to improve the accuracy of the results, but the conclusions would still be the same.

12. THE POTASSIUM HEAT PIPE

12.1 Introduction

As was indicated in chapter 11, liquid metal working fluids are well suited to use in heat pipes. The operating temperature for the system was originally calculated to be 400°C for a small pipe (Resizing due to the heat pipe limits reduced this temperature). This would have been just above the lowest temperature at which an alkali metal heat pipe would operate. Sodium, the usual heat pipe working fluid, is best suited to the temperature range 600°C to 1200°C and would be severely restricted by the sonic limit at 400°C. A eutectic of potassium and sodium is often used in heat transfer systems; however the properties of this too, would have meant that it would have had problems with the sonic limit at 400°C. Only potassium appeared likely to work, but again the limiting factor would also be the sonic limit.

12.2 Potassium

Potassium is a very reactive alkali metal which has a melting point at 63°C, and a critical temperature of 1950°C. Far from being poisonous, potassium is essential to life, where it shares a job with sodium in maintaining electrical neutrality, osmotic pressure, and control of enzyme activities (Chang 1984). However this is in the ionic state as potassium is so reactive that it will not last as a metal when exposed to water or air for any length of time. Potassium upon contact with the air will oxidise to the superoxide, KO_2, and upon contact with water will react violently to form potassium hydroxide and hydrogen (Chang 1984), as has been demonstrated in numerous high school chemistry classes.

$$2K_{(s)} + 2H_2O_{(l)} \rightarrow 2KOH_{(aqueous)} + H_{2(g)}$$

Should the metal get onto the skin or eyes, it will cause thermal, and alkali burns, while the oxide smoke or hydroxide mist will cause irritation, and be corrosive on the throat and lungs (Perry *et al* 1984). Should potassium escape into

the environment, it would react to a safe salt very quickly with the only real risk being that it might be able to hit a flammable object before it had all reacted, and set it on fire.

Aside from the low vapour pressure, potassium has excellent heat transfer properties, such as a low viscosity, good wetting characteristics, reasonable liquid density, high surface tension, large heat of vaporisation, and a very high thermal conductivity. However it is the vapour pressure that causes the problem. Being so low, the vapour has to travel very fast to transfer the heat, and to slow the vapour, a larger diameter pipe has to be used which increases the heat losses from the system. Having such a low vapour pressure the heat pipe is prone to loss of performance caused by only a very small amount of non-condensing gas. Therefore the heat pipe would have to be extremely clean and thoroughly degassed, degreased, and have had its surface deoxidised.

In its metallic form at room temperature it is a very soft metal, being the consistency of butter.

12.3 Potassium Heat Pipe Design

Being a wetting fluid, the design of the heat pipe is somewhat easier than that for the mercury heat pipe. With the full size system, it is again impossible to have the potassium wicking for the full 4m, so, again a gravity return with a condensate return tube would be used. In this case, a wrapped wire screen wick, would be fitted into the evaporator for spreading the liquid over the inside surface of the heated region.

The suggested improvements to the mercury heat pipe were included in this design with a water cooled gas-gap calorimeter, and a series of cartridge heaters to be used in a heated block which would be strapped firmly to the heat pipe evaporator section's bottom surface to simulate the heat from the solar concentrators.

12.3.1 Heat Pipe Operating Limits for Potassium

After a few trials, and a trip to the steel store, a plain carbon steel tube with an internal diameter of 38mm and an external diameter of 41.46mm was decided on

as it would give a suitable heat transfer at 400°C as originally calculated. Carbon steels, and low alloy steels, show good resistance to attack from potassium up to 538°C (Perry *et al* 1984). So, as the calculated temperature indicated that the heat pipe would be operating significantly below this temperature, it would be safe. Otherwise a stainless steel would have had to be used.

SONIC LIMIT

Chapter 7 gave the sonic limit as:

$$\dot{Q}_{sonic}=\lambda \rho_v A_{vap}\sqrt{\frac{\gamma R T_v}{2(1+\gamma)}} \qquad (12.1)$$

where λ is the latent heat of vaporisation.
ρ_v is the vapour density.
A_{vap} is the cross sectional area of the vapour space.
γ is the specific heat ratio of the working fluid which in the case of potassium is 1.67.
R is the gas constant for the working fluid which in this case is 212.65 J/kgK.
T_v is the vapour temperature (K).

At 400°C, with a pipe of 38mm internal diameter, the sonic limit is:

$$\dot{Q}_{sonic}=2181\times10^3\times0.0035\times\frac{\pi}{4}0.038^2\sqrt{\frac{1.67\times212.65\times673}{2(1+1.67)}}=1832\ W \qquad (12.2)$$

At the higher temperature used here, a potassium heat pipe of this size will transfer an axial heat rate that is barely enough to keep the 200W Stirling engine running on solar energy. The estimate here for the vapour density is conservative, and calculated from ideal gas laws. It does not agree with the figure given in Dunn (1982) which is about twice the density calculated, and therefore would give a higher heat transfer limit.

ENTRAINMENT LIMIT

The entrainment limit for the design to be outlined shortly is the same as that for a heat pipe with a wrapped screen wick, and capillary condensate return, because the liquid is being held within a porous wick which provides a good protection from

the vapour flow. The expression for the entrainment limit as given in chapter 7 is:

$$\dot{Q}_{ent}=A_{vap}\lambda\sqrt{\frac{\sigma\rho_v}{2r_{hs}}} \qquad (12.3)$$

where σ is the liquid surface tension.
r_{hs} is the hydraulic radius of the mesh tube apertures.
r_{hs} is taken to be ¼ of the aperture width of the wire mesh which in the case of a 150 mesh is 0.089mm, so r_{hs} equals 0.0223mm.

$$\dot{Q}_{ent}=\frac{\pi}{4}\times0.038^2\times2181\times10^3\sqrt{\frac{0.091\times3.5\times10^{-3}}{2\times22.3\times10^{-6}}}=6610\ W \qquad (12.4)$$

WICKING LIMIT AND BOILING LIMIT

Although potassium is a wetting fluid, its capillary pumping power is not strong enough to drive liquid for the full length of the large scale heat pipe that would be used on the solar concentrator, and so an alternative method for returning the liquid had to be found. The transport properties of potassium as a liquid make it well suited to a system similar to that used in the mercury heat pipe whereby the condensate is returned via a separate tube to the evaporator, by gravity. To distribute the condensate, the return tube would have a number of holes in it running the potassium into the wire mesh wick that would have the job of distributing the liquid around the heated wall. In the case of potassium, because the operation is at such a low temperature, neither the wicking or the boiling limit were very low, and so further calculations of the limits will not be shown here because they are in the many kilowatt range. However for the model system with 750W at 400°C, entering an evaporator of length 150mm, a check of the boiling limit was needed. The expression from chapter 7 was:

$$\dot{Q}_{boil}=\frac{2\pi L_{evap}k_{eff}T_v\left(\frac{2\sigma}{r_n}-P_c\right)}{\lambda\rho_v\ln\left(\frac{r_i}{r_v}\right)} \qquad (12.5)$$

Where T_v is the vapour temperature.

k_{eff} is the effective thermal conductivity of the saturated wick.
r_i is the internal wall radius of the heat pipe.
r_v is the radius of the vapour space.
r_n is the nucleation radius of the vapour bubbles which for this case is taken to be 10^{-6}m.
P_c is the capillary pumping pressure which is quite low, and will be negligible when compared to the pressure term due to boiling.

In the case of the evaporator, a porous wick is being used, and so an effective thermal conductivity is given by equation 12.6.

$$k_{eff}=\frac{k_l[(k_l+k_w)-(1-\varepsilon)(k_l-k_w)]}{[(k_l+k_w)+(1-\varepsilon)(k_l-k_w)]} \qquad (12.6)$$

In this k_l is the liquid thermal conductivity.
k_w is the thermal conductivity of the wick material.
ε is the volume fraction of liquid which is the ratio of the liquid volume to the total volume of the saturated wick.

ε in the case given here with a 200 wire screen wick wrapped with approximately 5 layers, = 0.594. The thermal conductivity k_l of the liquid is 49.08 W/mK at 400°C, while that of the screen wick k_w is 16.27W/mK, as it is stainless steel. Therefore the effective thermal conductivity is:

$$k_{eff}=\frac{49.08[(49.08+16.27)-(1-0.594)(49.08-16.27)]}{[(49.08+16.27)+(1-0.594)(49.08-16.27)]}=32\ W/mK \qquad (12.7)$$

Substituting this into the boiling limit expression gives:

$$\dot{Q}_{boil}=\frac{2\pi 0.1\times 32\times 670}{2181\times 10^3\times 3.5\times 10^{-3}\ln\left(\frac{19}{18.5}\right)}\left(\frac{2\times 0.091}{10^{-6}}\right)=120\ MW \qquad (12.8)$$

As can be seen, the boiling limit is definitely not a problem.

12.3.2 Potassium Heat Pipe Form Design

The method for returning condensate to the evaporator made use of a separate condensate return tube and a mesh wick to distribute the condensate around the evaporator as was described in the preceeding section. Because of the need to

evenly distribute the liquid, it was necessary to do more than just let the potassium run down the sides of the adiabatic region and into the wick. A catching gutter was needed that would guide the liquid into the condensate return tube.

It was desired that the pipe simulate the heat pipes to be fitted to the solar concentrators and Stirling engine. To this end it was made to be the same diameter as the full length ones, and to be easily adapted to fit over the heater head on the DMC3 Stirling engine (Clucas 1993) for preliminary tests. To simulate the heat flux from the solar concentrators, heating of the test heat pipe was to be through the bottom third of the evaporator surface.

To produce the wick, a spring was used to press the wrapped screen wick against the heat pipe wall. Using a special tool, the spring was wound up to decrease its diameter, and the wire mesh wrapped around it. Still with the torsion on the spring, the wick, spring, and tool were slid into the evaporator. Releasing the torque allowed the spring to expand, and press the wick against the heat pipe wall. The tool was disengaged, and removed. The end result was a heat pipe that looked like Figure 12.1.

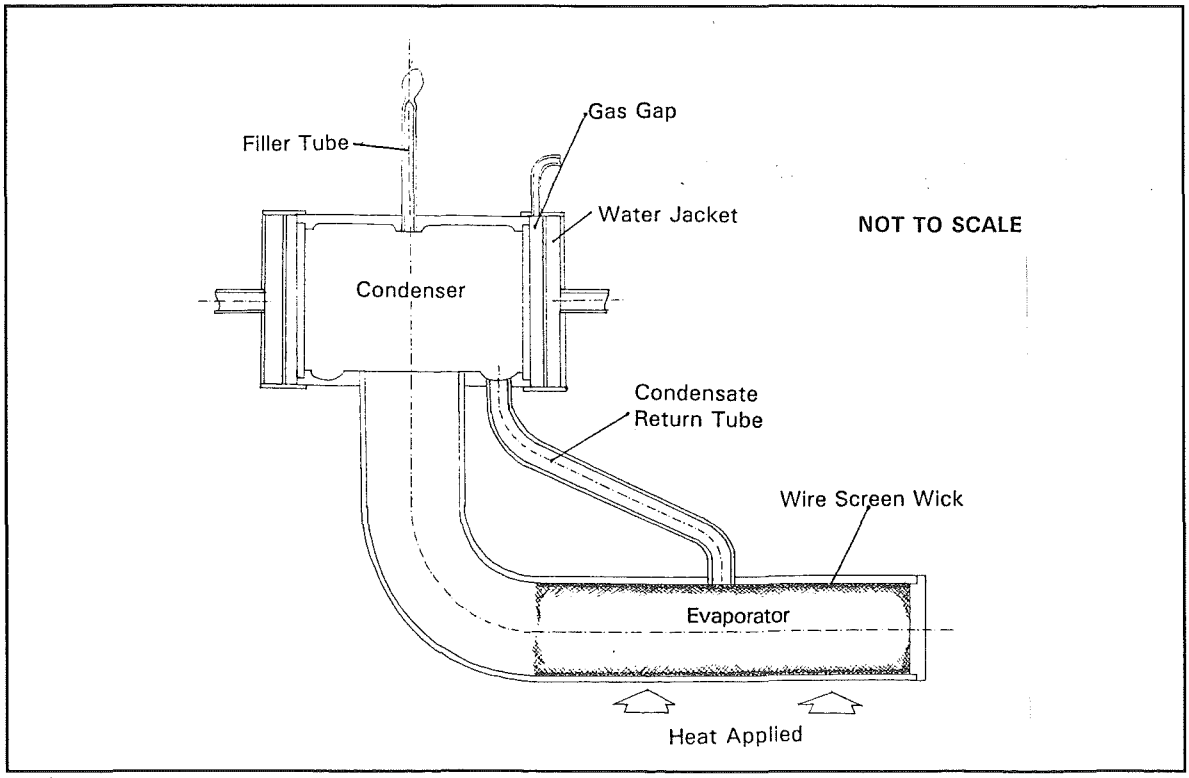

Figure 12.1 The potassium heat pipe for testing the concept. Note the wide diameter condenser section which can be easily adapted to fit over a DMC3 Stirling engine.

12.3.3 Heater

To improve the heating of the test heat pipe, it was desired to use a series of cartridge heaters within a block of metal in close contact with the heat pipe wall so as to allow conductive heat transfer to the heat pipe to occur instead of the radiant heat transfer as had been used with the previous heat pipe experiments. Heating was to occur only on the bottom third of the evaporator. The design that was built was a block containing three 260W ¼ inch OD cartridge heaters, and is shown in Figure 12.2.

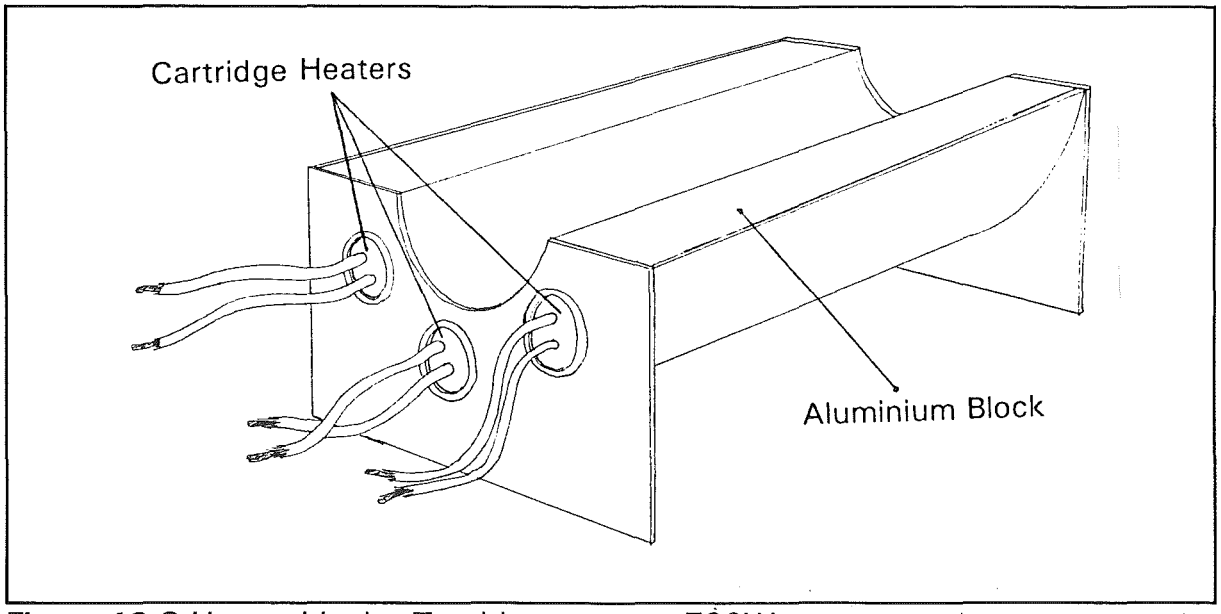

Figure 12.2 Heater block. Total heat output 780W.

12.3.4 Potassium Heat Pipe Surface Treatment

Because of the low vapour pressure, any oxygen in the heat pipe wall had to be removed to prevent it forming non-condensing gases which would act to stop the heat pipe. This process involved pickling the heat pipe in strong acid, and keeping it in a protective environment.

First the heat pipe (without the endcap on the evaporator) was washed with trichloroethylene to remove grease. It was then rinsed with water to flush out any solid particles that still remained inside. A solution of hot 50% sulphuric acid was poured into the pipe and left for approximately 1 minute. This removed the oxygen from the surface of the heat pipe and the wire screen wick. Another rinse of cold sulphuric acid mixed with hydrochloric acid was used, then the heat pipe was dried

potassium to allow the remaining impurities to settle out. The liquid potassium would then be poured into a mould for making small pellets which could be placed in the filling rig.(Figure 12.3)

When the pellets were in the rig, its valves could be closed, and it could be removed from the glove box, to be attached to the evacuation line. The empty heat pipe was also attached to the evacuation line. The ball valve on the filler rig could be opened and the protective nitrogen pumped out. By heating the bulb, the potassium could be melted, and then by tipping the rig, via the flexible metal bellows, the potassium would run down into the heat pipe, which could be then sealed up, and removed from the line.

However, the cleaning was halted when the potassium melted. Despite all the care and precautions taken, the potassium exploded. It seems that the perchloroethylene will form explosive compounds with sodium, and probably forms similar compounds with potassium. The compounds formed are a contact explosive and so any disturbance, in this case it may have been from a thermocouple probe being used to monitor the potassium temperature, would have caused it to explode.

12.4 Conclusion

Cut short, this experiment yielded no results for the use of potassium as a heat pipe working fluid other than it is very difficult and dangerous to handle. Given the right advice, and equipment, it would be possible to produce one.

In hindsight, now that the values for the system have been reassessed, (Chapter 6) it was shown that the optimum temperature was no longer the 400°C used here, but instead somewhat lower, making the sonic limit even more of a problem, and making it necessary to use an even larger heat pipe diameter which would increase the losses, and drop the optimum temperature even further. Potassium for this system as it stands now, would not work.

13. CONCLUSION

13.1 Final Concept Design Overview

Solar energy is a very clean and cheap source of renewable power for both domestic and industrial applications. Current systems using it are either, photovoltaic, dish/Stirling, or line focus concentrators with a Rankine cycle heat engine. These systems vary in size from many kilowatts of generating power to about 3-4kW. This project has found that a system to generate power for an isolated domestic situation, using a Stirling engine and line focus concentrators, has a very poor efficiency (Chapter 6). In the design presented here, heat pipes were found to be the best way for transporting the solar heat from the concentrators to the Stirling engine. Of the heat pipe working fluids tested, the best performance was from mercury. This does have the disadvantage of being a fluid which will not wet surfaces easily.

When vapour forms in the evaporator, which would run along the focus of the solar concentrators, the non-wetting fluid will break contact with the heated wall, forming an insulating layer. This results in large temperature drops between the heat pipe wall, and the working fluid. As the efficiency of the system is dependent on the absorber temperature and the heat pipe working fluid temperature, a temperature drop between the evaporator wall, and the liquid would reduce the efficiency. A higher evaporator surface temperature would increase the heat losses through reradiation, and convection-conduction. The reduced temperature in the heat pipe working fluid would decrease the heat engine thermal efficiency. In addition to the problems involved with the wetting, mercury is extremely toxic, and in a domestic environment would pose a severe health risk.

Figure 13.1 shows the system design as it was at the completion of this project. The design shown is the test arrangement for an electrical output of 200W from the engine. The temperature at the absorber would be between 330°C and 350°C, and would be monitored by a microcomputer connected to the tracking servos. This would allow the system to be tracked away from the sun should it begin to over-heat.

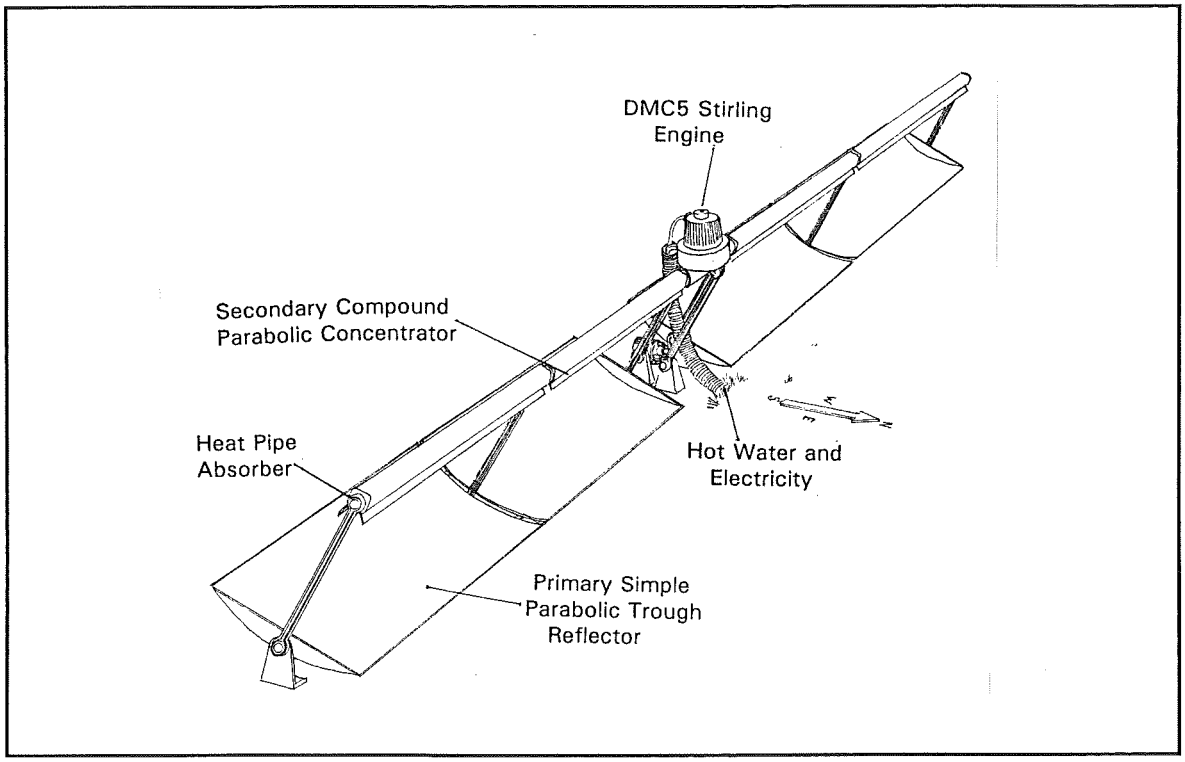

Figure 13.1 The test system for a line focus concentrator and Stirling engine generator set for domestic power 200W_e.

13.2 Optical System

The arrays would be set in an east-west orientation so that the movement of the array during the day is minimised, as well as ensuring that the arrays are in a horizontal plane (Section 5.4). A two stage concentrator system would be employed, with a simple parabolic primary concentrator, and a compound parabolic secondary concentrator. With an acceptance half angle of 1°, and a primary concentrator rim angle of 30°, the arrangement would be efficient on materials, and have a very good concentration ratio (Chapter 5). The simple parabolic primary concentrators would be surfaced with aluminised mylar and the secondary concentrators would be polished aluminium, due to their need to withstand high temperatures.

13.3 Heat Pipes

The chosen temperature of operation for the solar-Stirling system (600-625K), is within a range that there are very few suitable working fluids, being too high for organic fluids, and too low for most liquid metals.

13.3.1 The Sulphur Heat Pipe

It had been suggested that a mixture of sulphur and iodine would be a suitable working fluid for the temperature range 300°C-600°C. However, experiments (Chapter 9) showed that the iodine, which was added to keep the viscosity of the sulphur low, separated out, and formed a non-condensing gas during heat pipe operation.

13.3.2 Organic Heat Pipe Working Fluids

A search through the properties of a number of chemicals yielded some candidate organic working fluids. It was observed that although the properties were reasonable at the system operating temperature, the autoignition points of the fluids were close to the target temperature. A simple heat pipe operated for a number of hours showed that the dioctyl phthalate used to indicate the suitability of the other candidate fluids, broke down into lighter fraction chemicals (Chapter 10). This indicated that the other candidate fluids which had similar autoignition properties, would also break down at the high temperatures. Dowtherm A, another candidate fluid, though capable of withstanding the high temperatures for a time, would have problems with the boiling limit (Section 7.2.3).

13.3.3 The Mercury Heat Pipe

Mercury was the most promising candidate working fluid tried. Its performance was very good where condensation was concerned. The heat pipe design used a separate return tube for the return of the condensate from the condenser to the evaporator. Mercury is a non-wetting fluid, and this caused problems with boiling. Vapour forming adjacent to the heated evaporator wall would allow the liquid to break contact with the wall, thereby introducing a thermal resistance into the pipe. A high temperature drop between the evaporator heat pipe surface, and the rest of the heat pipe was evidence of this (Chapter 11).

For a project such as this, which is looking at a domestic oriented product, the use of large quantities of mercury at high temperatures, poses a very high health risk, due to mercury's high toxicity.

13.3.4 Potassium as a Heat Pipe Working Fluid

Potassium is a non-toxic, but very reactive alkali metal. It was observed that based on the preliminary system operating temperature, potassium would be able to work if the heat pipe diameter were to be enlarged to reduce the problem of sonic vapour velocities occurring (Chapter 12). In attempting to load the heat pipe, the potassium charge exploded, demonstrating how difficult it is to handle. Later reevaluation of the system operating temperature to account for the new absorber sizes, reduced the temperature to below that which potassium could successfully operate at.

13.4 Overall System Assessment

Experiments on the performance of a number of potential heat pipe working fluids demonstrated the difficulty in operating a heat pipe at the medium temperatures required for the line focus solar Stirling co-generation system. Of the fluids tested, the most promising was mercury which had the potential to be suitable if a technique to improve its wetting characteristics could be found. Unfortunately, because of the toxicity of mercury, the use of many small domestic solar Stirling co-generation units based around mercury heat pipes, is questionable from a safety point of view. Given a more controlled, and carefully monitored situation, mercury heat pipes could conceivably be used. Such a controlled environment could be found in a larger scale system for servicing a small community.

With a total system efficiency of 3% conversion of solar radiation to electricity as predicted by the performance prediction model, the economic viability of the line focus solar Stirling co-generation system is doubtful. Further economic assessment is recommended if a good working fluid (or solution to the wetting problem of mercury) was found and it was decided to continue with this design. From an energy point of view, the system must be able to produce more useful energy in its lifetime, than was used to manufacture the system.

14. REFERENCES

Amor,M.R., Raine,J.K., Tucker,A.S., "Double Diaphragm Solar-Powered Water Pump" *Proceedings of Solar World Congress of the International Solar Energy Society, vol2, part2, pp2141-2146,* 19-23 August, Denver, Colorado, 1991

Atkins,E.E., Ellison,W., Walker,G., Zylstra,S.G., "Wood-fired Ross-Stirling 3kW Power system" *Twenty five years of progress and Future Prospects - 25th Intersociety Energy Conversion Engineering Conference, vol.5, pp319-323,* IECEC, 12 -17 Aug, Reno, 1990

Beale,W., "Some practical Considerations for Cost Minimization of Solar Stirling Engines" *5th International Stirling Engine Conference, pp51-56,* ISEC-91012, 8-10 May, Dubrovnik, 1991

Bean,J.R., Diver,R.B., "The CPG 5-kW_e Dish Stirling Development Program." IECEC Paper No. 929181 *Proceedings of the 27th Intersociety Energy Conversion Engineering Conference, pp5.221-5.228, vol 5,* Warrendale, 1992

Billingham,B.M., "A new look at Hybrid Vehicles" *Electric Vehicle developments, pp10-11,* March 1979

Bonilla,C.F.,Busch,J.S.,Stalder,A.,Shaikhmahmud,N.S.,Ramachandran,A.,"Pool-Boiling Heat Transfer with Mercury" *Liquid Metals Technology - Part 1, Chemical Engineering Progress Symposium Series, pp51-57, No. 20, Vol. 53,* American Institute of Chemical Engineers, 1957.

Brown Copeland & Co.Ltd, "Guide to Sources of Data on National Energy Consumption" *New Zealand Energy Research and Development committee,* Publication P82, March 1984

Cao,Y., Faghri,A., "Closed-Form Analytical Solutions of High-Temperature Heat Pipe Startup and Frozen Startup Limitation." *Transactions of the ASME, Journal of Heat Transfer, pp1028-1035, Vol.114,* November 1992

Chang,R., "Chemistry - Second Edition" Random House, New York, 1984

Chi,S.W., "Heat Pipe Theory and Practice" Hemisphere Publishing Corporation, Washington, 1976

Chisholm,D., "The Heat Pipe" Mills & Boon Limited, London, 1971

Clucas,D.M., Raine,J.K., Tucker,A.S., "Stirling Cycle Battery Charger for Yachts" *Proc. IPENZ Annual Conference, vol.2, pp351-362,* Christchurch, 1992

Clucas,D.M., Raine,J.K., "The Design of a Stirling Engine Battery Charger for Yachts." *6th International Stirling Engine Conference, pp87-92*, ISEC-93017, 26-28 May, Eindhoven, 1993

Currie,A.M. (Managing Editor) "Collins Paperback Atlas of the World" William Collins Sons and Co. Ltd., 1989

Daubert,T.E., Danner,R.P., "Physical and Thermophysical Properties of Pure Chemicals - Data Compilation" Design Institute for physical Property data, American Institute of Chemical Engineers, Hemisphere Publishing Corporation, New York, 1989

Deverall,J.E., "Mercury as a Heat Pipe Fluid" Los Alamos Scientific Unclas Lab, LA-4300, October 1969

Douglas,J.F., Gasiorek,J.M., Swaffield,J.A., "Fluid Mechanics - Second Edition" Longman Scientific & Technical, Harlow, 1986

Dunn,P.D., Reay,D.A., "Heat Pipes - Third Edition" Pergamon Press, Oxford, 1982

Epstein,L.F., "Static and Dynamic Corrosion and Mass Transfer in Liquid Metal Systems" *Liquid Metals Technology - Part 1, Chemical Engineering Progress Symposium Series, pp67-81, No.20, Vol.53*, American Institute of Chemical Engineers, 1957

Erbeznik,R.M, White,M.A., Penswick,L.B., Neely,R.E., Ritter,D.C., Wallace,D.A., "Assessment of 25kW Free-Piston Stirling Technology Alternatives for Solar Applications" IECEC Paper No. 929186, *Proceedings of the 27th Intersociety Energy Conversion Engineering Conference, pp5.237-5.242, vol 5*, 3-7 August, San Diego, CA, Society of Automotive Engineers, 1992

Fox,M., "Model Stirling Engines" *5th International Stirling Engine Conference, pp141-148*, ISEC-91034, 8-10 May, Dubrovnik, 1991

Fox,M., "The 62nd Model Engineer Exhibition Hot Air Engine Competition", *Stirling Machine World, p3-6*, March 1993

Fraas,A.P., "Heat Exchanger Design - 2nd Edition" John Wiley and Sons, 1989

Gaegauf,C., Zumsteg,H., "Co-Generation With a Wood Chips Fueled Stirling Engine." *6th International Stirling Engine Conference, pp51-56*, ISEC-93008, 26-28 May, Eindhoven, 1993

Gerstmann,J., Schuetz,M.A., Berntell,J., Bratt,C., "Design of a Coal-Fired Stationary Stirling Engine" *C11/82, pp11-16* ,IMechE 1982

Goetz,P.W. (Editor in Chief), "The New Encyclopædia Britannica - 15th Edition" , *vol 10, p942, vol 11, p275, p387,* vol 18, p337,*vol 27, p507,* Encyclopædia Britannica Inc, Chicago, 1990

Grimmer,D.P., "A Comparison of Compound Parabolic and Simple Parabolic Concentrating Solar Collectors" *vol 22, pp21-25,* Solar Energy, 1979

Guyer,E.C. (Editor in Chief), **Brownell,D.L.**, "Handbook of Applied Thermal Design" McGraw-Hill Book Company, New York, 1988

Heiti,R.V., Thodos,G., " An experimental parabolic cylindrical concentrator: Its construction and thermal performance." *vol 30, No. 5, pp483-485,* Solar Energy, 1983

Hewitt,G.F. (Coordinating Editor) "Hemisphere Handbook of Heat Exchanger Design" Hemisphere Publishing Corporation, New York, 1990

Howell,J.R., Bannerot,R.B., "Optimum Solar Collector Operation For Maximizing Cycle Work Output" *vol 19, pp149-153,* Solar Energy, Pergamon Press, 1977

Isshiki,N., Terada,F., Yoshikawa,K., Nishiba,T., "Experiments on 2kW Stirling Engine with Bayonet Type Heaters and Coolers" *2nd International Conference on Stirling Engines, No.2-1* , June 21-24, Shanghai, China, 1984

Isshiki,N., Watanabe,H., Shishido,K., Watanabe,K., "Studies on Internally heated Solar Stirling Engine (TNT-1 Solar Stirling System)" *4th International Conference on Stirling Engines, pp183-188,* Paper No. 040, 7-10 Nov, Tokyo, Japan, 1988

Jang,J.H., "A Study of Start-up Characteristics of a Potassium Heat Pipe From The Frozen State" *Topics in Heat Transfer, pp63-69, Vol.3,* HTD-Vol.206-3, ASME, New York, 1992

Jenkins,B.M., Mehlschau,J.J., "Performance of a Biomass Fueled Stirling Engine" *1985 Winter Meeting American Society of Agricultural Engineers, ASAE,* Paper No. 85-3568, 17-20 December, Chicago, 1985

Jingwei,Y., "On the Combustion and Heat Transfer Problems of Coal-Fired Stirling Engines For Use on Locomotives" *2nd International Conference on Stirling Engines, No.3-6* , June 21-24, Shanghai, China, 1984

Johnson,R.J., Angleton,H.D., "Hot Water Usage in a Typical Single-Family Residence" *NAHB Research Foundation, Inc,* Rockville, Maryland, 1977

Karlekar,B.V., "Thermodynamics for Engineers" Prentice-Hall Inc., Englewood Cliffs, 1983

Kazumoto,Y., Fujiwara,M., Nomaguchi,T., "Effects of Drive Mechanism on Thermodynamic Performance of Piston-Displacer Type Stirling Engine"*2nd International Conference on Stirling Engines, No. 1-8*, June 21-24, Shanghai, China, 1984

Kolin,I., "Stirling Engines with Alternative Sources" *5th International Stirling Engine Conference, pp421-426*, ISEC-91079, 8-10 May, Dubrovnik, 1991

Kreider,J.F., Kreith,F., "Solar Energy Handbook" McGraw-Hill Book Company, New York, 1981

Levy,E.K., "Theoretical Investigation of Heat Pipes Operating at Low Vapor Pressures" *Transactions of the ASME, Journal of Engineering for Industry, pp547-552*, November 1968

Lista,P., "Commercial Stirling Machine Models: Technical Data and Availability" *5th International Stirling Engine Conference, pp399-410*, ISEC-91076, 8-10 May, Dubrovnik, 1991

Lockwood,L.M., "Development and Field Testing of a Four Kilowatt Rice Husk Fueled Hot Air Engine" *2nd International Conference on Stirling Engines, No.2-14* , June 21-24, Shanghai, China, 1984

Luo,G., Gong,J., "The Heating System of a Solar Stirling Engine Generator" *5th International Stirling Engine Conference, pp387-392*, ISEC-91074, 8-10 May, Dubrovnik, 1991

Massey,B.S., "Mechanics of Fluids - 5th Edition" Van Nostrand Reinhold (International), London, 1988

Meijer,R.J., "Prospects of the Stirling Engine for Vehicular Propulsion" *Philips Technical review, Vol.30, No. 5/6, pp169-185*, N.V. Philips Gloeilampenfabrieken, Eindhoven, 1970

Meijer,R.J., "The Evolution of the Stirling Engine at Philips",*4th International Conference on Stirling Engines, pp205-217*, ICSE 044, Nov 7-10, Tokyo, Japan Society of Mechanical Engineers, 1988

Meijer,R.J., "McGraw-Hill Encyclopedia of Science & Technology - 7th Edition" *vol 17 pp440-445*, McGraw-Hill Inc, New York, 1992

Meyer,B., "Elemental Sulfur - Chemistry and Physics", Interscience Publishers - John Wiley & Sons. 1965

Meyer,B., "Sulfur, Energy, and Environment", Elsevier Scientific Publishing Company, Amsterdam, 1977

Nakajima,N., Azetsu,A., Mori,Y., Tanimoto,K., "Study on Multi-Purpose Stirling Engine Driven with Wood Fuel"*2nd International Conference on Stirling Engines, No.2-11* , June 21-24, Shanghai, China, 1984

Nilsson,H., "Submarine Power Systems using the V4-275R Stirling Engine" *Proceedings of the Institute of Mechanical Engineers, vol 202, No.A4, pp257-267*, IMechE 1988

Peet,N.J., Carter,A.J., Baines,J.T., "Energy in the New Zealand Household - The Energy Cost of Living 1974-1980" *New Zealand Energy Research and Development Committee*, Publication P73, November 1982

Perlack,R.D., Jones,H.G., Waddle,D.B., "A Survey of Renewable Energy Technologies for Rural Applications" *Energy, vol15, No.5, pp1119-1127*, Pergamon Press 1990

Perry,R.H., Green,D., Maloney,J.O., "Perry's Chemical Engineering Handbook - 6th Edition" McGraw-Hill Book Company, New York, 1984

Polasek,F., Stulc,P., "Heat Pipes for the temperature range 200°C to 600°C", *Proceedings of the 2nd International Heat Pipe Conference*, Bologna, ESA Report SP112. 1976

Preston,J.(Editor), "EV's and Hybrids: Recent Developments" *Automotive Engineer, April\May, pp48-50*, Mechanical Engineering Publications Limited, Bury St. Edmunds, 1984

Rabl,A., " Optical and Thermal Properties of Compound Parabolic Concentrators" *vol 18, pp497-511*, Solar Energy, Pergamon Press, 1976

Rabl,A., " Comparison of Solar Concentrators" *vol 18, pp93-111*, Solar Energy, Pergamon Press, 1976

Reader,G.T., Hooper,C., "Stirling Engines", E.&F.N.Spon, London, 1983

Rice,G., "Heat Pipes For Stirling Engines" *2nd International Conference on Stirling Engines, No.3-1*, June 21-24, Shanghai, China, **1984**

Ross,A., "Small Stirling Air Engines"*2nd International Conference on Stirling Engines, No.2-3* , June 21-24, Shanghai, China, 1984

Ross,B.A., Bates,J.M., Larson,N.R., "Characterisation of Transients of Direct Solar Insolation Based on One-Minute Data." IECEC Paper No. 929180, *Proceedings of the 27th Intersociety Energy Conversion Engineering Conference, pp5.215-5.220, vol 5*, 3-7 August, San Diego, CA, Society of Automotive Engineers, 1992

San Martin,R.L., "McGraw-Hill Encyclopedia of Science & Technology, 7th Edition" *vol.16, pp608-622*, McGraw-Hill Inc, New York, 1992

Schiel,W., Schlaich,J., "Solar Dish/Stirling Systems - An option for the Future" *6th International Stirling Engine Conference, pp149-155*, ISEC-93027, 26-28 May, Eindhoven, 1993

Senft,J.R., "An Ultra Low Temperature Differential Stirling Engine" *5th International Stirling Engine Conference, pp1-8*, ISEC-91032, 8-10 May, Dubrovnik, 1991

Shah,R.K., "Plate-Fin and Tube-Fin Heat Exchanger Design Procedures" *Heat Transfer Equipment Design, pp255-266*, Hemisphere Publishing Corporation, 1988

Shah,R.K., Giovannelli,A.D., "Heat Pipe Heat Exchanger Design Theory" *Heat Transfer Equipment Design, pp609-653*, Hemisphere Publishing Corporation, 1988

Shaltens,R.K., Schreiber,J.G., Wong,W.A., "Update on the Advanced Stirling Conversion System Project for 25kW Dish Stirling Applications" IECEC Paper No. 929184, *Proceedings of the 27th Intersociety Energy Conversion Engineering Conference, pp5.229-5.235, vol 5*, 3-7 August, San Diego, CA, Society of Automotive Engineers, 1992

Shishido,K., Isshiki,N., Shibata,Y., Nagai,Y., Watanabe,H., Kikuchi,S., Ohtomo,M., "Characteristics of an Optical System for Driving a Kilowatt Range Solar Stirling Engine." *6th International Stirling Engine Conference, pp1-6*, ISEC-93001, 26-28 May, Eindhoven, 1993

Singh,P., "Incorporating Solar Electric Power into Rural Electrification Programs - A Case Study of Kenya" *Energy Sources, Vol 13, pp67-75*, Taylor & Francis, 1991

Sittig,M., "Manufacture and Availability of Alkali Metals" *Liquid Metals Technology-Part 1, Chemical Engineering Progress Symposium Series, pp35-41, No.20, Vol.53*, American Institute of Chemical Engineers, 1957

Starr,F., British Gas, Personal communication to Dr. J.K.Raine, February, 1994

Soumerai,H., "Practical Thermodynamic Tools for Heat Exchanger Design Engineers" John Wiley and Sons, 1987

Timrot,D.L., Serednitskaya,M.A., Medveditskov,A.N., Traktueva,S.A., "Thermophysical Properties of Sulphur-Iodine Binary System as a Promising Heat Transfer Medium for Heat Pipes" *Proceedings of the 4th International Heat Pipe Conference, pp429-437*, 7-10 September London, Pergamon Press. 1981

Trukhov,V.S. Toursounbaev,I.A., "Stirling Engine - Energy Converter of the Solar Power Plant" *6th International Stirling Engine Conference, pp303-314*, ISEC-93067, 26-28 May, Eindhoven, 1993

Walker,G., "Stirling Cycle Machines" Clarendon Press, Oxford, 1973

Walker,G., "The Stirling Engine" *Scientific American, 229(2), pp80-87*, August 1973

Walker,G., Fauvel,R., Srinivasan,S., Gustafson,R., Van Benthem,J., "Future Coal-Burning Stirling Engines" *C10/82,pp1-10*, IMechE 1982

Walker,G., Fauvel,R., " Applications for Stirling Engines - A Personal View." *3rd International Stirling Engine Conference, pp171-189*, ISEC 86-11-51, June 25-27, Rome, Italy, 1986

Walker,G., Scott,M.J., Bingham,E.R., "Ross-Stirling Silent Boat Engine" *5th International Stirling Engine Conference, pp327-333*, ISEC-91065, 8-10 May, Dubrovnik, 1991

Weinberg,C.J., Williams,R.H., "Energy From the Sun." *Scientific American, pp98-106*, September 1990

Welford,W.T., Winston,R., "The Optics of Nonimaging Concentrators - Light and Solar Energy" Academic Press, New York, 1978

Wenguang,W., "Heat Transfer Problems in the Heat Transport System of Coal Fired Locomotive Stirling Engine" *2nd International Conference on Stirling Engines, No.3-7*, June 21-24, Shanghai, China, 1984

West,C.D., "Principles and Applications of Stirling Engines." Van Nostrand Reinhold Company, New York, 1986

Western,B.E., "The Estimation of Solar Radiation in New Zealand" *Solar Energy, Vol.45, No.3, pp121-129*, Pergamon Press, 1990

Williamson,A.G., Chemical Engineering Department of the University of Canterbury, Personal communication 1993

Winston,R., "Nonimaging Optics" *pp52-57*, Scientific American, March 1991

Wright,J., Baines,J., "Supply Curves of Conserved Energy - The Potential for Conservation in New Zealand's Houses" *Centre for Resource Management University of Canterbury and Lincoln College*. Ministry of Energy, Wellington, New Zealand, Sept 1986

APPENDIX 1

MODEL SYSTEM SPECIFICATIONS

POWER AND PERFORMANCE

Total power produced in one day		0.84kWhr
Average electrical power from batteries		120W[1]
Mechanical Power from Stirling engine		333W
Overall solar to electrical conversion efficiency		3%
Energy Storage Device	Lead Acid Batteries	

CONCENTRATOR DATA

Collector Orientation	East-West	
Tracking	Single Axis Diurnal	
Concentrator Area		$7m^2$
Rim Angle		30°
Simple Parabolic Concentrator Acceptance Half Angle		1°
Compound Parabolic Concentrator Acceptance half Angle		29°
Concentration Ratio		48.6
Concentrator width		1m
Concentrator length	2 units	3.5m
Focal length of SPC		933mm
Absorber Diameter		25.4mm
Absorber Material		AISI C1020
Absorber Selective Coating	black sulphide or black oxide	
emissivity	0.15	
absorptivity	0.95	
Primary reflector material	Front surface Aluminised Mylar	
Secondary reflector material	Polished Aluminium	

THERMAL DATA

Absorber temperature		600K-625K
Cooling water temperature		333K
Proposed heat pipe working fluid		Mercury
Heat pipe insulation	●kaowool layer ●air gap ●ceramic casing ●evacuated pyrex segment covering the secondary exit aperture.	

STIRLING ENGINE

DMC5 Stirling engine with heat pipe working fluid condensation occurring directly on the heater heads. 200W electrical output, 4 cylinder Seimens configuration. Air charged.

---

[1] Assuming a collection time of 7hr per day with an insolation of $600W/m^2$

APPENDIX 2

FULL SCALE DOMESTIC POWER SYSTEM

POWER AND PERFORMANCE

Total power produced in one day		9.8kWhr
Average electrical power from batteries		1.4kW[2]
Mechanical Power from Stirling engine		3.88kW
Overall solar to electrical conversion efficiency		3%
Energy Storage Device	Lead Acid Batteries	

CONCENTRATOR DATA

Collector Orientation	East-West	
Tracking	Single Axis Diurnal	
Concentrator Area		81m²
Rim Angle		30°
Simple Parabolic Concentrator Acceptance Half Angle		1°
Compound Parabolic Concentrator Acceptance half Angle		29°
Concentration Ratio		48.6
Concentrator width		2m
Concentrator length	4 units	10m
Focal length of SPC		1.866m
Absorber Diameter		50.8mm
Absorber Material		AISI C1020
Absorber Selective Coating	black sulphide or black oxide	
emissivity	0.15	
absorptivity	0.95	
Primary reflector material	Front surface Aluminised Mylar	
Secondary reflector material	Polished Aluminium	

THERMAL DATA

Absorber temperature		600K-625K
Cooling water temperature		333K
Proposed heat pipe working fluid		Mercury
Heat pipe insulation	●kaowool layer ●air gap ●ceramic casing ●evacuated pyrex segment covering the secondary exit aperture.	

STIRLING ENGINE

4 cylinder seimens configuration engine with heat pipe condensation occurring directly on the heater heads. 2.33kW electrical output. Air charged.

---

[2] Assuming a collection time of 7hr per day with an insolation of 600W/m²

APPENDIX 3

BRIEF SPECIFICATIONS FOR THE DMC5 STIRLING ENGINE

Designed by Dr. Donald Clucas, of the University of Canterbury, New Zealand.

Figure A3 The DMC5 Prototype

Power Output	200W, 12V, Direct Current
Size	200mm diameter, 325mm high (without heater)
Mass	20kg
Configuration	4 cylinder double acting Siemens.
Mechanism	Wobble Yoke
Working Fluid	Air
Charge Pressure	10 Bar (for the Solar Application it would be 15 Bar)
Bore	40mm
Stroke	20mm
Shaft Speed	1200-1500 rpm

APPENDIX 4

SULPHUR PROPERTY CHART

Atomic Mass	32.064 g/mol
Melting Point	388.38K
Normal Boiling Point	717.82K
Critical Temperature	1313K
Critical Pressure	182.08 Bar
Toxicity	Non Toxic

Notes: Due to its changes in phase that see the break up of the S_8 rings, Sulphur exhibits some unusual viscous properties with increasing temperature. It will melt to a liquid of very low viscosity, then the viscosity will rise very rapidly within a few degrees until the liquid is a very thick substance with the consistency of molasses. By the addition of Iodine, the viscosity can be kept low.

TABLE A4 - Sulphur Thermal and Transport Properties

Temp K	Reduced Temp	Liquid Density kg/m^3	Vapour Pressure Pa	Heat of Vaporisation J/kg	liquid Heat Capacity J/kgK	Liquid Viscosity Pa.s	Liquid Thermal Conductivity W/mK	Surface Tension N/m	Vapour Density kg/m^3
613	0.467	1677	16584.55	295279	1062.20	0.34159845	0.171	0.0458	0.1043
400	0.305	1789	6.92	327513	987.40		0.130	0.0598	0.0001
410	0.312	1784	12.66	326109	1016.20		0.134	0.0591	0.0001
420	0.320	1779	22.35	324696	1103.77		0.137	0.0585	0.0002
430	0.327	1774	38.15	323273	1250.12		0.140	0.0578	0.0003
440	0.335	1769	63.13	321840	1455.24		0.143	0.0572	0.0006
450	0.343	1764	101.55	320397	1325.12		0.146	0.0565	0.0009
460	0.350	1759	159.09	318944	1290.57	106.627443	0.149	0.0559	0.0013
470	0.358	1754	243.24	317481	1259.33	81.4267587	0.151	0.0552	0.0020
480	0.366	1749	363.60	316006	1231.23	60.8542438	0.153	0.0546	0.0029
490	0.373	1744	532.24	314522	1206.06	44.596938	0.156	0.0539	0.0042
500	0.381	1738	764.07	313026	1183.65	32.1065551	0.158	0.0532	0.0059
510	0.388	1733	1077.20	311518	1163.79	22.7440972	0.160	0.0526	0.0081
520	0.396	1728	1493.29	309999	1146.29	15.8773198	0.162	0.0519	0.0111
530	0.404	1723	2037.86	308469	1130.97	10.9372553	0.163	0.0513	0.0148
540	0.411	1717	2740.58	306927	1117.62	7.44387771	0.165	0.0506	0.0196
550	0.419	1712	3635.57	305372	1106.07	5.01117964	0.166	0.0500	0.0255
560	0.427	1706	4761.63	303805	1096.11	3.34024562	0.167	0.0493	0.0328
570	0.434	1701	6162.40	302225	1087.56	2.20660269	0.168	0.0487	0.0417
580	0.442	1695	7886.60	300632	1080.22	1.44594655	0.169	0.0480	0.0524
590	0.449	1690	9988.08	299026	1073.90	0.94060315	0.170	0.0473	0.0653
600	0.457	1684	12526.00	297406	1068.41	0.60785785	0.171	0.0467	0.0805
610	0.465	1678	15564.88	295772	1063.56	0.39050676	0.171	0.0460	0.0984
620	0.472	1673	19174.67	294124	1059.16	0.24954682	0.171	0.0454	0.1193
630	0.480	1667	23430.82	292461	1055.01	0.15871468	0.172	0.0447	0.1434
640	0.487	1661	28414.32	290784	1050.92	0.10051917	0.172	0.0441	0.1712
650	0.495	1655	34211.76	289091	1046.71	0.06342415	0.171	0.0434	0.2030
660	0.503	1649	40915.42	287383	1042.17	0.03988646	0.171	0.0428	0.2391
670	0.510	1643	48623.28	285658	1037.12	0.02501138	0.171	0.0421	0.2799
680	0.518	1637	57439.21	283917	1031.36	0.0156442	0.170	0.0414	0.3258
690	0.526	1631	67473.03	282160	1024.71	0.00976389	0.169	0.0408	0.3771
700	0.533	1625	78840.70	280385	1016.98	0.00608253	0.169	0.0401	0.4344

APPENDIX 5

DIISODECYL PHTHALATE PROPERTY CHART

Molecular Mass 446.671 g/mol
Melting Point 227.59K
Normal Boiling Point 723K
Critical Temperature 887K
Critical Pressure 10 Bar
Toxicity Low order of toxicity

Notes: Diisodecyl Phthalate is a commercial plasticiser, with an auto ignition point at 674.82K.

TABLE A5 - Diisodecyl Phthalate Thermal and Transport Properties

Temp K	Reduced Temp	Liquid Density kg/m^3	Vapour Pressure Pa	Heat of Vaporisation J/kg	liquid Heat Capacity J/kgK	Liquid Viscosity Pa.s	Vapour Viscosity Pa.s	Liquid Thermal Conductivity W/mK	Surface Tension N/m	Vapour Density kg/m^3
613	0.691	753	6748.45	195468	2604.58	6.4632E-05	6.8104E-06	0.0547	0.0128	0.5915
400	0.451	908	0.84	262623	1959.39	0.003	4.3968E-06	0.0738	0.0275	0.0001
410	0.462	902	1.59	259610	1989.68	0.003	4.5142E-06	0.0729	0.0267	0.0002
420	0.474	895	2.92	256571	2019.97	0.003	4.6312E-06	0.0720	0.0260	0.0004
430	0.485	888	5.20	253509	2050.26	0.003	4.7478E-06	0.0711	0.0252	0.0006
440	0.496	881	9.01	250427	2080.55	0.003	4.864E-06	0.0702	0.0245	0.0011
450	0.507	875	15.20	247325	2110.84	0.003	4.9798E-06	0.0693	0.0238	0.0018
460	0.519	868	25.03	244206	2141.13	0.003	5.0952E-06	0.0684	0.0231	0.0029
470	0.530	861	40.31	241072	2171.42	0.003	5.2101E-06	0.0675	0.0223	0.0046
480	0.541	854	63.59	237926	2201.71	0.003	5.3247E-06	0.0667	0.0216	0.0071
490	0.552	847	98.39	234767	2232.01	0.003	5.4388E-06	0.0658	0.0209	0.0108
500	0.564	839	149.55	231599	2262.30	0.003	5.5526E-06	0.0649	0.0202	0.0161
510	0.575	832	223.56	228423	2292.59	0.003	5.6659E-06	0.0640	0.0195	0.0236
520	0.586	825	329.08	225240	2322.88	0.003	5.7788E-06	0.0631	0.0189	0.0340
530	0.598	818	477.51	222051	2353.17	0.003	5.8914E-06	0.0622	0.0182	0.0484
540	0.609	810	683.68	218858	2383.46	0.003	6.0035E-06	0.0613	0.0175	0.0680
550	0.620	803	966.71	215661	2413.75	0.003	6.1153E-06	0.0604	0.0168	0.0944
560	0.631	795	1351.07	212461	2444.04	0.003	6.2266E-06	0.0595	0.0162	0.1296
570	0.643	787	1867.81	209259	2474.33	0.003	6.3376E-06	0.0586	0.0155	0.1760
580	0.654	779	2556.04	206055	2504.62	0.003	6.4482E-06	0.0577	0.0149	0.2368
590	0.665	771	3464.71	202850	2534.91	0.003	6.5584E-06	0.0568	0.0142	0.3155
600	0.676	763	4654.74	199642	2565.20	0.003	6.6682E-06	0.0559	0.0136	0.4168
610	0.688	755	6201.50	196432	2595.50	0.003	6.7777E-06	0.0550	0.0130	0.5462
620	0.699	747	8197.80	193219	2625.79	0.003	6.8868E-06	0.0541	0.0123	0.7104
630	0.710	739	10757.45	190002	2656.08	0.003	6.9955E-06	0.0532	0.0117	0.9174
640	0.722	730	14019.37	186780	2686.37	0.003	7.1038E-06	0.0523	0.0111	1.1769
650	0.733	721	18152.54	183550	2716.66	0.003	7.2118E-06	0.0514	0.0105	1.5004
660	0.744	712	23361.81	180310	2746.95	0.003	7.3195E-06	0.0505	0.0100	1.9017
670	0.755	703	29894.74	177058	2777.24	0.003	7.4268E-06	0.0496	0.0094	2.3972
680	0.767	694	38049.63	173789	2807.53	0.003	7.5338E-06	0.0487	0.0088	3.0062
690	0.778	685	48185.03	170499	2837.82	0.003	7.6404E-06	0.0478	0.0082	3.7518

APPENDIX 6

BENZYL BENZOATE PROPERTY CHART

Molecular Mass 212.25 g/mol
Melting Point 292.55K
Normal Boiling Point 596.65K
Critical Temperature 820K
Critical Pressure 25.8 Bar
Toxicity Low order of toxicity

Notes: Benzyl Benzoate is a commercial plasticiser, also used as a chewing gum flavouring, with an auto ignition point at 674.82K.

TABLE A6 - Benzyl Benzoate Thermal and Transport Properties

Temp K	Reduced Temp	Liquid Density kg/m^3	Vapour Pressure Pa	Heat of Vaporisation J/kg	liquid Heat Capacity J/kgK	Liquid Viscosity Pa.s	Vapour Viscosity Pa.s	Liquid Thermal Conductivity W/mK	Surface Tension N/m	Vapour Density kg/m^3
613	0.748	796	139841.81	268408	2282.89	9.7519E-05	1.049E-05	0.0850	0.0124	5.8239
400	0.488	1020	109.21	355013	1669.73	0.00094625	6.3282E-06	0.1201	0.0339	0.0070
410	0.500	1011	189.23	351648	1698.52	0.00080674	6.5523E-06	0.1184	0.0328	0.0118
420	0.512	1001	317.63	348232	1727.30	0.000807	6.7728E-06	0.1168	0.0316	0.0193
430	0.524	991	517.73	344765	1756.09	0.000807	6.9899E-06	0.1151	0.0305	0.0307
440	0.537	982	821.23	341244	1784.88	0.000807	7.2036E-06	0.1135	0.0294	0.0476
450	0.549	972	1270.15	337666	1813.66	0.000807	7.4141E-06	0.1118	0.0283	0.0721
460	0.561	962	1918.91	334029	1842.45	0.000807	7.6215E-06	0.1102	0.0272	0.1065
470	0.573	952	2836.43	330330	1871.24	0.000807	7.8259E-06	0.1085	0.0261	0.1541
480	0.585	942	4108.29	326567	1900.02	0.000807	8.0273E-06	0.1069	0.0251	0.2185
490	0.598	931	5838.69	322737	1928.81	0.000807	8.226E-06	0.1052	0.0240	0.3042
500	0.610	921	8152.42	318835	1957.60	0.000807	8.4221E-06	0.1036	0.0230	0.4162
510	0.622	911	11196.42	314860	1986.38	0.000807	8.6156E-06	0.1019	0.0220	0.5605
520	0.634	900	15141.27	310805	2015.17	0.000807	8.8068E-06	0.1003	0.0210	0.7434
530	0.646	889	20182.17	306669	2043.96	0.000807	8.9957E-06	0.0986	0.0200	0.9721
540	0.659	879	26539.80	302445	2072.74	0.000807	9.1824E-06	0.0970	0.0190	1.2547
550	0.671	868	34460.71	298128	2101.53	0.000807	9.3671E-06	0.0953	0.0181	1.5996
560	0.683	857	44217.58	293714	2130.32	0.000807	9.5499E-06	0.0937	0.0171	2.0158
570	0.695	846	56109.13	289196	2159.10	0.000807	9.7308E-06	0.0921	0.0162	2.5130
580	0.707	834	70460.02	284568	2187.89	0.000807	9.9101E-06	0.0904	0.0153	3.1014
590	0.720	823	87620.56	279821	2216.68	0.000807	1.0088E-05	0.0888	0.0144	3.7913
600	0.732	811	107966.57	274948	2245.47	0.000807	1.0264E-05	0.0871	0.0135	4.5938
610	0.744	799	131899.37	269939	2274.25	0.000807	1.0438E-05	0.0855	0.0126	5.5201
620	0.756	787	159846.08	264783	2303.04	0.000807	1.0611E-05	0.0838	0.0118	6.5818
630	0.768	775	192260.25	259469	2331.83	0.000807	1.0783E-05	0.0822	0.0109	7.7909
640	0.780	762	229623.25	253983	2360.61	0.000807	1.0954E-05	0.0805	0.0101	9.1595
650	0.793	750	272446.09	248310	2389.40	0.000807	1.1124E-05	0.0789	0.0093	10.7005
660	0.805	736	321272.36	242431	2418.19	0.000807	1.1292E-05	0.0772	0.0086	12.4270
670	0.817	723	376681.92	236325	2446.97	0.000807	1.1459E-05	0.0756	0.0078	14.3528
680	0.829	709	439295.92	229968	2475.76	0.000807	1.1626E-05	0.0739	0.0071	16.4925
690	0.841	695	509783.08	223329	2504.55	0.000807	1.1791E-05	0.0723	0.0064	18.8614
700	0.854	681	588867.45	216375	2533.33	0.000807	1.1956E-05	0.0706	0.0057	21.4762

APPENDIX 7

DOWTHERM A PROPERTY CHART

Molecular Mass 166.0 g/mol average
Melting Point 285K
Normal Boiling Point 530K
Critical Temperature 770K
Critical Pressure 31.4 Bar
Toxicity Low order of Toxicity

Notes: Dowtherm A is a commercially produced heat transfer fluid also going by the name of Thermex. It is a eutectic mixture of diphenyl ($C_{12}H_{10}$), and diphenyl ether ($C_{12}H_{10}O$). Its autoignition temperature is 888K.

TABLE A7 - Dowtherm A Thermal and Transport Properties
As taken from Dunn&Reay 1982

Temp	Heat of Vaporisation	Liquid Density	Vapour Density	Liquid Thermal Conductivity	Liquid Viscosity	Vapour Viscosity	Vapour Pressure	Vapour Specific Heat	Surface Tension
°C	kJ.kg	kg/m^3	kg/m^3	W/mK	Pa.s	Pa.s	Bar	kJ/kgK	N/m
100	354	992	0.03	0.131	9.70E-04	6.70E-05	0.01	1.34	0.035
150	338	951	0.22	0.125	5.70E-04	7.80E-05	0.05	1.51	0.030
200	321	905	0.94	0.119	3.90E-04	8.90E-05	0.25	1.67	0.025
250	301	858	3.60	0.113	2.70E-04	1.00E-04	0.88	1.81	0.020
300	278	809	8.74	0.106	2.00E-04	1.12E-04	2.43	1.95	0.015
350	251	755	19.37	0.099	1.50E-04	1.23E-04	5.55	2.03	0.010
400	219	691	41.89	0.093	1.20E-04	1.34E-04	10.90	2.11	0.005
450	185	625	81.00	0.086	1.00E-04	1.45E-04	19.00	2.19	0.003

APPENDIX 8

MERCURY PROPERTY CHART

Atomic Mass 200.59 g/mol
Melting 234.29K
Normal Boiling Point 629.73K
Critical Temperature 1735K
Critical Pressure 1608 Bar
Toxicity Extremely toxic causing damage to brain, and lungs. It is not considered particularly toxic in the pure liquid metal state, but the vapour is very toxic, and most of the mercury compounds, particularly the organic compounds.
Notes: Mercury will readily form amalgams (alloys) with other metals

TABLE A8 - Mercury Thermal and Transport Properties

Temp K	Reduced Temp	Liquid Density kg/m^3	Vapour Pressure Pa	Heat of Vaporisation J/kg	liquid Heat Capacity J/kgK	Liquid Viscosity Pa.s	Vapour Viscosity Pa.s	Liquid Thermal Conductivity W/mK	Surface Tension N/m	Vapour Density kg/m^3
613	0.353	12802	74097.17	295511	135.40	0.00089282	0.0000641	12.07	0.5431	2.9164
410	0.236	13256	216.69	313488	136.56	0.00115023	3.7641E-05	9.92	0.5430	0.0128
420	0.242	13235	330.84	312645	136.38	0.00112944	3.7566E-05	10.04	0.5430	0.0190
430	0.248	13213	495.04	311799	136.21	0.00110997	3.7705E-05	10.16	0.5430	0.0278
440	0.254	13192	726.98	310949	136.05	0.0010917	3.8036E-05	10.27	0.5430	0.0399
450	0.259	13170	1049.06	310094	135.91	0.00107453	3.8538E-05	10.38	0.5430	0.0562
460	0.265	13148	1489.33	309235	135.78	0.00105836	3.9191E-05	10.50	0.5430	0.0781
470	0.271	13127	2082.30	308371	135.66	0.00104311	3.9976E-05	10.61	0.5430	0.1069
480	0.277	13105	2870.02	307503	135.56	0.0010287	4.0876E-05	10.72	0.5430	0.1443
490	0.282	13083	3902.99	306631	135.47	0.00101507	4.1872E-05	10.83	0.5430	0.1922
500	0.288	13061	5241.29	305754	135.39	0.00100216	4.295E-05	10.94	0.5430	0.2529
510	0.294	13038	6955.60	304873	135.33	0.00098991	4.4094E-05	11.04	0.5430	0.3291
520	0.300	13016	9128.26	303987	135.27	0.00097828	4.5289E-05	11.15	0.5430	0.4235
530	0.305	12993	11854.34	303096	135.23	0.00096721	4.6524E-05	11.25	0.5430	0.5396
540	0.311	12971	15242.67	302200	135.21	0.00095667	4.7786E-05	11.35	0.5430	0.6810
550	0.317	12948	19416.81	301300	135.19	0.00094663	4.9063E-05	11.46	0.5430	0.8518
560	0.323	12925	24516.04	300395	135.19	0.00093705	5.0347E-05	11.56	0.5431	1.0562
570	0.329	12902	30696.20	299484	135.20	0.0009279	5.1628E-05	11.65	0.5431	1.2993
580	0.334	12879	38130.53	298569	135.23	0.00091915	5.2898E-05	11.75	0.5431	1.5861
590	0.340	12856	47010.38	297648	135.26	0.00091077	5.415E-05	11.85	0.5431	1.9224
600	0.346	12833	57545.91	296723	135.32	0.00090275	5.5378E-05	11.94	0.5431	2.3140
610	0.352	12809	69966.61	295792	135.38	0.00089506	5.6577E-05	12.04	0.5431	2.7673
620	0.357	12786	84521.77	294855	135.45	0.00088768	5.7743E-05	12.13	0.5431	3.2891
630	0.363	12762	101480.86	293913	135.54	0.0008806	5.8873E-05	12.22	0.5431	3.8864
640	0.369	12738	121133.81	292966	135.65	0.00087379	5.9965E-05	12.31	0.5431	4.5665
650	0.375	12714	143791.18	292013	135.76	0.00086724	6.1019E-05	12.40	0.5431	5.3373
660	0.380	12690	169784.21	291055	135.89	0.00086094	6.2034E-05	12.49	0.5431	6.2066
670	0.386	12666	199464.85	290090	136.03	0.00085487	6.301E-05	12.57	0.5431	7.1828
680	0.392	12641	233205.63	289120	136.18	0.00084902	6.3952E-05	12.66	0.5431	8.2743
690	0.398	12617	271399.46	288144	136.35	0.00084338	6.486E-05	12.74	0.5431	9.4898

APPENDIX 9

POTASSIUM PROPERTY CHART

Atomic Mass 39.102 g/mol
Melting Point 336.35K
Normal Boiling Point 1037K
Critical Temperature 2223K
Critical Pressure 162.12 Bar
Toxicity Non toxic
Notes: Potassium is extremely reactive and a strong reducer

TABLE A9 - Potassium Thermal and Transport Properties

Temp K	Reduced Temp	Liquid Density kg/m^3	Vapour Pressure Pa	Heat of Vaporisation J/kg	liquid Heat Capacity J/kgK	Liquid Viscosity Pa.s	Vapour Viscosity Pa.s	Liquid Thermal Conductivity W/mK	Surface Tension N/m	Vapour Density kg/m^3
613	0.276	763	121.66	2187121	767.44	0.00021239		41.26	0.0957	0.000933
400	0.180	813	0.02	2186149	805.25	0.00038374		47.31	0.1119	0.000000
410	0.184	811	0.03	2186959	802.63	0.00036855		47.00	0.1111	0.000000
420	0.189	809	0.05	2187698	800.10	0.00035459		46.69	0.1103	0.000001
430	0.193	806	0.10	2188365	797.65	0.00034174		46.38	0.1096	0.000001
440	0.198	804	0.17	2188959	795.29	0.00032987		46.07	0.1088	0.000002
450	0.202	801	0.28	2189481	793.02	0.00031887		45.77	0.1080	0.000003
460	0.207	799	0.46	2189928	790.83	0.00030867		45.47	0.1073	0.000005
470	0.211	797	0.74	2190302	788.73	0.00029918		45.18	0.1065	0.000007
480	0.216	794	1.17	2190600	786.71	0.00029033		44.88	0.1057	0.000011
490	0.220	792	1.82	2190822	784.77	0.00028206		44.59	0.1050	0.000017
500	0.225	790	2.77	2190969	782.92	0.00027432		44.31	0.1042	0.000026
510	0.229	787	4.15	2191038	781.14	0.00026706		44.02	0.1034	0.000038
520	0.234	785	6.11	2191030	779.45	0.00026024		43.74	0.1027	0.000055
530	0.238	783	8.88	2190944	777.84	0.00025382		43.46	0.1019	0.000079
540	0.243	780	12.71	2190778	776.31	0.00024777		43.19	0.1012	0.000111
550	0.247	778	17.96	2190534	774.85	0.00024206		42.91	0.1004	0.000154
560	0.252	775	25.06	2190208	773.47	0.00023667		42.64	0.0997	0.000210
570	0.256	773	34.54	2189803	772.17	0.00023156		42.38	0.0989	0.000285
580	0.261	771	47.09	2189315	770.95	0.00022672	1.3506E-05	42.11	0.0981	0.000382
590	0.265	768	63.51	2188746	769.80	0.00022212	1.3903E-05	41.85	0.0974	0.000506
600	0.270	766	84.78	2188093	768.73	0.00021775	1.4274E-05	41.59	0.0966	0.000664
610	0.274	763	112.09	2187358	767.73	0.0002136	1.4616E-05	41.33	0.0959	0.000864
620	0.279	761	146.84	2186538	766.80	0.00020964	1.4928E-05	41.08	0.0952	0.001114
630	0.283	759	190.68	2185633	765.94	0.00020587	1.5209E-05	40.83	0.0944	0.001423
640	0.288	756	245.55	2184643	765.16	0.00020227	1.5456E-05	40.58	0.0937	0.001804
650	0.292	754	313.71	2183566	764.45	0.00019883	1.5669E-05	40.34	0.0929	0.002270
660	0.297	751	397.75	2182403	763.81	0.00019554	1.5846E-05	40.10	0.0922	0.002834
670	0.301	749	500.68	2181153	763.23	0.00019239	1.5985E-05	39.86	0.0914	0.003514
680	0.306	747	625.89	2179814	762.73	0.00018937	1.6084E-05	39.62	0.0907	0.004328
690	0.310	744	777.24	2178386	762.29	0.00018648	1.6143E-05	39.39	0.0900	0.005297
700	0.315	742	959.12	2176869	761.92	0.0001837	1.6158E-05	39.16	0.0892	0.006443

APPENDIX 10

SYSTEM PERFORMANCE AND RIM ANGLE

The following data was determined by the spreadsheet in Chapter 6. The system described here is for the 120W_e solar Stirling system (Appendix 1)

TABLE A10 - The Effect of Rim Angle on System Performance

Rim Angle	System Efficiency	Array Size	Absorber Temperature
45°	2.84%	7.03m²	605K
40°	2.87%	6.97m²	609K
35°	2.89%	6.92m²	613K
30°	2.91%	6.88m²	617K
25°	2.92%	6.85m²	618K
20°	2.93%	6.83m²	620K
15°	2.94%	6.81m²	622K

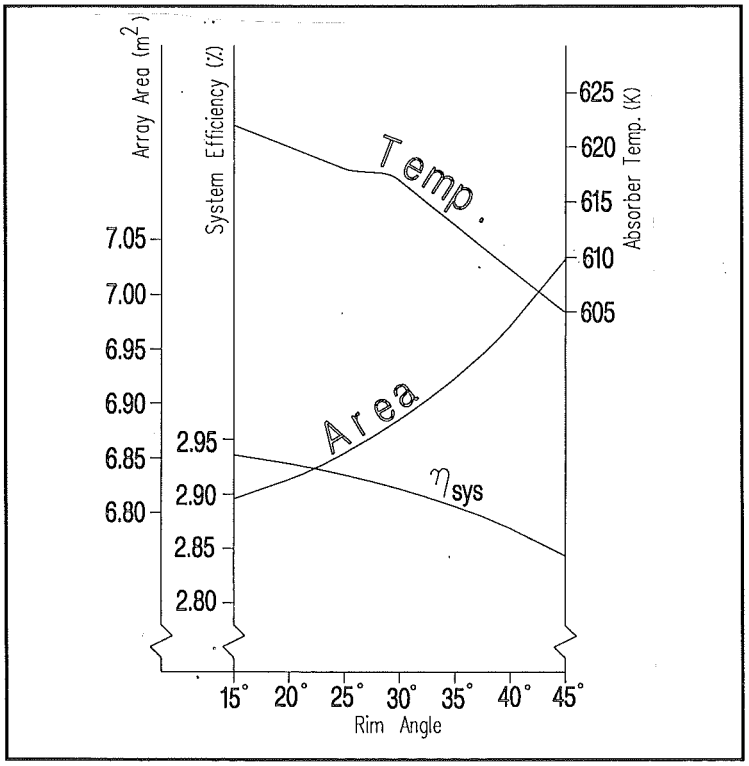

Figure A10 Variation of optimum absorber temperature, system efficiency, and array area with rim angle.

APPENDIX 11

SINGLE PHASE HEAT EXCHANGE CALCULATION

The following calculation is merely an estimate and has not been optimised or rigorously calculated. It deals with the temperature drop between the heat transfer fluid and the Stirling engine cylinder walls for the purposes of comparing the single phase heat transfer system to a heat pipe system (Section 7.3). No calculations have been done on the transfer of heat into the Stirling engine working fluid because this will be the same for both the heat pipe and the single phase heat transfer systems. The engine size for these calculations is the 120W_e system given in Appendix 1. The heat exchanger design used is the type with the heat transfer fluid flow paths external to the engine cylinder. A cutaway with the nomenclature used is presented in Figure A11. The working fluid is Marlotherm S, a product of Robert Bryce & Co. Ltd.

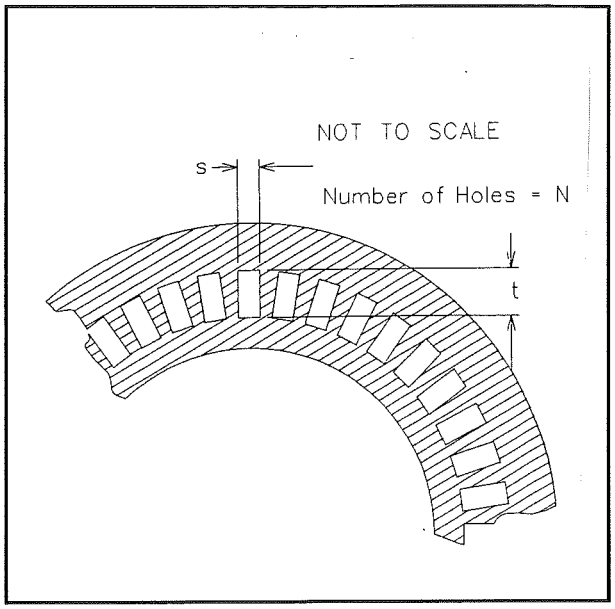

Figure A11 Cross-section through the heat exchanger showing the sizes and nomenclature used.

MARLOTHERM S DATA AT 600K

Marlotherm S is a mixture of isomeric dibenzyl toluenes, and has an ignition point above 500°C.

Vapour pressure $p \approx 210$mbar Specific heat capacity $c_p = 2.66$kJ/kgK

Liquid density $\rho = 813$kg/m^3 Liquid viscosity $\mu = 0.34 \times 10^{-3}$ Pa.s

Liquid thermal conductivity $k = 0.099$W/mK

Prandtl number (liquid phase) $Pr = 9.7$

HEAT TRANSFER CALCULATIONS

The free flow area in the heat transfer fluid path is:

$$A_{flow} = Nts = 80 \times 0.005 \times 0.002 = 8 \times 10^{-4} m^2 \qquad \text{(A1)}$$

where N is the number of channels.
s is the width of the channel.
t is the depth of the channel.

The velocity of the Marlotherm S through the heat exchanger is found through the temperature drop allowed, and the fluid properties. As the fluid flows through the exchanger, a temperature drop ,ΔT, of about 5°C will be assumed. Into each Stirling heater head will go 480W. This figure is arrived at through the heat transferred from the solar concentrators to the Stirling engine (Section 6.9) divided between the four cylinders. Therefore the heat transfer fluid flow rate is:

$$\dot{m}=\frac{\dot{Q}}{c_p\Delta T}=\frac{480}{2660\times5}=0.036kg/s \qquad \text{(A2)}$$

Knowing the free flow area A_{flow}, from equation A1, and the mass flow rate of the heat transfer fluid $\dot{m}$ from equation A2, the velocity of the liquid through the heat exchanger can be calculated:

$$v=\frac{\dot{m}}{\rho A_{flow}}=\frac{0.036}{813\times8\times10^{-4}}=0.055m/s \qquad \text{(A3)}$$

Before the Reynold's number can be calculated, the equivalent diameter D_e of one of the fluid flow paths must be calculated. This can be found through the hydraulic radius r_h of the tubes:

$$r_h=\frac{free\ flow\ area}{wetted\ perimeter}=\frac{2\times5}{2\times2+2\times5}=0.714mm$$
$$\therefore D_e=4r_h=4\times0.714=2.86mm \qquad \text{(A4)}$$

Thus the Reynold's number Re can be calculated:

$$Re=\frac{\rho vD_e}{\mu}=\frac{813\times0.055\times2.86\times10^{-3}}{0.34\times10^{-3}}=376 \qquad \text{(A5)}$$

The flow is therefore laminar. This is not desirable for good heat transfer because it relies on the fluid's thermal conductivity to transfer the heat. In the case of organic fluids, the thermal conductivity is quite low. The expression for the Nusselt number in a laminar flow is taken from Hewitt (1990).

$$Nu_T=\frac{hD_e}{k}=\sqrt[3]{3.66^3+1.61^3Pe\frac{D_e}{L}} \qquad \text{(A6)}$$

This expression is for the average Nusselt number over the length L of the heat exchanger. In the above expression:

h is the heat transfer coefficient

Pe is the Peclet number which is given by $Pe=RePr$ (Guyer 1988)

So, substituting the values into A6 yields.

$$Nu_T=\sqrt[3]{3.66^3+1.61^3\times376\times9.7\times\frac{2.86}{45}}=10.05$$

$$\therefore h=\frac{Nu_T k}{D_e}=\frac{10.05\times0.099}{2.86\times10^{-3}}=348 W/m^2K \quad \text{(A7)}$$

The area available for heat transfer is:

$$A=80\times(2\times2+2\times5)\times45\times10^{-6}=0.0504m^2 \quad \text{(A8)}$$

The heat transfer expression is given by:

$$\dot{Q}=hA\Delta T_{mean\ to\ wall} \quad \text{(A9)}$$

where $\Delta T_{mean\ to\ wall}$ is the temperature drop between the bulk fluid and the heat exchanger wall. To transfer the 480W into the cylinder head:

$$T_{mean\ to\ wall}=\frac{\dot{Q}}{hA}=\frac{480}{348\times0.0504}=27^\circ C \quad \text{(A10)}$$

APPENDIX 12

MERCURY HEAT PIPE PRODUCTION DIMENSIONS

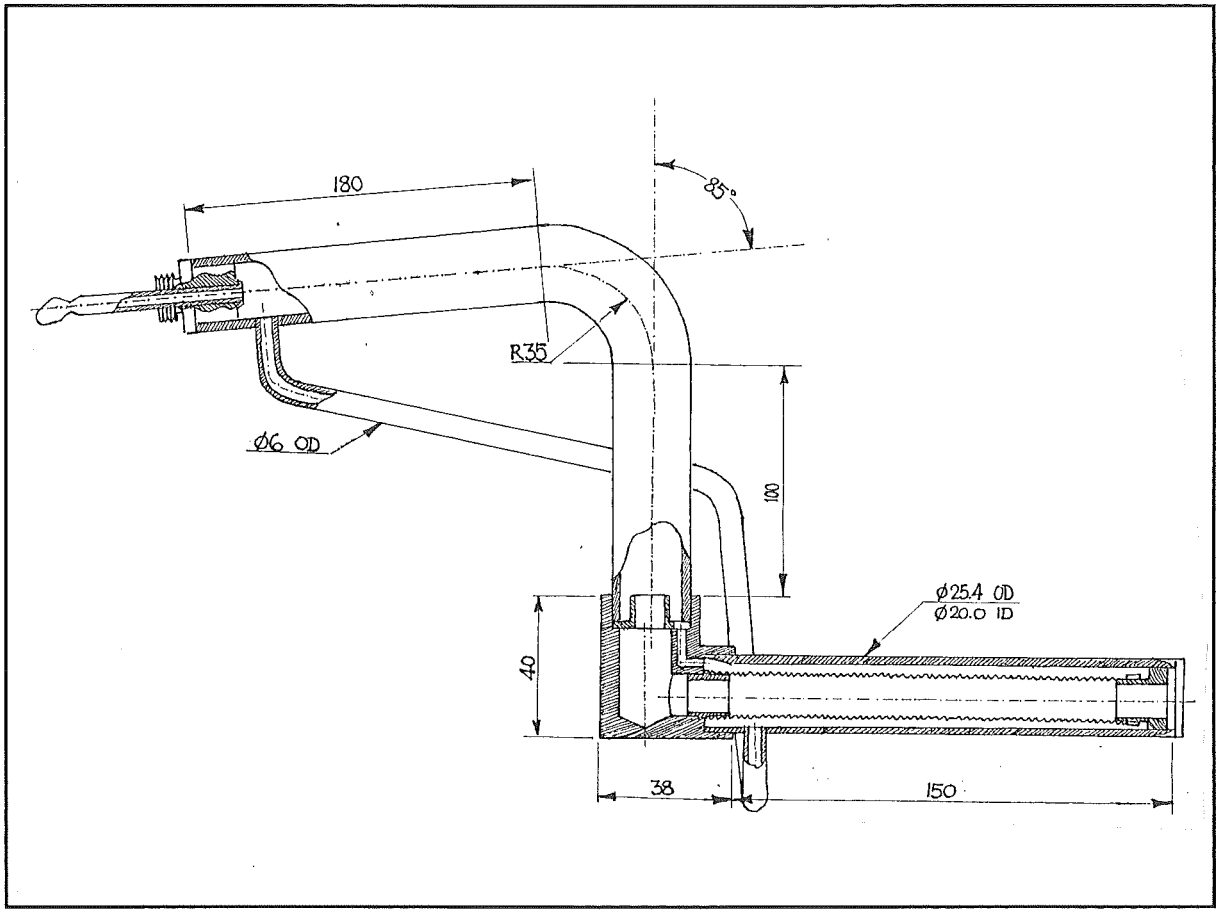

Figure A12 Basic dimensions of the mercury heat pipe. Not drawn to scale.

The heat pipe was loaded with 14.8mL of mercury. This quantity was calculated through the volume of the evaporator annular gap, and the volume of all of the condensate return tubes filled to a height level with the base of the catchment gutter. The density of the liquid mercury used in the calculation was that at 400°C, so a mass needed could be calculated. From this a volume of mercury at room temperature could be found.